

Advancing *in vitro* models of pulmonary epithelia  
for biomedical and biopharmaceutical research

Dissertation  
zur Erlangung des Grades  
des Doktors der Naturwissenschaften  
der Naturwissenschaftlich-Technischen Fakultät  
der Universität des Saarlandes

von

**Patrick Carius**

Saarbrücken 2023

Die dieser Dissertation zugrundeliegenden experimentellen Arbeiten wurden von März 2017 bis Juni 2021 unter der Leitung von Prof. Dr. Claus-Michael Lehr, zusätzlich unterstützt durch Dr. Nicole Schneider-Daum, am Helmholtz-Institut für Pharmazeutische Forschung Saarland (HIPS) in der Abteilung Wirkstofftransport (DDEL) durchgeführt.

Tag des Kolloquiums: 26. Januar 2024

Dekan: Prof. Dr. Ludger Santen

Berichterstatte:r: Prof. Dr. Claus-Michael Lehr

Prof. Dr. Jörn E. Walter

Dr. Otmar Schmid

Vorsitz: Prof. Dr.-Ing. Michael Vielhaber

Akad. Beisitzer: Dr. Britta Diesel



“Nothing in life is to be feared, it is only to be understood. Now is the time to understand more, so that we may fear less.”

*Marie Curie*

## Table of Contents

Summary.....	I
Zusammenfassung.....	II
List of Abbreviations.....	III
Introductory remarks & scientific output.....	1
1. General introduction – the role of <i>in vitro</i> models in the context of inhalation drug products.....	4
1.1 Animal testing and the “valley of death”.....	5
1.2 Fundamentals of lung biology.....	9
1.3 Transforming <i>in vivo</i> complexity into <i>in vitro</i> controllability.....	14
“Software” – state-of-the-art cellular models.....	16
“Hardware” – state-of-the-art <i>in vitro</i> devices.....	19
2. Aims of the thesis & extended summary.....	24
1. Implementation of the polyclonal hAELVi and differentiated THP-1 co-culture model into a novel microfluidic platform.....	25
2. Development of a novel perfusable platform (“PerfuPul”).....	26
3. Generation of a monoclonal human alveolar epithelial cell line named “Arlo” with pronounced barrier functions.....	28
3. Original Publications.....	30
„Capturing the Onset of Bacterial Pulmonary Infection in Acini-On-Chips“.....	30
„PerfuPul – A Versatile Perfusable Platform to Assess Permeability and Barrier Function of Air Exposed Pulmonary Epithelia“.....	43

## Table of Contents

---

„A Monoclonal Human Alveolar Epithelial Cell Line (“Arlo”) with Pronounced Barrier Function for Studying Drug Permeability and Viral Infections“ .....	83
4. Discussion and future perspectives .....	112
5. Acknowledgements.....	114
6. Publication bibliography .....	116

---

## Summary

Complex pulmonary *in vitro* models based on human cells and tissues are a potential alternative to animal testing, which could yield results with higher predictivity than current experimental models. Within this context, this thesis aimed to implement *in vitro* models of pulmonary epithelia, specifically cellular models of the human air-blood barrier, into a microfluidic platform to analyze aerosol transport and clearance. This primary goal evolved into three sub-objectives:

1. Implementation of the polyclonal hAELVi and differentiated THP-1 co-culture model into a morphologically inspired microfluidic platform.
2. Development of a novel perfusable platform (“PerfuPul”).
3. Generation of a monoclonal human alveolar epithelial cell line named “Arlo” with pronounced barrier functions.

The work conducted during this thesis led to the identification of practical issues with existing *in vitro* models as well as technologies. The critical lessons learned from these studies resulted in the generation and characterization of the perfusable platform “PerfuPul” as well as the monoclonal alveolar epithelial cell line “Arlo”, which both represent important building blocks to create complex pulmonary *in vitro* models in the future.

---

## Zusammenfassung

Komplexe pulmonale *in vitro* Modelle auf Basis menschlicher Zellen und Gewebe, stellen eine mögliche Alternative zum Tierversuch dar, welche zu Ergebnissen mit höherer Vorhersagekraft im Vergleich zu aktuellen experimentellen Modellen führen könnten. Das übergelagerte Ziel dieser Arbeit war es, *in vitro* Modelle pulmonaler Epithelien, insbesondere zelluläre Modelle der menschlichen Luft-Blut-Schranke der tiefen Lunge, in eine mikrofluidische Plattform zur Untersuchung des Aerosoltransports und -abbaus zu implementieren. Dieses Hauptziel entwickelte sich in drei Unterziele:

1. Die Implementierung eines Ko-Kultur Modells bestehend aus einer Zelllinie des Alveolarepithels (hAELVi-Zellen) und differenzierten THP-1-Zellen in eine anatomisch-inspirierte mikrofluidische Plattform.
2. Die Entwicklung einer neuartigen perfundierbaren Plattform für die Kultur von Lungenepithelzellen an einer Luft-Flüssigkeits-Grenzfläche („PerfuPul“).
3. Die Generierung einer monoklonalen humanen Alveolarepithelzelllinie namens „Arlo“, die ausgeprägte Barrierefunktionen aufweist.

Im Zuge dieser Arbeit wurden praktische Probleme in der Handhabung von etablierten *in vitro* Modellen und Technologien festgestellt. Die aus diesen Experimenten gewonnenen Erkenntnisse, führten zur Entwicklung und Charakterisierung der perfundierbaren *in vitro* Plattform „PerfuPul“ und der monoklonalen alveolaren Epithelzelllinie „Arlo“. Beide Erfindungen stellen wichtige Bausteine zur zukünftigen Entwicklung komplexer pulmonaler *in vitro* Modelle dar.

---

## List of Abbreviations

**ADME** - absorption, distribution, metabolism, excretion

**ALI** - air-liquid interface

**API** - active pharmaceutical ingredient

**AQP5** - aquaporin 5

**ATCC** - American Type Culture Collection

**AT-1** - alveolar type-1 pneumocyte

**AT-2** - alveolar type-2 pneumocyte

**BETA** - Biphasic Elastic Thin for Air-liquid culture conditions

**CIVIC** - Cyclic *In vitro* Cell-stretch

**CLDN18** - claudin 18

**COPD** - chronic obstructive pulmonary disease

**EMA** - European Medicines Agency

**FDA** - United States Food and Drug Administration

**hAELVi** - human alveolar epithelium lentivirus immortalized

**hAEPcs** - primary human alveolar epithelial cells

**HUVEC** - primary human umbilical vein endothelial cells

**iBCS** - inhalation-based biopharmaceutics classification system

**LPS** - lipopolysaccharide

**MALI** - moving air-liquid interface

**MHC II** - major histocompatibility complex 2

**PBS** - phosphate buffered saline

**PDMS** - polydimethylsiloxane

**PerfuPul** - perfusable platform to assess permeability and barrier function of air exposed pulmonary epithelia

**RAGE** - advanced glycation end products

**SARS-CoV-2** - severe acute respiratory syndrome coronavirus type 2

**SFTPC** - surfactant protein c

**TEER** - transepithelial electrical resistance

**TRPV4** - transient receptor potential cation channel subfamily V member 4

**ZO-1** - zona occludens-1

## Introductory remarks & scientific output

The ideas as well as the data from the following three publications constitute the core of this cumulative thesis:

1. Artzy-Schnirman, Arbel; Zidan, Hikaia; Elias-Kirma, Shani; Ben-Porat, Lee; Tenenbaum-Katan, Janna; **Carius, Patrick**; Fishler, Ramy; Schneider-Daum, Nicole; Lehr, Claus-Michael; Sznitman, Josué (2019): **Capturing the Onset of Bacterial Pulmonary Infection in Acini-On-Chips**. In *Advanced Biosystems*. 45, p. 1900026.

DOI: 10.1002/adbi.201900026.

2. **Carius, Patrick**; Dubois, Aurélie; Ajdarirad, Morvarid; Artzy-Schnirman, Arbel; Sznitman, Josué; Schneider-Daum, Nicole; Lehr, Claus-Michael (2021): **PerfuPul-A Versatile Perfusable Platform to Assess Permeability and Barrier Function of Air Exposed Pulmonary Epithelia**. In *Frontiers in bioengineering and biotechnology* 9, p. 743236.

DOI: 10.3389/fbioe.2021.743236.

3. **Carius, Patrick**; Jungmann, Annemarie; Bechtel, Marco; Grißmer, Alexander; Boese, Annette; Gasparoni, Gilles; Salhab, Abdulrahman; Seipelt, Ralf; Urbschat, Klaus; Richter, Clémentine; Meier, Carola; Bojkova, Denisa; Cinatl, Jindrich; Walter, Jörn; Schneider-Daum, Nicole; Lehr, Claus-Michael (2023): **A Monoclonal Human Alveolar Epithelial Cell Line ("Arlo") with Pronounced Barrier Function for Studying Drug Permeability and Viral Infections**. In *Advanced science* (Weinheim, Baden-Wurttemberg, Germany), e2207301. DOI: 10.1002/adv.202207301.

Other central ideas underlying the description of the state-of-the-art of the research presented in this thesis have already been described in more detail in the following two book chapters:

**Carius, Patrick;** Horstmann, Justus C.; Souza Carvalho-Wodarz, Cristiane de; Lehr, Claus-Michael (2021): **Disease Models: Lung Models for Testing Drugs Against Inflammation and Infection.** In Monika Schäfer-Korting, Silvy Stuchi Maria-Engler, Robert Landsiedel (Eds.): Organotypic models in drug development, vol. 265. Cham, Switzerland: Springer (Handbook of experimental pharmacology, 0171-2004, 265), pp. 157–186.

Schneider-Daum, Nicole; **Carius, Patrick;** Horstmann, Justus C.; Lehr, Claus-Michael (2019): **Reconstituted 2D Cell and Tissue Models.** In Hickey, Anthony J.; Da Rocha, Sandro R. (Eds.): Pharmaceutical inhalation aerosol technology. Third edition. Boca Raton: CRC Press/Taylor & Francis Group (Drugs and the pharmaceutical sciences), pp. 627–651.

In addition, the work related to this thesis was kindly supported by the German-Israeli Foundation for Scientific Research and Development (GIF) (Grant: I-101-409.8-2015) as well as by the German Federal Ministry of Education and Research as part of the COVID-protect project (Grant: 01KI20143C & 01KI20143A).

#### **Other publications related to this thesis:**

##### **2022**

Sengupta, A., Roldan, N., Kiener, M., Froment, L., Raggi, G., Imler, T., Maddalena, L., Rapet, A., May, T., **Carius, P.**, Schneider-Daum, N., Lehr, C. M., Kruihof-de Julio, M., Geiser, T., Marti, T. M., Stucki, J.D., Hobi, N., & Guenat, O. T. (2022). A new immortalized human alveolar epithelial cell model to study lung injury and toxicity on a breathing lung-On-Chip system. *Frontiers in toxicology*, 4.



## 2021

Huck, B., Hidalgo, A., Waldow, F., Schwudke, D., Gaede, K. I., Feldmann, C., **Carius, P.**, Autilio, C., Pérez-Gil, J., Schwarzkopf, K., Murgia, X., Loretz, B., Lehr, C.M. (2021). Systematic Analysis of Composition, Interfacial Performance and Effects of Pulmonary Surfactant Preparations on Cellular Uptake and Cytotoxicity of Aerosolized Nanomaterials. *Small Science*, 1(12), 2100067.

Horstmann, J. C., Thorn, C. R., **Carius, P.**, Graef, F., Murgia, X., de Souza Carvalho-Wodarz, C., & Lehr, C. M. (2021). A custom-made device for reproducibly depositing pre-metered doses of nebulized drugs on pulmonary cells *in vitro*. *Frontiers in Bioengineering and Biotechnology*, 9, 643491.

## Awards

**Ted Martonen Student Research Award (2021)** - for outstanding independent research in the field of aerosols in medicine received at the 23<sup>rd</sup> Congress of the International Society for Aerosols in Medicine. Boise, United States of America.

## 1. General introduction –

### the role of *in vitro* models in the context of inhalation drug products

A multi-stage process ensures that new drugs are safe and effective for patients (FDA 2018). In a simple depiction, this process often starts with an extensive exploratory research phase to identify and characterize potential targets, mostly proteins (Figure 1). Throughout the following drug discovery phase, thousands to millions of structures are often screened for the most favorable and selective interaction with the target until the most promising compounds are identified. During the preclinical research phase, selected lead compounds are chemically optimized for absorption, distribution, metabolism, and excretion (ADME) related properties, while potentially carcinogenic compounds are disqualified. Preclinical development begins if the preclinical research data indicate that a candidate compound is safe and shows a potential therapeutic efficacy.

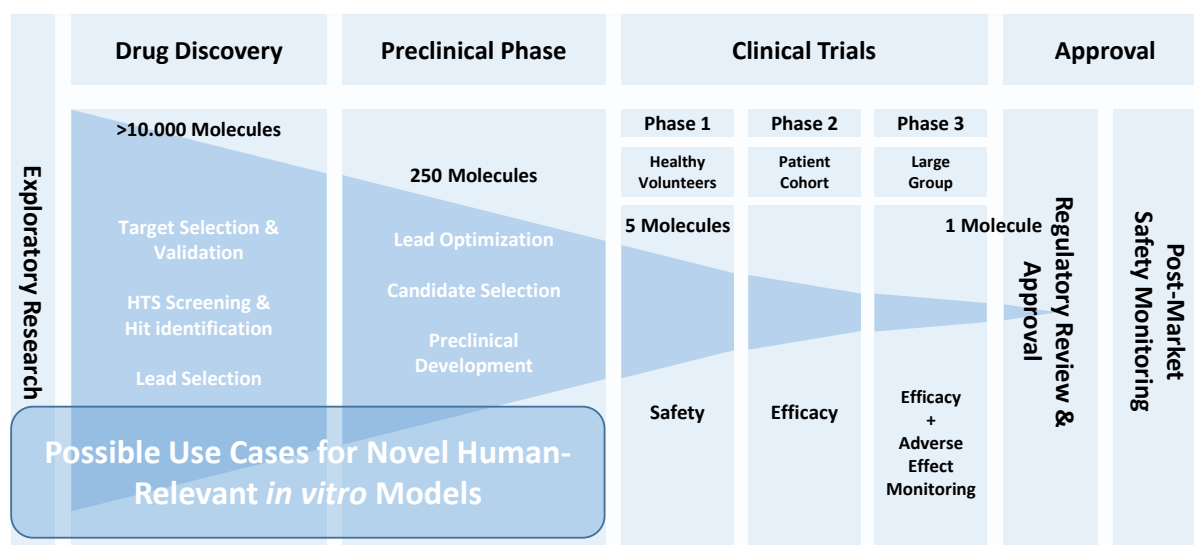


**Figure 1:** Schematic depiction of the different stages involved in drug development. Possible use cases for the application of novel human-relevant *in vitro* models are highlighted. Based on information from FDA (2018) and numbers from Ching et al. (2021).

During preclinical development, the active pharmaceutical ingredient (API) is united with selected excipients as part of the formulation process to derive an interim drug product. The development phase ensures that the API, in the predicted dose for the administration in the upcoming human clinical trial, remains stable and effective after administration as well as that it shows a favorable pharmacokinetic profile. Human clinical trials are then classically performed in three phases, where it is ensured that the drug is safe, effective, and applied at the correct dose. These phases are conducted with an increasing number of study participants from Phase I to Phase III to gather detailed information about the effects of the drug in a broad study population. As part of clinical development, the drug formulation is further refined during the clinical trial to enhance the efficacy of the final drug product by, e.g., optimizing the pharmacokinetic properties based on the gathered human data. Once these three phases are successfully completed, the regulatory authorities that chaperoned the clinical trial, such as the United States Food and Drug Administration (FDA) or the European Medicines Agency (EMA), review the data and finally evaluate whether the drug is safe and effective. After a positive review outcome, the drug is approved for marketing. A post-market safety monitoring ensures that rare side effects of the drug are also identified and reported to the authorities after the drug is released for marketing.

### **1.1 Animal testing and the “valley of death”**

The preclinical research phase (Figure 1) aims to mainly provide sufficient data that would allow predicting the pharmacological, pharmacokinetic, pharmacodynamic and potential toxic effects of a new drug before first-in-men studies. While in the drug discovery as well as exploratory research phase mainly *in vitro* and *in silico* data are generated, the preclinical research phase is mainly characterized by the generation of data from *in vivo* experiments, although *in silico*, *in vitro* and *in vivo* experiments are performed during all phases. A mandatory reliance on animal experiments to test for safety and efficacy further

stems from current regulatory guidelines. The ICHM3 (R2) guideline for small molecule new chemical entities, for example, requires to conduct experiments on a rodent (such as mouse or rat) as well as a non-rodent species (e.g., dog, mini-pig, or non-human primates) for assessing the potential toxicity of a new drug (Committee for Medicinal Products for Human Use - EMA 2009; Prior et al. 2020).

The experimental use of mammal model organisms that share many of their gene and organ functions with humans, historically, has tremendously influenced basic biomedical and biopharmaceutical research. Data from animal models have elucidated disease-related pathways and helped to identify new drug targets as well as new treatments (Bonniaud et al. 2018). Furthermore, living organisms possess interconnected organ systems, which allow the simultaneous monitoring of pharmacokinetic as well as pharmacodynamic processes after drug administration, such as the relationship between serum and tissue concentrations for example (Andes and Craig 2002).

There are, however, also obvious ethical concerns associated with sacrificing laboratory animals for biopharmaceutical and biomedical research. This is why every experiment that includes animals should be questioned according to the refine, reduce or replace (3R's) principles introduced by Russel and Burch more than 60 years ago (Russel and Burch 1959). In an example from another research area, such ethical concerns were raised by the public and led the European Parliament to introduce a phased-out ban on *in vivo* safety testing of cosmetic products as well as their ingredients, complementing focused efforts by animal welfare organizations (Knight et al. 2021). The ban partly took effect in 2009 for local health effects and finally in 2013 for systemic health effects (Buzek and Ask 2009). More recently, such considerations also resulted in the acceptance of the “FDA Modernization Act 2.0” by the United States Senate (Congress of the United States of America 2022). For the first time, this law legally authorized the use of validated human-

based models (*in vitro* or *in silico*) instead of animal models to investigate the safety and efficacy of a drug.

Apart from such ethical concerns, using animal models also comes with other disadvantages. Small molecules, for example, are known to be metabolized in a species-specific manner, resulting in the activation of different enzymatic pathways, changing metabolic rates as well as differently formed metabolites that all need to be individually assessed for each species of interest (Lin 1995; Hurst et al. 2007). Species-specific differences in the expression levels and physiological activities of efflux as well as uptake transporters between different animal models (e.g., rodents, dogs, or non-human primates) further aggravate the prediction of human ADME characteristics (Chu et al. 2013). More fundamentally, however, are scientific concerns about the general hypothesis that experimental data from animals are predictive for humans, since it has never been scientifically confirmed (Shanks et al. 2009; Pound and Ritskes-Hoitinga 2018; Leenaars et al. 2019).

In the specific case of respiratory diseases, these concerns are inter alia fueled by data from the pharmaceutical industry. Novel therapeutic drugs acting against respiratory diseases entering clinical trials were only successful in 7% of the cases during Phase I and only 15% successful during Phase II, with an overall success rate during all clinical trial phases smaller than 7% (Dowden and Munro 2019; Yaqub et al. 2022). By contrast, respiratory diseases are among the most common causes of serious disease and death worldwide (Vos et al. 2020; World Health Organization 2020; Forum of International Respiratory Societies 2021). This includes inflammatory diseases like asthma or chronic obstructive pulmonary disease (COPD) and infectious respiratory diseases caused by pathogenic microorganisms or viruses, such as severe acute respiratory syndrome coronavirus type 2 (SARS-CoV-2). While the reasons for the high attrition rate of pulmonary therapeutics during costly clinical trials – often referred to as the “valley of death” – are

multidimensional, a lack of preclinical models predictive for the human situation was often identified as a major reason in the recent literature of inhalation research (Fröhlich 2019; Seyhan 2019; Artzy-Schnirman et al. 2020; Ingber 2020). Such concerns are often linked to species-specific differences between the lungs of humans and the respective animal models, which encompass alterations in anatomical, functional as well as cellular properties. Rodents are, for example, obligatory nose-breathers, whereas humans can breathe through the oral or nasal cavity (Gautam and Verhagen 2012). Further, the airways of the lungs of mice and rats follow a monopodial architecture (Schittny 2017). This means that ramifications branch off asymmetrically from a central airway. In humans, however, the airways follow a dichotomous branching pattern, where each airway diverts into two roughly symmetrical daughter branches in each generation (Weibel et al. 1963; Labode et al. 2022). Particles within human lungs thus more often deposit at the bifurcations of the airways (Fröhlich 2021). Rats and mice further lack distinct respiratory bronchioles, a specialized human lung structure (Tyler and Julian 1992).

Being influenced also by other factors, such as the advances in the generation of *in vitro* models in the cosmetic industry after the ban on animal experimentation in 2013, complex *in vitro* models based on human cells and tissues were seen as a promising alternative to overcome some of the limitations imposed by animal models (European Commission, Joint Research Centre 2021). Figure 1 highlights such additional opportunities for the use of complex *in vitro* models in biopharmaceutical as well as biomedical research. As part of the generation of such predictive complex *in vitro* models for pulmonary research in the near future, however, reliable cell sources and robust technical platforms would be needed as essential building blocks to generate consistent experimental readouts (Carius et al. 2023; Carius et al. 2021a).

## 1.2 Fundamentals of lung biology

When comparing the human lung to other organs that give rise to major external epithelia, such as the skin or the gastrointestinal tract, one notices that the most proximal part of the trachea serves as a central in- as well as output. Using an allegorical simplification, the lung can thus be depicted as a sophisticated biological version of a balloon, which relies on elasticity, expansion and contraction to carry out its functions. In essence, these functions are effective gas exchange and protection from external noxae.

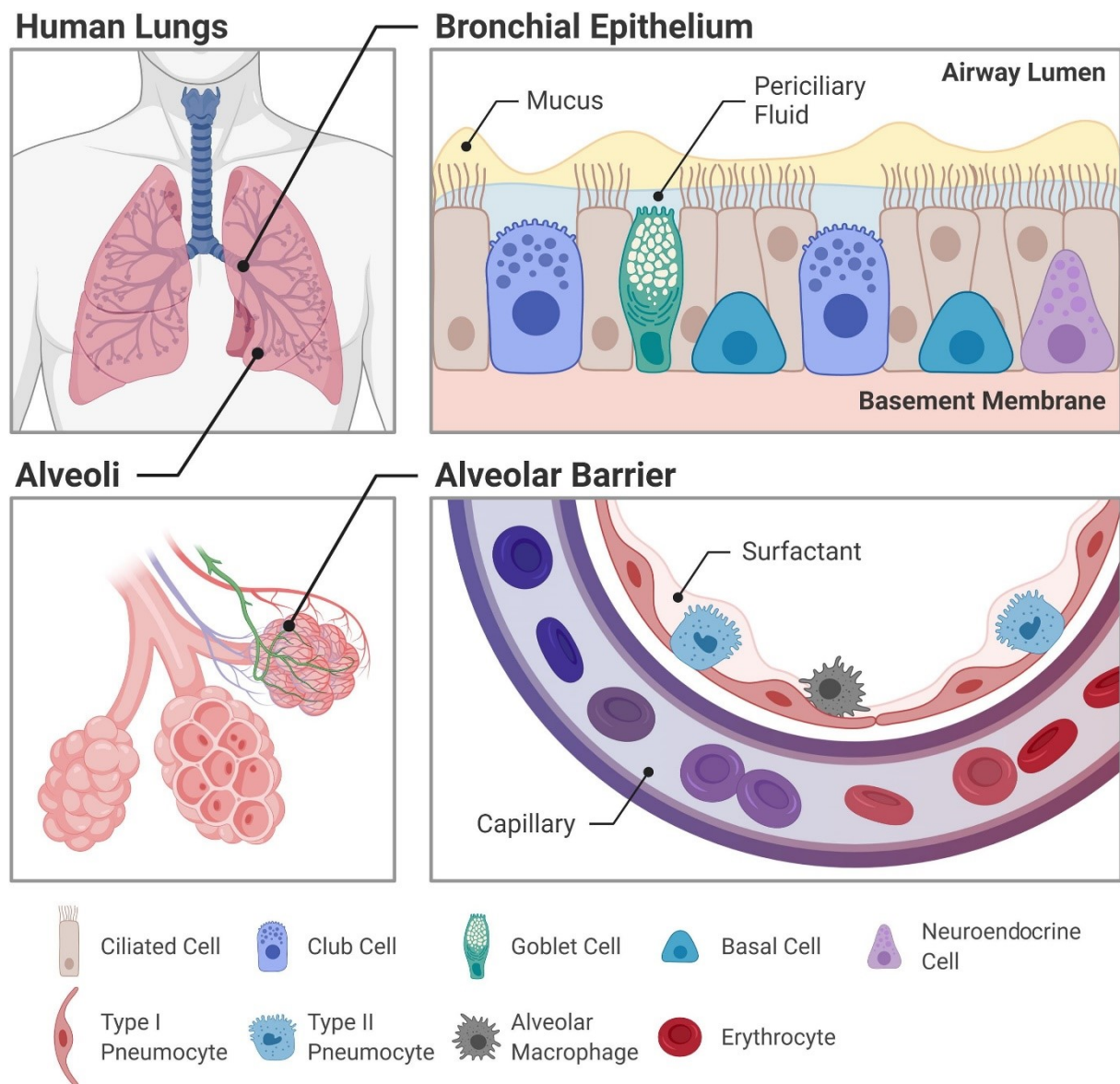


**Figure 2:** Epithelial barriers of the human respiratory tract. Cell composition of epithelial linings in the lungs varies in different segments. The pseudo-stratified, columnar epithelium in the bronchial and bronchiolar region is composed of ciliated, club, goblet, basal and neuroendocrine cells. A thin layer of periciliary fluid and mucus covers the cell layer. The alveolar epithelium is squamous in nature and comprises predominantly the extremely thin (for efficient gas exchange) AT-1 and the cuboidal AT-2 cells (responsible for the production, secretion and recycling of surfactant-(proteins)). Alveolar macrophages are also present.

Figure was taken from Selo et al. (2021) with slight modifications. Copyright © 2021 Mohammed Ali Selo, Johannes A. Sake, Kwang-Jin Kim, Carsten Ehrhardt. Distributed under the terms of the Creative Commons Attribution 4.0 International (CC BY 4.0).



The upper airways begin with the nasal or oral cavity and extend towards the larynx, thereby already starting to filter, moisten and warm the air we breathe. Distally from the larynx, the lower airways start to ramify. Following a dichotomous branching pattern, the airways branch into roughly two symmetrical daughter branches with each generation. The ~23 airway generations of the human lung can be roughly divided into the tracheo-bronchial airways (generation 0-10), the small to terminal bronchioles (generation 11-16), as well as the pulmonary acinar airways (generation >16) of the respiratory region of the peripheral lung (alveoli) (Haefeli-Bleuer and Weibel 1988; Koullapis et al. 2019). The tissue that lines the airways has evolved endoderm-derived epithelial cells that are part of the mucosa of the airways as well as of the respiratory region of the alveoli. In addition, cartilage, airway smooth muscle, fibroblasts, and vascular endothelium developed from mesenchymal derivatives (Kadzik and Morrisey 2012). Seen in the context of aerosol therapy or inhalation toxicology, the cellular epithelium but also non-cellular barriers, such as e.g. pulmonary mucus or surfactant, are the first structures with which an aerosol particle interacts (Ruge et al. 2013; Murgia et al. 2018). This makes them also potential barriers, which would need to be traversed if systemic drug delivery via the lungs is anticipated. It thus makes a difference whether particles initially deposit in the central or peripheral lung since these barriers will interact differently with particles based on their specific anatomical location and associated function.

The partially ciliated pseudo-stratified epithelial lining of the bronchial airways can reach a thickness of 50  $\mu\text{m}$  and is composed of columnar epithelial cells, club cells, mucus-secreting goblet cells, and interspersed basal cells, which serve as stem cells for the majority of airway epithelial cells (Rock et al. 2010). The bronchial epithelial lining is additionally protected by a mesh-forming hydrogel, the pulmonary mucus, which mainly consists of water (~95%), the glycoprotein mucin (2-5%) as well as of lipids in low concentrations (Boegh and Nielsen 2015). External noxae, such as particulate matter or

microorganisms, are often immobilized in the mucus and then subsequently transported out of the lung via the pharynx. This happens through a coordinated movement of the cilia of the epithelial lining termed “mucociliary clearance”. All non-cartilaginous airways are called bronchioles and are characterized by a pseudo-stratified epithelium with a similar cellular composition as observed in the bronchi (Rock et al. 2010). Yet, the number of basal cells as well as the airway diameter substantially decline from the early to the late airway generations, to less than 1 mm in the terminal bronchioles (van Michael J. Evans 2001). Distally, the terminal bronchioles develop into respiratory bronchioles, a structure exclusively found in the human lung and lined by a simple cuboidal epithelium (Have-Opbroek et al. 1991; Tyler and Julian 1992). The respiratory bronchioles fluently develop into pulmonary acini, which in turn extend into multiple alveolar sacs per acinus (Haefeli-Bleuer and Weibel 1988). Differing numbers of alveoli form a single alveolar sac; however, single alveoli represent the functional unit of gas exchange in the deep lung. In contrast to the decreasing luminal diameter of the airways from proximal to distal, the surface area coated by the epithelial lining increases from around 4 m<sup>2</sup> in the two bronchi to about 100 m<sup>2</sup> opened up by the, on average, 480 million alveoli within the two lobes of a human lung (Gehr et al. 1978; Ochs et al. 2004; Dombu and Betbeder 2013). Here, in the respiratory region of the peripheral lung, the epithelium is closely connected to the underlying endothelium. At the thinnest parts (<1 μm) of this interface, a structure also called the “air-blood barrier”, epi- and endothelial cells share a common basal lamina which reduces the distance for the diffusion of gases to the greatest possible extent (Weibel 1973; Knudsen and Ochs 2018). Unlike the bronchial tissue, which is connected to the systemic circulation, the highly perfused respiratory region of the peripheral lung is vascularized by the pulmonary circulatory system. This separate connection ensures the transport of oxygenated blood directly to the heart.

Two types of pneumocytes, alveolar type-1 (AT-1) and alveolar type-2 (AT-2), constitute the alveolar epithelium. AT-1 pneumocytes, which only account for around 8% of all lung cells, develop a squamous epithelial layer that has a share of 95-98% of the alveolar epithelium's total surface area, enabled by a surface area of  $\sim 5000 \mu\text{m}^2$  per cell (Gehr et al. 1978; Crapo et al. 1982). To withstand the fluid pressure stemming from the pulmonary circulatory system, which is directed towards the air-filled alveolar lumen, the flat AT-1 cells further evolved tight cell-to-cell connections to neighboring epithelial cells. At these intercellular junctions, adhesive transmembrane proteins that belong to the claudin family of tight junction proteins, in concert with other structural and tight junction proteins such as tight junction protein 1 (also known as zona occludens-1 (ZO-1)) and Occludin, play an essential role in regulating the paracellular permeability of ions and small hydrophilic molecules (Brune et al. 2015; Schlingmann et al. 2015). Particularly Claudin-18.1, which represents one of the two splice variants of the CLDN18 gene, is exclusively expressed in the lung and is the most abundant claudin found in AT-1 cells (Niimi et al. 2001; LaFemina et al. 2010; Brune et al. 2015). The tight barrier formed between the cells of the alveolar epithelium also allows for effective fluid homeostasis facilitated by active transporters, carrier or channel proteins that transport water, ions but also small molecules as well as macromolecules (Brune et al. 2015; Schlingmann et al. 2015; Wittekindt and Dietl 2019). As the most prevalent cell type, the cuboidal AT-2 cells account for  $\sim 18\%$  of the cells of the alveolar epithelium; however, their surface area contributes only 2-5% to the total epithelial surface area due to their cuboidal shape and positioning at the corners of the alveoli (Crapo et al. 1982; Perlman and Bhattacharya 2007; Herzog et al. 2008). On the contrary, they represent conditionally proliferative facultative progenitors, able to differentiate into AT-1 cells during epithelial growth or upon epithelial damage (Evans and Lee 2020). Another elementary function of AT-2 cells is their ability to secrete and recycle pulmonary surfactant, which acts as a non-cellular barrier composed of lipids as well as bioactive

proteins, which biophysically prevents the alveoli from collapsing by reducing the surface tension at the air-blood barrier (S. R. Bates et al. 1994; Knudsen and Ochs 2018; Garcia-Mouton et al. 2019). In addition, AT-2 cells contribute to immunological responses and immune signaling, e.g., by the secretion of antimicrobial peptides or the expression of major histocompatibility complex (MHC) II surface antigens, thereby assisting alveolar macrophages scavenging the lumen of the alveoli (Cunningham et al. 1994; Mieke A. Dentener et al. 2000; Hasegawa et al. 2017).

### 1.3 Transforming *in vivo* complexity into *in vitro* controllability

As outlined in the previous section, reproducing all dimensions of complexity (e.g., anatomical, biophysical, biochemical, and physiological) observed in the human lung can be deemed virtually impossible within a single experimental model and would thus not yield an effective assay for biopharmaceutical research. Utilizing animal models, however, comes with certain disadvantages, including species-specific differences in anatomical structures, cell types or enzymatic activities outlined in more detail in paragraph 1.2. Within this context, complex pulmonary *in vitro* models (in particular when based on human cells and tissues) were proposed as an imaginable alternative to animal testing (Artzy-Schnirman et al. 2020; Carius et al. 2021a). By isolating key elements, these models offer the possibility to unravel the multidimensionality of (patho-) physiological conditions observed in the human lung, which then could be individually controlled within an *in vitro* environment (Carius et al. 2021b).

Inspired by a useful comparison introduced by Artzy-Schnirman et al. (2019a), the building blocks needed to generate complex pulmonary *in vitro* models could be, in compliance with the basic design of computer systems, divided into two broad categories: "software" and "hardware". The "software" category would include biological factors, such as the different

cellular models or the cell culture medium needed to grow cells *in vitro*. The “hardware” category would thereby refer to all the technical accessories that constitute the (biomimetic) *in vitro* cell culture environment, such as traditional well-based permeable growth supports (e.g., Transwell®) or sophisticated microphysiological systems. This category would also include additional devices, e.g., for the generation and/or *in vitro* deposition of aerosols. Ideally, novel “software” could be combined interchangeably with state-of-the-art “hardware” to form predictive complex pulmonary *in vitro* models, which would resemble “higher-level anatomical and physiological aspects of human biology in practical experimental setups and are often referred to as 3D cell cultures, spheroids, bioprinted tissues, bioreactor cultures or microphysiological systems (e.g., tissue-/organ-/human-on-chip)” (European Commission, Joint Research Centre 2021).

**“Software” – state-of-the-art cellular models**

As essential requirements, cellular models of pulmonary epithelia should be cultured under air-liquid interface (ALI) conditions as well as develop tissue-specific barrier integrity, when they are selected for conducting *in vitro* biopharmaceutical or toxicological inhalation experiments (Bonniaud et al. 2018; Lacroix et al. 2018; Movia et al. 2020). Especially ALI conditions, which expose the apical cell surface to air, serve as an important biophysical stimulus that activates specific pathways involved in cellular differentiation and polarization (WU et al. 1986; Whitcutt et al. 1988; Jong et al. 1993; Dvorak et al. 2011). Primary bronchial epithelial cells fulfill these criteria and also differentiate into the cell types observed *in vivo* when cultured in a cell culture medium supplemented with retinoic acid for at least 14 days on collagen-coated Transwell®(-like) growth supports under ALI conditions (Karp et al. 2002). They are available from different clinical sources, such as patient-derived biobanks or via various commercial vendors. The latter, for instance, the American Type Culture Collection (ATCC) (USA), further distribute continuous cell lines such as the bronchial carcinoma cell line Calu-3, which also fulfills the needed basic criteria to perform transport experiments (Bosquillon et al. 2017). Other sources of *in vitro* models for the bronchial epithelium have been comprehensively discussed elsewhere (Gordon et al. 2015; Hittinger et al. 2017; Hiemstra et al. 2018; Selo et al. 2021).

In contrast to the bronchial cellular *in vitro* models described above, a substantially smaller fraction of cellular models is available to model the basic functional particularities of the alveolar epithelium *in vitro*. So far, primary human alveolar epithelial cells (hAEPs) are the present gold standard when assessing permeability in biopharmaceutical *in vitro* experiments (Selo et al. 2021). After isolation from resected lung tissue and seeded on porous growth supports, hAEPs reconstitute a polarized monolayer with functional tight junctional complexes under ALI conditions after a few days (Elbert et al. 1999; Kim et al. 2001; Fuchs et al. 2003; Bur et al. 2006; Daum et al. 2012). Unfortunately, however, after

the majority of AT-2 cells spontaneously differentiated into AT-1 cells, which is also indicated by changes in cellular morphology and accompanied by a peak in the transepithelial electrical resistance (TEER) reaching values  $>1000 \Omega \cdot \text{cm}^2$ , the cells further de-differentiate eventually losing barrier properties, which limits the experimental time scale to a few days (Dobbs et al. 1985; Foster et al. 2007; Bove et al. 2014; Hittinger et al. 2016; Carius et al. 2023). Yet the de-differentiation is only one of the disadvantages when working with hAEPs, which can hardly be passaged and thus not expanded after the isolation procedure. The cell isolations only yield a modest number of cells, consume a considerable amount of working time as well as labor costs and donor-to-donor variations hamper the successful establishment of barrier properties, thus introducing difficult-to-control experimental variability.

A promising development over recent years was the generation of cellular models that are based on induced pluripotent or adult stem cells. By now, experimental protocols are available to maintain the proliferative capacity of these stem cells *in vitro* but also to further differentiate them into multi-cellular, self-organizing organoid cultures, which resemble some morphological hallmarks of *in vivo* tissues (Kratochvil et al. 2019). In expansion culture, organoids are usually cultured in submerged cell culture conditions on titer plates to retain their stemness, where they form multiple micron-sized spherical *in vitro* tissues that are embedded in hydrogel domes. To achieve differentiation under ALI conditions, the organoids from the proliferative expansion culture need to be extracted from the hydrogel domes, and are then dissociated into smaller fragments, before seeding them on Transwell® inserts or other growth supports. Such procedures yielded cellular models of the alveolar epithelium that expressed AT-1 associated markers such as aquaporin 5 (AQP5) or podoplanin (PDPN) but also AT-2 markers, for example surfactant protein c (SFTPC) (Jacob et al. 2017; van Riet et al. 2020; van Riet et al. 2022; Tindle et al. 2021; Yang et al. 2022). Currently, however, such models have not been characterized to be used

in biopharmaceutical permeability experiments, or are unsuitable for such studies. Reasons include the lack of tissue-specific barrier properties (He et al. 2022; Yang et al. 2022; Tindle et al. 2021; van Riet et al. 2020), formation of stratified epithelia (Lamers et al. 2021) or their exclusive culture as closed alveospheres (Jacob et al. 2017; Katsura et al. 2020).

Another alternative to using primary cells was, and still is, the generation and steady advancement of continuous cell lines of alveolar epithelial cells. These cellular models have been isolated from resections of cancerous lung tissue or were genetically modified to retain their proliferative capacity *in vitro*. A key example in this regard are A549 cells, which are a patient-derived AT-2-like cell line isolated from an adenocarcinoma (Giard et al. 1973). Cultured for several weeks in a modified cell culture medium, these cells contain cytoplasmic lamellar inclusions and show gene expression signatures similar to primary AT-2 cells (Cooper et al. 2016). Their use as a reliable cellular model to perform biopharmaceutical permeability experiments involving small molecules, however, is limited by the lack of functional tight junctions (Winton et al. 1998). A recent report further identified three sub-clones within A549 *in vitro* cultures, which hampers experimental robustness and might be an explanation for contradictory results that described either the secretion or the lack of functional surfactant proteins within A549 cultures (Mahto et al. 2014; Tièche et al. 2019). Alternatively, immortalized cell lines can be generated by inserting transgenes or additional genes, which all should influence essential cellular mechanisms regulating proliferation, into the genome of primary cell cultures using, e.g., (lenti-) viral vectors (Lipps et al. 2018).

Although continuous cell lines can develop genetic instabilities or yield phenotypes that divert from *in vivo*, an immortalized cell line, the human alveolar epithelium lentivirus immortalized (hAELVi) cell line, as well as the adenocarcinoma-derived NCI-H441 cell line, have been recently proposed as useful cellular models to reconstitute the alveolar



epithelium *in vitro* (Kuehn et al. 2016; Hiemstra et al. 2019; Selo et al. 2021). By forming electrically tight monolayers that ensure tissue-specific barrier integrity under ALI conditions together with the expression of markers relevant for alveolar epithelial cells, these two cell lines principally fulfill the requirements to perform biopharmaceutical or toxicological inhalation experiments (Kuehn et al. 2016; Lochbaum et al. 2020). Nevertheless, they were also reported to cause experimental inconsistencies that might be *inter alia* linked to their polyclonality, which is more extensively discussed as part of this thesis in Carius et al. (2023).

#### **“Hardware” – state-of-the-art *in vitro* devices**

Permeable growth supports (e.g., Transwell® inserts) including a microporous membrane, can be inserted into multi-well cell culture plates and are the prevailing standard for culturing pulmonary cellular *in vitro* models. As a key feature, these technical accessories allow the spatial separation of the cell culture environment into an apical and basolateral compartment. This separation enables the culture of different cell types (e.g., epi- vs. endothelial cells) on opposite sides of a membrane, but more importantly, also allows to expose the cells to air at the apical surface. Biologically, the establishment of ALI conditions enabled by these growth supports leads to the enhanced differentiation and polarization of pulmonary epithelial cells *in vitro* (Hiemstra et al. 2018; Lacroix et al. 2018). Technically, they further allow the measurement of electrophysiological metrics, such as the epithelial potential difference as well as TEER, but also the deposition of nebulized aerosols or aerosolized dry powders (Lenz et al. 2014; Horstmann et al. 2021; Metz et al. 2018). Even though these growth supports have additional advantages, such as the possibility to perform high throughput experiments due to their compatibility with lab-automation systems, they also face significant disadvantages, namely the stiffness of the growth supports as well as their static culture conditions.

In order to overcome the disadvantages posed by cells cultured on static Transwell®-like growth supports, research efforts that shaped the field of microphysiological systems introduced devices that allow to culture cells in organ-specific biomimetic *in vitro* environments (Low et al. 2021). In particular, lung-on-chip systems introduced physiologically relevant biophysical stimuli into pulmonary *in vitro* cultures, such as continuous perfusion or stretch, which more realistically mimic certain features of the complex biological environment as it is observed in the human lung (described in section 1.2) (Artzy-Schnirman et al. 2019a).

In one of the earliest lung-on-chip studies described, the AT-2-like continuous cell line A549 could be cultured under ALI conditions and constant perfusion for up to 21 days in a simple polydimethylsiloxane (PDMS)-based lung-on-chip (Nayalanda, 2009). Shortly after, the seminal work by Huh et al. (2010) introduced a sophisticated PDMS-based lung-on-chip, which enabled the co-culture of primary alveolar epithelial cells under ALI conditions (apical channel) in close contact with primary human microvasculature cells (basolateral channel) to mimic the air-blood barrier *in vitro*. The device, which is by now in a similar version commercially distributed by Emulate Inc. (USA) as Chip-S1®, for the first time, enabled the implementation of cyclic stretch as well as perfusion-like continuous fluid flow in a pulmonary *in vitro* system (Emulate 05.04.23). Recently, this system has been used to demonstrate that breathing motions suppress innate immune responses in primary epithelial as well as endothelial cells, partly orchestrated by stimulation of the mechanosensitive ion channel transient receptor potential cation channel subfamily V member 4 (TRPV4) and the receptor for advanced glycation end products (RAGE) (Bai et al. 2022).

Implementing continuous fluid flow into an inflammation lung model based on a Transwell®-like device, for example, has further been shown to positively influence the transmigration of fibrocytes by creating a concentration gradient as a guide (Punde et al.

2015). Another important contribution to the field was the lung-on-chip device by Stucki et al. (2015), which introduced a thin PDMS-based permeable membrane that is passively deflected by the movement of a biomimetic micro-diaphragm. This lung-on-chip enabled cyclical three-dimensional stretch of hAEPs grown on the apical side as well as the culture of primary human umbilical vein endothelial cells (HUVEC) grown on the basolateral side of the membrane (Stucki et al. 2015). A medium-throughput version of this breathing lung-on-chip harboring 12 separate culture wells (Stucki et al. 2018), distributed by the company Alveolix AG (Switzerland) under the name AX12 (AlveoliX 24.03.23), was also recently combined with an AX12-compatible exposure chamber (Vitrocell Systems GmbH (Germany)). This setup was used to deposit different nebulized aerosols as fine mist on a cell line based model of the air-blood barrier cultured under ALI conditions (Sengupta et al. 2022; Sengupta et al. 2023).

As another promising system, the moving air-liquid interface (MALI) bioreactor also allows the culture of epithelial cells grown in monoculture on a flexible membrane under the influence of ALI conditions and three-dimensional biodynamic stretch. However, the system additionally adds perfusion as another physiologically relevant stimulus and clearance mechanism (Cei et al. 2021). In contrast to the breathing lung-on-chip introduced by Stucki et al. (2015), the membrane of the MALI bioreactor is deflected by above-ambient positive air pressure in the apical chamber and only yields a single experiment per unit. The design of the MALI bioreactor moreover includes the direct integration of a clinically relevant nebulizer for the direct deposition of aerosols onto the epithelial cells grown in the apical chamber. A further developed version of the MALI bioreactor, the Cyclic *In vitro* Cell-stretch (CIVIC) system, which includes a thinner and optimized Biphasic Elastic Thin for Air-liquid culture conditions (BETA) stretchable membrane, showed the establishment of tissue-specific barrier integrity determined by TEER measurements for the bronchial epithelial cell line 16HBE14o- (Doryab et al. 2021; Doryab and Schmid 2022). Recently, this system was

used to demonstrate the anti-fibrotic effects of the drug nintedanib (inhaled vs. systemic dosing) in an *in vitro* model of idiopathic pulmonary fibrosis, where a triple co-culture consisting of A549 cells and primary fibroblasts in the apical compartment and an endothelial cell line (EA.hy926) in the basolateral compartment, was induced via a pro-fibrotic cocktail (Doryab et al. 2023).

Other developments in the field focused on culturing pulmonary cellular models on biomimetic extracellular matrices resembling curved micro-alveoli. This includes a porous hydrogel made of gelatin methacryloyl in a breathing lung-on-chip (Di Huang et al. 2021), micro-curved track-etched membranes in a PDMS-based lung-on-chip (Baptista et al. 2022) or a reconstituted basal membrane on a hexagonally structured grid in static culture (He et al. 2022). A hexagonally structured gold grid was also implemented in the next generation of the breathing lung-on-chip originally introduced by Stucki et al. (2015), allowing the culture of hAEPs and endothelial cells on opposite sides of a biodegradable collagen-elastin membrane (Zamprogno et al. 2021).

The polyclonal hAELVi cell line was co-cultured with THP-1 macrophage-like cells in an anatomically inspired acini-on-chip that aimed to mimic the airflows observed in the acinar airways of the human lung, as a part of this thesis (Artzy-Schnirman et al. 2019b). The branching apical channel of the platform possesses micron-sized true-scale acinar dimensions and could be used to expose the co-cultured cells to an aerosolized lipopolysaccharide (LPS) suspension. Recently the same lab also created an anatomically inspired multi-compartment airways-on-chip platform, which interconnected a nasal-chip, a bronchial airway-on-chip, as well as the aforementioned acini-on-chip in an effort to replicate the viral transmission of, e.g. SARS-CoV-2, from the nose to the pulmonary acini (Nof et al. 2022).

All of the aforementioned devices, however, demand a vast amount of labor and/or cost investment to be set up and used in routine experiments. The devices stemming from

academic labs additionally often demand a high level of engineering expertise. As another part of this thesis, we thus described and discussed a minimalistic perfusable platform that non-experts could produce in any lab by (Carius et al. 2021a).

With a strong focus on *in vitro* models of the alveolar epithelium, the present thesis includes an early example of combining “software” and “hardware” (Artzy-Schnirman et al. 2019b) as well as individual contributions to both categories: “hardware” (Carius et al. 2021a) and “software” (Carius et al. 2023).

## **2. Aims of the thesis & extended summary**

The overall goal of this thesis was to implement prevailing *in vitro* models of pulmonary epithelia, in particular cellular models of the human air-blood barrier, into a novel microfluidic platform in order to robustly analyze the transport and clearance of established or newly engineered aerosols within a complex pulmonary *in vitro* model. Based on the learnings that were generated during the course of the current thesis, this primary goal evolved into three sub-objectives:

- 1. Implementation of the polyclonal hAELVi and differentiated THP-1 co-culture model into a morphologically inspired microfluidic platform.**
- 2. Development of a novel perfusable platform (“PerfuPul”).**
- 3. Generation of a monoclonal human alveolar epithelial cell line named “Arlo” with pronounced barrier functions.**

**1. Implementation of the polyclonal hAELVi and differentiated THP-1 co-culture model into a novel microfluidic platform**

The results described in Artzy-Schnirman et al. (2019b) emerged as the first research contribution from the current thesis and could be seen as a fulfillment of the overall project goal. As part of the study mentioned above, the polyclonal hAELVi cell line was cultured in co-culture with human macrophage-like differentiated THP-1 cells in an anatomically inspired acini-on-chip platform. As the first of its kind, this *in vitro* platform allowed to culture an immuno-competent cell line based model of the alveolar epithelium within a morphologically relevant cell culture environment. The platform was furthermore connected to a standard mini compressor nebulizer, which allowed to expose the epithelial mono- and the co-culture to droplets from an aerosolized solution of LPS in phosphate buffered saline (PBS). The acinar structures thereby led to the formation of *in vivo*-like micro-airflows, as typically observed in human respiratory airways. While exposure to LPS generally caused a higher secretion of interleukin 8 compared to unstimulated controls, this effect was significantly higher in the epithelial co-culture with differentiated THP-1 cells than in the epithelial monocultures.

Additionally, this study represented the first time that the polyclonal hAELVi cell line was successfully integrated into a microfluidic platform. Even more, the polyclonal hAELVi cell line formed a dense network of tight junction protein 1 (also known as ZO-1) as well as Occludin, both representative for functional tight junctions. Based on these encouraging results, we adjusted our strategy to create a novel platform that could be used and, more importantly, reproduced within any bio-/pharmaceutical laboratory as a widespread as well as robust tool for biopharmaceutical studies.

## **2. Development of a novel perfusable platform (“PerfuPul”)**

Working with the acini-on-chip platform described above, as well as with other lung-on-chip platforms, it became clear to us that these devices are challenging to manufacture and/or to maintain within standard bio-/pharmaceutical laboratories because the routine production as well as maintenance demand specialized techniques and equipment. At the same time, the research underlying this thesis was additionally influenced by *in vitro* infection studies, which were conducted within the same department. In these studies, the establishment of long-term pulmonary *in vitro* models of chronic bacterial infections was limited by the short life span of the epithelial cell cultures (Montefusco-Pereira et al. 2020; Juntke et al. 2021; Horstmann et al. 2022). We thus hypothesized that continuous perfusion of cell culture medium would not only serve as a physiologically relevant clearance mechanism in the context of drug transport studies but could in addition, also enhance the survival time of the infected co-culture models through the elimination of bacterial toxins and virulence factors. Based on these considerations, we identified ALI conditions, aerosol deposition, TEER measurements, and especially perfusion, in contrast to the anatomical relevance in the case of the acini-on-chip platform, as needed prerequisites for a novel platform that could support the generation of such (infected) complex pulmonary *in vitro* models.

In the second research article that emerged from this thesis, we thus introduced a blueprint as well as a technical proof-of-principle study for the versatile perfusable platform to assess permeability and barrier function of air-exposed pulmonary epithelia (PerfuPul) (Carius et al. 2021a). The perfusable platform maintains the principle design as well as the advantages of traditional Transwell®-based systems; however, also enables perfusion of the basolateral compartment. Among the platform’s advantages are the culture of pulmonary epithelial cells at an air-liquid interface with subsequent aerosol deposition and



the measurement of TEER - all within the same system. The development of barrier integrity of Calu-3 cells grown in the platform, which was measured via TEER, and the results from transport experiments using fluorescein sodium, matched well with results obtained from similar experiments performed on Transwell®-inserts. TEER measurements inside the perfusable platform were made possible via a custom-made electrode. The custom-made electrode thereby determined TEER values of Calu-3 cells grown on Transwell® inserts as precise as a chopstick electrode, which is the standard electrode for determining TEER on porous growth supports.

Additionally, based on a design initially introduced by Horstmann et al. (2021), an adapted custom-made deposition chamber enabled the deposition of aerosols on the perfusable platform using a clinically relevant Aerogen lab nebulizer. As a technical proof-of-principle, we compared the transport of nebulized fluorescein sodium under static conditions and under the influence of perfusion; however, observing no apparent differences between the two conditions. In order to make the simple but versatile perfusable *in vitro* platform accessible to researchers unfamiliar with microfabrication techniques, we published the detailed protocols, construction drawings, and material lists needed to reproduce all of the parts of the platform so that it could be replicated in any bio-/pharmaceutical laboratory.

**3. *Generation of a monoclonal human alveolar epithelial cell line named “Arlo” with pronounced barrier functions***

During the work with the polyclonal hAELVi cell line in the context of the acini-on-chip studies, we also already started to recognize inconsistencies in the development of barrier properties for some cell batches, which were notably different from the results described in Kuehn et al. (2016). Depending on which cell culture vial was taken out of the cryo storage and put into culture, cells from certain vials would show a strongly delayed formation of barrier properties or completely impaired barrier formation, as indicated by TEER value measurements. As a working hypothesis for the Carius et al. (2023) article, which emerged as a third paper from the current thesis, we initially assumed that the inconsistencies observed for the hAELVi cell line must be linked to a heterogeneous cell population. To support this hypothesis, we isolated single-cell clones via single-cell printing from a heterogeneous hAELVi population, which showed TEER value development in a previous passage. After the single-cell clones had been expanded to a high enough cellular yield, they were seeded on Transwell® inserts and characterized for developing barrier properties. Originating from such a single cell, the “Arlo” cell line reliably developed monolayers with functional tight junctions when exposed to an air interface. “Arlo” robustly developed TEER values  $>3000 \Omega \cdot \text{cm}^2$  under ALI conditions and expressed gene signatures most probably representative of proliferating AT-2 cells. The human monoclonal cell line “Arlo”, in addition, showed high similarity to hAEPcs related to the expression of genes involved in the formation of the junctional barriers in the human lung and in the epithelial immune response. Further, we demonstrated that the cell line “Arlo” could be productively infected by different variants of SARS-CoV-2, which paves the way for various viral infection experiments. “Arlo” will be of direct experimental use to researchers from various disciplines seeking for a human alveolar epithelial cell line that maintains robust barrier

Generation of a monoclonal human alveolar epithelial cell line named “Arlo” with pronounced barrier functions

---

properties and grows in a polarized cellular monolayer. Moreover, the monoclonal “Arlo” cell line was made commercially available to all interested researchers via the company Inscreenex GmbH (Germany) (InSCREENex 07.05.23).

During this thesis, we identified issues with the applicability of some of the cellular models and technologies described in the state-of-the-art section, which so far might have limited the widespread use of these technologies by a broader research community. In sum, the studies described in this thesis represent robust and reliable building blocks for developing future complex pulmonary *in vitro* models, which can be used to conduct biopharmaceutical permeability experiments.

### 3. Original Publications

#### *„Capturing the Onset of Bacterial Pulmonary Infection in Acini-On-Chips“*

Arbel Artzy-Schnirman, Hikaia Zidan, Shani Elias-Kirma, Lee Ben-Porat, Janna Tenenbaum-Katan, **Patrick Carius**, Ramy Fishler, Nicole Schneider-Daum, Claus-Michael Lehr, Josué Sznitman

Published in *Advanced Biosystems*, 2019, Volume 3, Issue 9

(<http://dx.doi.org/10.1002/adbi.201900026>)

Copyright © Wiley-VCH Verlag GmbH & Co. KgaA. Reproduced with permission.

Contributions to co-authorship:

Patrick Carius planned and assisted in parts of the cell culture experiments involving the hAELVi cell line. He further assisted in designing the study and critically revised the paper before publication.

# Capturing the Onset of Bacterial Pulmonary Infection in Acini-On-Chips

Arbel Artzy-Schnirman, Hikaia Zidan, Shani Elias-Kirma, Lee Ben-Porat, Janna Tenenbaum-Katan, Patrick Carius, Ramy Fishler, Nicole Schneider-Daum, Claus-Michael Lehr, and Josué Sznitman\*

Bacterial invasion of the respiratory system leads to complex immune responses. In the deep alveolar regions, the first line of defense includes foremost the alveolar epithelium, the surfactant-rich liquid lining, and alveolar macrophages. Typical *in vitro* models come short of mimicking the complexity of the airway environment in the onset of airway infection; among others, they neither capture the relevant anatomical features nor the physiological flows innate of the acinar milieu. Here, novel microfluidic-based acini-on-chips that mimic more closely the native acinar airways at a true scale with an anatomically inspired, multigeneration alveolated tree are presented and an inhalation-like maneuver is delivered. Composed of human alveolar epithelial lentivirus immortalized cells and macrophages-like human THP-1 cells at an air–liquid interface, the models maintain critically an epithelial barrier with immune function. To demonstrate, the usability and versatility of the platforms, a realistic inhalation exposure assay mimicking bacterial infection is recapitulated, whereby the alveolar epithelium is exposed to lipopolysaccharides droplets directly aerosolized and the innate immune response is assessed by monitoring the secretion of IL8 cytokines. These efforts underscore the potential to deliver advanced *in vitro* biosystems that can provide new insights into drug screening as well as acute and subacute toxicity assays.

## 1. Introduction

Lung inflammation plays a critical role in many respiratory diseases including acute respiratory distress syndrome (ARDS), chronic obstructive pulmonary disease (COPD), asthma, and cystic fibrosis (CF) amongst others.<sup>[1]</sup> Traditionally, the immunological mechanisms underlying such conditions have been studied using animal models and/or *in vitro* models. While animal models of lung inflammation remain an invaluable tool for both basic research and preclinical trials, their use is known to be limited by the underlying differences between such *in vivo* models and the human body.<sup>[2–4]</sup> Concurrently, *in vitro* models,<sup>[5]</sup> most commonly consisting of submerged cell cultures seeded in well plates or grown on transmembrane well inserts, are not only limited in their ability to faithfully recapitulate critical biological functions of the innate organ, they also lack essential phenotypes that range from anatomical traits to physiological flows and mechanical stresses applied


*in vivo*. To overcome the aforementioned shortcomings, there is a growing need for alternative *in vitro* platforms that better mimic the pulmonary milieu.<sup>[6]</sup>

In the last decade microfluidics, and so-called organ-on-chips in particular, have gained significant momentum in laying the foundations for constructing advanced *in vitro* models that can mimic more faithfully physiologically relevant organ functions. This includes, for example, the critical role played by (air and blood) flows in the respiratory zone (i.e., pulmonary acinus). Multiple groups have leveraged lung-on-chip models to recreate breathing phenomena; yet, the bulk of such efforts has relied on single channels or isolated airsacs,<sup>[7–9]</sup> thereby neglecting important anatomical features of the deep lung environment that lead to acinar-specific aerosol deposition outcomes and may play a significant role in drug distribution.<sup>[10]</sup> A faithful reconstitution of the underlying lung architecture, and in particular the intricate foam-like structure of deep alveolated airways, remains technically challenging and is still widely beyond reach.<sup>[6]</sup> Although the aforementioned studies as well as others represent major advances in investigating alveolar

Dr. A. Artzy-Schnirman, H. Zidan, S. Elias-Kirma, L. Ben-Porat, Dr. J. Tenenbaum-Katan, Dr. R. Fishler, Prof. J. Sznitman  
Department of Biomedical Engineering  
Technion-Israel Institute of Technology  
32000 Haifa, Israel  
E-mail: sznitman@bm.technion.ac.il

P. Carius, Dr. N. Schneider-Daum, Prof. C.-M. Lehr  
Helmholtz Institute for Pharmaceutical Research Saarland (HIPS)  
Helmholtz Center for Infection Research (HZI)  
Saarland University  
66123 Saarbrücken, Germany

P. Carius, Prof. C.-M. Lehr  
Biopharmaceutics and Pharmaceutical Technology  
Department of Pharmacy  
Saarland University  
66123 Saarbrücken, Germany

 The ORCID identification number(s) for the author(s) of this article can be found under <https://doi.org/10.1002/adbi.201900026>.

DOI: 10.1002/adbi.201900026

physiology,<sup>[7,8,11–14]</sup> they come short in both mimicking accurately the morphology and ensuring respiratory airflow distributions pertinent to acinar airways in vivo.<sup>[6,15]</sup> This latter aspect is critical when considering that by and large in vitro inhalation exposure assays on airway barriers have relied on instilling liquid suspensions directly onto cell cultures. More recent efforts have pushed to deliver aerosols via direct spraying,<sup>[16–18]</sup> yet there is still a gap in capturing physically realistic aerosol transport at an air liquid interface (ALI) in mimicking more truthfully the fate of aerosols depositing on the airway lumen.

Beyond the anatomical and physiological flow determinants of the acinar regions, three main cell types line the lumen of the deep lungs in vivo. These include alveolar epithelial cells type 1 (AT1) that enable gas exchange and barrier function, alveolar epithelial cells type 2 (AT2) responsible for surfactant-secretion, and alveolar macrophages that orchestrate the innate immune response at the barrier site. AT2 cells also serve as progenitor cells, maintaining the regenerative capacity of the alveolar sacs and alveolar macrophages. Importantly, epithelial cells together with alveolar macrophages are known to have immunomodulatory functions characterized by the secretion of proinflammatory cytokines.<sup>[19,20]</sup> To date, the majority of microfluidic-based in vitro alveolar models have advocated the use of primary pulmonary cells. While it is generally accepted that primary alveolar cells directly isolated from human lungs better preserve physiological properties of the lung tissue, ongoing hurdles include difficulties in obtaining such cells and the huge variability between donors, in addition to the challenges of cell culturing alone.<sup>[21,22]</sup> Most significantly, benchmarking standardized assays with primary cells is critically challenging whereas past cell lines do not hold sufficient. In circumventing such challenges, a novel alternative and highly relevant epithelial model was recently developed, i.e., human alveolar epithelial lentivirus immortalized (hAELVi) cells. Briefly, hAELVi cells feature AT1-like phenotypes corresponding to the normal composition of the alveolar epithelium.<sup>[23]</sup> Furthermore, they maintain critical epithelial barrier functions leading to high transepithelial electrical resistance (TEER), in analogy to primary cells harvested from human tissue.<sup>[21]</sup> Such characteristics render them most suitable for drug delivery and cytotoxicity assays amongst others but have never been leveraged beyond traditional in vitro assays.

Here, we have developed a novel anatomically inspired acini-on-chip platform that mimics more closely native acinar airways at true scale in a multigeneration alveolated tree. Together with hAELVi cells and a model for human monocyte derived macrophages, differentiated to macrophage-like cells at an ALI, our in vitro devices underline the reconstitution of a functional alveolar barrier including immune functions. To model alveolar macrophages, we use the THP-1 cell line; a cell line that has been extensively used<sup>[23,24]</sup> to study monocyte and macrophage functions, signaling pathways, and drug transport among others. In addition, it is an established cell line to induce pro-inflammatory activation of lung epithelial cells.<sup>[25]</sup> As a proof-of-concept of the model's potential, we recapitulate in vitro an aerosol exposure assay and monitor the proinflammatory response of the alveolar epithelial barrier. To model inflammatory events typically going along with bacterial infections we used lipopoly saccharide (LPS), a notorious stimulator of the innate immune

system and constituting a major outer surface membrane protein expressed on Gram-negative bacteria,<sup>[26]</sup> i.e., in mycobacterium tuberculosis. The reconstituted alveolar epithelium in coculture with the macrophages is exposed to LPS-laden aerosols via a realistic inhalation-like exposure composed of airborne droplets under airflow, whereby ensuing cell response is assessed by monitoring IL8 secretion. Overall, our versatile model captures anatomical and physiological characteristics while preserving essential functions of the homeostatic cellular microenvironment. Such platform represents an important milestone toward the realization of new in vitro tools that could better predict clinical outcomes.

## 2. Results and Discussion

### 2.1. Acini-On-Chip Establishment

To assess the biological applicability of our acini-on-chip bio systems, two anatomically inspired microfluidic devices of increasing complexity were designed. First, a microfluidic device featuring an anatomically inspired, multigeneration alveolated airway tree was established (Figure 1a). The device consists of six asymmetric dichotomously branching generations, where saccular airspaces, corresponding to early stages during pulmonary development, are mimicked by enlarged cavities at the distal generations (see Figure 1a, blue arrows). Underalveolated branches, on the other hand, are depicted by cavity depletions off from the proximal ducts (see Figure 1a, red arrows). To adequately capture the acinar length scales of developing acinar airways, our designs feature characteristic channels of 170 μm width by 100 μm height with alveolar diameters of 155 μm, following morphometric data from lung casts.<sup>[27,28]</sup> As the measured data are acquired in fully inflated lungs representative of total lung capacity, our acinar airway anatomies are scaled to match lung volumes corresponding to functional residual capacity (FRC) in line with respiratory volumes representative of tidal breathing. The selected FRC values are matched to pediatric populations exhibiting height and weight distributions as obtained from lung cast measurements.<sup>[29]</sup> A notable feature of our microfluidic design is given in the matched flow rates at the distal ends of the acinar tree (see Figure 1a, stars); such requirement stems from the in vivo environment, where no slip flow conditions on the alveolar walls assure zero flow across all terminal ends of the acinus.<sup>[15]</sup> Here, we have established an analogous condition by adjusting the pathways between each terminal end of the microfluidic tree and the common outlet. This ensures matching the same pressure drop across all paths by having channels of equal length within the microfluidic-based in vitro device.

The acinar airway tree model (Figure 1a) offers an anatomically relevant model that demonstrates the versatility of microfluidic-based lung models in realizing intricate morphologies of the developing deep airways. Concurrently, it poses technical difficulties in achieving full epithelial coverage due to the vast surface area combined with such intricate length scales and morphological features (e.g., bifurcations, alveoli, etc.). In parallel, we thus opted for an anatomically simpler, alveolated airway model based on a recent design useful for investigating

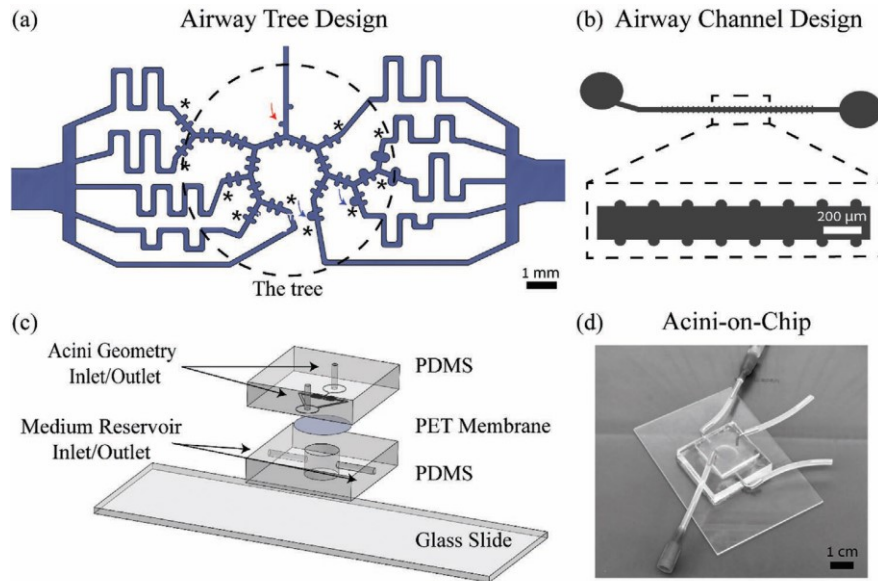


**Figure 1.** Anatomically inspired microfluidic model of acinar airways. a) Microfluidic alveolated acini-on-chip design featuring a multigeneration asymmetrically bifurcating model of subacinar airway structures. Distal airways are modeled by saccular alveoli (blue arrows) and underpopulated air-ducts (red arrows). Note that the model provides equal flow at each terminal end, by adjusting and matching the length of a channel connecting the common microfluidic outlet and the last generation of our acinar tree. b) A microfluidic device combining straight ducts (resembling airways) lined with cylindrical cavities (mimicking alveolar spaces). c) Exploded view of the computer-aided drawing of the acini-on-chip. A compartmentalized sandwich structure is assembled on a glass slide, and a porous membrane is positioned between the PDMS alveolated airway tree (apical side) and a bottom reservoir (basal side) to perfuse culture media (with integrated openings for inlet and outlet). On the apical side, two openings (inlet and outlet) allowing selective insertion of desired components to the upper tree, e.g., cells for seeding followed by airflow to reproduce physiological flow conditions. d) Snapshot of the assembled acini-on-chip.

barrier functions<sup>[30]</sup> (Figure 1b). This design mimics underlying features of the acinar ducts only. The microfluidic model combines straight channels of 160 μm width and 100 μm height, regularly lined with cylindrical cavities of 40 μm radius. The alveolar opening angle ( $\alpha = 60^\circ$ ) was selected to match closely that frequently used to model fully developed adult alveoli.<sup>[31]</sup>

To render our microfluidic acinar designs compatible for cell culture and thereby recapitulate underlying characteristics of the alveolar epithelial barrier at an ALI, devices were assembled by integrating the poly(dimethylsiloxane) (PDMS) polymer microfluidic channels (on the apical side) to a PDMS pool containing cell medium (on the basal side), separated by a 100 μm thick porous polyester (PET) membrane (Dow Corning) with 0.4 μm pore sizes (see Figure 1c). These so-called microfluidic “sandwich” structures, namely device assemblies featuring an ALI separated by an epithelial barrier with medium perfusion from the basal side, have been increasingly utilized in recent years.<sup>[6,8,32]</sup> Finally, tubing is connected to the apical and basal compartments, respectively, to allow easy access of fluid and/or airflow at the hands of the end user (Figure 1d).

## 2.2. Epithelial Barrier Characteristics

A growing number of cell lines derived from different regions of the airways are available for in vitro studies of the respiratory environment.<sup>[33]</sup> To date, the most commonly used and

widely characterized cell type to model the alveolar epithelium remains the A549 (American Type Culture Collection, ATCC CL-185) cell line; an epithelial model immortalized and derived from human lung adenocarcinoma.<sup>[34]</sup> The morphology and biochemical features of this cell line resemble the characteristics of human alveolar type 2 cells in situ. A major limitation of the A549 cells remains their inability to form functional intercellular tight junctions, resulting in so-called “leaky” monolayers of the epithelium; a major limitation in realizing attractive in vitro models for drug permeability and absorption assays. In the past few years, alveolar primary cells have become more commonly used to overcome the limitations of A549 cells.<sup>[11,35–38]</sup> Nevertheless, the limited number of cells that can be received during each isolation, the short life span and the uncertainty due to donor variation represent important drawbacks.<sup>[39]</sup> Here, we present acini-on-chip cultured with hAELVi cells (Figure 2). Unlike primary cells, hAELVi cells can be cultured up to passage 75, under liquid–liquid as well as ALI conditions. Furthermore, and in contrast to A549 cells, hAELVi cells resemble AT1 cells and maintain their capacity to form tight intercellular junctions, with high transepithelial electrical resistance ( $>1000 \Omega \text{ cm}^2$ ).<sup>[23]</sup>

To the best of our knowledge, the present acini-on-chip constitutes the first use of hAELVi cells as an in vitro functional biosystem of the alveolar epithelial barrier. Namely, the epithelial barrier was established by coating the device’s membranes with type I collagen and fibronectin solution. Following



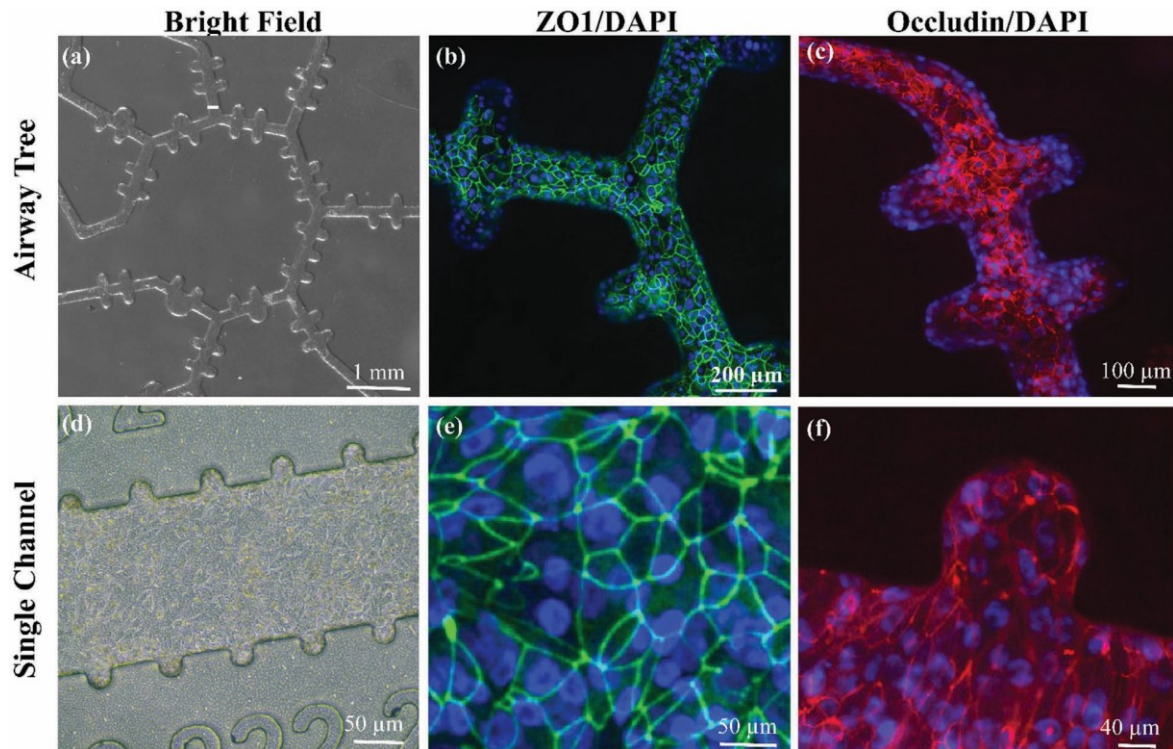


**Figure 2.** Anatomically inspired microfluidic models of alveolated airways seeded with hAELVi cells in the full alveolated airway tree (top row) and acinar ducts (bottom row). a,d) Brightfield image. b,e) Immunofluorescence micrographic views of hAELVi cells immunolabeled with anti-ZO-1 (green) and DAPI (blue) at (a) day 17, and (b) day 18 cultivated at an ALI from day 2. c,f) Immunofluorescence micrographic views of hAELVi cells immunolabeled with antioccludin (red) DAPI (blue).

coating, hAELVi cells were seeded in the apical compartment and allowed to adhere under liquid–liquid conditions. To mimic *in vivo* conditions, medium was removed after 48 h from the apical compartment and cells were allowed to grow at the ALI for at least 12 days. At that time point, a densely packed monolayer of cells can be observed under light microscopy (see Figure 2a,d). To confirm the formation of tight junctions, the expression of two characteristic proteins were examined: zona occludens (ZO-1) and occludin. Clearly labeled tight junction complexes appeared as a continuous thin line between adjacent cells in both the alveolated tree (Figure 2b,c) and the airway channel design (Figure 2e,f), similar to those observed on traditional Transwell inserts (see Figure S1, Supporting Information).

To recapitulate relevant immune functions of the acinar environment with alveolar macrophages, THP-1 monocytes were differentiated into macrophage-like cells. Differentiated THP-1 cells were then trypsinized and seeded on top of-pre formed hAELVi monolayer and the devices were further cultivated for up to 7 days. In each experiment, two sets of devices were seeded simultaneously; cocultures of hAELVi cells and THP-1 macrophage-like cells and monocultures of hAELVi cells, for direct comparison. The differentiation of THP-1 cells into macrophage-like cells was determined by using antihuman CD11b antibody, which stains macrophages<sup>[40]</sup> (Figure 3a,b).

Notably, TEER measurements were used to evaluate the integrity of the epithelial monolayer and have thus become a standard experimental method. Here as a control, each passage of hAELVi cells, seeded in a device, was also seeded on an insert and TEER was monitored over time (see Figure S2, Supporting Information) to ensure the capability of each specific cell passage to deliver a functional barrier, with values reaching well within  $1000\Omega\text{ cm}^2$ . In the acini-on-chip platforms, however, TEER measurements are still challenging as no practical and validated approach has yet been developed.<sup>[41]</sup> The minute dimensions of the channels together with the stringent requirement for a closed and controlled environment to support cell growth creates limited access to the epithelial layer leading to difficulties in measuring adequately TEER.

To circumvent such challenges, we have evaluated the barrier properties of the coculture using a hydrophilic molecule, i.e., sodium fluorescein (FluNa). This follows as high TEER correlates with low transepithelial transport and provides a viable alternative to TEER measurements.<sup>[23]</sup> Briefly, FluNa was added to the apical compartment and a transport buffer was introduced to the basolateral compartment. At different time points, 30  $\mu\text{L}$  samples were taken from the basolateral compartment and the volume lost during sampling was replaced with fresh buffer. The sodium fluorescein amount in the samples was measured and the apparent permeability ( $R_{app}$ ) was calculated



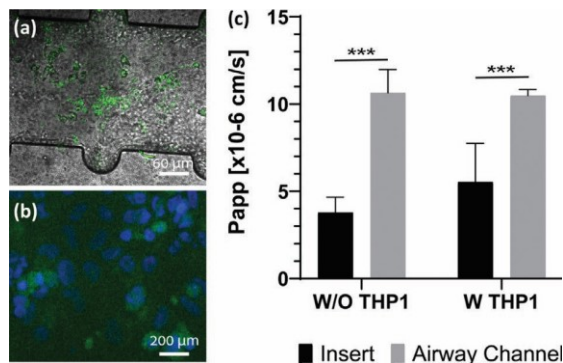


**Figure 3.** Morphology and barrier properties of hAELVi/THP-1 cocultures. a) Airway channel seeded with coculture of hAELVi (day 21) cells and THP-1 (day 7), overlaying of bright field image and on THP-1 cells stained with anti-CD11b antibody (Green). b) Immunofluorescence micrographic views of THP-1 cultured on-chip for 7 days at the ALI, stained with anti-CD11b antibody (green) and DAPI (blue). c) Transport of FluNa across a monolayer of hAELVi. The THP-1 cells were seeded between day 17 and 20 on a preformed hAELVi monolayer on insert and devices. Data shown as mean  $\pm$  SD (insert: W-THP-1 with  $n = 8$ , WO-THP-1 with  $n = 4$ , airway channel W-THP-1 with  $n = 7$ , and WO-THP-1 with  $n = 4$ )  $^{***}p < 0.001$ .

following Elbert et al.<sup>[22]</sup> To compare between the different culturing conditions in the device and the traditional insert, cells were grown until a full confluent monolayer was achieved (i.e., 14–35 days) to allow the formation of tight junctions. At that time point, differentiated THP-1 cells were seeded respectively in the Transwell inserts and the microfluidic devices, and the transport assay was performed after 72 h following a previous protocol reported by Kletting et al.<sup>[40]</sup> on inserts. As can be seen in Figure 3c, no statistical differences were found in  $P_{app}$  measurements between the airway channels and the Transwell inserts; both in the absence or presence of THP-1 cells (i.e., mono- vs cocultures). Indeed, measured  $P_{app}$  yields values within the same order of magnitude, as previously highlighted for hAELVi cells monolayer specifically,<sup>[23]</sup> although transepithelial transport is slightly higher within the microfluidic device compared to the Transwell insert. We hypothesize that the main reason for such discrepancy may arise due to the interface between the PET membrane and the channel walls made of PDMS since the cells grow only on the membrane but FluNa may nevertheless translocate across the interface between the two materials (PET and PDMS).

As a final remark in considering epithelial barrier characteristics, we open here a short parenthesis in evaluating the benefits of both advocated platforms, i.e., the complex acinar airway network (Figure 1a) compared with straight alveolated channels (Figure 1b). As presented in Figure 2, a functional epithelial barrier is established across the full airway tree that carefully adheres to the geometrical constraints of the underlying substrate. Yet, it has been recently shown that a mere 0.4% lack in epithelial coverage of the surface leads to an 80% decrease in TEER measurements,<sup>[42]</sup> correlating with high  $P_{app}$  values. With this in mind, guaranteeing a strict 100% surface coverage across the intrinsically complex airway network featuring a large number of bifurcations, branches, and alveolar cavities

is not realistic. Thus, we have introduced a device platform (i.e., acinar ducts) that delivers a compromise in anatomical complexity (i.e., straight channels) while still offering relevant anatomical features of the acinus (i.e., alveoli). Together, our two complementary platforms offer benefits for different applications depending on the specific endpoints. While in both devices functional tight junctions are formed (Figure 2b,e), if the scope of the in vitro assay is targeted at pure transport assays, the simpler device anatomy would be preferential as guaranteed by  $P_{app}$  values (Figure 3).

### 2.3. Aerosol Inflammation Exposure Assay

In the alveolar regions, the first line of defense includes the alveolar epithelium, the surfactant-rich alveolar fluid lining and the alveolar macrophages. AT1 and AT2 are known to have immunomodulatory functions characterized by the secretion of proinflammatory cytokines.<sup>[19]</sup> AT1 contain toll-like receptor 4 (TLR4), i.e., a receptor for LPS, a cell wall protein found on Gram-negative bacteria. LPS is a strong stimulator of the innate arm of the immune system, which is known to cause acute lung injury in vivo<sup>[43]</sup> and has been widely used to simulate bacterial infections in vitro.<sup>[44]</sup> Notably, LPS stimulation of alveolar epithelial cells and macrophages has been shown to produce proinflammatory cytokines. As a proof-of-concept of the potential and suitability of our in vitro platforms for various aerosol exposure assays, our acini-on-chip were exposed to nebulized aerosols. While inhalation therapies often aim at tracheobronchial delivery in the context of asthma and obstructive diseases (e.g., COPD), delivering therapeutics to the deeper pulmonary alveolar regions has drawn increased attention in recent years with potential applications for systemic delivery<sup>[45,46]</sup> (e.g., vaccinations<sup>[47,48]</sup> and insulin delivery<sup>[49]</sup>) as well as antibiotics for targeted treatments of pulmonary infections,<sup>[50]</sup> such as in pneumonia and CF. Our in vitro biosystems lend themselves as a potent alternative for conducting early-stage, preclinical studies in assessing inhalation therapies.

To induce an inflammatory response, the acini-on-chips were directly connected to a standard mini compressor nebulizer. All chips were exposed to nebulized aerosols for up to 4 min, with phosphate buffered saline (PBS) as the carrier liquid (i.e., deposition field inside device, Figure 4a). 48 h after the exposure assay, the medium from the basal compartment was collected and analyzed for IL8 secretion using an enzyme-linked immunosorbent assay (ELISA). IL8 plays a role in the pathogenesis of various diseases, including ARDS and asthma. IL8 has a major role in neutrophil chemoattractant and activating, one of the major immune cell types that accumulate in the airway when inflamed. As can be seen in Figure 4b, IL8 secretion levels were higher upon LPS exposure in both the airway channel and tree for hAELVi cells alone, thereby supporting the role played by the epithelial monolayer itself. The IL-8 levels of the co- and monocultures with nebulized PBS show similar values as exposing the samples to PBS without the nebulizer (data not shown), representing the basal secretion levels. Coculturing of hAELVi cells with THP-1 macrophage-like cells (Figure 4c) resulted in a similar yet enhanced trend in secretion, i.e., IL-8 levels were higher compared to the control in both models. As

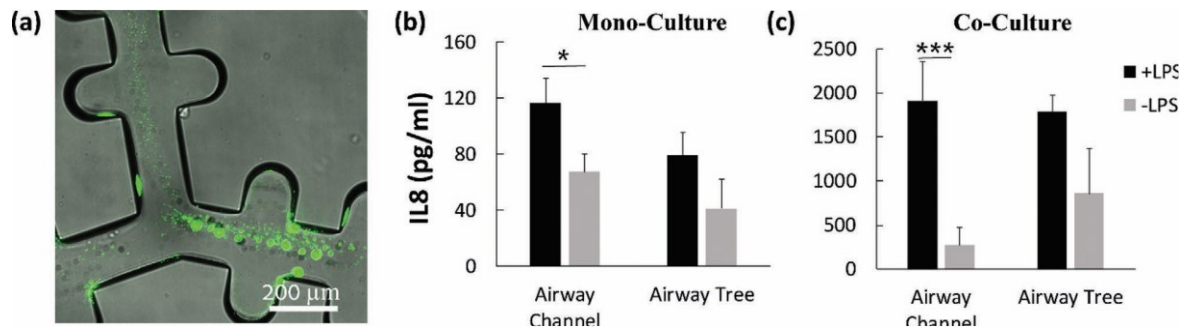


**Figure 4.** Mimicking bacterial inflammation in the acini-on-chip. a) Qualitative snapshot of a local deposition field after 2 min exposure with a commercial nebulizer: dry channel on a glass slide, FluNa  $2.5 \mu\text{g mL}^{-1}$  in PBS. b,c) Plots show the secretion of IL8 cytokines following 48 h poststimulation with LPS nebulization ( $10 \mu\text{g mL}^{-1}$ ) or PBS nebulization as a control, measured by ELISA: (b) monoculture (hAELVi) and (c) coculture (hAELVi and THP-1). Cells were grown until a full confluent monolayer was achieved (14–35 days). Data shown as mean  $\pm$  SD (airway channel: mono- $n = 3$ , coculture  $n = 6$ , alveolated airway tree: mono- and coculture  $n = 3$  independent experiments); \*\*\* $p < 0.001$ , (ANOVA). \* $p < 0.05$ , compared with controls (i.e., cells cultured without LPS).

expected from the coculture, the THP-1 augments IL-8 secretion by more than an order of magnitude, thus demonstrating the important role played by THP-1 in recapitulating realistic immune functions within the acini-on-chip. The influence of the LPS exposure on the epithelial integrity was examined by staining of the tight junction proteins, i.e., ZO-1 and Occludin, 72 h after the LPS exposure, with no change in the epithelial monolayer integrity (not shown for brevity); a result consistent with previous findings.<sup>[38]</sup>

### 3. Conclusions

The acini-on-chips presently described are the first in vitro platforms, to the best of our knowledge, that integrate characteristic airflows of the respiratory zone within a morphologically relevant anatomy while guaranteeing underlying epithelial barrier characteristics. To date, all efforts within lung-on-chip platforms have been performed in straight channels. For the first time, we have expanded such concept to complex airway tree networks mimicking more closely native acinar airway anatomies. Using a novel cell model system (hAELVi), we have successfully reconstructed relevant cell populations of the alveolar region and demonstrated the establishment of a functional epithelial barrier in an anatomically relevant manner. We used two complementary techniques to demonstrate a functional barrier in a coculture system where macrophage-like cells are grown on top of the epithelial cell layer: staining of tight junction proteins as well as permeability assays. Within the scope of establishing an in vitro acinar benchmark, THP-1 cells have been used to mimic alveolar macrophages and deliver valuable insight that can be developed in the future into a biosystem consisting of lung primary cells. We successfully demonstrated a long-term cell culture inside the lung-on-chip while maintaining functional barrier properties. The presented assays were performed following up to 35 days from seeding, providing a promising platform for both acute (normally, 48–72 h) and subacute (14–28 days) toxicity assays in the deep alveolar regions. As a proof-of-concept, the devices were leveraged to mimic the onset

of bacterial infection. Following a realistic aerosol exposure scenario with inhaled airborne droplets in airflow, LPS was introduced into the devices and cell response was measured by IL8 secretion. Our in vitro biosystem was able to recapitulate the protective responses from the epithelium and its further enhancement by the immune cells. Possible directions include integrating additional cell types that play a critical role in the orchestra of the immune response, such as endothelia and neutrophils. Here, we have used the hAELVi cells with a unique opportunity to help bridge between in vivo and in vitro studies in respiratory research. With the practical difficulty in obtaining human alveolar primary cells and alveolar macrophages, the variability between different donors can mask effects and jeopardize delivering clear conclusions. As such, the hAELVi and THP-1 cells provide an attractive alternative in establishing a novel in vitro benchmark for other researchers and scientists to compare with (e.g., control), allowing for example to “normalize” differences between different donors. Such biological functionality in conjunction with mimicking more closely morphological constraints (i.e., airway anatomy) and physiological conditions (e.g., respiratory airflows) offer tangible opportunities for drug toxicity screens and aerosol deposition assays amongst other.

### 4. Experimental Section

**Microdevice Fabrication:** Standard soft-lithography techniques were adopted for microfabrication of PDMS-based microfluidic devices;<sup>[51]</sup> such techniques were combined with a modified method for master production using deep reactive ion etching of a silicon on insulator<sup>[10]</sup> wafer to manufacture delicate features of the acinar model.

A clean 2 in. wafer was dehydrated on a hot plate (300, 5 min). SU-8 2150 photoresist (Microchem) was spin-coated on the wafer at 500 rpm for 10 s using a  $100 \text{ rpm s}^{-1}$  acceleration rate, then 3000 rpm for 30 s with acceleration of  $300 \text{ rpm s}^{-1}$ . The wafer was kept overnight on a leveled surface in a sealed petri dish to improve surface flatness, then baked on a hot plate (65°C 5 min, 90°C 30 min), and exposed to UV light through a photomask at a total dose of  $400 \text{ mJ cm}^{-2}$  using an MA6 mask aligner (Karl Suss). Postexposure bake was performed on a hot plate (65 °C 5 min, 95 °C 13 min) and then the substrate was

developed in propylene glycol monomethyl ether acetate, rinsed with isopropyl alcohol, and spin dried. The resulting SU-8 pattern on the silicon wafer is then continuously used as a master template for PDMS casting, and manufacture of PDMS microdevices. PDMS was mixed with a curing agent (DOWSIL 184 Silicon Elastomer Kit) at a 10:1 volume ratio, poured on the template, and baked for 60 min at 65 °C. Cured PDMS was peeled from the wafer, punched using a 1 mm biopsy punch (Miltex, 3331) to create inlets and outlets, and rinsed with 70% ethanol. The PET membrane with 0.4 μm pore size (Corning), was irreversibly bonded to the acinar microchannels using a “stamping” technique.<sup>[52]</sup> Briefly, liquid PDMS (10:1) was spin-coated on a glass slide (500 rpm for 20 s acceleration 100 rpm s<sup>-1</sup>, 4000 rpm for 20 min acceleration 127 rpm s<sup>-1</sup>), creating a thin liquid layer. Thereafter, a readily made PDMS microdevice was gently brought into contact with the thin layer (for 30 s) and immediately attached to the PET membrane from one side. The structure was cured at 65 °C for an hour to accomplish a complete bonding, and placed using stamping on top of a PDMS well to be further filled with culture media. Finally, a glass cover slip (Corning) was prepared and cleaned with ethanol and bonded to the bottom side (reservoir) of the device.

**Cell Culture:** hAELVi cells (InSCREENeX, INS-CI-1015) were cultured as previously described.<sup>[23]</sup> In brief, hAELVi cells were cultured in small airway epithelial cell growth medium (SAGM) BulletKit (Lonza CC-3118) supplemented with 1% FBS and 1% penicillin/streptomycin (P/S) (Life Technologies, 15140-122). Prior to seeding, flasks were coated with coating buffer (1% (v/v) fibronectin; (Corning, 33016015) and 1% (v/v) collagen (Sigma, C4243)). The medium was changed every two to three days. When cells reached 90% confluency, they were trypsinized and used for maintenance or experiments, as described below.

The THP1 cells were cultured in RPMI-1640 (Biological Industries Israel Beit-Haemek Ltd. 01-100-1A) supplemented with 10% FBS and 1% penicillin–streptomycin (P/S). THP-1 monocytes (ATCC, TIB-202) were differentiated to macrophage-like cells using 7.5 ng mL<sup>-1</sup> of phorbol 12-myristate 13-acetate (PMA; Sigma, P8139) following incubation of 16 h. Differentiated THP-1 cells were trypsinized and used in the experiments.

All cells were grown under 37 °C, 5% CO<sub>2</sub>, and 95% humidity.

Mycoplasma controls were performed routinely and never showed infection.

**Insert Cell Culture:** hAELVi cells (2 × 10<sup>5</sup> cells cm<sup>-2</sup>) were seeded on coated Transwell polyester membranes (Corning 3460; growth area 1.12 cm<sup>2</sup>; pore size 0.4 μm). Under liquid–liquid conditions, 500 μL of medium was perfused in the apical side and 1.5 mL at the basolateral. The medium was changed every second day. For air–liquid conditions (ALI), at 2 days postseeding, the medium from the apical compartment was aspirated and the cells were further fed from the basolateral compartment with 500 μL of medium.

**Microfluidic Cell Culture:** The devices were sterilized following three rounds of UV (254 nm), 15 min each. Following sterilization, the apical side was incubated with coating buffer for 1 h in 3% CO<sub>2</sub>, and 95% humidity. All devices were washed with PBS and seeded with cells without drying the membrane.

**Monocultures:** 10 μL or 5 μL of a hAELVi cell suspension (3 × 10<sup>7</sup> cells mL<sup>-1</sup>), were seeded on the membrane of a coated full tree or the airway channel, respectively. Both the basolateral and apical compartments were filled with medium. Following 48 h in liquid–liquid conditions the medium from the apical compartment was aspirated, allowing the cells to grow at the ALI. The cells were further fed every second day from the basolateral compartment, by withdrawing the liquid from the basolateral side and then injecting fresh medium changed the medium.

**Cocultures:** hAELVi monocultures pregrown for 20–35 days were used to set up the coculture with THP-1 cells. Differentiated THP-1 cells (1 × 10<sup>7</sup> cells mL<sup>-1</sup>), 10 or 5 μL of the suspended cells were seeded on top of hAELVi cells in the full tree or the airway channel, respectively. In the basolateral compartment, SAGM was applied. The coculture was cultivated between 1 and 7 days at 37 °C, 5% CO<sub>2</sub>.

**Scanning Electron Microscopy:** The samples were washed three times with PBS and fixed in primary fixative buffer (1% paraformaldehyde

(PFA) and 2% GA in 0.1 M NaP pH 7.4 and 3% sucrose) for 60 min at RT. Following three washes with 0.1 M cacodylate buffer, pH 7.4 the samples postfixed with 1% osmium tetroxide in 0.1 M cacodylate buffer for 15 min at RT. Next, the samples dehydrated through a graded ethanol series, processed by critical point drying and sputter coated with chromium (5 nm). Images were taken with a Zeiss ULTRA plus field-emission scanning electron microscope.

**Immunostaining:** hAELVi and differentiated THP-1 cells were washed with PBS, fixed with 3.6% PFA (Sigma-Aldrich, 47608) in PBS for 15 min at RT, following a rinse with PBS. Next, the cells were permeabilized with 0.5% Triton X-100 (Sigma-Aldrich, T8787) in PBS for 5 min at RT. The cells were washed with PBS and blocked with 10% serum in PBS for 1 h. For DAPI nucleic acid staining cells were incubated with DAPI solution (ThermoFisher Scientific, D1306), diluted with PBS (ratio of 1:1000) for 5 min at RT. For tight junction proteins, Zonula occludens-1 (ZO-1) and Occludin staining, cells were incubated with the primary antibodies rabbit anti-ZO1 (ThermoFisher Scientific, 617300)/mouse antioccludin (ThermoFisher scientific, 331500) diluted with PBS (ratio of 1:200) overnight at 4 °C, followed by incubation with secondary antibody Alexa Fluor 488 antirabbit/antimouse (Jackson ImmunoResearch, 111-545-144/115-545-062), diluted with PBS (ratio of 1:400) for 1 h at RT. The differentiation of THP-1 toward macrophage-like cells was examined with FITC antihuman CD11b (BioLegend, 301329), diluted with PBS (ratio of 1:20) for 1 h at RT. Confocal microscopy imaging of fluorescent immunostaining was performed (Nikon Eclipse Ti with spinning disk, Yokogawa, Japan).

**Transport Studies:** The devices were seeded with mono- or coculture as previously described. The cells were allowed to grow for 14–25 days (in ALI from day 2). Transport experiments were then performed according to Elbert et al.<sup>[22]</sup> Briefly, the cells were washed twice with prewarmed Krebs–Ringer buffer (KRB; NaCl 142.08 × 10<sup>-3</sup> M, KCl 2.95 × 10<sup>-3</sup> M, K<sub>2</sub>HPO<sub>4</sub>·3H<sub>2</sub>O 1.49 × 10<sup>-3</sup> M, HEPES 10.07 × 10<sup>-3</sup> M, D-glucose 4.00 × 10<sup>-3</sup> M, MgCl<sub>2</sub>·6H<sub>2</sub>O 1.18 × 10<sup>-3</sup> M, CaCl<sub>2</sub>·2H<sub>2</sub>O 4.22 × 10<sup>-3</sup> M; pH 7.4), and incubated in KRB for 45 min. Next, medium was aspirated and 10 μL FluNa (10 μg mL<sup>-1</sup> in KRB) were added to the apical compartment and 500 KRB were added to the basolateral compartment. The devices were placed in the incubator and 300 μL samples were taken every 30 min, from the basolateral compartment only, and transferred into a 384-well plate to measure FluNa concentrations. Sampled volumes were refilled with 300 μL KRB. The samples in the 384-well plates were measured with a Varioskan LUX plate reader using wavelengths of 495 nm (em) and 520 nm (ex).

**TEER Measurement:** The TEER was measured as previously described.<sup>[23]</sup> Briefly, 100000 cells cm<sup>-2</sup> cells were seeded on precoated PET membrane with a pore size of 0.4 μm and a growth area of 0.33 cm<sup>2</sup> (Corning, CLS3460). 48 h after seeding the medium from the apical side was aspirated to allow ALI. Before measuring TEER, the apical side was refilled with 300 μL prewarmed medium and the basolateral compartments were filled up to a final volume of 500 μL. Following 1 h of incubation, the TEER was measured in all samples using an epithelial volt-ohm meter (Millicell ERS-2) equipped with chopstick electrodes (MERSSTX01, Millicell). The electrical resistance was calculated by subtracting the value of blank inserts containing medium from all samples, and multiplication with the cultivation area of the inserts (0.33 cm<sup>2</sup>).

**LPS Stimulations:** The exposure assay was conducted using a Mini Compressor Nebulizer (Bio-rich). The nebulizer plastic parts were rinsed with soap (Ariel Clean liquid soap) followed by ethanol, and then sterilized for 15 min under UV radiation (254 nm). The nebulizer cup was loaded with PBS or LPS diluted with PBS (10 μg mL<sup>-1</sup>) (L4516 SIGMA). Using an adaptor, the outlet of the nebulizer cup was connected to the apical compartment of the acini-on-chip devices using Cole–Parmer tubing (cat # 06400–90). Each exposure assay was conducted for up to 4 min.

**IL8 Secretion Assay:** Cell culture supernatants were assayed using ELISA for IL-8 (Thermo fisher scientific) following the manufacturer's instructions.

**Statistical Analysis:** Data are representative of 3–9 independent experiments and shown as mean ± SD. Two-way ANOVA was performed using GraphPad Prism 8 software (GraphPad).



## Supporting Information

Supporting Information is available from the Wiley Online Library or from the author.

## Acknowledgements

The authors thank Prof. Netanel Korin (Technion) and Dr. Enas Abu-Shah (Oxford University, UK) for helpful discussions. The authors thank Dr. Shaulov from the Biomedical Core Facilities (Technion) for technical support with the electron microscopy. This work was supported by the German Israel Foundation (GIF, Grant Agreement No. I-1348-409.10/2016) and the European Research Council (ERC) under the European Union's Horizon 2020 research and innovation program (Grant Agreement No. 677772). Microfabrication was conducted at the Micro-Nano Fabrication & Printing Unit (MNF & PU) of the Technion and supported by the Russel Berrie Nanotechnology Institute (RBNI, Technion).

## Conflict of Interest

The authors declare no conflict of interest.

## Keywords

epithelial barrier, in vitro assays, microfluidics, organ-on-chip, pulmonary infection

Received: February 26, 2019

Revised: June 30, 2019

Published online: July 31, 2019

- [1] T. C. J. Mertens, H. Karmouty-Quintana, C. Taube, P. S. Hiemstra, *Pulm. Pharmacol. Ther.* **2017**, *45*, 101.
- [2] J. Seok, H. S. Warren, A. G. Cuenca, M. N. Mindrinos, H. V. Baker, W. Xu, D. R. Richards, G. P. McDonald-Smith, H. Gao, L. Hennessy, C. C. Finnerty, C. M. López, S. Honari, E. E. Moore, J. P. Minei, J. Cuschieri, P. E. Bankey, J. L. Johnson, J. Sperry, A. B. Nathens, T. R. Billiar, M. A. West, M. G. Jeschke, M. B. Klein, R. L. Gamelli, N. S. Gibrán, B. H. Brownstein, C. Miller-Graziano, S. E. Calvano, P. H. Mason et al. *Proc. Natl. Acad. Sci. USA* **2013**, *110*, 3507.
- [3] C. H. Wong, K. W. Siah, A. W. Lo, *Biostatistics* **2019**, *20*, 273.
- [4] J. Rice, *Nature* **2012**, *484*, S9.
- [5] P. S. Hiemstra, G. Grootaers, A. M. van der Does, C. A. M. Krul, I. M. Kooter, *Toxicol. Vitro* **2018**, *47*, 137.
- [6] J. Tenenbaum-Katan, A. Artzy-Schnirman, R. Fishler, N. Korin, J. Sznitman, *Biomicrofluidics* **2018**, *12*, 042209.
- [7] A. O. Stucki, J. D. Stucki, S. R. R. Hall, M. Felder, Y. Mermoud, R. A. Schmid, T. Geiser, O. T. Guenat, *Lab Chip* **2015**, *15*, 1302.
- [8] D. Huh, B. D. Matthews, A. Mammoto, M. Montoya-Zavala, H. Y. Hsin, D. E. Ingber, *Science* **2010**, *328*, 1662.
- [9] N. J. Douville, P. Zamankhan, Y.-C. Tung, R. Li, B. L. Vaughan, C.-F. Tai, J. White, P. J. Christensen, J. B. Grotberg, S. Takayama, *Lab Chip* **2011**, *11*, 609.
- [10] R. Fishler, P. Hofemeier, Y. Etzion, Y. Dubowski, J. Sznitman, *Rep.* **2015**, *5*, 14071.
- [11] D. Huh, D. C. Leslie, B. D. Matthews, J. P. Fraser, S. Jurek, G. A. Hamilton, K. S. Thorneloe, M. A. McAlexander, D. E. Ingber, *Sci. Transl. Med.* **2012**, *4*, 159ra147.
- [12] K. H. Benam, R. Novak, J. Nawroth, M. Hirano-Kobayashi, T. C. Ferrante, Y. Choe, R. Prantil-Baun, J. C. Weaver, A. Bahinski, K. K. Parker, D. E. Ingber, *Cell Syst.* **2016**, *3*, 456.
- [13] A. Jain, R. Barrile, A. D. van der Meer, A. Mammoto, T. Mammoto, K. De Ceunynck, O. Aisiku, M. A. Otieno, C. S. Louden, G. A. Hamilton, R. Flaumenhaft, D. E. Ingber, *Clin. Pharmacol. Ther.* **2018**, *103*, 332.
- [14] C. Blume, R. Reale, M. Held, T. M. Millar, J. E. Collins, D. E. Davies, H. Morgan, E. J. Swindle, *PLoS One* **2015**, *10*, e0139872.
- [15] J. Sznitman, *J. Biomech.* **2013**, *46*, 284.
- [16] F. Blank, B. M. Rothen-Rutishauser, S. Schurch, P. Gehr, *J. Aerosol Med.* **2006**, *19*, 392.
- [17] A. G. Lenz, T. Stoeger, D. Cei, M. Schmidmeir, N. Semren, G. Burgstaller, B. Lentner, O. Eickelberg, S. Meiners, O. Schmid, *Am. J. Respir. Cell Mol. Biol.* **2014**, *51*, 526.
- [18] M. Röhm, S. Carle, F. Maigler, J. Flamm, V. Kramer, C. Mavoungou, O. Schmid, K. Schindowski, *Int. J. Pharm.* **2017**, *532*, 537.
- [19] M. H. Wong, M. D. Johnson, *PLoS One* **2013**, *8*, e55545.
- [20] A. J. Byrne, S. A. Mathie, L. G. Gregory, C. M. Lloyd-Jones, *Thorax* **2015**, *70*, 1189.
- [21] N. Daum, A. Kuehn, S. Hein, U. F. Schaefer, H. Huwer, C. Lehr, *Methods Mol. Biol.* **2012**, *806*, 31.
- [22] K. J. Elbert, U. F. Schäfer, H. J. Schäfers, K. J. Kim, V. H. Lee, C. M. Lehr, *Pharm. Res.* **1999**, *16*, 601.
- [23] A. Kuehn, S. Kletting, C. de Souza Carvalho-Wodarz, U. Repnik, G. Griffiths, U. Fischer, E. Meese, H. Huwer, D. Wirth, T. May, N. Schneider-Daum, C. M. Lehr, *ALTEX* **2016**, *33*, 251.
- [24] W. Chanput, J. J. Mes, H. J. Wichers, *Int. Immunopharmacol.* **2014**, *23*, 37.
- [25] C. Schulz, X. Lai, W. Bertrams, A. L. Jung, A. Sittka-Stark, C. E. Herkt, H. Janga, K. Zscheppang, C. Stielow, L. Schulte, S. Hippenstiel, J. Vera, B. Schmeck, *Sci. Rep.* **2017**, *7*, 11988.
- [26] C. Alexander, E. T. Rietschel, *J. Endotoxin Res.* **2001**, *7*, 167.
- [27] A. A. Hislop, J. S. Wigglesworth, S. R. Desai, *Early Hum. Dev.* **1986**, *13*, 1.
- [28] M. G. Ménache, W. Hofmann, B. Asgharian, F. J. Milleghalation, *Toxicol.* **2008**, *20*, 101.
- [29] J. Stocks, P. H. Quanjer, *Eur. Respir. J.* **1995**, *8*, 492.
- [30] J. Tenenbaum-Katan, R. Fishler, B. Rothen-Rutishauser, J. Sznitman, *Biomicrofluidics* **2015**, *9*, 014120.
- [31] A. Tsuda, F. S. Henry, J. P. Butler, *J. Appl. Physiol.* **1995**, *79*, 1055.
- [32] M. Humayun, C. W. Chow, E. W. K. Young, *Lab Chip* **2018**, *18*, 1298.
- [33] R. Bhowmick, H. Gappa-Fahlenkamp, *Lung* **2016**, *194*, 419.
- [34] K. A. Foster, C. G. Oster, M. M. Mayer, M. L. Avery, K. L. Audus, *Exp. Cell Res.* **1998**, *243*, 359.
- [35] D. Konar, M. Devarasetty, D. V. Yildiz, A. Atala, S. V. Murphy, *Biomed. Eng. Comput. Biol.* **2016**, *2016*, 17.
- [36] B. Zhang, M. Radisic, *Lab Chip* **2017**, *17*, 2395.
- [37] D. E. Ingber, *Cell* **2016**, *164*, 1105.
- [38] K. H. Benam, R. Villenave, C. Lucchesi, A. Varone, C. Hubeau, H. H. Lee, S. E. Alves, M. Salmon, T. C. Ferrante, J. C. Weaver, A. Bahinski, G. A. Hamilton, D. E. Ingber, *Nat. Methods* **2016**, *13*, 151.
- [39] C.-M. Lehr, *Cell Culture Models of Biological Barriers: In Vitro Test Systems for Drug Absorption and Delivery*, CRC Press, London, UK **2002**.
- [40] S. Kletting, S. Barthold, U. Repnik, G. Griffiths, B. Loretz, N. Schneider-Daum, C. deS. Carvalho-Wodarz, C. M. Lehr, *ALTEX – Altern. Anim. Exp.* **2018**, *35*, 211.
- [41] O. Y. F. Henry, R. Villenave, M. J. Crouce, W. D. Leineweber, M. A. Benz, D. E. Ingber, *Lab Chip* **2017**, *17*, 2264.
- [42] Y. B. Arlik, M. W. Van Der Helm, M. Odijk, L. I. Segerink, R. Passier, A. Van Den Berg, A. D. Van Der Meer, *Biomicrofluidics* **2018**, *12*, 042218.
- [43] F. Liu, W. Li, J. Pauluhn, H. Trübel, C. Wang, *Toxicology* **2013**, *304*, 158.

- [44] A. K. Mayer, M. Muehmer, J. Mages, K. Gueinzus, C. Hess, K. Heeg, R. Bals, R. Lang, A. H. Dalpke, *J. Immunol.* **2007**, 178, 3134.
- [45] B. L. Laube, *Respir. Care* **2005**, 50, 1161.
- [46] B. L. Laube, *Transl. Respir. Med.* **2014**, 2, 1.
- [47] W. F. Tonnis, G. F. Kersten, H. W. Frijlink, W. L. J. Hinrichs, A. H. de Boer, J.-P. Amorij, *J. Aerosol Med. Pulm. Drug Delivery* **2012**, 25, 249.
- [48] C. A. Fromen, G. R. Robbins, T. W. Shen, M. P. Kai, J. P. Y. Ting, J. M. DeSimone, *Proc. Natl. Acad. Sci. USA* **2015**, 112, 488.
- [49] L. D. Mastrandrea, *Vasc. Health Risk Manag.* **2010**, 6, 47.
- [50] S. B. Fiel, *Expert Rev. Respir. Med.* **2008**, 2, 479.
- [51] D. C. Duffy, J. C. McDonald, O. J. A. Schueller, G. M. Whitesides, *Anal. Chem.* **1998**, 70, 4974.
- [52] B. Chueh, D. Huh, C. R. Kyrtosos, T. Houssin, N. Futai, S. Takayama, *Anal. Chem.* **2007**, 79, 3504.

# ADVANCED BIOSYSTEMS

## Supporting Information

for *Adv. Biosys.*, DOI: 10.1002/adbi.201900026

### Capturing the Onset of Bacterial Pulmonary Infection in Acini-On-Chips

*Arbel Artzy-Schnirman, Hikaia Zidan, Shani Elias-Kirma, Lee Ben-Porat, Janna Tenenbaum-Katan, Patrick Carius, Ramy Fishler, Nicole Schneider-Daum, Claus-Michael Lehr, and Josué Sznitman\**

Supporting Information

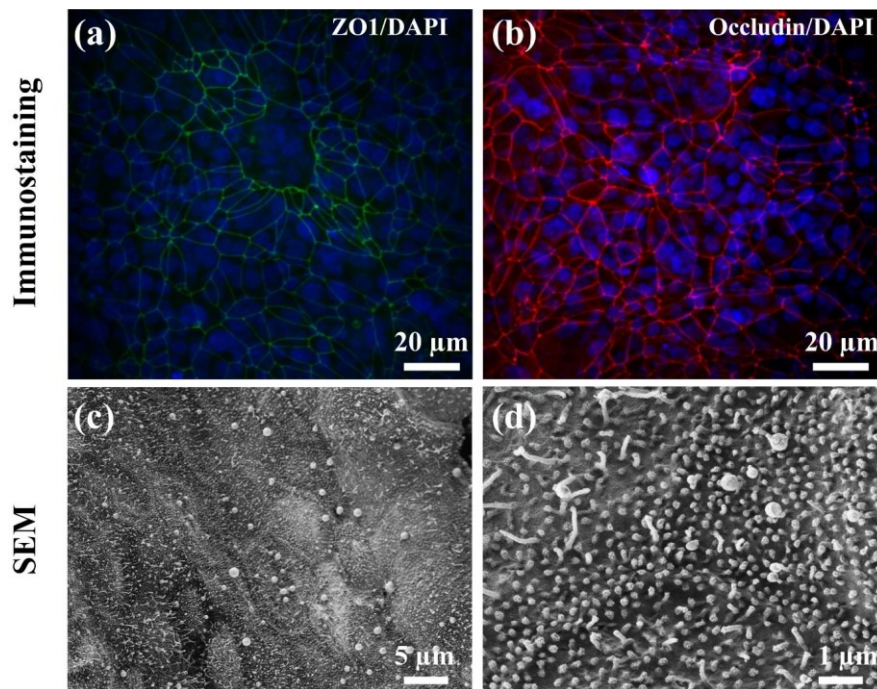


**Figure S1:**hAELVi cell characterization on inserts. Z-stacks of images acquired from confocal laser scanning microscopy of hAELVi cells. (a) ZO1 (green) and nuclei stained with DAPI (blue). (b) Occludin (red) DAPI (blue). (c, d) Scanning electron microscopic (SEM) images of hAELVi cells showing the monolayer with clear cell-cell contacts.

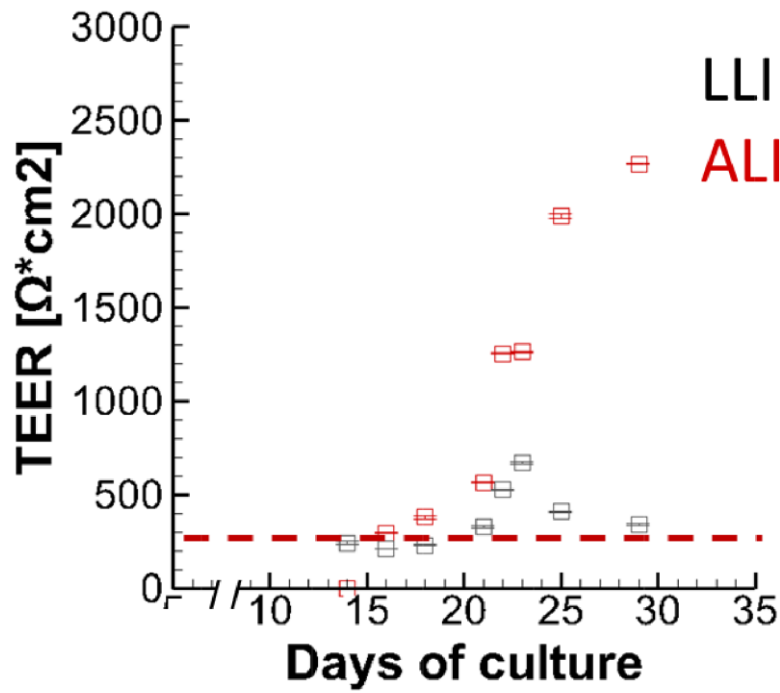


**Figure S2:** TEER measurement of hAELVi growing up to 29 days under immersed conditions (gray) and at air-liquid conditions (red); the red line represents the threshold for guaranteeing a functional barrier. Data shown as mean  $\pm$  SD corresponds n=3.



***„PerfuPul – A Versatile Perfusable Platform to Assess Permeability and Barrier Function of Air Exposed Pulmonary Epithelia“***

**Patrick Carius**, Aurélie Dubois, Morvarid Ajdarirad, Arbel Artzy-Schnirman, Josué Sznitman, Nicole Schneider-Daum and Claus-Michael Lehr

Published in *Frontiers in Bioengineering and Biotechnology*, 2021, Volume 3, Issue 9  
(<http://dx.doi.org/10.3389/fbioe.2021.743236>)

Copyright © 2021 Carius, Dubois, Ajdarirad, Artzy-Schnirman, Sznitman, Schneider-Daum and Lehr. This is an open-access article distributed under the terms of the Creative Commons Attribution License (CC BY).

Contributions to co-authorship:

Patrick Carius had the idea for the perfusable platform, designed, planned as well as performed the experiments and wrote the manuscript. Aurélie Dubois helped in the creation of the custom-made electrode and helped in improving the molds. Morvarid Ajdarirad helped in the creation of the Supplementary Information. Josué Sznitman and Arbel Artzy-Schnirman helped in planning the concept as well as the experiments for the perfusable platform. They further helped to write and enhance the manuscript. Nicole Schneider-Daum helped in revising the manuscript. Claus-Michael Lehr shares the idea for the perfusable platform and helped in planning the experiments. He also helped writing and enhancing the manuscript.



# PerfuPul—A Versatile Perfusable Platform to Assess Permeability and Barrier Function of Air Exposed Pulmonary Epithelia

Patrick Carius<sup>1,2</sup>, Aurélie Dubois<sup>1</sup>, Morvarid Ajdarirad<sup>1,2</sup>, Arbel Artzy-Schnirman<sup>3</sup>,  
Josué Sznitman<sup>3</sup>, Nicole Schneider-Daum<sup>1</sup> and Claus-Michael Lehr<sup>1,2\*</sup>

<sup>1</sup>Department of Drug Delivery (DDEL), Helmholtz-Institute for Pharmaceutical Research Saarland (HIPS), Helmholtz Centre for Infection Research (HZI), Saarbrücken, Germany, <sup>2</sup>Department of Pharmacy, Biopharmaceutics and Pharmaceutical Technology, Saarland University, Saarbrücken, Germany, <sup>3</sup>Department of Biomedical Engineering, Technion—Israel Institute of Technology, Haifa, Israel

## OPEN ACCESS

### Edited by:

Mariana B. Oliveira,  
University of Aveiro, Portugal

### Reviewed by:

Paola Petrini,  
Politecnico di Milano, Italy  
Jyothi U. Menon,  
University of Rhode Island,  
United States

### \*Correspondence:

Claus-Michael Lehr  
Claus-Michael.Lehr@helmholtz-hips.de

### Specialty section:

This article was submitted to  
Biomaterials,  
a section of the journal  
Frontiers in Bioengineering and  
Biotechnology

Received: 17 July 2021

Accepted: 16 September 2021

Published: 06 October 2021

### Citation:

Carius P, Dubois A, Ajdarirad M,  
Artzy-Schnirman A, Sznitman J,  
Schneider-Daum N and  
Lehr C-M (2021) PerfuPul—A Versatile  
Perfusable Platform to Assess  
Permeability and Barrier Function of Air  
Exposed Pulmonary Epithelia.  
Front. Bioeng. Biotechnol. 9:743236.  
doi: 10.3389/fbioe.2021.743236

Complex *in vitro* models, especially those based on human cells and tissues, may successfully reduce or even replace animal models within pre-clinical development of orally inhaled drug products. Microfluidic lung-on-chips are regarded as especially promising models since they allow the culture of lung specific cell types under physiological stimuli including perfusion and air-liquid interface (ALI) conditions within a precisely controlled *in vitro* environment. Currently, though, such models are not available to a broad user community given their need for sophisticated microfabrication techniques. They further require systematic comparison to well-based filter supports, in analogy to traditional Transwells<sup>®</sup>. We here present a versatile perfusable platform that combines the advantages of well-based filter supports with the benefits of perfusion, to assess barrier permeability of and aerosol deposition on ALI cultured pulmonary epithelial cells. The platform as well as the required technical accessories can be reproduced *via* a detailed step-by-step protocol and implemented in typical bio-/pharmaceutical laboratories without specific expertise in microfabrication methods nor the need to buy costly specialized equipment. Calu-3 cells cultured under liquid covered conditions (LCC) inside the platform showed similar development of transepithelial electrical resistance (TEER) over a period of 14 days as cells cultured on a traditional Transwell<sup>®</sup>. By using a customized deposition chamber, fluorescein sodium was nebulized *via* a clinically relevant Aerogen<sup>®</sup> Solo nebulizer onto Calu-3 cells cultured under ALI conditions within the platform. This not only allowed to analyze the transport of fluorescein sodium after ALI deposition under perfusion, but also to compare it to transport under traditional static conditions.

**Keywords:** air-liquid interface (ALI), permeability, perfusion, transepithelial electrical resistance (TEER), aerosol deposition, drug testing, pulmonary epithelia

## INTRODUCTION

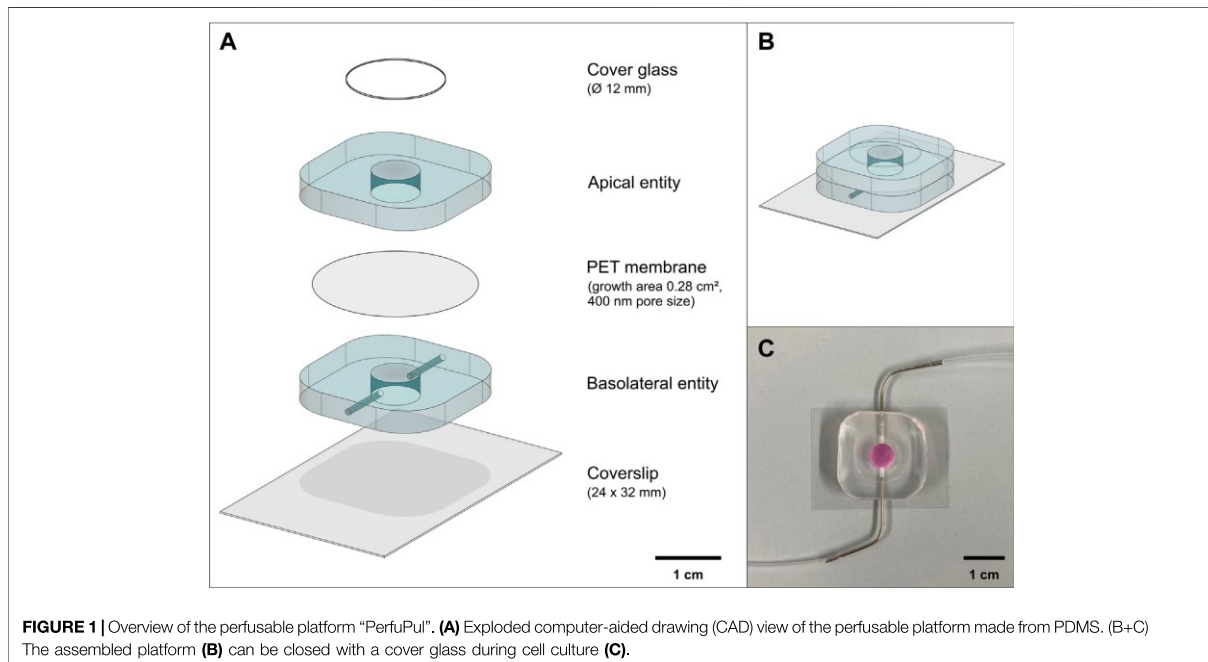
Animal models have undoubtedly been essential for the development of oral inhalation drug products, especially for demonstrating safety as well as, at least for some diseases, also efficacy in preclinical research. But it must be realized that, already in healthy state, animal models hardly reflect the human respiratory tract with regard to the administration and deposition of aerosolized medicines. While forced inhalation or tracheobronchial instillation may still allow to draw some conclusion about pulmonary toxicity, the problem becomes more challenging for efficacy studies. This is especially true for inhalable anti-infective drugs, where the available animal models fail to adequately replicate how such diseases affect the human respiratory tract (Lorenz et al., 2016). This can be attributed to evident species-species variations between humans and model organisms (e.g., in lung anatomy, airway histology, cellular composition of epithelial and sub epithelial compartments) that amongst other reasons eventually slow down the development of orally inhaled drug products (Barnes et al., 2015; Artzy-Schnirman et al., 2019a; Jimenez-Valdes et al., 2020).

In contrast to animal models, complex *in vitro* models, especially when human based, allow to focus on key elements of underlying (patho-) physiological conditions as observed in the clinic and to model such conditions within a controlled *in vitro* environment (Carius et al., 2021). Because at present no such predictive *in vitro* models are available yet, their technological development and subsequent validation represent important and demanding scientific tasks (European Commission Joint Research Centre, 2021). Pulmonary *in vitro* models thereby profited from utilizing well-based permeable growth supports (e.g., Transwell®) as a cell culture environment, because these substrates most importantly enable the establishment of air-liquid interface (ALI) conditions as well as polarized differentiation of pulmonary epithelial cells (Lacroix et al., 2018). The easy accessibility to the apical as well as to the basolateral compartment further supports aerosol deposition and/or permeability studies, along with the biophysical measurement of barrier properties *via* transepithelial electrical resistance (TEER). Various simple pulmonary *in vitro* models, usually consisting of bronchial or alveolar epithelial cell monocultures, but also complex models comprising pulmonary epi- and/or endothelial cells in co-culture with other cell types like immune cells (e.g., dendritic cells, macrophages or neutrophils) or fibroblasts have been extensively reviewed (Gordon et al., 2015; Hittinger et al., 2015; Hittinger et al., 2017; Ehrmann et al., 2020).

In moving beyond simple Transwell® cultures that are mainly limited by static culture conditions, organ-on-chip systems have advanced miniaturized biomimetic devices that allow the *in vitro* culture of human cells under physiological conditions similar to *in vivo*, including continuous perfusion and mechanical deflection (Tenenbaum-Katan et al., 2018). Lung-on-chip devices may moreover replicate the characteristics of specific regions of the lung (e.g., cell composition, exposure to air (flow), or breathing dynamics) and comprise tissue relevant cell types.

Among the earliest efforts, Nalayanda et al. (2009) described the ALI culture of the A549 carcinoma cell line A549 under low flow conditions (0.35 µl/min) in a PDMS-based lung-on-chip for up to 3 weeks. Following the pioneering work of Huh et al. (2010), that introduced an alveolar-capillary model able to co-culture pulmonary epithelial cells under ALI and flow conditions together with endothelial cells, both stretched by cyclic mechanical strain, the field rapidly advanced. Punde et al. (2015) followed the concept of a dynamic Transwell®-like device, thereby showing that the implementation of dynamic flow created a concentration gradient that effectively guided the transmigration of fibrocytes in an inflammation lung model. An anatomically inspired true-scale acini-on-chip allowed the investigation of the immune response of alveolar epithelial cells in co-culture with differentiated THP-1 macrophage-like cells to nebulized lipopolysaccharide (LPS) as a surrogate for bacterial infections (Artzy-Schnirman et al., 2019a). Recently, the same group used a branching airway-on-chip platform to realistically mimic the transport and deposition of aerosolized particulate matter and study its cytotoxic effect on normal human bronchial epithelial (NHBE) cells (Elias-Kirma et al., 2020). Other devices worth mentioning enable the displacement of a flexible membrane in a diaphragm-like motion (Stucki et al., 2015) in combination with perfusion (Ceï et al., 2020) as well as the membrane-free culture of airway smooth muscle cells in co-culture with epithelial cells embedded within a hydrogel (Humayun et al., 2018) or the culture of human alveolar epithelial cells in a gelatin methacryloyl hydrogel resembling alveoli-like hemispheres in a breathing lung-on-chip (Huang et al., 2021).

Despite such advances, the lung-on-chip models described above are technically cumbersome to manufacture and unfortunately need either sophisticated microfabrication techniques, stemming from academic labs with a high level of bioengineering expertise and equipment, or are too costly to be introduced in a standard bio-/pharmaceutical laboratory. Inspired by these devices, we here provide the blueprint as well as a technical proof of principal study of a novel versatile perfusable platform to assess permeability and barrier function of air exposed pulmonary epithelia (PerfuPul), using the bronchial carcinoma cell line Calu-3. Furthermore, to mimic chronic infections of epithelial cells and to enable repetitive treatment of these cultures *in vitro* with aerosolized drug products, survival times should be spanning multiple days, ideally even weeks. Hence, we hypothesized that constant perfusion of cell culture medium could not only prolong the survival time of such complex infected co-culture models, by removal of bacterial toxins and virulence factors, but also accelerate and enhance cellular differentiation, as supported by others (Chandorkar et al., 2017). To this end, we identified ALI conditions, aerosol deposition, TEER measurements and especially perfusion as a physiological relevant clearance mechanism as needed prerequisites for the intended infection studies. Our platform fulfills the technical requirements for the intended infection models and can easily be reproduced in any bio-/pharmaceutical laboratory with a moderate time as well as financial investment.



## MATERIALS AND METHODS

### Design and Fabrication of the Perfusable Platform

The perfusable platform consists of two well-based entities (apical and basolateral) separated *via* a permeable membrane and mounted on a glass coverslip (**Figure 1A**). The apical entity (chamber volume: 85  $\mu$ l) can be closed with a removable cover glass (cover glass round 12 mm; Carl Roth GmbH, P231.1). Channels embedded in the basolateral entity (chamber volume: 85  $\mu$ l) allow access to the basolateral chamber, to connect flexible 22ga polyethylene tubing (Inotech, BTPE-50) or to insert a pair of electrodes for TEER measurements (**Figures 1B,C, 3A,B**).

The production of the perfusable platform is based on an adapted version of the protocol described by Artzy-Schnirman et al. (2019b), where the main steps of the production process are shown in **Figure 2**. Detailed engineering drawings and all steps that are needed to reproduce the platform are depicted in the Supplementary information (**Supplementary Figures S3–S25; Supplementary Table S1**). Engineering drawings and technical figures were created using Fusion360™ (Autodesk®; version 2.0.7402) under an education license. In short, two separate molds serve as a negative for the castings. The castings yield 6 apical or 6 basolateral entities respectively (**Supplementary Figure S5**). They were machined at the workshop of Saarland University (Saarbrücken, Germany) from polytetrafluoroethylene (PTFE). In case of the basolateral mold, the negatives for the channels were formed by insertion of 6 needles (Sterican size 12; B. Braun, 4657624). Polydimethylsiloxane (PDMS) (Sylgard 184 Elastomer Kit; Dow Corning, 1673921) was mixed with curing agent [10:1 (v/v)

ratio; base/curing agent] and degassed using a desiccator. After pouring degassed PDMS onto the molds, the molds were degassed additionally and baked for 60 min at 100°C. The cured castings were peeled off from the molds, the entities were excised out of the castings and centrally punched using a biopsy punch (6 mm; Kai medical, BP-60F) to generate the wells. Apical entities were attached to polyethyleneterephthalat (PET) membranes (0.4  $\mu$ m pore size; Corning, 3450) and basolateral entities to a 24  $\times$  32 mm coverslip (coverslip 24  $\times$  32 mm; Carl Roth GmbH, H 877) *via* a “stamping” method (Chueh et al., 2007). In brief, degassed liquid PDMS [10:1 (v/v) ratio] is poured on a microscopy slide (microscope slide 76  $\times$  52  $\times$  1 mm; Paul Marienfeld GmbH & Co. KG, 1,100,420) that was previously cleaned, first with water followed by 100% isopropanol and then dried. After that, PDMS was spin-coated (3,000 rpm; acceleration 100 rpm/s for 60 s), resulting in a thin layer. Entities were carefully applied on to the thin layer of PDMS and subsequently attached, either to PET membranes (apical entities) or to microscopy slides (basolateral entities). After degassing, the processed entities were baked for 15 min at 100°C. Basolateral entities were combined with the apical entities repeating this process, resulting in the final perfusable platform (**Figure 2**, step 5-6).

### Cell Culture

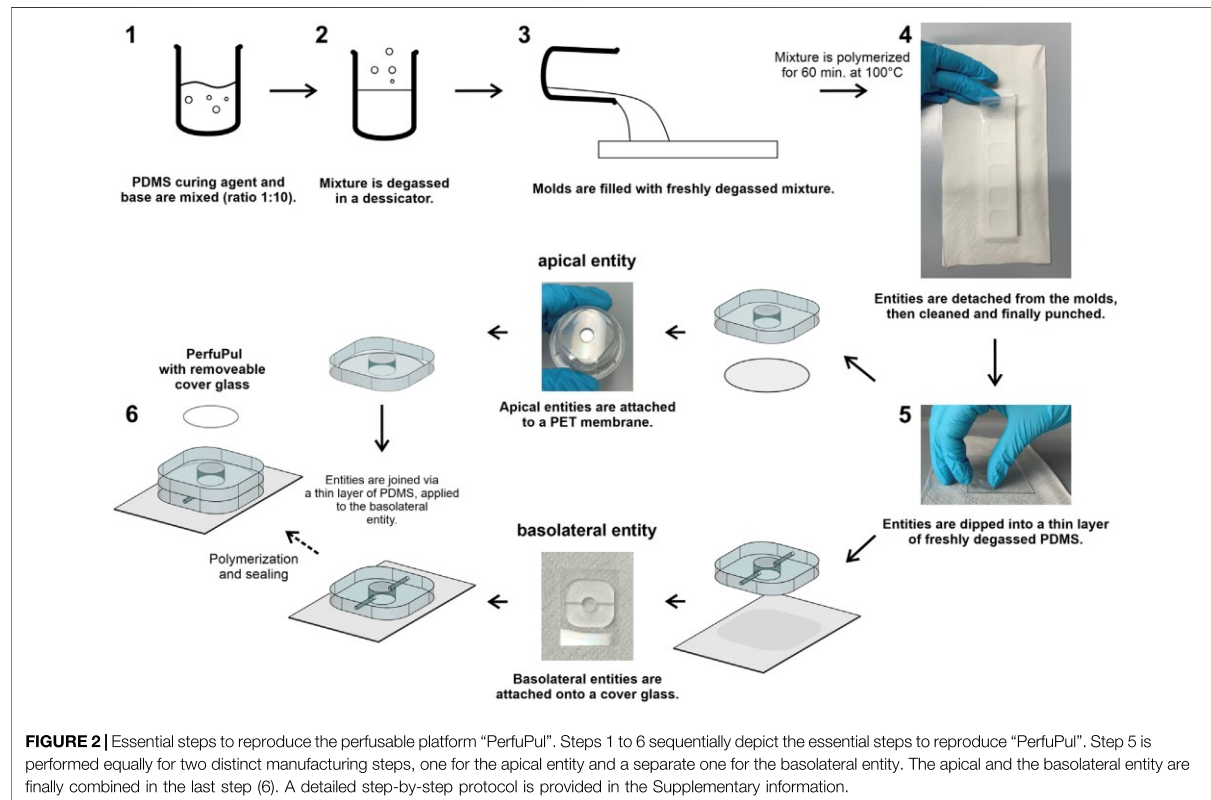
#### General Cell Culture

Calu-3 cells (HTB-55™; ATCC) passages 35 to 55 were cultured in a T75-flask supplemented with 13 ml fresh minimum essential medium (MEM) containing Earle’s salts and L-glutamine (11095080), 1% non-essential amino acids (NEAA, 40035), 1 mM sodium pyruvate (11360070), 100 U/ml penicillin,

# „PerfuPul – A Versatile Perfusable Platform to Assess Permeability and Barrier Function of Air Exposed Pulmonary Epithelia“

Carius et al.

Perfusable Platform for Pulmonary Epithelia



100 µg/ml streptomycin (15140122) and 10% fetal calf serum (FCS) (all Gibco™, Thermo Fisher Scientific Inc.) every two to 3 days. Cells were maintained at 37°C in a humidified atmosphere containing 5% CO<sub>2</sub>. When reaching 80–90% confluency, cells were detached with Trypsin-EDTA 0.05% (Gibco™, Thermo Fisher Scientific Inc.) and then seeded into a new T75-flask (2 × 10<sup>6</sup> cells per flask) and/or used for the experiments detailed in the following paragraphs. All solutions were pre-warmed to 37°C before use.

## Transwell® Experiments

0.33 × 10<sup>5</sup> Calu-3 cells were seeded in 200 µl MEM including all supplements per apical compartment of a Transwell® insert (0.33 cm<sup>2</sup>; 400 nm pore size; Corning, 3,470) (1 × 10<sup>5</sup> cells/cm<sup>2</sup>). The basolateral compartment was supplemented with 800 µl MEM including all supplements. Every two to 3 days used medium was aspirated from the basolateral compartment first and then from the apical compartment. Fresh MEM including all supplements was supplemented first in the apical compartment (200 µl) followed by the basolateral compartment (800 µl).

## Perfusable Platform

Before cell culture, all platforms including tubing (Supplementary Figure S24) were transferred to one Petri dish (Petri dish 145 × 20 mm; Greiner Bio-One, 6052085) per

platform and decontaminated for 30 min on each side (apical side facing up first, then basolateral side facing up) *via* UV light (254 nm) within a safety cabinet. Filling of the perfusable platform was achieved by manually flushing 800 µl of MEM including all supplements carefully through the basolateral compartment using a bubble-free 1 ml syringe (Injekt®-F SOLO; B. Braun, TZ-2180), leaving 200 µl of medium in the syringe. 0.28 × 10<sup>5</sup> Calu-3 cells were seeded apically in a volume of 85 µl MEM including all supplements (1 × 10<sup>5</sup> cells/cm<sup>2</sup>) and the perfusable platform was closed with an autoclaved cover glass. Every two to 3 days medium exchange was performed by carefully removing the cover glass with a sterile forceps, then aspirating the used medium from the apical compartment. After that the basolateral compartment was flushed with 800 µl from a bubble-free 1 ml syringe filled with MEM including all supplements leaving 200 µl medium in the syringe. The outlet of the basolateral compartment was closed with an autoclaved tubing clamp (Th.Geyer, 6200838). In a final step, 85 µl of MEM including all supplements was added to the apical compartment to restore LCC and the perfusable platform was closed apically with an autoclaved cover glass. The same procedure was performed for ALI conditions, with the exception, that when cells were confluent on day 7 or 8 of culture all medium in the apical compartment was aspirated. Additionally, the apical compartment of perfusable platforms containing Calu-3 cells grown under ALI conditions were washed with 85 µl



pre-warmed PBS on days of medium exchange. If not stated otherwise, the perfusable platforms were always closed with an autoclaved cover glass and placed in a 145 mm diameter Petri dish at 37°C in a humidified atmosphere containing 5% CO<sub>2</sub>.

## Confocal Laser Scanning Microscopy

### Immunofluorescence Staining

For the representative immunofluorescence staining only inserts with TEER values > 500 Ω\*cm<sup>2</sup> were selected. After washing the apical and basolateral entity with pre-warmed PBS (apical: 85 μl, basolateral: 800 μl) all liquid was flushed out the basolateral compartment by a bolus injection of air. Cells were fixated with 85 μl of 4% paraformaldehyde (in PBS) for 10 min at room temperature (RT) from apical only. Permeabilization and blocking of unspecific epitopes was performed with blocking buffer [1% BSA (Bovine Serum Albumin heat shock fraction; Sigma-Aldrich, A9647-50G), 0.05% Saponin (Saponin Quillaja sp.; Sigma-Aldrich, S4521-10G) in PBS (w/w/v)] for 1 h at RT. Primary antibodies against tight junction proteins Occludin (monoclonal antibody, Thermo Fisher Scientific, Cat# 33-1500, RRID:AB\_2533101) and ZO-1 (monoclonal antibody, BD Biosciences, Cat# 610966, RRID:AB\_398279) were both diluted [1:200 (v/v)] in blocking buffer and incubated for 12 h at 4°C. The secondary antibody [1:2000 (v/v) in blocking buffer] was incubated for 1 h at RT. Nuclei were stained with DAPI [1 μg/ml in PBS (v/v)] for 30 min at RT. All steps were performed with a volume of 85 μl and the perfusable platforms were washed in between steps with PBS at RT three times. After staining, the apical compartment including the membrane was carefully detached from the basolateral entity using a forceps, by slowly inserting a scalpel underneath the membrane but not touching the growth area. Briefly, the growth area of the membrane was cut from the basolateral side of the membrane as a squared shape, roughly 1 × 1 cm in size, using a scalpel, mounted on a microscope slide (Superfrost; Menzel, AAAA000080##32E) and embedded with fluorescence mounting medium (DAKO, S3023). Samples were always kept moist by careful addition of PBS during the cutting and mounting procedure.

## Image Acquisition and Processing

Z-stacks were acquired with an inverted confocal laser scanning microscope (TCS SP8, Leica) equipped with a ×25 water objective, using a zoom of 1, a resolution of 1,024 × 1,024, and a scan speed of 200 Hz. Maximum projections were equally created for all images with FIJI/Image J (Schindelin et al., 2012) and further processed using the BIOP Channel tools plugin ([https://c4science.ch/w/bioimaging\\_and\\_optics\\_platform\\_biop/image-processing/imagej\\_tools/ijab-biop\\_channel\\_tools/](https://c4science.ch/w/bioimaging_and_optics_platform_biop/image-processing/imagej_tools/ijab-biop_channel_tools/)).

## TEER Measurements

### Transwell Insert

In case of Calu-3 cultured in Transwell® inserts under LCC, TEER was measured with a chopstick electrode connected to a Volt-Ohm-meter (STX2 and EVOM 2; World Precision instruments) according to the manufacturer's instructions. During the time of the measurement the Transwell® plate was placed on a heating

plate (37°C). Ohmic resistance values were corrected for the area of the Transwell® insert (0.33 cm<sup>2</sup>) as well as the related value of a blank and reported as Ω\*cm<sup>2</sup>. If not described differently, all cultures were fed after TEER measurement.

## Perfusable Platform

### Custom Electrode Fabrication

Two Ag/AgCl electrodes were created by following the procedure described by Rootare and Powers (1977), with the exception that the silver disk from the method described was replaced by a silver wire with an outer diameter of 0.5 mm (silver wire 0.5 mm diameter; neoLab, 2-3309) for each electrode. Pre-coated electrodes are also commercially available. The two Ag/AgCl electrodes (V1 and V2) and two additional pieces of silver wire (I1 and I2) were cut to a length of 15 mm, soldered to the stranded wires of a RJ14 (6P4C) telephone cable as described in **Supplementary Figure S3** and insulated with a shrinkage tube per strand. The custom-made electrode was equilibrated in 100 mM KCl overnight connected to a switched off EVOM 2 in “Ohm” mode before its first use, in order to stabilize its electrical potential. After this, the electrode was stored and handled in the same way as the STX2 electrode according to the manufacturer's instructions. To validate the custom-made electrode against the STX2 electrode, the TEER of the same Transwell® with Calu-3 cells (day 16–day 19) grown under LCC was first measured with the STX2 electrode and then with the custom-made electrode. For measuring TEER in the Transwell® with the custom-made electrode the electrode pair I2/V1 was placed in the basolateral compartment and I1/V2 in the apical compartment.

### TEER Measurements in the Perfusable Platform

The custom-made electrode was first soaked in 70% isopropanol [in sterile MilliQ water (v/v)] for 5 min and then dried before each measurement. Briefly, TEER measurements of Calu-3 cells grown under LCC were performed as described for the Transwell®, by placing the electrode pair I2/V1 in the basolateral compartment and the electrode pair I1/V2 in the apical compartment (**Figure 3A**). In the case of Calu-3 cells grown under ALI conditions, LCC were reestablished by following the procedure described for medium exchange. After an incubation time of 1 h TEER measurements were performed as described for LCC. The TEER value for each platform measured on day 3 was used as a blank for the LCC cultures. In order to not disturb the development of an ALI, for all experiments under ALI conditions the blank was set to 178 Ω\*cm<sup>2</sup> for these experiments. This was the upper deviation from the mean of all blanks measured for the LCC cultures at day 3 (155 Ω\*cm<sup>2</sup> ± 23 Ω\*cm<sup>2</sup>; n = 6). Ohmic resistance values were corrected for the area of the perfusable platform (0.28 cm<sup>2</sup>) as well as for the related value of a blank and reported as Ω\*cm<sup>2</sup>.

## Aerosol Deposition

### Deposition Chamber Design and Fabrication

The custom-made deposition chamber was machined at the workshop of Saarland University (Saarbrücken, Germany) from a polyoxymethylene (POM) rod (**Supplementary Figure**

S4). The design was modified based on the device published by Horstmann et al. (2021) in order to fit the perfusable platform. The chamber was designed in such a way that the wider inlet of the cylindrical device fits tightly against an Aeroneb<sup>®</sup> Lab nebulizer (Aerogen<sup>®</sup>, Galway, Ireland) and the narrow outlet seals against the apical compartment of the perfusable platform (Figure 5A). In the upper to middle part of the deposition chamber, the inner diameter of the chamber matches the inner diameter of the nebulizer and then conically tapers towards the outlet, where a nozzle protrudes 2 mm from the main body of the deposition chamber. The nozzle is inserted into the apical entity of the perfusable platform and leaves a distance of 1 mm towards the apical surface area, ensuring that it will not interfere with any cells. The distance between the vibrating mesh of the nebulizer and the cell layer is ~50 mm and was chosen due to handling reasons. It can be extended by lengthening the upper to middle part of the custom-made deposition chamber as needed. Aerosol loss is avoided by insertion of a sealing ring (22 mm inner diameter; 2 mm cord size) in the nebulizer-fitting cavity of the deposition chamber and a tight fit of the nozzle inside the perfusable platform.

## Deposition Protocol

The Aeroneb<sup>®</sup> Lab nebulizer as well as the deposition chamber were disinfected with 70% isopropanol and allowed to dry before the experiments. Before each use, the Aeroneb<sup>®</sup> Lab nebulizer (standard VMAD, 2.5–4.0 µm droplet diameter) connected to an Aerogen<sup>®</sup> USB controller (both Aerogen<sup>®</sup>, Galway, Ireland) was tested for a constant liquid output rate which was not allowed to differ more than 10% from 0.5 ml/min. Therefore 200 µl of sterile PBS was nebulized and the time needed to nebulize all liquid was taken. For aerosol deposition experiments the Aeroneb<sup>®</sup> Lab nebulizer was connected to the custom-made deposition chamber and inserted into the open apical cavity of the perfusable platform. If not stated otherwise, 20 µl of a fluorescein sodium solution (1 mg/ml in PBS) were allowed to nebulize completely and the generated aerosol settled for 1 min before the nebulizer and the deposition chamber were removed from the perfusable platform. After aerosol deposition the perfusable platform was immediately closed with a sterile cover glass.

For the determination of the deposited dose (Figure 5B), single apical entities of the perfusable platform were directly attached to a 24 × 32 mm microscopy slide using the “stamping” method described for the fabrication of the perfusable platform. 20 µl of a fluorescein sodium solution (1 mg/ml in PBS) were nebulized into 30 µl of PBS which were previously pipetted into each apical entity and served as a surrogate for the cell layer. Fluorescence intensity of nebulized fluorescein sodium was measured in 96-well plates at 485 nm excitation and 530 nm emission wavelength with a plate reader (Infinite M200 Pro; Tecan Trading AG) and the deposited dose was calculated from a standard curve. This was done for 5 separate entities. The deposition efficiency was reported as the percentage of the measured dose from the invested dose before nebulization.

## Transport Studies

Before each transport experiment, TEER values of Calu-3 cells cultured between day 17 and day 19 were measured while cells remained under LCC to ensure barrier integrity (before). Samples were only used for transport experiments when TEER values reached  $>300 \Omega \cdot \text{cm}^2$  before the transport study in accordance with Ehrhardt et al. (2002).

## Transwell<sup>®</sup> System

Calu-3 cells were washed once with pre-warmed Hanks' Balanced Salt Solution (HBSS) with  $\text{CaCl}_2$  as well as  $\text{MgCl}_2$  (HBSS (1x); Gibco<sup>™</sup>, Thermo Fisher Scientific Inc., 14025050) and then equilibrated in HBSS (200 µl apical; 800 µl basolateral) for 1 h (1 h after switch). After measuring TEER, HBSS was aspirated from both, the apical and basolateral compartment. 200 µl fluorescein sodium solution (2.5 µg/ml in HBSS) were added apically (donor) and 800 µl HBSS were added to the basolateral compartment (acceptor). From the same solutions 200 µl each were transferred into a 96-well plate to determine the starting concentrations for each compartment. All steps were performed on a heating plate at 37°C. Afterwards, the Transwell<sup>®</sup> plates were placed on a MTS orbital shaker (150 rpm; IKA, Germany) in the incubator and 200 µl samples were taken every 1 h for a total of 7 h, from the basolateral compartment only. 200 µl sampled at time points were immediately replenished with 200 µl pre-warmed HBSS. TEER was measured 30 min after the last sample was taken (after 8 h), 200 µl from the apical as well as the basolateral compartment were sampled to determine the end concentrations and all samples were measured with a plate reader in a 96-well plate at 485 nm excitation and 530 nm emission wavelength. The concentration of fluorescein sodium in each sample was calculated using a calibration curve of defined concentrations of fluorescein sodium in HBSS.

## Perfusable Platform

Calu-3 cells were washed once with pre-warmed HBSS, by repeating the procedures described for medium exchange. After 1 h of equilibration TEER was measured again (1 h after switch). After connecting a fresh set of tubing including a new syringe filled with pre-warmed HBSS, the basolateral compartment was filled bubble free, while the HBSS from the equilibration step remained in the apical compartment. Immediately after the basolateral compartment was filled and closed with a tubing clamp (receiver), the HBSS in the apical compartment was aspirated and 85 µl fluorescein sodium solution (2.5 µg/ml in HBSS) was added apically (donor). Shortly after, the syringe that was connected to the basolateral compartment was placed into a syringe pump (Harvard industries, PHD Ultra) and 80 µl samples were taken every 1 h for a total of 7 h, while the perfusable platform was placed on an orbital shaker (150 rpm). The flow rate of the syringe pump was set to 1 ml/min in order to sample 80 µl in a short period of time from the basolateral compartment while additionally preventing the sampling maneuver from exerting too much pressure on the cell layer. TEER was measured 30 min after the last sample was taken (after 8 h) and 80 µl from the apical as well as the

basolateral compartment were sampled to determine end concentrations.

Transport studies under ALI conditions in the perfusable platform followed the same procedure as transport studies under LCC with only a few exceptions. Calu-3 cells were set to ALI conditions between day 7 or 8 of culture and cultured until day 16–18. The first TEER measurement (1 h after switch) was performed 1 h after LCC was restored by the addition of HBSS to both compartments. After the first TEER measurement ALI conditions were restored again and Calu-3 cells were allowed to equilibrate for 30 min. Then 20  $\mu$ l of a sterile fluorescein sodium solution (1 mg/ml in PBS) were nebulized onto the apical compartment. The apical compartment was closed with an autoclaved cover glass immediately after the aerosol settled for 1 min. The perfusable platform was placed on an orbital shaker (150 rpm) and 80  $\mu$ l samples (ALI discontinuous sampling) were taken every 1 h for a total of 5 h, while shortly perfused (1 ml/min) with a syringe pump during the time of sample collection. For transport studies of ALI cultures under perfusion, a peristaltic pump (flow rate: 80  $\mu$ l/min; Gilson, minipuls 3) equipped with a PharMed<sup>®</sup> BPT tubing (internal diameter: 0.38 mm; Saint Gobain Performance Plastics<sup>™</sup>, 070539-04) was connected to the basolateral compartment and 80  $\mu$ l samples (ALI continuous sampling) were taken every 1 h for a total of 5 h. Although the same dose of fluorescein sodium was used for the transport studies under ALI conditions and LCC, we reduced the duration of the transport studies under ALI conditions to 5 h due to an increased concentration gradient.

All samples were analyzed in the same way as described for the Transwell<sup>®</sup> samples. The area under the curve (AUC; a. u.),  $C_{max}$  (ng/ml) and  $t_{max}$  (min) were determined from the cumulative concentration-time curve using GraphPad Prism<sup>®</sup> 9 (GraphPad software).

## Calculation of the Apparent Permeability Coefficient ( $P_{app}$ )

From the linear portion of a cumulative concentration-time curve (LCC: 240–360 min), where drug concentration in the receiver compartment did not exceed 10% of the drug concentration originally added to the donor compartment (Supplementary Figure S2) and at which no lag time was observed, the slope was calculated and divided by the area ( $A$ ;  $cm^2$ ) of the growth support to get the flux of fluorescein sodium ( $J$ ;  $ng/cm^2 \cdot s$ ). To obtain the  $P_{app}$  ( $cm \cdot s^{-1}$ ) the following equation was applied, where  $c_0$  ( $ng/cm^3$ ) is the initial concentration in the donor compartment at the beginning of the experiment:

$$P_{app} = \frac{J}{c_0}$$

The measured concentrations were converted into absolute masses of compound by multiplication with the acceptor volume of the perfusable platform which was 120  $\mu$ l ( 85  $\mu$ l for the chamber +35  $\mu$ l for the connected tubing).

## Statistical Analysis

If not stated otherwise, numerical data were reported as individual values or mean values  $\pm$  standard deviation (SD).

2-way ANOVA was performed not assuming sphericity and with a Šidák's multiple comparisons test. Unpaired  $t$ -test was performed with Welch's Correction.  $p$  values were defined as: ns:  $p > 0.5$ ; \*:  $p < 0.05$ ; \*\*:  $p < 0.005$ ; \*\*\*:  $p < 0.0005$ . Calculations were made using GraphPad Prism<sup>®</sup> 9.

## RESULTS

### Concept of the Perfusable Platform

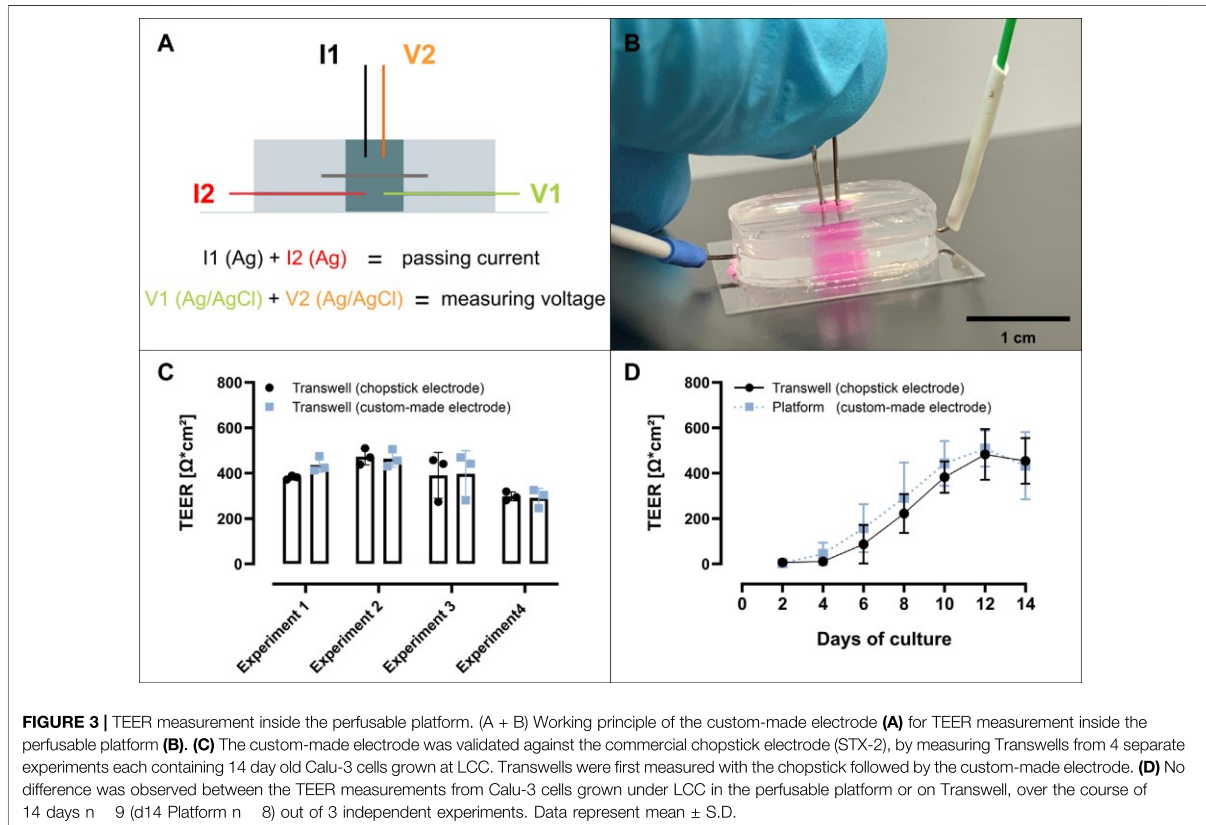
The perfusable platform has been designed in such a way, that it is both easy to produce and operable by non-experts. It encompasses an apical compartment, which is open to the top, and a basolateral compartment, which can be perfused *via* two lateral channels (Figure 1A). This design allows to keep experimental conditions similar to the established static Transwell<sup>®</sup> systems or analogues thereof, and to generate analogous readouts. The open design of the apical entity enables aerosol deposition as well as easy access to the apical cell layer, and the lateral orientation of the in- and outlet enables the insertion of a custom-made electrode for measuring TEER. In addition, the apical entity can be closed with a sterile cover glass to protect the cell layer during cell culture. The two entities are separated *via* a PET membrane that is cut from a Transwell<sup>®</sup>, which ensures that composition and quality of the growth support are essentially the same, requiring minimal adaptations of the protocol. By keeping the height of the assembled perfusable platform to a minimum, cell growth can be monitored microscopically under sterile conditions, while the assembled perfusable platform (Figures 1B,C) remains in a Petri dish. This was demonstrated in a model experiment for the growth of Calu-3 cells, which were seeded on the apical side of the membrane within the apical entity of the perfusable platform under LCC (Supplementary Figure S1). After seeding, Calu-3 cells reached confluency within 7–8 days of cell culture, indicating that neither the setup nor the handling of the platform impaired reproducible cell growth.

### Analyzing Barrier Integrity Inside the Perfusable Platform

TEER measurements prove to be a non-destructive, reliable and functional tool for the assessment of barrier integrity. The increase in ohmic resistance of an *in vitro* culture grown on a permeable support thereby serves as a convenient readout to monitor the development of functional tight junctions and other cell-to-cell connections. To measure TEER in case of the Transwell<sup>®</sup>, the shorter leg of an Ag/AgCl chopstick electrode is inserted into the apical compartment, while the longer leg is simultaneously placed into the basolateral compartment. The electrode is then connected to an epithelial Volt-Ohm-Meter, which calculates the ohmic resistance.

The design of the perfusable platform, however, required another type of Ag/AgCl electrode to measure TEER values, since the narrow channels are incompatible with the commercial chopstick electrodes provided with a standard epithelial Volt-Ohm-Meter (EVOM 2) instrument. We decided





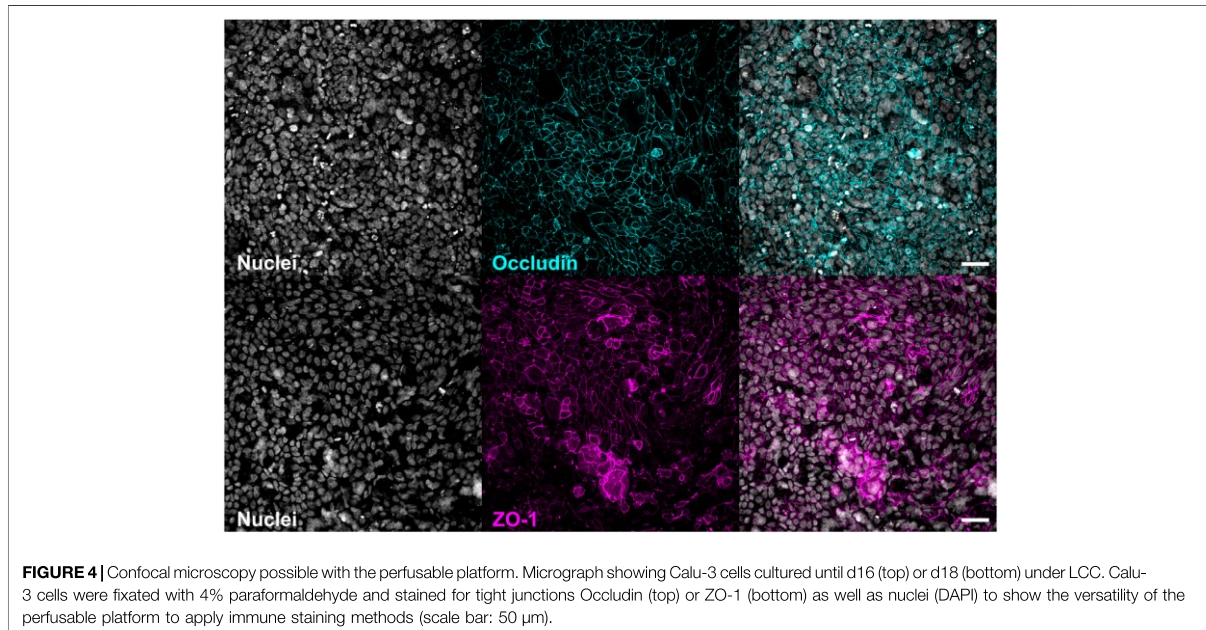
for a custom-made electrode connected to the four cords of a RJ14 (6P4C) telephone cable as described in the methods section. This is the same type of cable used to connect the chopstick electrode to a regular EVOM 2. As depicted in **Figure 3A**, two cords of the electrode are passing current [I1 (Ag) + I2 (Ag)] and voltage is measured *via* the other two cords [V1 (Ag/AgCl) + V2 (Ag/AgCl)]. In order to measure TEER, I1/V2 need to be inserted into the apical compartment of the perfusable platform and I2/V1 need to be inserted into the basolateral compartment, while connected to an epithelial Volt-Ohm-Meter (**Figures 3A,B**).

The chopstick electrode, however, comprises a combination of Ag as well as Ag/AgCl electrodes per leg, one Ag pellet on the side of each leg that faces away from the Transwell® insert (passing current) and an Ag/AgCl pellet per leg that faces the Transwell® insert (measuring voltage). In order to show that the design of the custom-made electrode, which is based on individual silver wires and not on silver pellets attached to each leg, does not impair TEER measurements, the functionality of the custom-made electrode was compared to the chopstick electrode. Both measurements were conducted in the same Transwell® (**Figure 3C**). For this, TEER values from 12 Transwells® out of four experiments (3 Transwells® per experiment) carrying Calu-3 cells grown for 14 days under LCC were measured. After 14 days TEER values were measured first with the chopstick electrode and then with the custom-made electrode. The mean of all TEER

values determined with the custom-made electrode showed a deviation of +3% from the mean of all TEER values determined with the chopstick electrode (custom-made electrode:  $398 \pm 54 \Omega \cdot \text{cm}^2$ ; chopstick electrode  $386 \pm 41 \Omega \cdot \text{cm}^2$ ). These differences between the two electrodes were in an acceptable error range covering not more than  $15 \Omega \cdot \text{cm}^2$ , which suffices for the determination of TEER values during *in vitro* culture of pulmonary epithelial cells.

The development of TEER values of Calu-3 cells inside the perfusable platform was compared side-by-side with Calu-3 cells grown on Transwells®, under LCC over the course of 14 days (**Figure 3D**). As displayed in **Figure 3D**, TEER values developed equally in the perfusable platform as well as in the Transwell® during 14 days of culture, reaching a maximum (perfusable platform:  $510 \pm 81 \Omega \cdot \text{cm}^2$ ; Transwell®:  $484 \pm 112 \Omega \cdot \text{cm}^2$ ) after 12 days of culture. These results indicated that the combination of the custom-made electrode and the perfusable platform could be used to reliably determine the development of TEER values in the same quality as the traditional combination of the chopstick electrode and the Transwell®.

Another common technique to demonstrate the integrity of a pulmonary epithelial barrier *in vitro* is the visualization of proteins that form functional tight junctions *via* fluorescent immunocytochemistry staining. **Figure 4** exemplifies how such methods can be conducted within the perfusable platform in the



same manner as they are applied for the Transwell<sup>®</sup>. As described in the methods section, Calu-3 cells were fixated and treated with the respective antibodies to visualize the tight junction forming proteins Occludin (d16) and ZO-1 (d18). Both micrographs show the development of a densely connected network representative of functional tight junctions together with a homogenously distributed cell layer indicated *via* staining of cell nuclei with DAPI.

The combination of non-destructive TEER measurements to assess barrier integrity together with the ability to perform immunocytochemistry staining after cells have been fixated demonstrates that the perfusable platform can be used for the quantitative and mechanistic characterisation of barrier function during *in vitro* culture of pulmonary epithelial cells.

### Pre-Metered Aerosol Deposition on the Perfusable Platform

The *in vitro* culture of pulmonary epithelial cells under ALI conditions exposes the epithelial cell layer apically to air, which creates a physiologically relevant interface to mimic the *in vivo* situation more closely. Other than LCC, which for good reasons are standard for intestinal epithelial or blood vessel forming endothelial cells, ALI conditions also allow the controlled deposition of aerosols to the apical surface of the cell layer. Since the apical compartment of the perfusable platform can be opened, by removing the cover glass whenever needed, switching to ALI conditions and the deposition of aerosols are easily possible. In this context, we adapted the design of a recently published custom-made deposition chamber (Horstmann et al., 2021) which fits to an Aeroneb<sup>®</sup> Lab vibrating mesh nebulizer (Figure 5A). The functional unit, consisting of an Aeroneb<sup>®</sup> Lab

nebulizer connected to an Aerogen<sup>®</sup> USB controller as well as to the deposition chamber, is placed on the apical compartment of the perfusable platform. The nebulizer generates an aerosol from an aqueous drug solution through a vibrating mesh, which is released into the deposition chamber and finally settles as a mist onto the apical compartment of the perfusable platform. Reproducible deposition of pre-metered doses of an aqueous drug solution, can be achieved by controlling the concentration and/or the volume of the solution before nebulization. While increasing the settling time beyond 30-s was found to not further affect the deposited dose, a settling time of 1 min was chosen as routine to facilitate the experimental procedure (Horstmann et al., 2021).

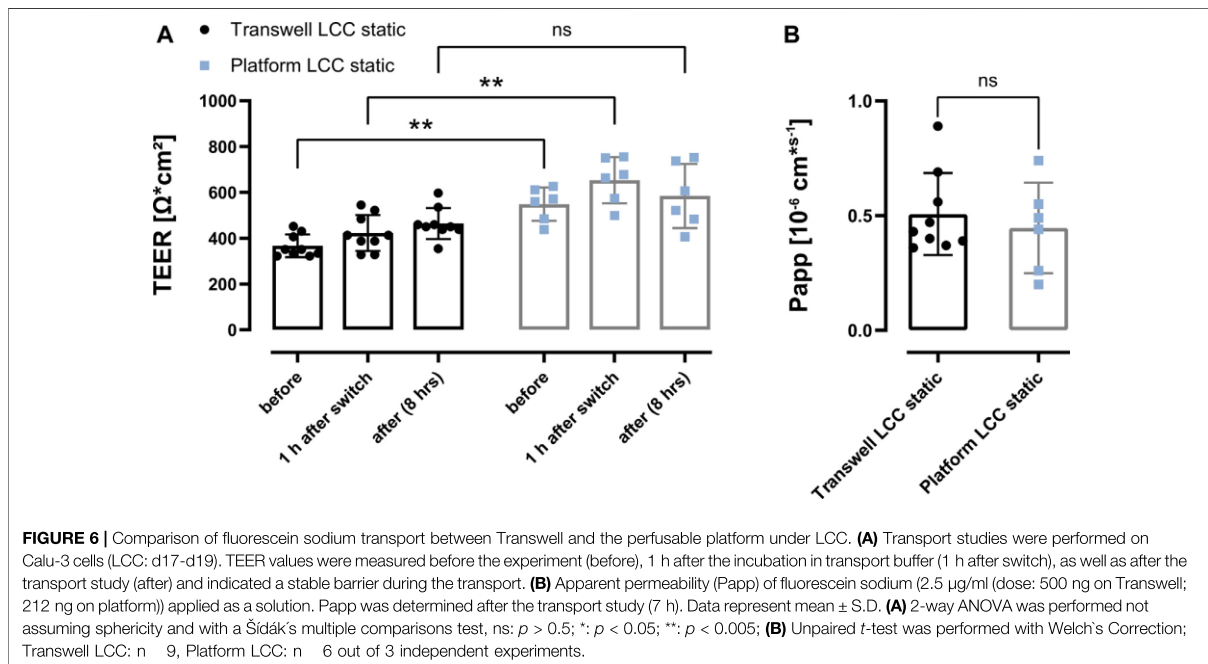
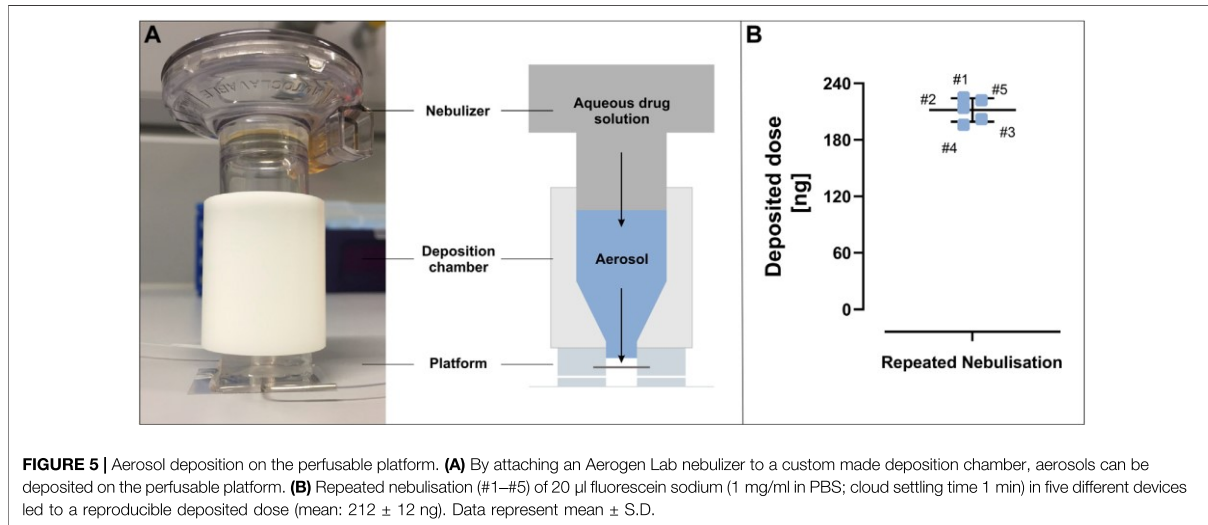
This was demonstrated by nebulizing 20  $\mu$ l of fluorescein sodium solution (1 mg/ml in PBS) onto five perfusable platforms, which comprised only the apical compartment attached to a glass slide. By keeping the settling time of the mist to 1 min after each nebulization, a delivered dose of  $212 \pm 12$  ng could be reproducibly deposited (Figure 5B).

### Comparison of Fluorescein Sodium Transport Between the Transwell<sup>®</sup> and the Perfusable Platform

To carry out comparative transport experiments on Calu-3 cells grown under LCC on Transwell<sup>®</sup> versus cells grown under LCC in the perfusable platform, fluorescein sodium was used as a well-defined low-permeability marker.

Before, during and after each transport experiment, TEER values were measured to ensure that barrier integrity was not compromised by the transport buffer or over the duration of the experiment. In case of the cells grown under ALI conditions, the

# „PerfuPul – A Versatile Perfusable Platform to Assess Permeability and Barrier Function of Air Exposed Pulmonary Epithelia“



first TEER measurements were performed 1 h after LCC conditions were re-established. Before the transport experiments, Calu-3 cells grown under LCC in the Transwell® presented a significantly lower TEER (before,  $367 \pm 49 \Omega \cdot \text{cm}^2$ ) than Calu-3 cells grown in the perfusable platform under the same conditions (before,  $548 \pm 73 \Omega \cdot \text{cm}^2$ ) (Figure 6A). After the switch to HBSS as a transport buffer (1 h after switch) TEER values slightly increased in both the Transwell® cultures ( $423 \pm$

$78 \Omega \cdot \text{cm}^2$ ) as well as in the cultures grown in the perfusable platform (to  $653 \pm 100 \Omega \cdot \text{cm}^2$ ). After 7 h of transport experiments (Transwell®:  $464 \pm 67 \Omega \cdot \text{cm}^2$ ; perfusable platform:  $584 \pm 140 \Omega \cdot \text{cm}^2$ ), TEER values did not decline when compared to the condition before the transport experiments for either system, indicating that barrier properties remained intact during the course of the experiment. Without reaching statistical significance, however, it was observed that in the

perfusable platform TEER values after the transport slightly decreased ( $-69 \pm 4 \Omega \cdot \text{cm}^2$ ) compared to 1 h after the switch to transport buffer, whereas the TEER values of the cells cultured on Transwells<sup>®</sup> showed a slight increase ( $41 \pm 3 \Omega \cdot \text{cm}^2$ ).

The Papp values further supported the assumption of the formation of a functional diffusional barrier to fluorescein sodium within Calu-3 cell layers, which TEER value measurements already indicated (Figure 6B). The transport of fluorescein sodium over Calu-3 cell layers grown under LCC within Transwell<sup>®</sup> inserts showed no significant differences indicated by the respective Papp values when compared to cell layers grown in the perfusable platform (Transwell<sup>®</sup>:  $0.51 \pm 0.18 \cdot 10^{-6} \text{ cm}^2 \cdot \text{s}^{-1}$ ; perfusable platform:  $0.45 \pm 0.20 \cdot 10^{-6} \text{ cm}^2 \cdot \text{s}^{-1}$ ). In addition, permeability of fluorescein sodium in a perfusable platform without any cells grown inside was increased 20-fold (Supplementary Figure S2).

This set of experiments showed that the perfusable platform performs as good as the Transwell<sup>®</sup> under the experimental requirements of a transport study, in terms of reproducibility and consistency of results.

## Transport Studies Under Perfusion

The essential advantage of the perfusable platform in comparison to the Transwell<sup>®</sup> system is the option to perfuse the basolateral compartment. In order to demonstrate one of the various possibilities enabled by perfusing the acceptor compartment, we compared the transport of fluorescein sodium after nebulization under static conditions and under the influence of perfusion (Figure 7A). For the static conditions, the experimental setup for sampling was the same as for the transport studies under LCC described earlier (Figure 6), where the basolateral compartment was only subjected to a short perfusion (80  $\mu\text{l}$ , ALI discontinuous sampling) from a syringe pump during sample timepoints, while the platform remained on a shaker during the transport experiment. In the case of the samples that were taken from perfusion, samples were collected as fractions (80  $\mu\text{l}$ , ALI continuous sampling) from perfusion (80  $\mu\text{l}/\text{h}$ ) generated by a peristaltic pump. During transport experiments TEER seemed not to be affected from perfusion when compared to static conditions (Figure 7B), demonstrating that perfusion did not disturb barrier properties during a 5 h transport experiments. Neither the comparison of the different concentration time curves nor the comparison of the area under the concentration time curve (AUC) (Figure 7C), yielded a significant difference between the two conditions (ALI continuous sampling:  $22,525 \pm 6,248 \text{ a. u.}$ ; ALI discontinuous sampling:  $20,850 \pm 6,900 \text{ a. u.}$ ), indicating that similar mass transport occurred under both conditions. When comparing the mean of  $C_{\text{max}}$  (ALI continuous sampling:  $135 \pm 47 \text{ ng/ml}$ ; ALI discontinuous sampling:  $115 \pm 41 \text{ ng/ml}$ ) as well as  $t_{\text{max}}$  (ALI continuous sampling:  $140 \pm 31 \text{ min}$ ; ALI discontinuous sampling:  $165 \pm 30 \text{ min}$ ) of the individual platforms, there seems to be - without being statistically significant - at least some trend towards higher  $C_{\text{max}}$  as well as shorter  $t_{\text{max}}$  for the transport studies under perfusion (Figure 7D), but this would need further investigation.

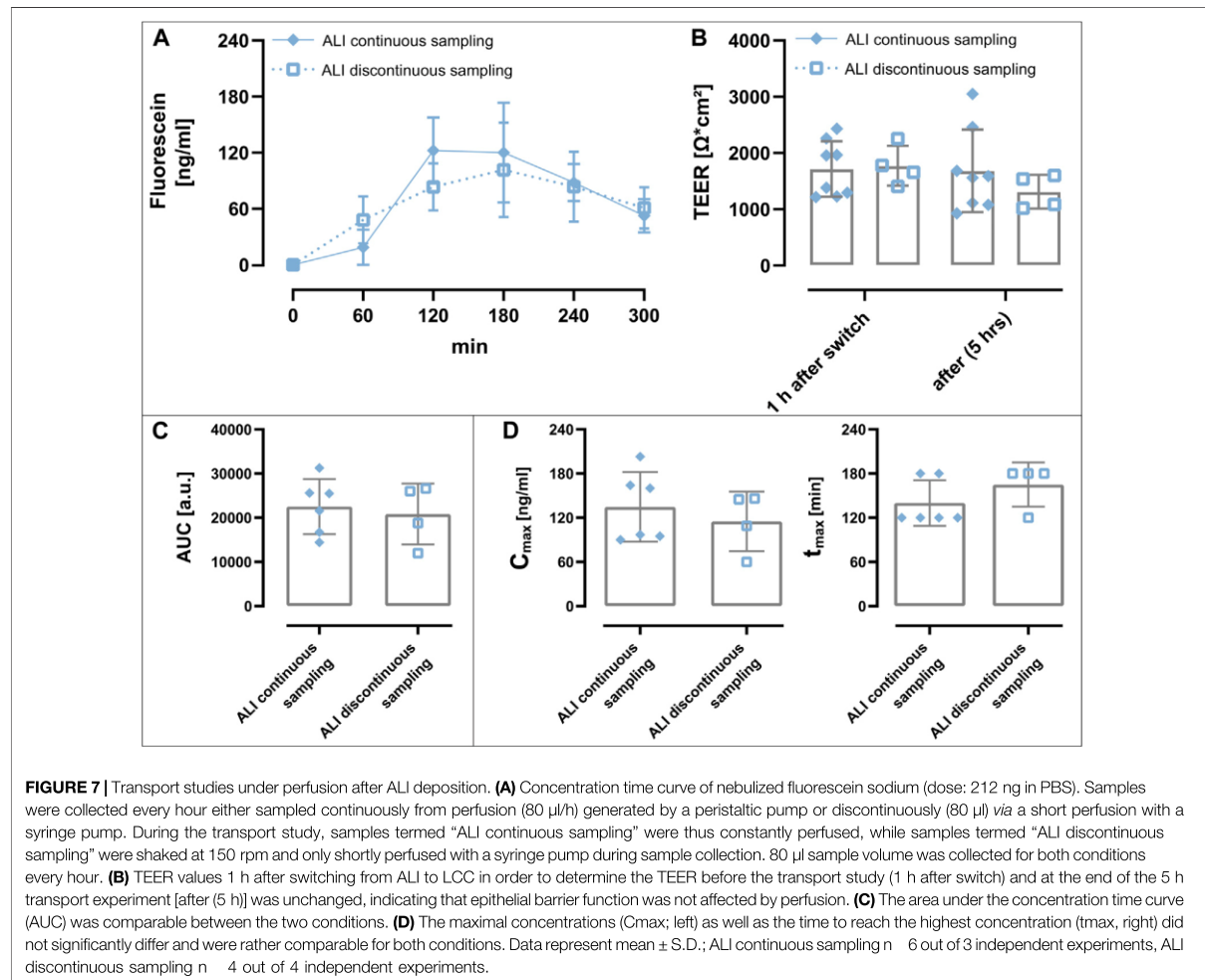
## DISCUSSION

In spite of their physiological advantages, perfusable transport chambers have only rarely found their way into *in vitro* models of epithelial cell culture, in particular for the lungs (Artzy-Schnirman et al., 2020). Complex designs, mostly encompassing micron-sized rectangular channels, as well as the underlying problems of impaired aerosol deposition and/or complexity of handling by non-experts, might restrict the exploitation of the full potential of lung-on-chip devices as preclinical research tools (Junaid et al., 2017; Ehrmann et al., 2020). Perfusable systems offer particular advantages for studying infectious diseases, as concentration of e.g., bacterial virulence factors can be kept at lower levels by continuous supply and dilution with fresh media. Before this can be studied in more detail, however, it is necessary to ensure to what extent data generated on novel perfusable setups can be compared to those obtained on established Transwells<sup>®</sup> under static conditions (Ainslie et al., 2019). We therefore here first describe the development as well as the characterization of a simple perfusable platform for pulmonary epithelial cell cultures at ALI conditions. This platform maintains the advantages of traditional Transwell<sup>®</sup>-based systems, but adds the possibility to implement perfusion as a prerequisite to develop longer-lasting *in vitro* models of chronic pulmonary diseases in the future. In addition, we want to share the protocol needed to produce the platform with a broad scientific community, in order to make this technology available to end-users that might not yet be familiar with microfabrication techniques.

Apart from standardized readouts to assess cell viability or cytotoxicity *in vitro*, such as the MTT or lactate dehydrogenase (LDH) assay respectively, information from TEER measurements or permeability studies appear extremely helpful for the preclinical evaluation of orally inhaled drug products (Wilson 2000; Hittinger et al., 2017). For such purposes, these models must allow ALI conditions together with the subsequent deposition of aerosols. Although pulmonary epithelial cells grown on Transwell<sup>®</sup> inserts meet all of these technical specifications, they are limited to static culture conditions. Recent studies, however, demonstrated that normal human bronchial epithelial (NHBE) cells cultured under ALI conditions and simultaneous perfusion of cell culture medium showed improved barrier properties in comparison to static conditions (Chandorkar et al., 2017; Bovard et al., 2018). Perfusion is, amongst other physiological important mechanical stimuli, also recognized as a central element to be implemented in organ-on-chip systems in general to improve cellular development (Thompson et al., 2020).

The new platform thus was designed to comply with the familiar technical standards and features of Transwell<sup>®</sup> inserts, but at the same time also enabling perfusion as a physiological relevant clearance mechanism not present in Transwell<sup>®</sup>-based culture plates. Major specifications are: 1) a comparable surface area (24-well based Transwell<sup>®</sup>:  $0.33 \text{ cm}^2$ ; perfusable platform:  $0.28 \text{ cm}^2$ ), 2) the possibility to routinely inspect cell layers under a microscope while maintaining sterile culture conditions, 3) the option to measure TEER, and 4.) the implementation of ALI





conditions as well as subsequent aerosol deposition (Figures 1, 3, 5; Supplementary Figure S1). The access to the basolateral compartment *via* a combination of a channel-based inlet connected to a flexible tubing enables the culturing of cells under static culture conditions, but also adds the possibility to perform experiments under perfusion (Figure 7).

In a side-by-side comparison using Calu-3 cells grown on regular Transwell® inserts or within the perfusable platform we could show that both, the resistance readings from the two electrodes (chopstick vs. custom-made electrode) within the same Transwell® insert as well as the measurements performed in the perfusable platform and on Transwell® inserts under equal experimental conditions agree by good approximation (Figure 3C, D). Notably, this was irrespective of the fact that in the case of the custom electrode, when compared with the chopstick electrode within the same Transwell®, four separate cables needed to be arranged in each well. The custom-made Ag/AgCl electrode used by us can be connected to existing instrumentation (e.g., EVOM 2) with only little technical effort

needed to solder the different silver wires to a 4-cord cable (Figure 3A), as already described for organ-on-chip systems in similar ways (Douville et al., 2010; Ferrell et al., 2010; Huh et al., 2010; Kim et al., 2012; Griep et al., 2013). Most of these studies reported significantly higher TEER values in case of the organ-on-chip systems when compared to results obtained for the same cell models cultured on Transwell® inserts. However, these higher TEER values could be related to the geometry of the rectangular micron-sized channels within these organ-on-chips, that generate a non-uniformly distributed electrical current, rather than showing a biological effect (Odijk et al., 2015). The perfusable platform reported in the present paper, however, is based on a design encompassing two equally sized wells separated by a circular membrane that has a cell culture area identical to that of a 24-well Transwell® insert (Figure 1A). Limiting the use of micron-sized channels only to the in- and outlet that enable access to the basolateral well, further generates similarity to the Transwell®.

Especially during permeability studies within the same lab, TEER value measurements using an EVOM 2 or similar direct current based Voltohmmeters are widely accepted as a valuable non-invasive readout to routinely assess barrier integrity. This holds still true while some more advanced bioelectrical methods (e.g., impedance spectroscopy) might be more precise in determining information about actual barrier integrity (Günzel et al., 2012; Odijk et al., 2015; Srinivasan et al., 2015; Henry et al., 2017).

As already indicated by the stable TEER values during the course of the 7 h transport experiments, the apparent permeability of fluorescein sodium transported under LCC also did not reveal any significant differences between the perfusable platform and the Transwell® (Figure 6B). Further were the obtained Papp values in this study, in relation to the respective TEER values, consistent with reported Papp values in the literature performed under similar study conditions on Transwell® inserts using Calu-3 cells (Ehrhardt et al., 2002; Fiegel et al., 2003; Grainger et al., 2006; Haghi et al., 2010). To our knowledge, these historical data from Transwells® inserts have not been confirmed using any perfusable, microfluidic or lung-on-chip system so far.

To assess barrier integrity by staining for relevant cellular markers, techniques to perform immunofluorescence staining and subsequent confocal laser scanning microscopy or other imaging methods can be used with the perfusable platform in the same way as for Transwell® inserts. This was demonstrated by the example of the visualization of the proteins Occludin and ZO-1 that are involved in the formation of functional tight junctions (Figure 4). For that purpose, the apical as well as basolateral entity can be separated from the membrane, independently from each other. This procedure allows to flexibly conduct staining and cell fixation methods.

One of the unique features of the perfusable platform as presented here is the possibility to reproducibly deposit pre-metered aerosols from aqueous drug solutions on pulmonary epithelial cells grown at an ALI using a clinically relevant vibrating mesh nebulizer (Aeroneb® Lab). The removable cover glass, that allows to easily open and close the top of the apical compartment, thereby enables the establishment of ALI conditions after cells have been grown to confluency under LCC. The flexibility to open and close the top of the apical compartment is what creates the possibility to connect a vibrating mesh nebulizer to the perfusable platform by using the custom-made deposition chamber. The custom-made deposition chamber presented here was modified to fit the opening of the apical compartment of the perfusable platform, but mostly retains the design as well as dimensions of the device described by Horstmann et al. (2021) to be used with a single 12-well (12 mm) Transwell® insert or a single 24-well. Since we extensively discussed the obtained results and characterized the deposition chamber in the work mentioned above, we limited the characterization for its use with the perfusable platform to the experiments described in Figure 5, to ensure that reproducibility of results is consistent with our previous findings. While reproducibility could be maintained in good approximation (5.6% relative standard deviation (deposition on perfusable

platform) vs. 4.8% relative standard deviation [12-well Transwell®]), the deposition efficiency showed a 4-fold reduction [ $1.06 \pm 0.06\%$  (perfusable platform) vs.  $\sim 4\%$  (12-well Transwell®)]. When all parameters, such as the used nebulizer, the volume to be nebulized in the same concentration and the settling time are kept constant, the deposition efficiency in these chambers is mainly limited by the inner diameter of the outlet (Horstmann et al., 2021). The inner diameter amounts to  $\sim 5$  mm in the version for the perfusable platform and  $\sim 11$  mm for the 12-well Transwell® version. A substantial amount of the aerosol mist generated by the vibrating mesh nebulizer thus deposits on the walls of the deposition chamber and therefore is not channeled through the outlet. A similar concept, also including a vibrating mesh nebulizer and a connected chamber, was recently introduced by Cei et al. (2020) in a dynamic *in vitro* stretch lung model. The outlet of the aerosol chamber in their model was about 20 mm in inner diameter and resulted in an impressive deposition efficiency of about 52% after nebulization.

Although we acknowledge the fact that a deposition efficiency of 1% from the invested dose seems relatively low, the dose delivered per surface area provides better comparability in this case. Based on an equally invested dose of 20  $\mu\text{g}$  (20  $\mu\text{l}$  from a 1 mg/ml solution) which would be nebulized, the delivered dose per surface area would result to  $\sim 0.7 \mu\text{g}/\text{cm}^2$  (perfusable platform, 0.28  $\text{cm}^2$ ; deposition efficiency: 1%),  $\sim 0.8 \mu\text{g}/\text{cm}^2$  (12-well Transwell®, 1.12  $\text{cm}^2$ ; deposition efficiency: 4.8%) or  $\sim 2.2 \mu\text{g}/\text{cm}^2$  [(Cei et al., 2020), 4.67  $\text{cm}^2$ ; deposition efficiency: 52%]. Ultimately, between different devices the dose delivered per surface area should be used for comparison instead of the isolated deposition efficiency. This considerably mitigates the major differences observed when focusing on the isolated deposition efficiency while enhancing comparability, despite the fact that the delivered dose per surface area is still about three times higher in the device of Cei et al. (2020) when compared to the perfusable platform, since less compound is deposited on the walls of the deposition chamber. The foregoing notwithstanding, although the main share of compound is deposited on the walls of the deposition chamber and not reaching the cellular layer, the quantity of compound invested to obtain meaningful *in vitro* results with the devices mentioned before is still substantially lower than that normally required for conducting *in vivo* inhalation studies (Phalen and Mendez 2009).

As demonstrated by the data of Figure 7, transport studies under static as well as perfused conditions were successfully conducted after the reproducible deposition of a pre-metered aerosol from an aqueous fluorescein sodium solution. Interestingly enough, under perfusion we only observed a negligible decrease in TEER values ( $-2\%$ ) after 5 h of transport after ALI deposition of fluorescein sodium under perfusion (Figure 7B) while the difference after 5 h of transport under static conditions amounted to ( $-26\%$ ) when comparing only the mean values. Although this difference was not statistically supported, it could suggest a positive effect of perfusion on barrier properties during the course of the transport experiment in comparison to static conditions, but would need

more thorough investigation. The ability to implement perfusion into the perfusable platform, further allowed the comparison of transport of nebulized fluorescein sodium as a model compound under static conditions to transport under perfusion. Although we also could only observe a slight trend towards higher  $C_{max}$  and lower  $t_{max}$  in case of the fluorescein sodium transported under continuous perfusion, we think that if such experiments would be performed under different parameters (shorter sampling intervals, drugs with different permeation, different flow rates etc.) meaningful insights into the transport of experimental drugs intended for inhalation under physiological relevant conditions could be provided.

We are well aware that the features that make up the perfusable platform are built upon the work of other researchers active in the lung-on-chip field. A similar concept comprising a PDMS-based chip which possessed an open apical compartment, thereby allowing the establishment of ALI conditions, which was also able to provide perfusion and TEER measurements was already introduced by Nalayanda et al., in 2009. Although the authors compared their findings systematically to Transwell® inserts at an ALI using the alveolar type 2-like cell line A549, they did not show the deposition of aerosols. The importance of flow in lung-on-chip systems initially demonstrated by Punde et al. (2015), was used by others to follow the concept of a flowable Transwell® (Blume et al., 2015; Blume et al., 2017; Chandorkar et al., 2017; Bovard et al., 2018; Schimek et al., 2020). The problem with such systems is that the Transwell® inserts where the cells are cultured during perfusion need to be taken out of the sophisticated culture devices that provide the perfusion, and are then transferred to separate culture wells or devices before TEER measurements can be performed or aerosols could be deposited. Especially for substances that are rapidly absorbed after aerosol deposition, such delays could aggravate subsequent analysis. Sophisticated aerosol deposition on cells grown at an ALI was described by Artzy-Schnirman et al. (2019a) for a morphologically inspired acinus-on-chip and also recently for a bronchial bifurcation mimic by Elias-Kirma et al. (2020). Unfortunately, these devices were not characterized in terms of TEER measurements nor in the application of perfusion. In addition, the former device needs sophisticated microfabrication during production and the latter device requires a complex set of devices for the generation of aerosols as well as the related physiologically relevant airflows. Researchers that consider implementing lung-on-chip devices for their research or just want to try out if the physiological features provided by these devices, such as perfusion, could benefit their work, are thus facing considerable difficulties, if they do not have the needed technical expertise in micro-fabrication or the financial resources to invest in commercial platforms. Although companies like Alveolix, CN bio, Emulate, Kirkstall or TissUse introduced innovative lung-on-chip devices or perfusable Transwells®, the material costs of the chips and the related infrastructure needed to operate them could add up to sums which are difficult to finance for academic labs (Kirkstall Ltd 2020; AlveoliX 2021; Chips - TissUse GmbH 2021; CN Bio Innovations 2021; Emulate 2021).

The perfusable platform presented here holds some limitations. The platform is based on a PET membrane, which is cut from Transwell® inserts and known to be rather rigid and bio-inert in comparison to the extracellular matrix found *in vivo* (Humayun et al., 2018). The used PDMS is also known to absorb small, hydrophobic molecules (Toepke and Beebe 2006). This technical characteristic can be corrected though, by pre-equilibrating the devices or adjusting for the loss of substance (Jimenez-Valdes et al., 2020). Depending on the skill of the operator but also on the used peristaltic pump, results obtained from the perfusable platform are in the low- to mid-throughput range depending on the extent of the intended studies.

## CONCLUSION

The minimalistic design of the presented perfusable platform “PerfuPul” allows its production by non-experts in most lab environments without the need for specialized equipment. Furthermore, the platform combines TEER measurements, aerosol deposition as well as the implementation of perfusion as a physiological relevant clearance mechanism in a single device that matches the design as well as the quality of results known from Transwell® inserts. The open apical entity not only allows the establishment of ALI conditions but could be also utilized for working with cutting-edge techniques such as 3D bio printing. Moreover, the easy access to the basolateral compartment would permit co-culture studies, for instance, by also growing endothelial cells on the basal side of the membrane. Taking all of these factors in consideration, we are convinced that this perfusable platform will enable the development of novel pulmonary *in vitro* models especially to study long-term diseases, such as e.g., bacterial lung infections and their treatment by aerosolized drugs and nanoscale carriers thereof.

## DATA AVAILABILITY STATEMENT

The raw data supporting the conclusions of this article will be made available by the authors, without undue reservation.

## AUTHOR CONTRIBUTIONS

PC had the idea for the perfusable platform, designed, planned as well as performed the experiments and wrote the manuscript. AD helped in the creation of the custom-made electrode and helped in improving the molds. MA helped in the creation of the Supplementary Information. JS, AA-S helped in planning the concept as well as the experiments for the perfusable platform. They further helped to write and enhance the manuscript. NS-D helped in revising the manuscript. C-ML shares the idea for the perfusable platform and helped in planning the experiments. He also helped writing and enhancing the manuscript.

## FUNDING

PC, AA-S, and JS were financially supported by the German-Israeli Foundation for Scientific Research and Development (GIF) (Grant: I-101-409.8-2015).

## ACKNOWLEDGMENTS

We would like to express our sincere thanks to Rudolf Richter (Workshop, Department of Physical Chemistry and Didactics of Chemistry, Saarland University) for his

## REFERENCES

- Ainslie, G. R., Davis, M., Ewart, L., Lieberman, L. A., Rowlands, D. J., Thorley, A. J., et al. (2019). Microphysiological Lung Models to Evaluate the Safety of New Pharmaceutical Modalities: a Biopharmaceutical Perspective. *Lab. Chip* 19, 3152–3161. doi:10.1039/c9lc00492k
- AlveoliX (2021). *Information | the Latest News about Our Projects and Our Team - AlveoliX*. Available at: <https://www.alveolix.com/information/> (Accessed March 30, 2021).
- Artzy-Schnirman, A., Hobi, N., Schneider-Daum, N., Guenat, O. T., Lehr, C.-M., and Sznitman, J. (2019a). Advanced *In Vitro* Lung-On-Chip Platforms for Inhalation Assays: From prospect to Pipeline. *Eur. J. Pharm. Biopharm.* 144, 11–17. doi:10.1016/j.ejpb.2019.09.006
- Artzy-Schnirman, A., Zidan, H., Elias-Kirma, S., Ben-Porat, L., Tenenbaum-Katan, J., Carius, P., et al. (2019b). Capturing the Onset of Bacterial Pulmonary Infection in Acini-On-Chips. *Adv. Biosys.* 3, 1900026. doi:10.1002/adbi.201900026
- Artzy-Schnirman, A., Lehr, C.-M., and Sznitman, J. (2020). Advancing Human *In Vitro* Pulmonary Disease Models in Preclinical Research: Opportunities for Lung-On-Chips. *Expert Opin. Drug Deliv.* 17, 621–625. doi:10.1080/17425247.2020.1738380
- Barnes, P. J., Bonini, S., Seeger, W., Belvisi, M. G., Ward, B., and Holmes, A. (2015). Barriers to New Drug Development in Respiratory Disease. *Eur. Respir. J.* 45, 1197–1207. doi:10.1183/09031936.00007915
- Blume, C., Reale, R., Held, M., Millar, T. M., Collins, J. E., Davies, D. E., et al. (2015). Temporal Monitoring of Differentiated Human Airway Epithelial Cells Using Microfluidics. *PLoS One* 10, e0139872. doi:10.1371/journal.pone.0139872
- Blume, C., Reale, R., Held, M., Loxham, M., Millar, T. M., Collins, J. E., et al. (2017). Cellular Crosstalk between Airway Epithelial and Endothelial Cells Regulates Barrier Functions during Exposure to Double-Stranded RNA. *Inflamm. Dis.* 5, 45–56. doi:10.1002/iid3.139
- Bovard, D., Sandoz, A., Luettich, K., Frentzel, S., Iskandar, A., Marescotti, D., et al. (2018). A Lung/liver-On-A-Chip Platform for Acute and Chronic Toxicity Studies. *Lab. Chip* 18, 3814–3829. doi:10.1039/c8lc01029c
- Carius, P., Horstmann, J. C., Souza Carvalho-Wodarz, C. de., and Lehr, C.-M. (2021). “Disease Models: Lung Models for Testing Drugs against Inflammation and Infection,” in *Organotypic Models in Drug Development*. Editors M. Schäfer-Korting, S. Stuchi Maria-Engler, and R. Landsiedel (Cham: Springer International Publishing), 157–186.
- Cei, D., Doryab, A., Lenz, A. G., Schröppel, A., Mayer, P., Burgstaller, G., et al. (2020). Development of a Dynamic *In Vitro* Stretch Model of the Alveolar Interface with Aerosol Delivery. *Biotechnol. Bioeng.* 118, 690–702. doi:10.1002/bit.27600
- Chandorkar, P., Posch, W., Zaderer, V., Blatzer, M., Steger, M., Ammann, C. G., et al. (2017). Fast-track Development of an *In Vitro* 3D Lung/immune Cell Model to Study Aspergillus Infections. *Sci. Rep.* 7, 11644. doi:10.1038/s41598-017-11271-4
- Chips - TissUse GmbH (2021). HUMIMIC Chips – Superpowers for Superb Insights. Berlin, Germany: TissUse GmbH. Available at: <https://www.tissuse.com/en/humimic/chips/> (Accessed March 29, 2021).

help in the technical realization and construction of the deposition device. In addition we would like to cordially thank Petra König and Jana Westhues for their help in routine cell culture.

## SUPPLEMENTARY MATERIAL

The Supplementary Material for this article can be found online at: <https://www.frontiersin.org/articles/10.3389/fbioe.2021.743236/full#supplementary-material>

- Chueh, B.-h., Huh, D., Kyrtos, C. R., Houssin, T., Futai, N., and Takayama, S. (2007). Leakage-free Bonding of Porous Membranes into Layered Microfluidic Array Systems. *Anal. Chem.* 79, 3504–3508. doi:10.1021/ac062118p
- CN Bio Innovations (2021). Barrier Models. Available at: <https://cn-bio.com/barrier-models/> (Accessed March 29, 2021).
- Douville, N. J., Tung, Y.-C., Li, R., Wang, J. D., El-Sayed, M. E. H., and Takayama, S. (2010). Fabrication of Two-Layered Channel System with Embedded Electrodes to Measure Resistance across Epithelial and Endothelial Barriers. *Anal. Chem.* 82, 2505–2511. doi:10.1021/ac9029345
- Ehrhardt, C., Fiegel, J., Fuchs, S., Abu-Dahab, R., Schaefer, U. F., Hanes, J., et al. (2002). Drug Absorption by the Respiratory Mucosa: Cell Culture Models and Particulate Drug Carriers. *J. Aerosol Med.* 15, 131–139. doi:10.1089/089426802320282257
- Ehrmann, S., Schmid, O., Darquenne, C., Rothen-Rutishauser, B., Sznitman, J., Yang, L., et al. (2020). Innovative Preclinical Models for Pulmonary Drug Delivery Research. *Expert Opin. Drug Deliv.* 17, 463–478. doi:10.1080/17425247.2020.1730807
- Elias-Kirma, S., Artzy-Schnirman, A., Das, P., Heller-Algazi, M., Korin, N., and Sznitman, J. (2020). In Situ-Like Aerosol Inhalation Exposure for Cytotoxicity Assessment Using Airway-On-Chips Platforms. *Front. Bioeng. Biotechnol.* 8, 91. doi:10.3389/fbioe.2020.00091
- Emulate (2021). Lung-Chip — Emulate. Available at: <https://www.emulatebio.com/lung-chip> (Accessed March 29, 2021).
- European Commission Joint Research Centre (2021). *Establishing the Scientific Validity of Complex in Vitro Models: Results of a EURL ECVAM Survey*. Available at: <https://publications.jrc.ec.europa.eu/repository/handle/JRC122394> (Accessed May 18, 2021).
- Ferrell, N., Desai, R. R., Fleischman, A. J., Roy, S., Humes, H. D., and Fissell, W. H. (2010). A Microfluidic Bioreactor with Integrated Transepithelial Electrical Resistance (TEER) Measurement Electrodes for Evaluation of Renal Epithelial Cells. *Biotechnol. Bioeng.* 107, 707–716. doi:10.1002/bit.22835
- Fiegel, J., Ehrhardt, C., Schaefer, U. F., Lehr, C.-M., and Hanes, J. (2003). Large Porous Particle Impingement on Lung Epithelial Cell Monolayers—Toward Improved Particle Characterization in the Lung. *Pharm. Res.* 20, 788–796. doi:10.1023/a:1023441804464
- Gordon, S., Daneshian, M., Bouwstra, J., Caloni, F., Constant, S., Davies, D. E., et al. (2015). Non-animal Models of Epithelial Barriers (Skin, Intestine and Lung) in Research, Industrial Applications and Regulatory Toxicology. *ALTEX* 32, 327–378. doi:10.14573/altex.1510051
- Grainger, C. I., Greenwell, L. L., Lockley, D. J., Martin, G. P., and Forbes, B. (2006). Culture of Calu-3 Cells at the Air Interface Provides a Representative Model of the Airway Epithelial Barrier. *Pharm. Res.* 23, 1482–1490. doi:10.1007/s11095-006-0255-0
- Griep, L. M., Wolbers, F., de Wagenaar, B., ter Braak, P. M., Weksler, B. B., Romero, I. A., et al. (2013). BBB on Chip: Microfluidic Platform to Mechanically and Biochemically Modulate Blood-Brain Barrier Function. *Biomed. Microdevices* 15, 145–150. doi:10.1007/s10544-012-9699-7
- Günzel, D., Zakrzewski, S. S., Schmid, T., Pangalos, M., Wiedenhoef, J., Blasse, C., et al. (2012). From TER to Trans- and Paracellular Resistance: Lessons from Impedance Spectroscopy. *Ann. N. Y. Acad. Sci.* 1257, 142–151. doi:10.1111/j.1749-6632.2012.06540.x



# „PerfuPul – A Versatile Perfusable Platform to Assess Permeability and Barrier Function of Air Exposed Pulmonary Epithelia“

Carius et al.

Perfusable Platform for Pulmonary Epithelia

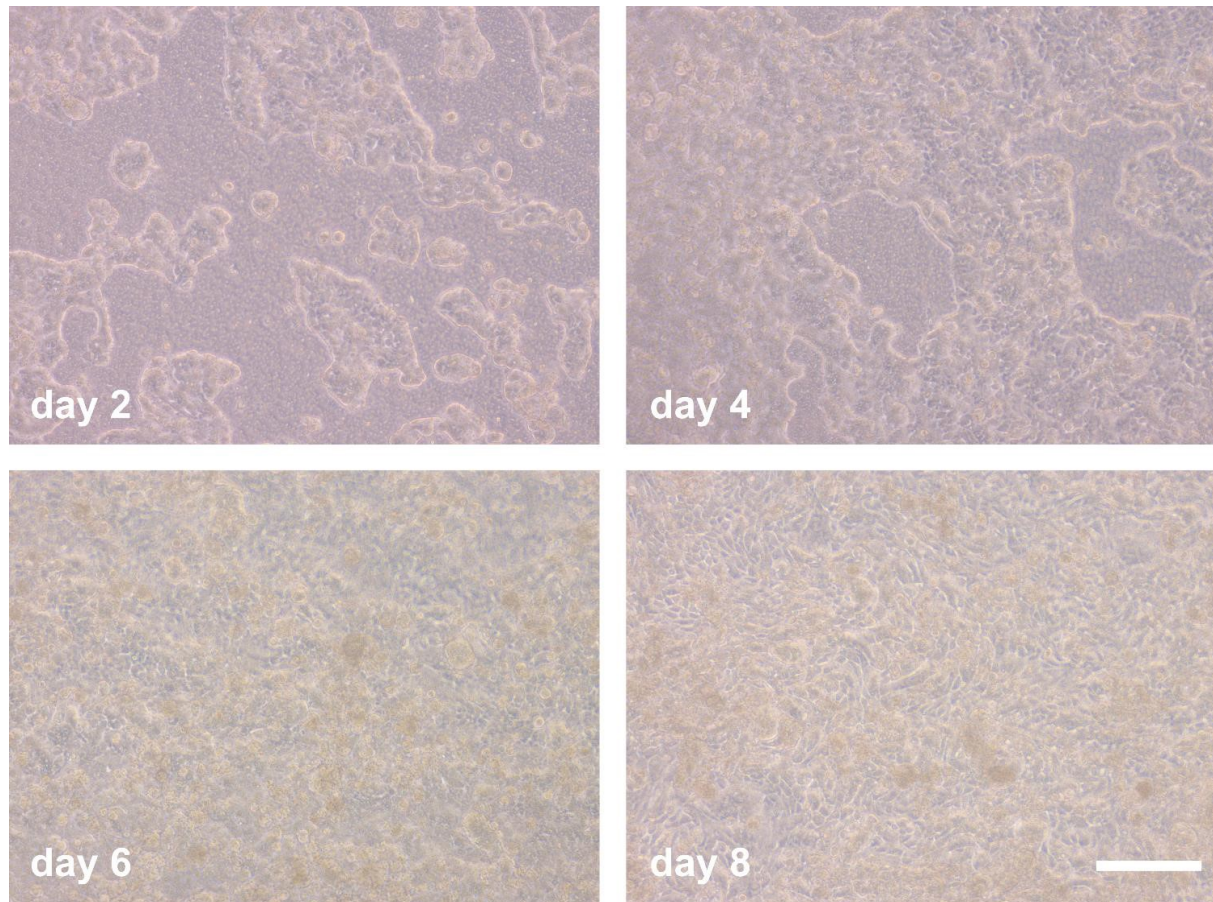
- Haghi, M., Young, P. M., Traini, D., Jaiswal, R., Gong, J., and Bebawy, M. (2010). Time- and Passage-dependent Characteristics of a Calu-3 Respiratory Epithelial Cell Model. *Drug Dev. Ind. Pharm.* 36, 1207–1214. doi:10.3109/03639041003695113
- Henry, O. Y. F., Villenave, R., Cronce, M. J., Leineweber, W. D., Benz, M. A., and Ingber, D. E. (2017). Organs-on-chips with Integrated Electrodes for Trans-epithelial Electrical Resistance (TEER) Measurements of Human Epithelial Barrier Function. *Lab. Chip* 17, 2264–2271. doi:10.1039/c7lc00155j
- Hittinger, M., Juntke, J., Kletting, S., Schneider-Daum, N., de Souza Carvalho, C., and Lehr, C.-M. (2015). Preclinical Safety and Efficacy Models for Pulmonary Drug Delivery of Antimicrobials with Focus on *In Vitro* Models. *Adv. Drug Deliv. Rev.* 85, 44–56. doi:10.1016/j.addr.2014.10.011
- Hittinger, M., Schneider-Daum, N., and Lehr, C.-M. (2017). Cell and Tissue-Based *In Vitro* Models for Improving the Development of Oral Inhalation Drug Products. *Eur. J. Pharm. Biopharm.* 118, 73–78. doi:10.1016/j.ejpb.2017.02.019
- Horstmann, J. C., Thorn, C. R., Carius, P., Graef, F., Murgia, X., de Souza Carvalho-Wodarz, C., et al. (2021). A Custom-Made Device for Reproducibly Depositing Pre-metered Doses of Nebulized Drugs on Pulmonary Cells *In Vitro*. *Front. Bieng. Biotechnol.* 9, 643491. doi:10.3389/fbioe.2021.643491
- Huang, D., Liu, T., Liao, J., Maharjan, S., Xie, X., Pérez, M., et al. (2021). Reversed-engineered Human Alveolar Lung-On-A-Chip Model. *Proc. Natl. Acad. Sci. USA* 118, e2016146118. doi:10.1073/pnas.2016146118
- Huh, D., Matthews, B. D., Mammoto, A., Montoya-Zavala, M., Hsin, H. Y., and Ingber, D. E. (2010). Reconstituting Organ-Level Lung Functions on a Chip. *Science* 328, 1662–1668. doi:10.1126/science.1188302
- Humayun, M., Chow, C.-W., and Young, E. W. K. (2018). Microfluidic Lung Airway-On-A-Chip with Arrayable Suspended Gels for Studying Epithelial and Smooth Muscle Cell Interactions. *Lab. Chip* 18, 1298–1309. doi:10.1039/c7lc01357d
- Jimenez-Valdes, R. J., Can, U. I., Niemeyer, B. F., and Benam, K. H. (2020). Where We Stand: Lung Organotypic Living Systems that Emulate Human-Relevant Host-Environment/Pathogen Interactions. *Front. Bieng. Biotechnol.* 8, 989. doi:10.3389/fbioe.2020.00989
- Junaid, A., Mashaghi, A., Hankemeier, T., and Vulto, P. (2017). An End-User Perspective on Organ-On-A-Chip: Assays and Usability Aspects. *Curr. Opin. Biomed. Eng.* 1, 15–22. doi:10.1016/j.cobme.2017.02.002
- Kim, H. J., Huh, D., Hamilton, G., and Ingber, D. E. (2012). Human Gut-On-A-Chip Inhabited by Microbial flora that Experiences Intestinal Peristalsis-like Motions and Flow. *Lab. Chip* 12, 2165–2174. doi:10.1039/c2lc40074j
- Kirkstall Ltd (2020). *Quasi Vivo® | Commercially Available Organ-On-A-Chip Technology*. York, United Kingdom: Kirkstall Ltd. Available at: <https://www.kirkstall.com/> (Accessed March 30, 2021).
- Lacroix, G., Koch, W., Ritter, D., Gutleb, A. C., Larsen, S. T., Loret, T., et al. (2018). Air-Liquid Interface *In Vitro* Models for Respiratory Toxicology Research: Consensus Workshop and Recommendations. *Appl. Vitro Toxicol.* 4, 91–106. doi:10.1089/avt.2017.0034
- Lorenz, A., Pawar, V., Häussler, S., and Weiss, S. (2016). Insights into Host-Pathogen Interactions from State-Of-The-Art Animal Models of respiratory Pseudomonas Aeruginosa Infections. *FEBS Lett.* 590, 3941–3959. doi:10.1002/1873-3468.12454
- Nalayanda, D. D., Puleo, C., Fulton, W. B., Sharpe, L. M., Wang, T.-H., and Abdullah, F. (2009). An Open-Access Microfluidic Model for Lung-specific Functional Studies at an Air-Liquid Interface. *Biomed. Microdevices* 11, 1081–1089. doi:10.1007/s10544-009-9325-5
- Odijk, M., van der Meer, A. D., Levner, D., Kim, H. J., van der Helm, M. W., Segerink, L. I., et al. (2015). Measuring Direct Current Trans-epithelial Electrical Resistance in Organ-On-A-Chip Microsystems. *Lab. Chip* 15, 745–752. doi:10.1039/c4lc01219d
- Phalen, R. F., and Mendez, L. B. (2009). Dosimetry Considerations for Animal Aerosol Inhalation Studies. *Biomarkers* 14 (Suppl. 1), 63–66. doi:10.1080/13547500902965468
- Punde, T. H., Wu, W.-H., Lien, P.-C., Chang, Y.-L., Kuo, P.-H., Chang, M. D.-T., et al. (2015). A Biologically Inspired Lung-On-A-Chip Device for the Study of Protein-Induced Lung Inflammation. *Integr. Biol. (Camb)* 7, 162–169. doi:10.1039/c4ib00239c
- Rootare, H. M., and Powers, J. M. (1977). Preparation of Ag/AgCl Electrodes. *J. Biomed. Mater. Res.* 11, 633–635. doi:10.1002/jbm.820110416
- Schimek, K., Frentzel, S., Luettich, K., Bovard, D., Rüttschle, I., Boden, L., et al. (2020). Human Multi-Organ Chip Co-culture of Bronchial Lung Culture and Liver Spheroids for Substance Exposure Studies. *Sci. Rep.* 10, 7865. doi:10.1038/s41598-020-64219-6
- Schindelin, J., Arganda-Carreras, I., Frise, E., Kaynig, V., Longair, M., Pietzsch, T., et al. (2012). Fiji: an Open-Source Platform for Biological-Image Analysis. *Nat. Methods* 9, 676–682. doi:10.1038/nmeth.2019
- Srinivasan, B., Kolli, A. R., Esch, M. B., Abaci, H. E., Shuler, M. L., and Hickman, J. J. (2015). TEER Measurement Techniques for *In Vitro* Barrier Model Systems. *J. Lab. Autom.* 20, 107–126. doi:10.1177/2211068214561025
- Stucki, A. O., Stucki, J. D., Hall, S. R. R., Felder, M., Mermoud, Y., Schmid, R. A., et al. (2015). A Lung-On-A-Chip Array with an Integrated Bio-Inspired Respiration Mechanism. *Lab. Chip* 15, 1302–1310. doi:10.1039/c4lc01252f
- Tenenbaum-Katan, J., Artzy-Schnirman, A., Fishler, R., Korin, N., and Sznitman, J. (2018). Biomimetics of the Pulmonary Environment *In Vitro*: A Microfluidics Perspective. *Biomicrofluidics* 12, 042209. doi:10.1063/1.5023034
- Thompson, C. L., Fu, S., Heywood, H. K., Knight, M. M., and Thorpe, S. D. (2020). Mechanical Stimulation: A Crucial Element of Organ-On-Chip Models. *Front. Bieng. Biotechnol.* 8, 602646. doi:10.3389/fbioe.2020.602646
- Toepke, M. W., and Beebe, D. J. (2006). PDMS Absorption of Small Molecules and Consequences in Microfluidic Applications. *Lab. Chip* 6, 1484–1486. doi:10.1039/B612140C
- Wilson, A. P., and Richards, S. A. (2000). Consuming and Grouping: Recourse-Mediated Animal Aggregation. *Ecol. Lett.* 3, 175–180. doi:10.1046/j.1461-0248.2000.00135.x

**Conflict of Interest:** The authors declare that the research was conducted in the absence of any commercial or financial relationships that could be construed as a potential conflict of interest.

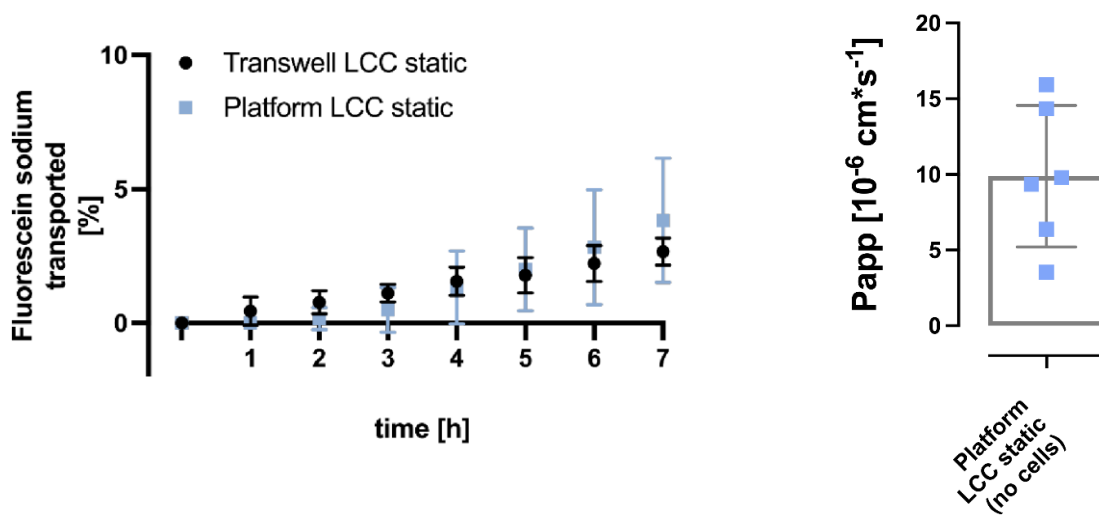
**Publisher's Note:** All claims expressed in this article are solely those of the authors and do not necessarily represent those of their affiliated organizations, or those of the publisher, the editors and the reviewers. Any product that may be evaluated in this article, or claim that may be made by its manufacturer, is not guaranteed or endorsed by the publisher.

Copyright © 2021 Carius, Dubois, Ajdarirad, Artzy-Schnirman, Sznitman, Schneider-Daum and Lehr. This is an open-access article distributed under the terms of the Creative Commons Attribution License (CC BY). The use, distribution or reproduction in other forums is permitted, provided the original author(s) and the copyright owner(s) are credited and that the original publication in this journal is cited, in accordance with accepted academic practice. No use, distribution or reproduction is permitted which does not comply with these terms.

*Supplementary Material*



**Supplementary Figure 1:** Representative micrograph showing undisturbed growth of Calu-3 cells inside the perfusable platform. Calu-3 cells (10.000 cells/cm<sup>2</sup> seeded) become confluent between day 6 and day 8 of culture. Calu-3 cells were cultured under liquid covered conditions (LCC) and fed every second day. (scale bar : 200  $\mu$ m)



**Supplementary Figure 2:** Transport studies were performed on Calu-3 cells (LCC: d17-d19). **Left:** The transported Fluorescein sodium derived from the concentration within the acceptor compartment at sampling time points is cumulatively displayed in relation [%] to the concentration within the acceptor compartment at the beginning of the experiment ( $2.5 \mu\text{g/ml}$ , (dose: 500 ng on Transwell; 212 ng on platform)). **Right:** Apparent permeability (Papp) of Fluorescein sodium applied as a solution to perfusable platforms without any cells. Papp was determined after the transport study (100 min.). Data represent mean  $\pm$  S.D.; Transwell LCC: n=9, Platform LCC & Platform LCC (no cells): n=6 out of 3 independent experiments.

The following pages contain all information needed to reproduce the platform as well as the described experiments.

# „PerfuPul – A Versatile Perfusable Platform to Assess Permeability and Barrier Function of Air Exposed Pulmonary Epithelia“

**Supplementary Table 1:** Parts and devices needed for the production of the perfusable platform “PerfuPul” as well as other accessories.

	Name	Specifications	Item number	Supplier
Devices needed	Desiccator	not specified	not specified	not specified
	Lab oven	Temperature: 100°C	not specified	not specified
	(optional) Spin coater	should fit a 76x53 mm glass slide; min. 3000 rpm; 100 rpm/s	not specified	not specified
Custom-made electrode	RJ14 (6P4C*) telephone cable	*: 6 pins, 4 connected to stranded wires	not specified	not specified
	Silver wire	0.5 mm outer diameter	2-3309	NeoLab
	Shrinkage tubing	not specified	not specified	not specified
	Soldering iron + soldering tin	not specified	not specified	not specified
Perfusable platform	PDMS preparation			
	Plastic weighing dish	not specified	not specified	not specified
	Polydimethylsiloxane (PDMS)	Sylgard 184 Elastomer Kit (curing agent + base)	1673921	Dow Corning
	Mold filling			
	Needle (channel negative)	Sterican, size 12 (0.7 x 40 mm)	4657624	B. Braun
	Entity production			
	Scissors	not specified	not specified	not specified
	6 mm Biopsy punch	6 mm diameter	BP-60F	Kai medical
	Adhesive tape	Scotch® Magic™ 810 matt	7100026960	Scotch®
	Blunt needle	Sterican blunt, 21 G, 7/8 inch (0.8 x 22 mm)	9180109	B. Braun
	Platform assembly			
	Microscopy slide (76x52 mm)	Microscope slide 76x52x1 mm	1100420	Paul Marienfeld GmbH & Co. KG
	Transwell insert	24 mm, 0.4 µm pore size	3450	Corning
	Scalpel	not specified	not specified	not specified
	Cover glass (24x32 mm)	cover glass 24x32 mm	H877	Carl Roth GmbH
	Tube assembly			
	Tubing	flexible 22 G Polyethylene tubing	BTPE-50	Instech
	2 ml reaction tube	not specified	not specified	not specified
	Cell culture			
	Petri dish	145x20 mm	6052085	Greiner Bio-One
	Perfusion setup			
	15 ml reaction tube	not specified	not specified	(e.g. Falcon®)
	Sterile filter cap	from T25 cm <sup>2</sup> cell culture flask	C6481-200EA	Greiner Bio-One

## 1 Custom-made electrode

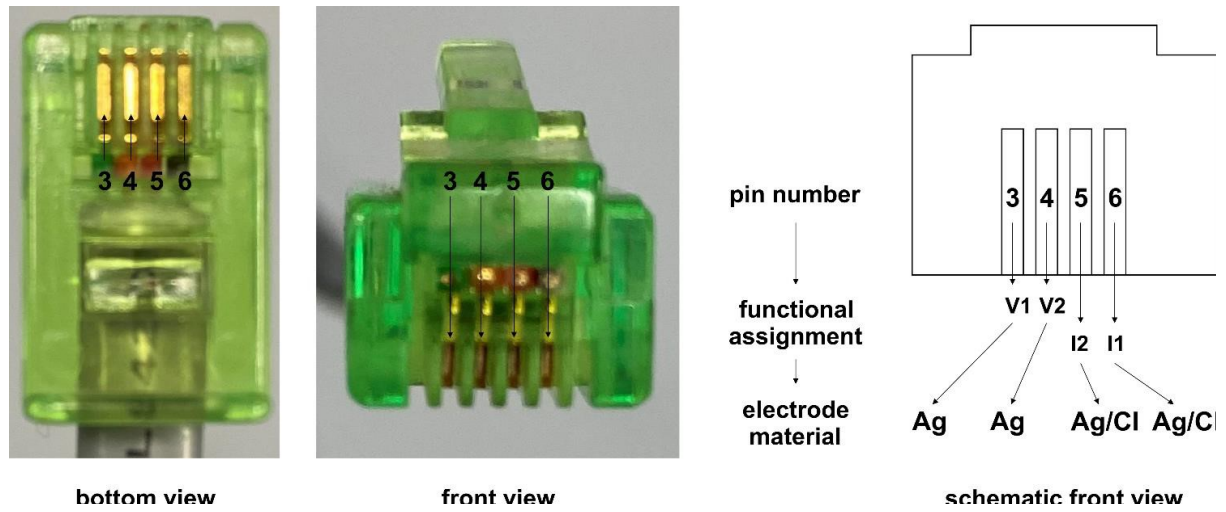
**Materials needed:** RJ14 (6P4C) telephone cable, silver wire (length; ~ 7 cm), shrinkage tubing (4 pieces), soldering iron, soldering tin

1. Cut a RJ14 cable to a length of ~ 60 cm.
2. Cut a silver wire (0.5 mm diameter; neoLab, 2-3309) into 4 pieces with a length of 15 mm per piece.
3. Coat two of the silver wire pieces with chloride using the following method:

Rootare, H. M.; Powers, J. M. (1977): Preparation of Ag/AgCl electrodes. In *Journal of biomedical materials research* 11 (4), pp. 633–635. DOI: 10.1002/jbm.820110416.

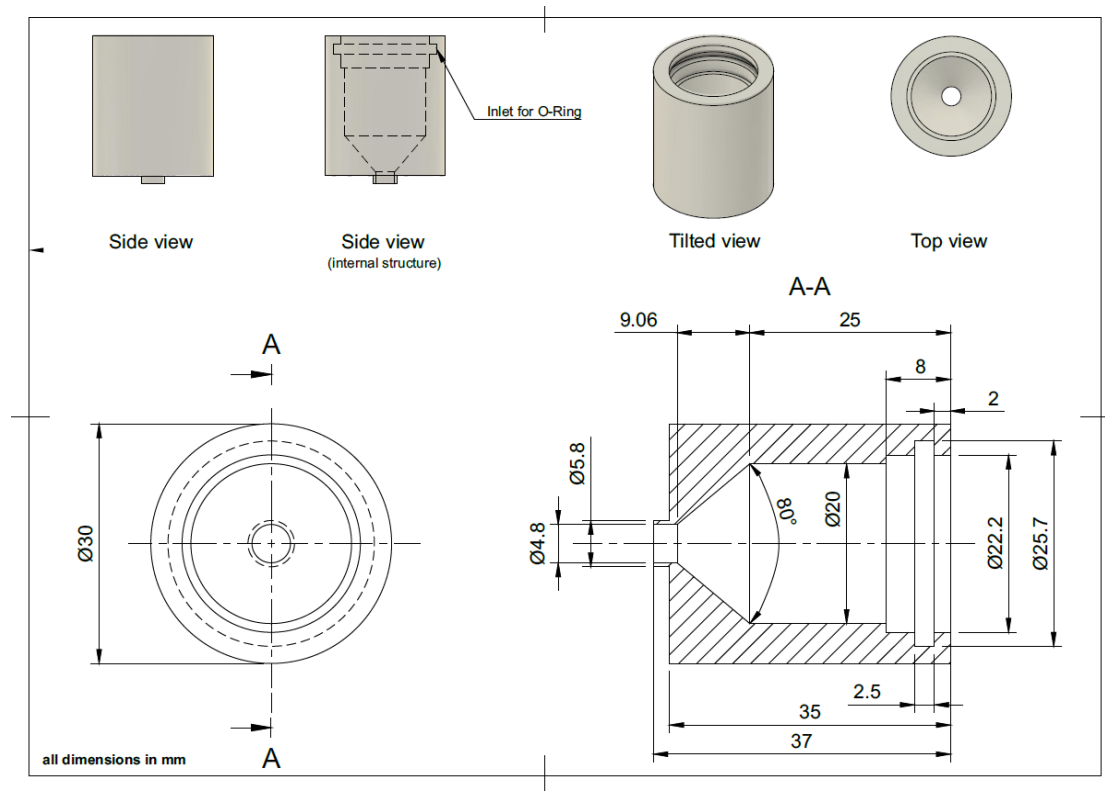
4. **(optional)** Pre-coated electrodes are also available commercially.
5. Solder one of the uncoated silver wires (Ag) to the stranded wire of the RJ 14 cable that connects to pin 3 and the other uncoated silver wire to the stranded wire that connects to pin 4. Then solder one of the coated silver (Ag/Cl) wires to the stranded wire of the RJ 14 cable that connects to pin 5 and the other coated silver wire to the stranded wire that connects to pin 6 (Supplementary Figure 3).
6. Insulate each junction where an electrode is connected to a stranded wire with a shrinkage tube.
7. Before first use, equilibrate the custom-made electrode in 100 mM KCl (in H<sub>2</sub>O) overnight connected to a switched off EVOM2 in “Ohm” mode connected to a charger. This stabilizes the electrical potential of the electrode.

The custom-made electrode needs to be disinfected with 70% Isopropanol (in sterile MilliQ water, (v/v)) for 5 min and then fully dried before each measurement.



**Supplementary Figure 3:** Pin assignment scheme of the RJ14 (6P4C) telephone cable for the custom made electrode.

## 2 Deposition chamber

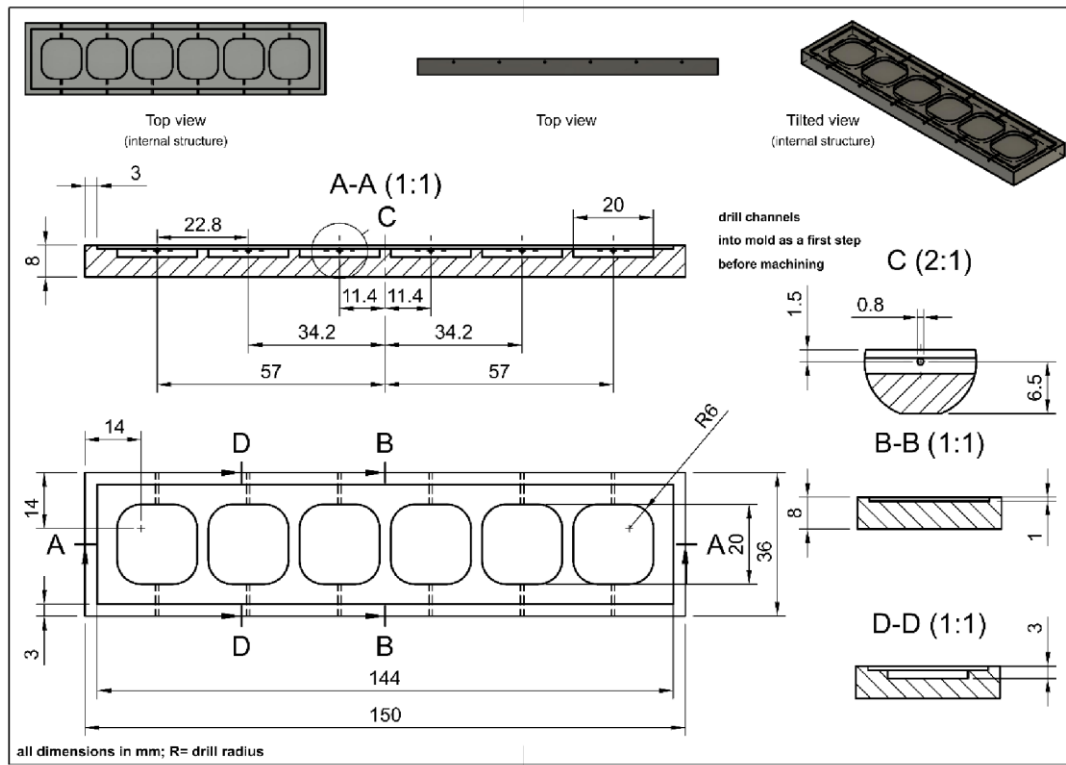


**Supplementary Figure 4:** Technical drawing of the deposition chamber. After the deposition chamber has been created, an O-Ring needs to be inserted into the inlet. This step is shown in the side view with the included internal structure. The files to 3D print the deposition chamber (.dwg/.stl), as well as the unscaled .pdf file of the technical drawing can be found in the download section of the supplementary information.



### 3 Perfusable platform “PerfuPul”

#### 3.1 Design of the molds



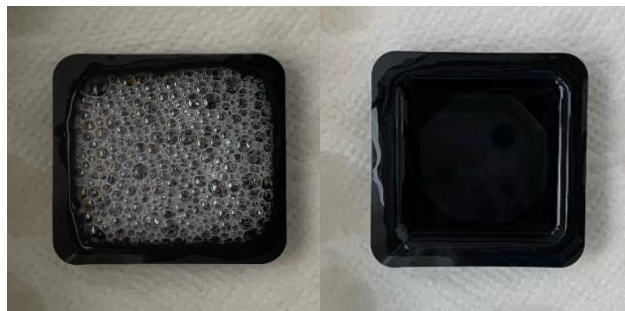
**Supplementary Figure 5:** Technical drawing of the mold (mold B) for creating the basolateral entities. It is important to note that the holes that later form the channels should be already drilled in the blank material, before the indentations are machined. In case of the mold to create the apical entities (mold A), the channel drilling step is just omitted. The files to 3D print the molds (A+B; .dwg/.stl), as well as the unscaled .pdf file of the technical drawing can be found in the download section of the supplementary information.



### 3.2 PDMS preparation

**Materials needed:** weighing dish (plastic), PDMS base + curing agent, desiccator, oven

1. Pre-heat oven to 100°C.
2. In a weighing dish add curing agent to Polydimethylsiloxane (PDMS) in a ratio of 1:10 (1:10 (w/w); curing agent/base) and mix thoroughly (> 2 min).
3. Carefully transfer mixed PDMS to a desiccator and degas. If big bubbles form during degassing (**Supplementary Figure 6**, left), ventilate and repeat desiccation process. Degas until PDMS-mixture displays a smooth air bubble free surface (**Supplementary Figure 6**, right) (~ 20 min).

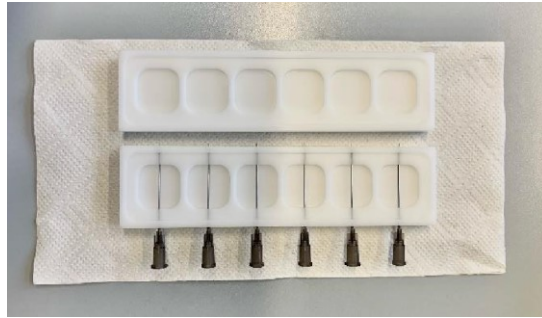


**Supplementary Figure 6:** Bubble creation during degassing of PDMS (left). After degassing a smooth bubble free surface should be obtained (right).

### 3.3 Mold filling

**Materials needed:** Needle (channel negative), mold A, mold B, oven, desiccator, freshly degassed PDMS (at least 25 g)

4. Insert eight needles (channel negative) in mold B that contains the inlets (**Supplementary Figure 7**, bottom). These entities will later form the basal part of the perfusable platform.



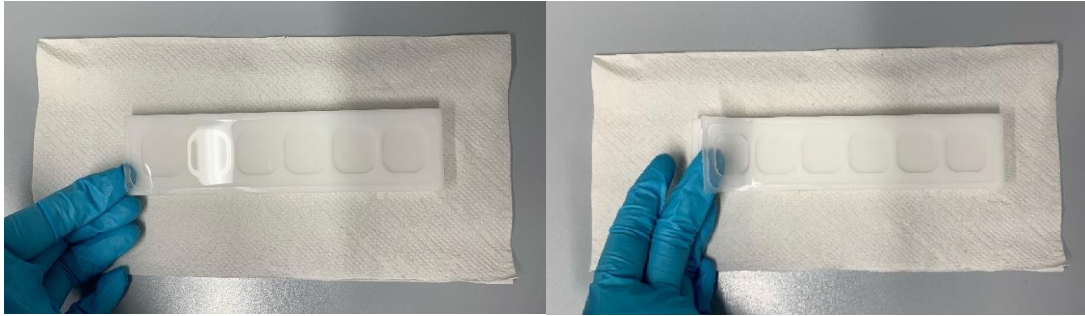
**Supplementary Figure 7:** top: mold A (designated for apical entities); bottom: mold B (designated for the basolateral entities). Use one needle to connect two perpendicular oriented channels.

5. Fill molds with freshly degassed PDMS using 8.5 g for mold B (basolateral entities, containing needles) and 9 g for mold A (apical entities).
6. After checking if molds are filled evenly and in their entirety, carefully transfer to desiccator and degas again until air bubble free (~ 20 min), opening the desiccator carefully if needed to insert air when strong bubble formation is observed.
7. Insert in preheated oven (100°C, 60 min).
8. Remove molds from oven and let them cool down completely before removing the previously inserted needles. Remove needles in a steady motion.

### 3.4 Entity production

**Materials needed:** scissors, biopsy punch, adhesive tape, blunt needle

9. Cautiously elevate the thin layer of polymerized PDMS surrounding the entities (Supplementary Figure 8, left) before carefully detaching it from the mold (Supplementary Figure 8, right).



**Supplementary Figure 8:** Cautiously elevate the thin layer of polymerized PDMS surrounding the entities (a) before carefully detaching the PDMS from the mold (b).

10. Cut away protruding PDMS that surrounds the entities using scissors (Supplementary Figure 9).



**Supplementary Figure 9:** Remove protruding PDMS that surrounds the entities with scissors.

11. Punch a centred hole using a 6 mm biopsy punch into the center of each entity.
12. Remove any PDMS residues that might block the channels of the basal entity with a blunt needle.
13. Use a stripe of adhesive tape to remove any leftover PDMS cuttings or dirt from the entities. Make sure to repeat until entity surfaces are clean.

### 3.5 Platform assembly

**Materials needed:** apical entities, basolateral entities, freshly degassed PDMS (at least 5 g), microscopy slide (76x52 mm), Transwells insert, scalpel, microscopy slides (24x32 mm), desiccator, oven, spin coater (if available)

Spin coater method (if no spin-coater is available, see step 16):

14. Clean microscopy slide (76x52 mm) (fits maximum 8 entities) by rinsing them with 100% Isopropanol first and afterwards with deionized water. Repeat this step twice. Check whether slides are clean, if not repeat. Dry slides using compressed air.
15. Cast a spot of freshly degassed PDMS (roughly 3 cm in diameter) onto one freshly dried microscopy slide (76x52 mm) and place it on a spin-coater (3000 rpm; 100 rpm/s; 60 s). Continue with **step 17**.

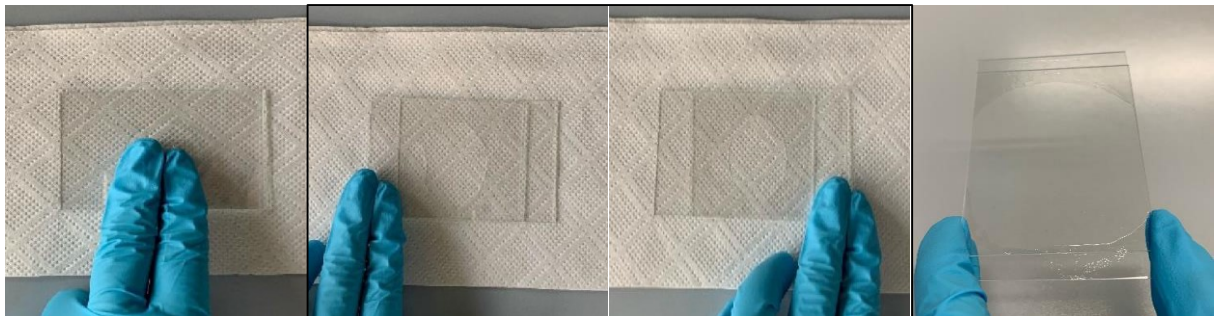
**16. Alternatively, in case no spin-coater is available:**

Add 150 mg of freshly degassed PDMS in-between two freshly cleaned microscope slides (step 14) and first apply firm pressure (

**Supplementary Figure 10**, left). Then slide them back and forth (

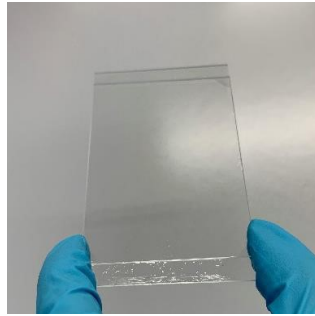
**Supplementary Figure 10**, center: left + right) until PDMS is well-distributed (

**Supplementary Figure 10**, right).



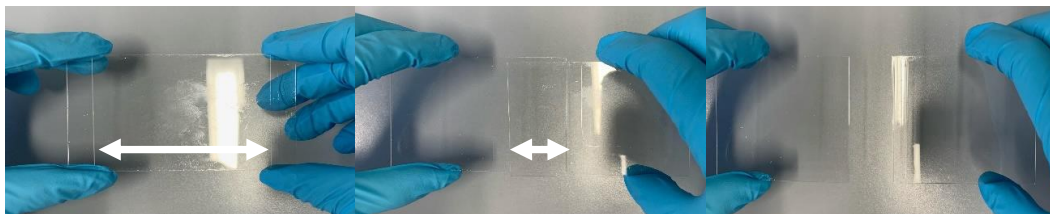
**Supplementary Figure 10:** First apply pressure on top of microscopy slides (76x52 mm) layered with PDMS (left), then slide them back and forth to distribute PDMS layered in-between (center: left + right). Apply firm but controlled pressure to ensure that the slides do not completely overlap and the PDMS is spread equally (right).

- Place microscopy slides (76x52 mm) in such a way into the desiccator that the slides do not overlap congruent. Degas in two intervals (2 x 10 min) and ventilate in-between. Air bubbles will not disappear completely but PDMS will be distributed more regularly (**Supplementary Figure 11**).

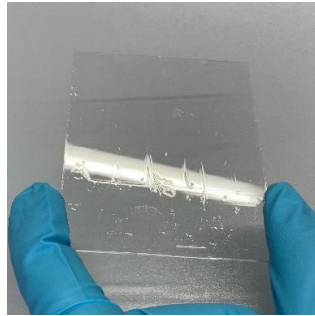


**Supplementary Figure 11:** More regular distributed PDMS-spot after first cycle of spreading and degassing.

- Remove microscopy slides (76x52 mm) from desiccator and separate them via a bilateral pulling motion, resulting in each of the separated slides coated with PDMS (**Supplementary Figure 12**, right). This step distributes the PDMS even more regular on both glass slides. Trapped air bubbles will also be eliminated, which can form unwanted streaks (**Supplementary Figure 13**).

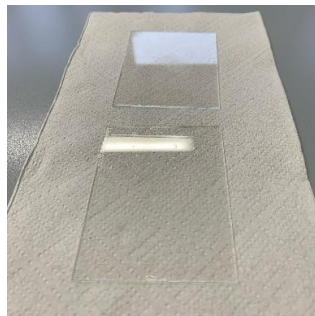


**Supplementary Figure 12:** Separation of microscopy slides (76 x 53 mm) by pulling them apart (left to right) in a steady bilateral pulling motion. (white arrows display the area where the slides overlap)



**Supplementary Figure 13:** Unwanted streaks formed during first separation.

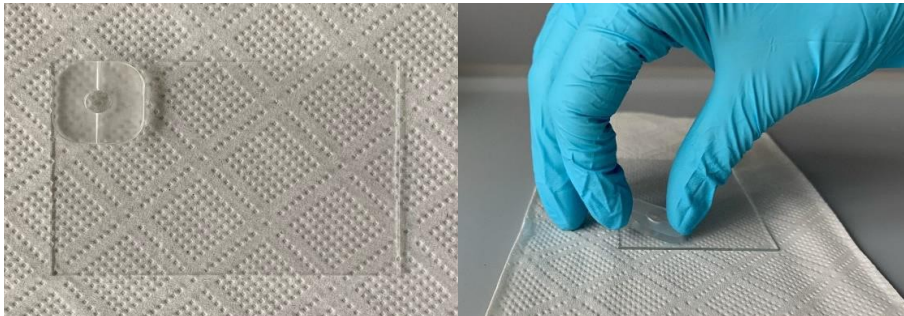
- Place both microscopy slides (76x52 mm) congruent on top of each other and repeat sliding them back and forth as previously shown (**Supplementary Figure 12**). Afterwards degas and check whether unwanted streaks did form during separation (**Supplementary Figure 13**).
- If necessary, repeat until slides show a homogenous surface without any streaks (**Supplementary Figure 14**).



**Supplementary Figure 14:** Two microscopy slides (76x52 mm) covered with PDMS; no streaks, plain surface.

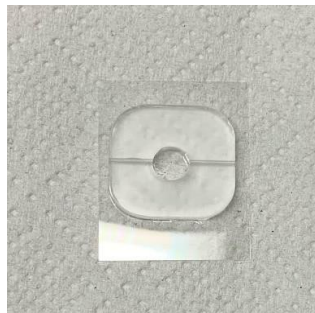
17. Place basolateral entity (resulting from mold B) onto one PDMS-covered microscopy slide (**Supplementary Figure 14**; fits 8 entities) and carefully apply firm pressure (**Supplementary Figure 15**, left). Avoid shifting entity. Then carefully lift entity from slide using index finger and thumb (**Supplementary Figure 15**, right).





**Supplementary Figure 15:** First place basolateral entity on PDMS-covered microscopy slide (fits 8 entities, left) using firm pressure. Then use index finger and thumb to carefully lift PDMS-covered entity (right).

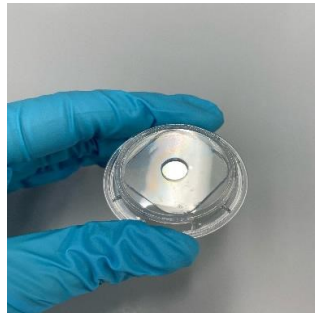
18. Attach PDMS-covered basolateral entities one after the other on a cover slide (24x32 mm). Pay attention to arrange channels in parallel to the short side of the microscopy slide. Apply pressure to ensure binding while simultaneously avoiding shifting the entities after placement. Be careful not to form new air bubbles after degassing.



**Supplementary Figure 16:** Place basolateral entity onto microscopy slide, arrange channel in parallel to the short side of the microscopy slide. Be careful not to form new air bubbles after degassing.

19. Place all assemblies in desiccator and degas until air bubble free (10 min).
20. Carefully insert in preheated oven (100°C, 10 min).

21. Cover basolateral entities with adhesive tape and let cool.
22. Repeat **step 15** and coat apical entity (resulting from mold A) with PDMS. Alternatively use second microscopy slide from **step 16** if no spin-coater was available.
23. Place entity centrally on a Transwell insert so that the whole entity is in contact with the membrane area (Supplementary Figure 17). Carefully apply pressure to ensure bonding. Avoid pushing entity around the membrane, as overflowed PDMS might decrease the cell growth area (Supplementary Figure 18).



**Supplementary Figure 17:** Apical entity centrally placed on Transwell insert.

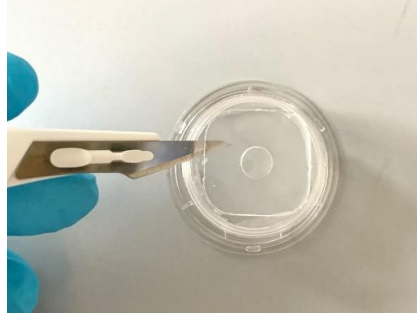


**Figure 18:** Reduced growth area due to unwanted entity movement after placed on transwell membrane.

24. Repeat for all apical entities.
25. Place assemblies in desiccator and degas until air bubble free (10 min).

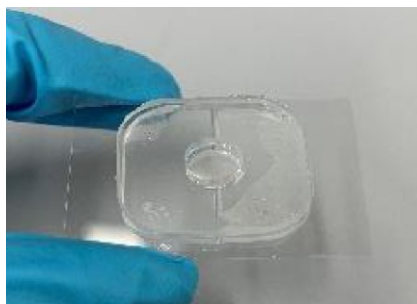


26. Carefully insert assemblies in preheated oven (100°C, 10 min).
27. Cut entities from the Transwell insert using a scalpel (Supplementary Figure 19). Remaining air bubbles can be eliminated manually with a dull object, by carefully pushing against the membrane from the bottom side of the entity.



**Supplementary Figure 19:** Cut entity from Transwell membrane using a scalpel.

28. Repeat **step 15** (or alternatively **step 16** if no spin-coater is available) and apply PDMS onto basolateral entities from **step 21** (remove adhesive tape before applying PDMS).
29. Place the basolateral entity on membrane side of apical entity. Pay attention to align the pre-punched holes congruent.
30. Place the assembled platform in a desiccator and degas. Big air pockets may form during degassing in desiccator (Supplementary Figure 20). Fix it with PDMS in sealing step (step 31).



**Supplementary Figure 20:** Unwanted air pockets may form during degassing in desiccator. Fix it with PDMS in sealing step.

31. To remove any leftover air pockets, seal the platform. Therefore, carefully add liquid degassed PDMS (from step 15 or 16, or alternatively freshly mixed (~ 3 g)) on the edge that seals the basolateral and apical entity. Be careful not to put any PDMS in the openings of the channels.
32. Degas in desiccator (10 - 15 min). If needed repeat until there are no air bubbles left.
33. Place sealed platform in preheated oven (100°C, 10 min). The assembled perfusable platform should have the following characteristics: no air pockets, no reduced growth area as well as aligned wells.

### 3.6 Tube assembly

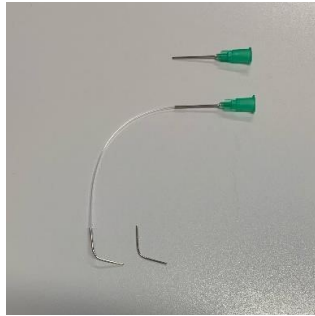
**Materials needed:** Tubing, scissors, blunt needle, spade, pliers, 2 ml reaction tube

34. Cut tubing into 10 cm fragments using scissors.
35. Isolate the metal cannula tube from a blunt needle using pliers. First crush the needle's resin using pliers (Supplementary Figure 21, left). Be careful not to dent or crease the metal cannula tube. Then apply a firm use of pressure and repeatedly compress the resin to detach it from metal cannula tube (Supplementary Figure 21, center).



**Supplementary Figure 21:** Carefully crush the needle's resin using pliers (left); Resin successfully detached from metal cannula tube (center). Process of bending the connection piece for tube assembly: an isolated metal cannula tube is generated from a blunt needle. The cannula tube is bent around a 2 ml reaction tube to create the curvy connection piece (right).

36. Grab the plastic adhesive with pliers and use the other hand to pull on metal cannula tube. Disintegrate the needle in a steady motion.
37. Clean the isolated metal cannula tube of any resin residues. If necessary, use a laboratory spade.
38. Lastly take a 2 ml reaction tube and bend previously isolated metal cannula tube around to create a bow (Supplementary Figure 21, right). The curvy connection piece must not be pointy or sharp.
39. Each perfusable platform will need an inlet and outlet tubing: the inlet tubing has a curvy connection piece connected at one end and a blunt needle connected at the other end of the tubing (Supplementary Figure 22). The outlet tubing (not shown) is assembled leaving the blunt needle away.

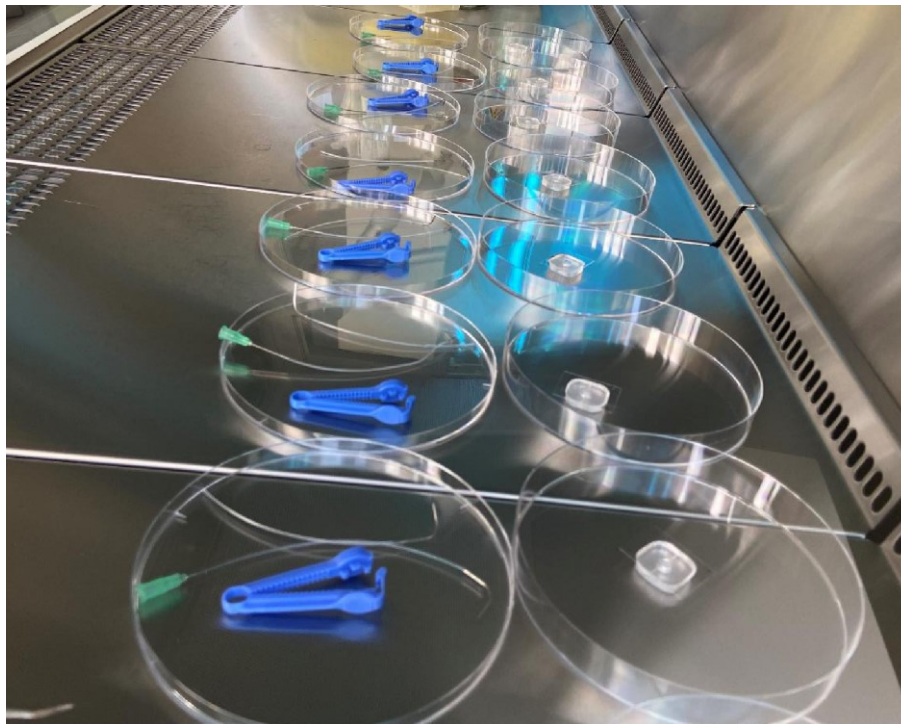


**Supplementary Figure 22:** Inlet tubing assembly as seen; Outlet tubing (not shown) re-assembled by connecting the curvy connection piece to a tubing, leaving one end of the tubing unmodified.

### 3.7 Preparing the perfusable platform for cell culture

To prepare the perfusable platforms for experiments that require sterilization such as cell culture, prepare: 1x petri dish, 1x assembled inlet tubing, 1x assembled outlet tubing, 1x tubing clamp, 1x autoclaved cover glass ( $\varnothing$  12 mm) and 1x fully assembled platform per functional unit.

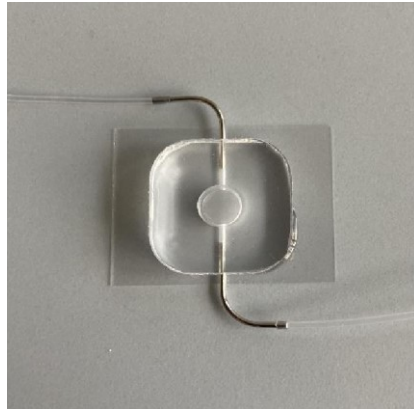
40. Immerse the inlet and outlet tubes as well as the tubing clamp for 10 min in 70% Isopropanol to disinfect them.
41. Put the material needed to assemble the functional unit (platform, inlet- and outlet tubes) into one petri dish each under a sterile lab hood (Supplementary Figure 23). Position the platform with the glass side facing up.



**Supplementary Figure 23:** Decontamination of functional unit.

42. Decontaminate the functional unit with UV light for 30 min.
43. Flip the platform as well as all other parts, except for the petri dish, towards the side that has not been in contact with UV.
44. Decontaminate again under UV light for 30 min.

45. Connect the tubes with the channel in- and outlet of the perfusable platform by inserting the curvy connection piece of each tubing into the channel opening. The fully assembled perfusable platform should look like the one displayed in Supplementary Figure 24. Close the platform with an autoclaved cover glass ( $\varnothing$  12 mm) whenever needed.



**Supplementary Figure 24:** Fully assembled and sealed perfusable platform. Characteristics: no air pockets, no reduced growth area as well as aligned wells.

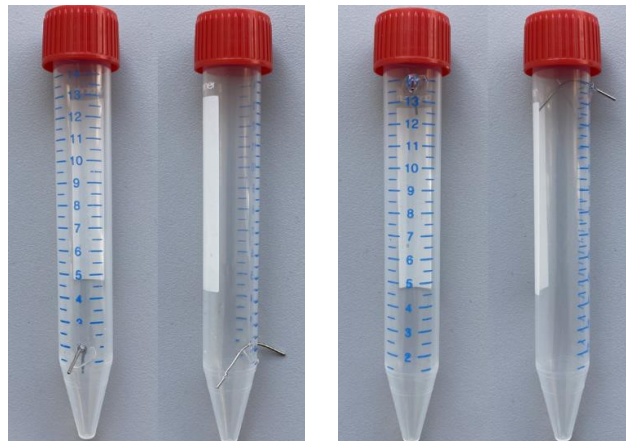
46. Place all sterilized parts into the petri dish and close.
47. Please see the Material and Methods section of the main manuscript for details on cell culture.

### 3.8 Perfusion setup

**Materials needed:** 2x 15 ml reaction tubes (e.g. Falcon®), needle (channel negative) (step 4), 2x curvy connection pieces (step 38), 5 g freshly degassed PDMS (step 2+3), oven, sterile filter cap, tubing (step 34)

48. Punch a hole using a needle (channel negative) (step 4) at the 2 ml mark of one 15 ml reaction tube and also at the 14 ml mark of the other 15 ml reaction tube.
49. The 15 ml reaction tube with the hole at the 2 ml mark will be used as the inlet reservoir and the 15 ml reaction tube with the hole at the 14 ml mark will be used as the outlet reservoir.

50. Insert a curvy connection piece in each of the punched holes and place the curvy connection piece in such a way, that the curvy connection piece is stabilized by the inside of the reaction tube. Exemplarily shown in Supplementary Figure 25.
51. Seal the tubes with the inserted curvy connection pieces with freshly degassed PDMS from the inside as well as outside of the tube, put them in a desiccator, and degas for 15 min.
52. Insert the tubes in preheated oven (100°C) for 10 min.
53. Wash tubes with 10 ml distilled water.
54. Steam autoclave inlet and outlet reservoir with connected curvy connection pieces.
55. Close inlet and outlet reservoir with sterile filter cap under a sterile workbench.



**Supplementary Figure 25:** Fully assembled inlet reservoir (left) and outlet reservoir (right) with sterile filter cap.

56. For perfusion experiments, connect the inlet reservoir to a peristaltic pump of your choice with tubing (step 34).
57. Fill the inlet reservoir with a liquid of your choice (e.g. cell culture medium) and flush all connecting tubing by using the peristaltic pump.
58. Once the tubing is cleared from any remaining air bubbles, connect a perfusable platform (fully assembled and sterilized) first to the peristaltic pump (which is connected to the inlet reservoir, step 57) and then to the outlet reservoir.

59. During the experiment watch that the liquid level in the inlet reservoir is in line with the membrane of the perfusable platform, to prevent an increase of hydrodynamic pressure.



„A Monoclonal Human Alveolar Epithelial Cell Line (“Arlo”) with Pronounced Barrier Function for Studying Drug Permeability and Viral Infections“

---

***„A Monoclonal Human Alveolar Epithelial Cell Line (“Arlo”) with Pronounced Barrier Function for Studying Drug Permeability and Viral Infections“***

**Patrick Carius**, Annemarie Jungmann, Marco Bechtel, Alexander Grißmer, Annette Boese, Gilles Gasparoni, Abdulrahman Salhab, Ralf Seipelt, Klaus Urbschat, Clémentine Richter, Carola Meier, Denisa Bojkova, Jindrich Cinatl, Jörn Walter, Nicole Schneider-Daum and Claus-Michael Lehr

Published in *Advanced Science*, 2023, Volume 10, 2207301

(<https://doi.org/10.1002/advs.202207301>)

Copyright © 2023 Patrick Carius, Annemarie Jungmann, Marco Bechtel, Alexander Grißmer, Annette Boese, Gilles Gasparoni, Abdulrahman Salhab, Ralf Seipelt, Klaus Urbschat, Clémentine Richter, Carola Meier, Denisa Bojkova, Jindrich Cinatl, Jörn Walter, Nicole Schneider-Daum and Claus-Michael Lehr. This is an open-access article distributed under the terms of the Creative Commons Attribution 4.0 International (CC BY 4.0).

Contributions to co-authorship:

Claus-Michael Lehr, Nicole Schneider-Daum and Patrick Carius are the creators of the cell line “Arlo”. Patrick Carius conceptualized the research idea, was mainly responsible for the methodological design of the study and performed most of the experiments as well as analyzed the data. Exceptions were the RNA-sequencing studies, the histological sample preparation and microscopy as well as the viral infection studies, where he assisted in. Patrick further wrote the original draft of the manuscript and visualized the data. In addition, he was mainly involved in reviewing and editing the revision of the manuscript.

# A Monoclonal Human Alveolar Epithelial Cell Line (“Arlo”) with Pronounced Barrier Function for Studying Drug Permeability and Viral Infections

Patrick Carius, Annemarie Jungmann, Marco Bechtel, Alexander Grißmer, Annette Boese, Gilles Gasparoni, Abdulrahman Salhab, Ralf Seipelt, Klaus Urbschat, Clémentine Richter, Carola Meier, Denisa Bojkova, Jindrich Cinatl, Jörn Walter, Nicole Schneider-Daum,\* and Claus-Michael Lehr\*

In the development of orally inhaled drug products preclinical animal models regularly fail to predict pharmacological as well as toxicological responses in humans. Models based on human cells and tissues are potential alternatives to animal experimentation allowing for the isolation of essential processes of human biology and making them accessible in vitro. Here, the generation of a novel monoclonal cell line “Arlo,” derived from the polyclonal human alveolar epithelium lentivirus immortalized cell line hAELVi via single-cell printing, and its characterization as a model for the human alveolar epithelium as well as a building block for future complex in vitro models is described. “Arlo” is systematically compared in vitro to primary human alveolar epithelial cells (hAEPcs) as well as to the polyclonal hAELVi cell line. “Arlo” cells show enhanced barrier properties with high transepithelial electrical resistance (TEER) of  $\approx 3000 \Omega \text{ cm}^2$  and a potential difference (PD) of  $\approx 30 \text{ mV}$  under air–liquid interface (ALI) conditions, that can be modulated. The cells grow in a polarized monolayer and express genes relevant to barrier integrity as well as homeostasis as is observed in hAEPcs. Successful productive infection with severe acute respiratory syndrome coronavirus 2 (SARS-CoV-2) in a proof-of-principle study offers an additional, attractive application of “Arlo” beyond biopharmaceutical experimentation.

## 1. Introduction

The translational value of results from animal experiments for predicting the human response to orally inhaled compounds or drug products has been questioned in past years in inhalation research.<sup>[1–3]</sup> Reasons include essential species-species differences in anatomical structures as well as in physiological functions between different non-human species and humans. For example, although genomic responses to inflammatory stimuli as observed in acute respiratory distress syndrome (ARDS) are highly similar within humans, these could not be reproduced using current mouse models.<sup>[4]</sup> Complex in vitro models based on human cells and tissues were raised as a potential alternative to animal experimentation because they allow to reduce the complexity of human biology to an extent that can be consistently reproduced in vitro.<sup>[5]</sup> The generation of such complex in vitro models, however, requires reliable human-relevant

P. Carius, A. Boese, C. Richter, N. Schneider-Daum, C.-M. Lehr  
Helmholtz Institute for Pharmaceutical Research Saarland (HIPS) –  
Helmholtz Centre for Infection Research (HZI)  
Campus E8.1, 66123 Saarbrücken, Germany  
E-mail: nicole.schneider-daum@helmholtz-hips.de;  
claus-michael.lehr@helmholtz-hips.de  
P. Carius, C. Richter, C.-M. Lehr  
Department of Pharmacy  
Saarland University  
Campus E8.1, 66123 Saarbrücken, Germany

A. Jungmann, G. Gasparoni, A. Salhab, J. Walter  
Department of Genetics and Epigenetics  
Saarland University  
Campus A2 4, 66123 Saarbrücken, Germany  
M. Bechtel, D. Bojkova, J. Cinatl  
Institute of Medical Virology  
University Hospital Frankfurt  
Paul-Ehrlich-Str. 40, 60596 Frankfurt am Main, Germany  
A. Grißmer, C. Meier  
Department of Anatomy and Cellular Biology  
Saarland University  
Kirrberger Straße  
Building 61, 66421 Homburg Saar, Germany  
R. Seipelt, K. Urbschat  
Section of Thoracic Surgery of the Saar Lung Center  
SHG Clinics Völklingen  
Richardstraße 5-9, 66333 Völklingen, Germany

 The ORCID identification number(s) for the author(s) of this article can be found under <https://doi.org/10.1002/adv.202207301>

© 2023 The Authors. Advanced Science published by Wiley-VCH GmbH. This is an open access article under the terms of the Creative Commons Attribution License, which permits use, distribution and reproduction in any medium, provided the original work is properly cited.

DOI: 10.1002/adv.202207301

cell sources as the essential building blocks, necessarily demonstrating reproducible experimental readouts *in vitro*.

In the case of the human lung, a morphologically and histologically complex organ, this means that different cell types prevailing in the diverse epithelial linings of the tracheobronchial region, the airways (bronchi) as well as the respiratory region (alveoli) of the peripheral lung would need to be considered.<sup>[6]</sup> The highest number of different epithelial cell types exists in the approximately 50  $\mu\text{m}$  thick epithelial lining of the bronchial airways. It is mainly characterized by a pseudostratified epithelium formed by columnar ciliated epithelial cells, club cells, mucous-secreting goblet cells as well as basal cells that serve as progenitors to most of the airway epithelial cells.<sup>[7]</sup> From proximal to distal, the surface that is covered by the epithelial lining of the human lung increases from around 4  $\text{m}^2$  in the two bronchi to around 100  $\text{m}^2$  spanning the alveolar epithelium.<sup>[8,9]</sup> This squamous epithelial layer has on average a delicate thickness of 1  $\mu\text{m}$  and is formed by AT-1 pneumocytes together with the cuboidal AT-2 cells.<sup>[10]</sup> While only representing about 8% of all lung cells, AT-1 cells account for 95–98% of the total surface area of the alveolar epithelium due to a cell surface area of  $\approx 5.000 \mu\text{m}^2$  per cell, ensuring effective gas exchange.<sup>[8,11]</sup> To prevent fluid leakage from the highly perfused vascular system underlying the alveolar epithelium into the air-filled alveoli, a structure which is also called the air–blood barrier, the thin AT-1 cells maintain tight cell-to-cell connections as well as effective fluid homeostasis by regulating water and ion transport. On the contrary, the cuboidal AT-2 cells make up  $\approx 18\%$  of the cells of the alveolar epithelium but only contribute to 2–5% of the surface area, since they are mostly located at the corners of the alveoli.<sup>[12,13]</sup> AT-2 cells produce pulmonary surfactant, a complex mixture of lipids and bioactive proteins, which prevents the alveolar sacs from collapsing by lowering the surface tension at the air–liquid interface above the epithelial lining.<sup>[14]</sup> Furthermore, they contribute to the innate immune response and serve as facultative progenitors that differentiate into AT-1 cells, but also replicate during epithelial homeostasis or after epithelial damage.<sup>[15]</sup>

When modeling pulmonary epithelia *in vitro* in the context of biopharmaceutical or toxicological inhalation experiments, air–liquid interface (ALI) conditions as well as tissue-specific barrier integrity should be considered as standard requirements.<sup>[16–18]</sup> For the bronchial epithelia described above, such cellular models are commercially available as primary cells from different donors supplied by various vendors or as continuous cell lines from recognized sources such as the American Type Culture Collection (ATCC) (extensively reviewed recently:<sup>[19–21]</sup>). In case of the alveolar epithelium though, cellular *in vitro* models that recapitulate tissue-specific barrier integrity, provided by polarized alveolar epithelial cells that grow in a monolayer and show the formation of functional tight junctional complexes, were so far limited to primary human alveolar epithelial cells (hAEPs) grown on porous growth supports (e.g., Transwell inserts)<sup>[22–25]</sup> or within advanced lung-on-chip devices.<sup>[26–28]</sup>

Freshly isolated primary hAEPs seeded on Transwell inserts are still considered as a gold standard when replicating the human alveolar epithelium *in vitro*, especially during biopharmaceutical *in vitro* permeability experiments.<sup>[20]</sup> Nevertheless, they come with several disadvantages such as costly isolation procedures, donor-to-donor variations or low yields that limit the ex-

perimental scale. Further, the isolated cells which are by the majority AT-2 cells tend to transdifferentiate into AT-1 cells when cultured on permeable growth supports, which is a wanted effect to reach proper barrier integrity, but then continue to further de-differentiate resulting in a loss of barrier integrity and a limited experimental window of several days.<sup>[29–32]</sup> Impressive advances that were achieved by optimizing the differentiation protocols used to culture adult stem cells or human induced pluripotent stem cells and differentiate them further into organoids, yielded models that recapitulate the phenotypic as well as many other functional characteristics of the cells of the alveolar epithelium over an enhanced culture period.<sup>[33]</sup> Whereas these models have the potential to overcome the limitations underlying the use of freshly isolated hAEPs such as limited yield or availability in general, they currently face weak barrier properties,<sup>[34–37]</sup> inhomogeneous multiple cellular layers<sup>[38]</sup> or multilayered closed alveospheres.<sup>[39,40]</sup>

Continuously growing cell lines, derived from tumor biopsies or functionally immortalized by different genetic modifications, offer experimental convenience due to higher yields and flexible expansion, but might suffer from genetic instability as well as phenotypes distinct from epithelial cells *in situ*.<sup>[20,41]</sup> For example, the quite commonly used continuous cell line A549, originally derived from a human adenocarcinoma patient and showing some AT-2-like characteristics, lacks functional tight junctions, which disqualifies it for transport studies, at least as far as small molecules are concerned.<sup>[42]</sup> Another report further demonstrated that the cell line is polyclonal and might yield up to three different sub-clones.<sup>[43]</sup>

Recently though, two continuous cell lines, the adenocarcinoma-derived NCI-H441 as well as the human alveolar epithelial lentivirus immortalized (hAELVi) cell line, have been proposed as promising models for the alveolar epithelium especially in the context of biopharmaceutical experiments.<sup>[44]</sup> While both cell lines present electrically tight epithelial layers with intercellular junctions forming a diffusion barrier as well as certain markers representative for alveolar epithelial cells, the hAELVi cell line maintains tight barrier properties under ALI conditions over a longer culture period than NCI-H441.<sup>[45–47]</sup>

Unfortunately, the original hAELVi cell line presents a heterogeneous cell population due to the initial immortalization of a mixed population of CD326-positive hAEPs, without further monoclonal selection.<sup>[45,48]</sup> This led to inconsistencies in the development of barrier properties depending on the used cell culture vial, experienced by the authors of this study as well as by other laboratories leading to irreproducible experimental results.<sup>[49–51]</sup>

We here report the development as well as the characterization of a new monoclonal cell line named “Arlo.” The cell line is based on a single-cell clone of the polyclonal hAELVi cell line generated by single-cell printing and shows enhanced barrier properties while preserving a monolayer morphology. A transcriptomic analysis of “Arlo” in comparison to hAEPs, both cultured under ALI conditions on Transwell inserts for a total of 14 days, demonstrated high similarity in gene expression relevant to barrier integrity and homeostasis. To show the versatility of “Arlo” beyond biopharmaceutical experimentation, we additionally report the infection of the new cell line with SARS-CoV-2 in a proof of principle study. In addition, the data from the tran-

scriptomic analysis are publicly available as a resource for other researchers.

## 2. Results

### 2.1. Generation of the Single Cell Clone “Arlo”

The hAELVi cell line was generated based on the immortalization of a single-donor hAEPc isolation of CD326-positive (also known as an epithelial cell adhesion molecule (EpCAM)) cells that have been cultured on a six-well cell culture plate for 5 d.<sup>[45,48]</sup> Functional immortalization was achieved by using self-inactivating lentiviral vectors, comprising 33 genes under the control of a SV40 promoter.<sup>[52]</sup> This procedure yielded two continuously growing polyclonal cell lines that were selected upon developing transepithelial electrical resistance (TEER) values  $>1000 \Omega \text{ cm}^2$  that were named hAELVi.A and hAELVi.B.

hAELVi.A was renamed to CI-hAELVi and distributed by the company Inscreenex GmbH. CI-hAELVi comprises a heterogeneous cell population that, depending on the initially thawed culture vial, would either demonstrate barrier formation indicated by TEER values  $>1000 \Omega \text{ cm}^2$  or would show impaired barrier formation (Figure S1, Supporting Information).

In an initial effort to ensure reproducibility of experimental results from the hAELVi cell line, single-cell clones were generated by single-cell printing from a polyclonal hAELVi cell suspension that demonstrated barrier formation in the previous passage (Figure 1A). The parameters needed for the single-cell printing were determined via counting of the cell suspension with a Casy cell counter (Figure 1B). The image-based algorithm of the Cytena c.sight single-cell printer detected single cells and precisely deposited them within a drop via an inkjet-like technique into a single well of a 96-well cell culture plate. A series of pictures documents this process, and is exemplarily shown for well D4 that resembles the single cell clone “Arlo” (Figure S2, Supporting Information). After single-cell printing, the single-cell clone “Arlo” was serially expanded in multiple sized well-formats until it eventually could be transferred into a T25  $\text{cm}^2$  cell culture flask (Figure 1A). For reasons of consistency, we use the naming “single cell clone “Arlo”” whenever “Arlo” is compared to the polyclonal hAELVi cell line and the term “Arlo” in all other cases, including comparisons with hAEPcs. A visual comparison of the growth of the polyclonal hAELVi cell line (Figure 1C) and the single cell clone “Arlo” (Figure 1D) in T25  $\text{cm}^2$  cell culture flasks already indicated a more homogeneous appearance in the case of the single cell clone “Arlo” in comparison to the polyclonal hAELVi cell line, especially on day 2 and day 5 of culture.

### 2.2. Electrophysiological and Functional Characterization of Barrier Properties of the Single Cell Clone “Arlo”

When epithelial cells are cultured on permeable growth supports, the increase in ohmic resistance of the in vitro tissue over time reported as TEER values serve as a non-destructive, accepted measure to assess and monitor the formation of tight junctions as well as other cell-to-cell connections. When using traditional direct current based voltohmmeter such as the EVOM 2 to measure

TEER values, epithelial potential difference (PD) can be measured as well using the same experimental setup. PD delivers additional information about the formation as well as homeostasis of an ion gradient by the epithelial cells in in vitro culture.

In order to assess the capability of the single-cell clone “Arlo” to develop and maintain an electrically tight barrier, we compared its barrier development against the polyclonal hAELVi cell line as well as hAEPcs over a course of 14 d either cultured under ALI (Figure 2A) or under liquid-covered conditions (LCC) (Figure 2B).

hAEPcs grown under ALI conditions showed an increase in TEER values from day 2 to day 6 (peak:  $1624 \pm 501 \Omega \text{ cm}^2$ ), then TEER values declined towards day 14 ( $772 \pm 1122 \Omega \text{ cm}^2$ ). Under LCC, TEER values peaked at day 7 ( $1428 \pm 656 \Omega \text{ cm}^2$ ) until they eventually declined to  $654 \pm 397 \Omega \text{ cm}^2$  on day 14. PD followed the same development as the TEER values, peaking at  $14 \pm 11 \text{ mV}$  on day 8 under ALI conditions, as well as on day 7 at  $13 \pm 8 \text{ mV}$  under LCC. Electrophysiological properties under both growth conditions were in accordance with our historic measurements.<sup>[25,29]</sup> The polyclonal hAELVi cell line showed a stepwise increase in TEER as well as PD development beginning from day 7 under LCC or day 10 under ALI conditions, respectively. TEER values reached a peak (ALI:  $1436 \pm 397 \Omega \text{ cm}^2$ ; LCC:  $1148 \pm 151 \Omega \text{ cm}^2$ ) on day 14, in a similar development as the PD values (ALI:  $20 \pm 7 \text{ mV}$ ; LCC:  $31 \pm 4 \text{ mV}$ ).

The single cell clone “Arlo” however, demonstrated a steadily increasing TEER development with TEER values about twice as high as the polyclonal hAELVi cell line on day 14 (ALI:  $3112 \pm 607 \Omega \text{ cm}^2$ ; LCC:  $2136 \pm 711 \Omega \text{ cm}^2$ ). A similar development could be observed for PD values, although these were appreciably higher under LCC (LCC:  $64 \pm 12 \text{ mV}$ ) than under ALI conditions (ALI:  $37 \pm 14 \text{ mV}$ ).

In order to assess whether the high TEER values developed by the single-cell clone “Arlo” also correspond to the formation of functional tight junction complexes, we performed a transport experiment with the well-defined low-permeability marker fluorescein sodium (Figure 2C, left). One of the two experimental groups was treated with 2,2',2'',2'''-(ethane-1,2-diyl)dinitrilo) tetra acetic acid (EDTA) for 1 h during the equilibration with transport buffer. EDTA leads to the reversible opening of tight junction complexes by primarily chelating extracellular  $\text{Ca}^{2+}$ . The resulting change in intracellular  $\text{Ca}^{2+}$  concentrations eventually activates Protein Kinase C which increases paracellular permeability.<sup>[53]</sup> TEER values were measured to monitor barrier integrity before, 1 h after the switch to transport buffer, which was supplemented with  $16 \times 10^{-3} \text{ M}$  EDTA in one group, as well as after the transport experiment. Before the transport experiment, where cells were cultured 14 d under LCC in cell culture medium, no significant differences in TEER values were observed between the two groups ( $3988 \pm 512 \Omega \text{ cm}^2$  (HBSS) vs  $3971 \pm 473 \Omega \text{ cm}^2$  (HBSS + EDTA [ $16 \times 10^{-3} \text{ M}$ ])). The switch to the transport buffer HBSS led to a strong decrease in TEER values after the 1 h incubation in case of the untreated group ( $1509 \pm 420 \Omega \text{ cm}^2$  (HBSS)), but still remained above  $1000 \Omega \text{ cm}^2$ . In case of the group that was treated with EDTA, TEER values decreased significantly to  $120 \pm 31 \Omega \text{ cm}^2$  indicating a successful opening of tight junctional complexes. After 5 h of transport with only HBSS as a transport buffer in both groups, the TEER values of the control group still differed significantly from the group treated with EDTA during the 1 h incubation ( $2491 \pm 586 \Omega \text{ cm}^2$  (HBSS) vs  $379 \pm 128 \Omega \text{ cm}^2$  (HBSS



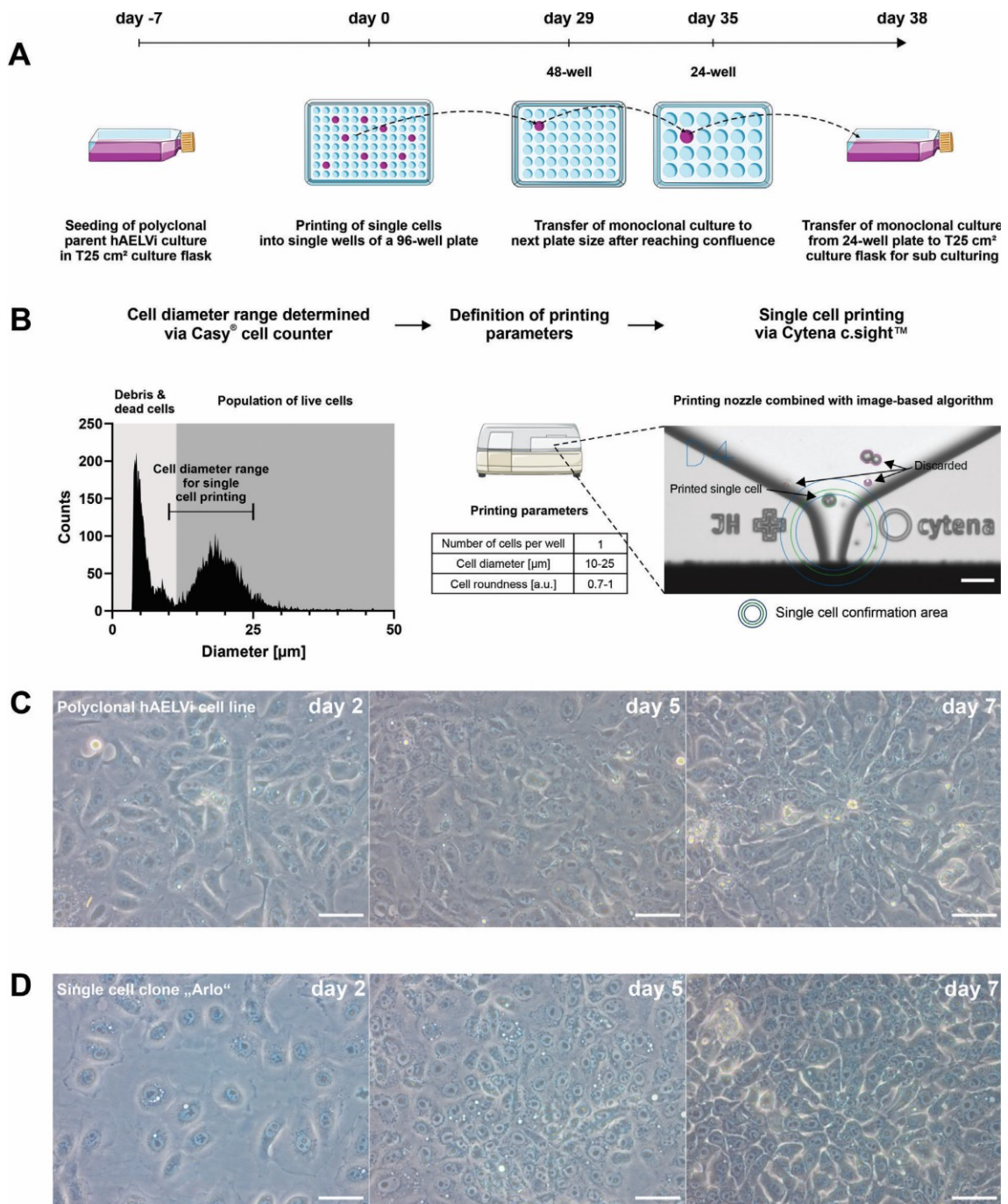


**Figure 1.** Generation of the single cell clone ‘‘Arlo.’’ A) Schematic depicting the single-cell printing procedure (detailed in B) and subsequent passaging strategy for the single-cell clone ‘‘Arlo’’ originating from a polyclonal hAELVi suspension that demonstrated TEER values >1000 Ω cm<sup>2</sup> in the previous passage. B) Before single-cell printing, the cell diameter of the polyclonal hAELVi cell suspension was determined via a Casy cell counter to define the printing parameters. Single cells within the printing parameters (bordered green) were confirmed by an image-based algorithm and then deposited into a single well of a 96-well plate. Cells that did not meet the printing criteria were discarded via vacuum aspiration after ejection from the printing nozzle (bordered purple or red). C,D) Light microscopic images showing morphological differences between C) the polyclonal hAELVi cell line and D) the single cell clone ‘‘Arlo’’ when cultured in T25 cm<sup>2</sup> culture flasks for 7 d. Scale: 50 µm for all images displayed. Panel A) was partly generated using Servier Medical Art, provided by Servier, licensed under a Creative Commons Attribution 3.0 unported license.

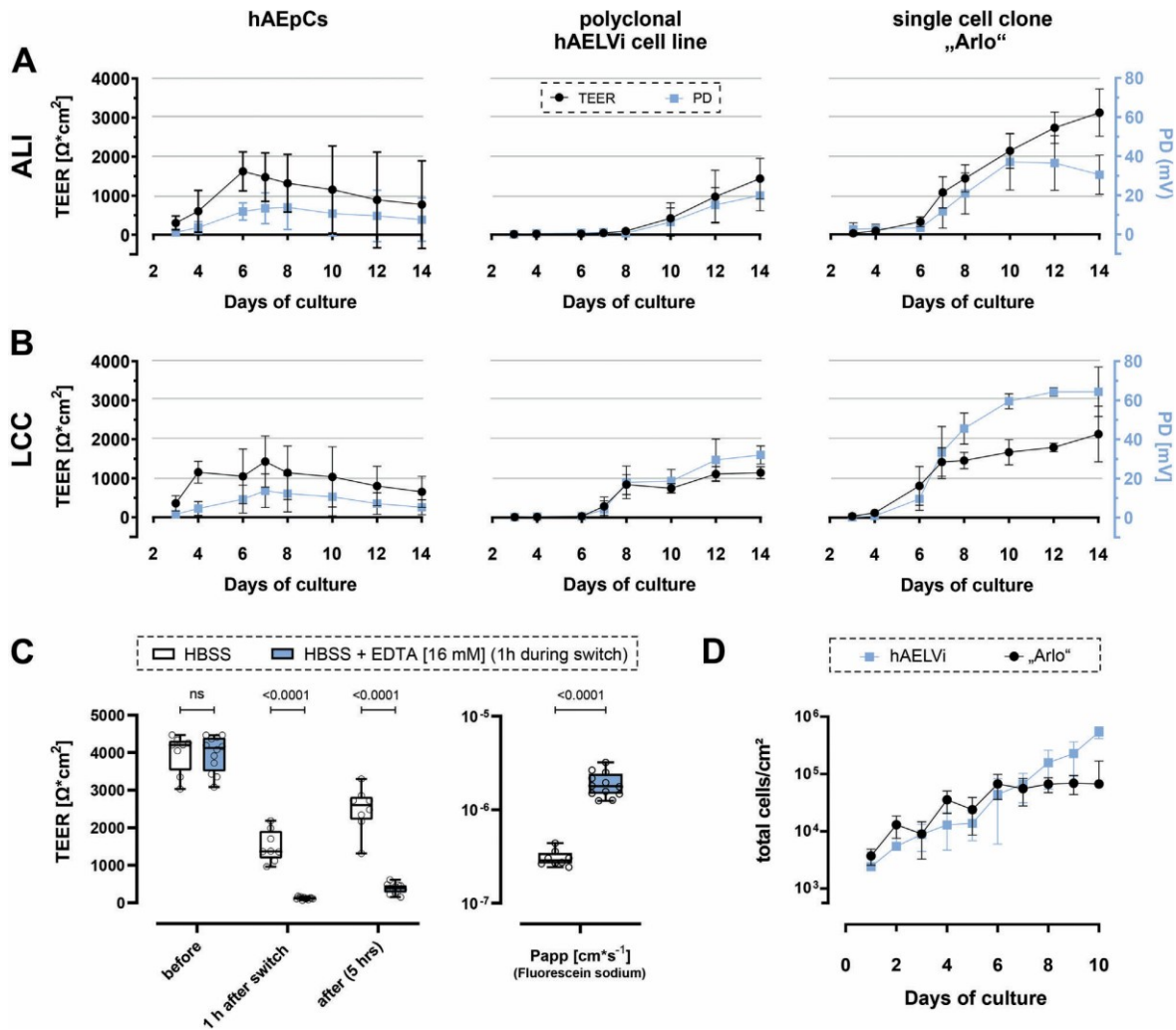


**Figure 2.** Electrophysiological and functional characterization of barrier properties of the single cell clone ‘‘Arlo.’’ A, B) TEER values ( $\Omega^2\text{cm}^2$ , black curve) as well as epithelial potential difference (PD) (mV, blue curve) of hAEPcs, the polyclonal hAELVi cell line and the single cell clone ‘‘Arlo’’ grown on Transwell inserts either under A) ALI or B) LCC conditions for 14 d. Data represent mean  $\pm$  S.D. from 12 TWs and three independent biological replicates (hAEPcs day 4: 8 TWs; 2 bio. replicates). C) Apparent permeability of Fluorescein sodium ( $1\text{ mg mL}^{-1}$  in HBSS) transported over ‘‘Arlo’’ monolayers after 14 d of culture under LCC. TEER values were measured with cells cultured in the medium before the experiment (before), 1 h after the incubation in transport buffer (1 h after switch), as well as after the transport study (after). Transport buffer (HBSS) was supplemented with EDTA ( $16 \times 10^{-3}\text{ M}$ ) during the 1 h incubation to disrupt tight junction complexes in one group. (TEER) 2-way ANOVA was performed not assuming sphericity and with a Šidák’s multiple comparisons test. ( $P_{\text{app}}$ ) Unpaired *t*-test was performed with Welch’s Correction; Data represent mean  $\pm$  S.D.; HBSS:  $n = 9$ , HBSS+EDTA:  $n = 12$  from 3 independent biological replicates. D) Growth curve comparing the polyclonal hAELVi cell line with the single cell clone ‘‘Arlo’’. Data represent mean  $\pm$  S.D. from at least 2 technical replicates of 3 biological replicates (‘‘Arlo’’d10: single biological replicate).

+ EDTA [ $16 \times 10^{-3}\text{ M}$ ]). This significant difference was also reflected in the Papp values for fluorescein sodium, which was significantly lower in the control group ( $3 \times 10^{-7} \pm 6 \times 10^{-8}\text{ cm s}^{-1}$  (HBSS)) in comparison to the group treated with EDTA ( $2 \times 10^{-6} \pm 6 \times 10^{-7}\text{ cm s}^{-1}$  (HBSS + EDTA [ $16 \times 10^{-3}\text{ M}$ ])) (Figure 2C, right). This indicated that the paracellular permeability of the single-cell clone ‘‘Arlo’’ could be experimentally modulated regardless of its strong barrier properties indicated by high TEER values.

To exclude that the higher TEER values in case of the single-cell clone ‘‘Arlo’’ originated from a higher number of cells present in the culture and thereby generating a higher electrical resistance, we performed a growth curve to compare the growth of the single-cell clone ‘‘Arlo’’ against the growth of the polyclonal hAELVi cell line. The data of the growth curve indicated that the cells of both cell lines equally proliferated until day 6 of the culture (Figure 2D). From day 6 onwards the polyclonal cell line hAELVi seemed to have further proliferated until day 10, whereas

the total cell number of the single-cell clone “Arlo” seems to enter an equilibrium. Interestingly, day 6 is also the day that marks the formation of TEER values for both cell lines under LCC (Figure 2B).

### 2.3. Morphological Comparison of the Single Cell Clone “Arlo” and the Polyclonal hAELVi Cell Line

In theory, the increase of the electrical resistance of an epithelial in vitro tissue to the net ion flux could be caused by cells growing in a monolayer, where the cells are developing tightly connected functional tight junctions as well as other cell-to-cell connections. Another possibility would be that cells are growing in multiple cellular layers, thereby increasing resistance to the net ion flux.

To evaluate the tissue morphology of the single-cell clone “Arlo” as well as the polyclonal hAELVi cell line, micrographs from confocal z-stacks were analyzed (Figure 3A,B).

Computed orthogonal sections within the horizontal plane of z-stacked images, already indicated differences between the two cell lines in terms of layer morphology. In case of the single-cell clone “Arlo” grown for 14 d under ALI conditions the top-view micrograph as well as the orthogonal section of the representative z-stacked image suggested that cells predominantly grew within a monolayer (Figure 3A). The polyclonal hAELVi cell line cultured under the same conditions as the single cell clone “Arlo” indicated the formation of multiple layers, as demonstrated by the top-view micrograph as well as the orthogonal section of the z-stacked image (Figure 3B).

Using only orthogonal image-based sections of an in vitro tissue to assess the morphology of the cellular layer impairs the unbiased evaluation of the tissue. Sections need to be selected first and then assessed individually to deduce the layer morphology of the whole micrograph. In order to quantitatively assess the layer morphology of the single-cell clone “Arlo” as well as the polyclonal hAELVi cell line, a computational image analysis was conducted (Figure 3C). For computational analysis, the signal of the nuclei from each cell was calculated as a single object within the 3D space of each z-stack. The extracted z-positions were then compared between the two cell lines (Figure 3D). The comparison of the distribution of the nuclear signal as a surrogate for the cellular position on the z-axis in relation to the Transwell-membrane within each layer showed, that the single cell clone “Arlo” grew in a monolayer on day 7 of culture under ALI conditions and also displayed a monolayer morphology until day 14 of culture. The polyclonal cell line hAELVi however, showed the formation of multiple layers already at day 7 of culture under ALI conditions. This was also observed on day 14, differing significantly from the single-cell clone “Arlo” as well as from the condition on day 7.

Representative histological sections of the in vitro tissue further supported the results of the computational image analysis, which was based on immunofluorescence staining, by another method. The single cell clone “Arlo” maintained a monolayer morphology over the 14 days of culture under ALI conditions, whereas the polyclonal cell line hAELVi seemed to develop multiple layers already on day 7 of culture under ALI conditions and even more pronounced on day 14 (Figure 3D).

### 2.4. Similarities in Gene Expression Relevant to Barrier Integrity between hAEpCs and “Arlo”

Notably enough, the newly created “Arlo” cells demonstrated remarkably high TEER values, experimentally adaptable tight junction complexes as well as stringent monolayer morphology. To assess whether “Arlo” could be used as a model for the alveolar epithelium, not only on the functional but also on the molecular level, a bulk RNA-Sequencing analysis (RNA-seq) was conducted. The RNA-seq results from “Arlo” were compared to results from hAEpCs both cultured under the same conditions for 14 days under ALI. Samples for RNA-seq have been collected before seeding cells on Transwell inserts (day 0), as well as on day 7 and day 14 of culture. The day 0 samples from the hAEpCs used for RNA-seq were generated from the CD326/EpCAM-positive cellular fraction of the donor tissue on the day the tissue was resected and thus stand representative for the RNA expression status of the epithelial fraction of the native tissue. The day 0 samples from “Arlo” used for RNA-seq were generated from freshly passaged cells, which were continuously cultured in T25 cm<sup>2</sup> culture flasks for 7 d prior to passaging.

First, the expression of 35 genes whose products are associated with regulating lung barrier integrity or barrier homeostasis were identified in the literature and compared between hAEpCs as well as “Arlo” (Figure 4A).<sup>[54–56]</sup>

The genes were assigned to the following classes: adherence junctions, desmosomes, gap junctions, receptors, and tight junctions based on the associated function of their gene products. The tight junction class of gene products directly regulates the paracellular permeability of ions and hydrophilic small molecules, specifically through adhesive transmembrane proteins (e.g., Claudins). However, gene classes whose products contribute to structural epithelial integrity (e.g., adherence junctions) as well as cellular communication (e.g., gap junctions) were also included in this comparison to additionally cover other important epithelial functions. The striking majority of the 35 genes showed similar expression levels in both hAEpCs as well as “Arlo,” as indicated by 4 broader categorized apparent clusters. Clearly distinguishable differences in gene expression were observed within the receptor class. The genes coding for the integrin subunits ITGA2, ITGA5, ITGAV, and to a lesser extent the genes ITGA6, ITGB4 as well as ITGB6 demonstrated differing expression levels either in general or at specific time points between the two cellular models. Further, the gene CLDN18 that codes for the alveolar-relevant tight junctional protein claudin-18 did not show a detectable expression in “Arlo” whereas its expression declined in hAEpCs from day 0 to day 14 of culture under ALI conditions on Transwell inserts. In addition, the gene ERBB4 (HER4), that codes for the disease-relevant Erb-b2 receptor tyrosine kinase 4, could also not be detected within “Arlo” whereas a moderate expression was observed within hAEpCs.

From these 35 genes, the resulting structural junctional proteins Occludin as well as tight junction protein 1 (ZO-1) were chosen as empirically-defined molecules representative for functional tight junction complexes mainly located apically in polarized epithelial cells.<sup>[57,58]</sup> The elevated gene expression of the respective genes OCLN (Occludin) as well as TJP1 (Tight junction protein 1) observed for “Arlo” already indicated that the respective proteins might also be detectable (Figure 4A–C). Micrographs of



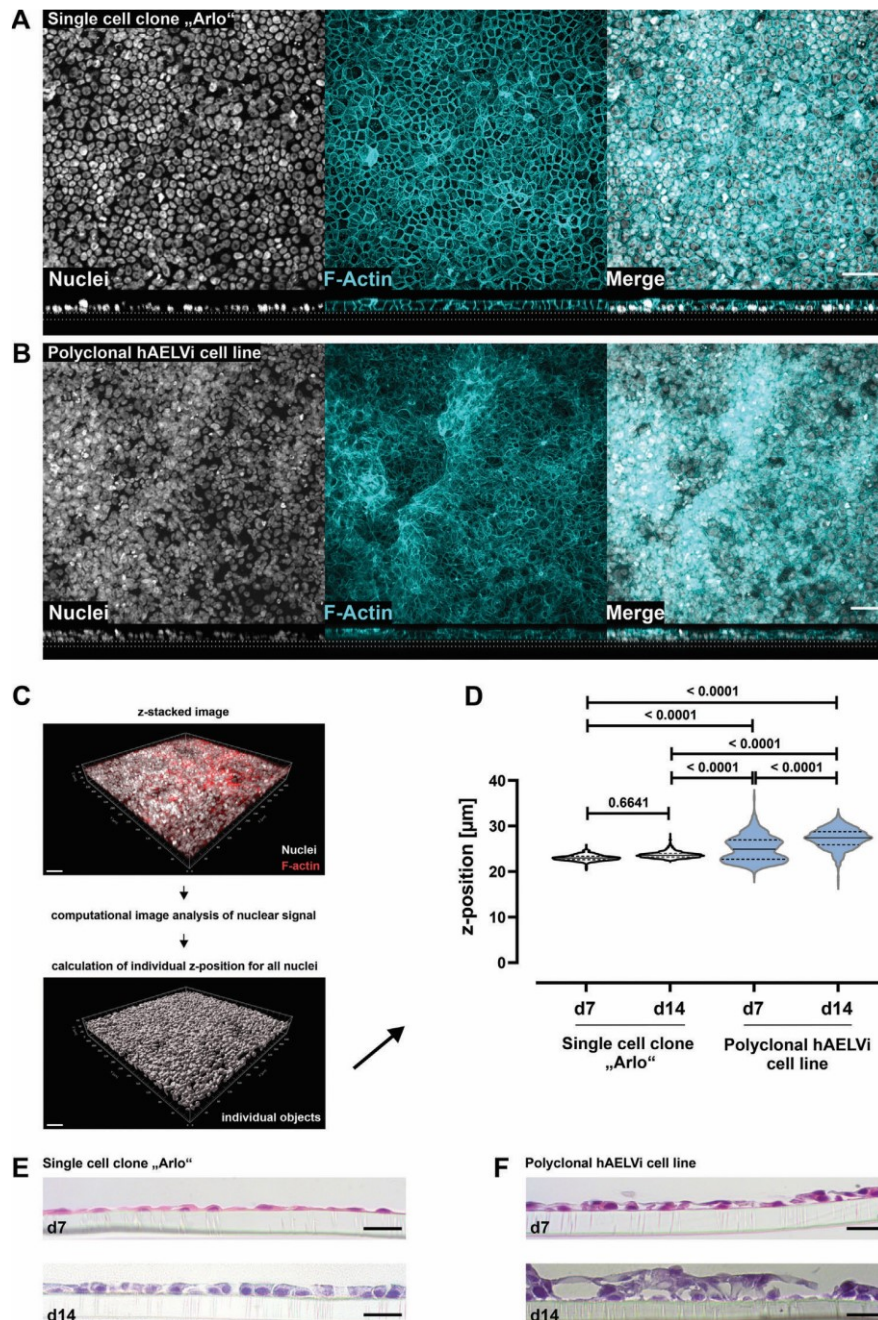
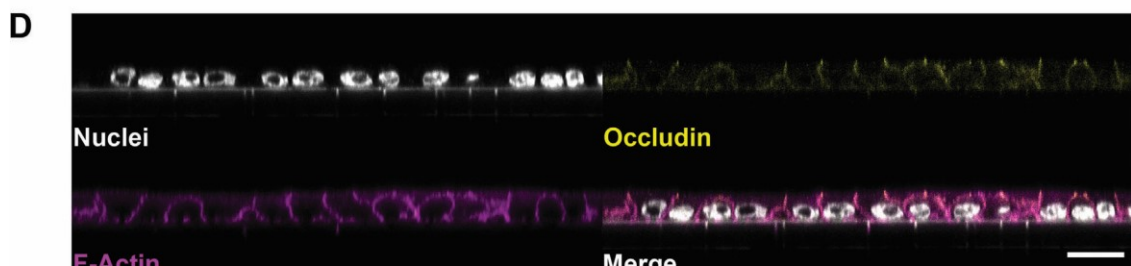
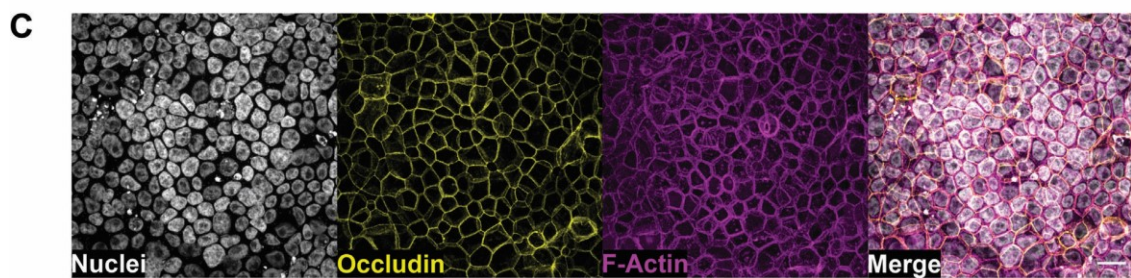
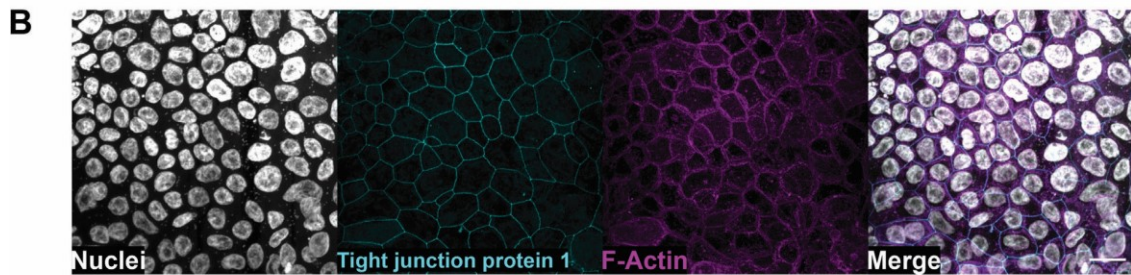
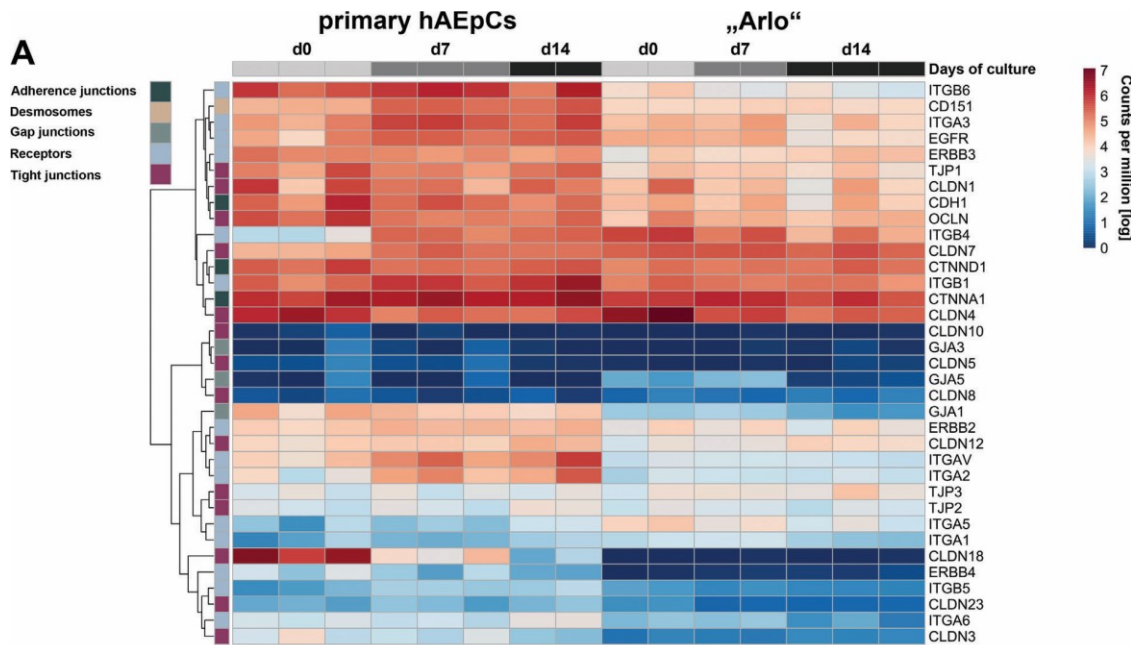


**Figure 3.** Different tissue morphology between the polyclonal hAELVi cell line and the single cell clone ‘‘Arlo.’’ A,B) Maximum projections from immunofluorescence staining showing cellular distribution as top view (upper panel) and the tissue morphology as orthogonal projections from z-stacked images (lower panel) for A) the single cell clone ‘‘Arlo’’ as well as B) the polyclonal hAELVi cell line. Nuclei stained with DAPI (gray) as well as F-Actin stained with phalloidin (cyan). Images are representative for 3 independent biological replicates. Scale bar: 50  $\mu\text{m}$ . C) Schematic depicting the generation of individual digital objects for each cell, based on its nuclear signal by computational image analysis, computed from the information contained in z-stacked confocal images. D) Computational image analysis of cellular z-position computed from nuclear signal within different z-stacks as a quantitative measure of the vertical cellular distribution within each in vitro tissue. 2-way ANOVA was performed with a Tukey’s multiple comparisons test. E,F) Histological tissue sections from the single cell clone ‘‘Arlo’’ as well as from the polyclonal hAELVi cell line stained with hematoxylin and eosin. Cells were grown under ALI conditions for 7 or 14 d. Representative for at least 2 biological replicates. Scale bar: 20  $\mu\text{m}$ . A,B) For details concerning the deviating apparent scale bar please refer to the Experimental section.





fluorescent immunocytochemistry staining showed a homogeneously distributed and continuously connected network of Tight junction protein 1 (Figure 4B) as well as an Occludin signal (Figure 4C). Orthogonal optical sections obtained from confocal microscopy additionally showed an overlap of Occludin and F-Actin signal at the apical cellular junction, further indicating that “Arlo” demonstrates physiologically relevant cellular polarization. In addition, the same data also again showed the monolayer morphology displayed by “Arlo.”

The ability of “Arlo” to form a polarized epithelium with functional tight junctions is also the basis for the establishment of vectorial ion transport. “Arlo” already demonstrated elevated PD values under ALI conditions (Figure 2A, right; ALI:  $37 \pm 14$  mV) when compared to the polyclonal hAELVi cell line as well as to hAEPcs. To assess whether the elevated PD values are related to an elevated synthesis of proteins involved in molecular transport, the expression of 52 genes whose products are involved in the active or passive transport of ions, small- and macromolecules as well as drugs was assessed (Figure 5).

The selected genes were shown to be expressed in the human lung and were derived from literature.<sup>[56,59–62]</sup> The following classes categorize the genes based on the function of their respective gene products: ABC transporters, aquaporins, ATPases, ion channels, ion transport associated, lipid transporter and solute carrier. Gene expression was compared between “Arlo” and hAEPcs over 14 d of culture under ALI conditions. The expression level of many genes was comparable between samples of “Arlo” and hAEPcs, including the genes coding for the sodium/potassium-transporting ATPase catalytic ( $\alpha$ ) and regulatory ( $\beta$ ) subunits (ATP1A1, ATP1A2, ATP1B1) or the sodium channel epithelial 1 subunits (also known as ENaC) subunits (SCNN1A, SCNN1B) within the ATPases class. Among the genes with comparable expression were also the ones coding for drug transporters: ABCB1 (also known as MDR1 or P-gp), ABCC1 (MRP1), ABCC4 (MRP4), ABCC5 (MRP5), ABCG2 (BCRP), SLC15A2 (PEPT2) or SLC22A5 (OCTN2). The gene coding for the sodium channel epithelial 1 subunit gamma (SCNN1G), showed a slight increase in expression within samples of “Arlo” during the course of ALI culture. The expression of the CFTR gene, which codes for the cystic fibrosis transmembrane conductance regulator, seems to be absent in “Arlo,” while CFTR expression was well present in hAEPcs, especially in day 0 samples.

Two genes of the ion transport associated class, however, FXYD3 and CLCA2, showed an elevated gene expression within “Arlo” samples. The respective protein (FXYD domain containing ion transport regulator 3), which the FXYD3 gene codes for, regulates the activity of the sodium/potassium-transporting ATPase.<sup>[63]</sup> The gene product of the CLCA2 gene, the Chloride channel accessory 2 protein modulates calcium-activated chloride channel currents.<sup>[64]</sup> Further, the genes ABCA3 within the

ABC transporter class, the genes AQP1, AQP3, AQP4 within the aquaporin class, ATP11A within the ATPases class, MFSD2A within the lipid transporter class and SLC6A14 within the solute carrier class showed an elevated expression within hAEPcs samples.

## 2.5. Cellular Identity of “Arlo”

The polyclonal hAELVi cell line was considered to have an AT-1-like character.<sup>[45]</sup> Given that the cell line demonstrated elevated TEER values under different culture conditions, the AT-1-like assumption was in parts based on the observed elevated expression of CAV1 as well as on a nondetectable SFTPC expression. The expression of CAV1, the gene coding for the protein Caveolin 1, is enhanced in ATI pneumocytes and SFTPC expression, the gene coding for Surfactant protein C, is considered a specific molecular marker for AT-2 pneumocytes.<sup>[65,66]</sup>

In an effort to determine cell type-specific gene signatures present within the hAEPcs in vitro cultures as well as in the cultures of “Arlo,” the bulk RNA-seq data generated in this study was mapped against the most current set of consensus marker genes for epithelial cells in the human lung.<sup>[59]</sup> The marker genes provided by the integrated Human Lung Cell Atlas define a set of genes that in their specific combination show an elevated expression within the different cell types of the human lung and are used to identify the respective cell types. The data underlying the Human Lung Cell Atlas are consensus-based and represent the most recent re-annotation of 46 single-cell RNA-seq data sets of the human respiratory system.

The data presented here is broadly categorized into the analysis of airway epithelial cells (Figure 6A) and alveolar epithelial cells (Figure 6B). The airway epithelial cell analysis covers basal cells (subdivided into: basal resting, suprabasal), multiciliated cells (subdivided into: deuterosomal, multiciliated nasal, multiciliated non-nasal), secretory cells (sub-divided into: club nasal, club non-nasal, goblet nasal, goblet bronchial, goblet subsegmental) and rare cells (sub-divided into: ionocyte, Tuft). The analysis of the alveolar epithelial cells covers AT-1 cells, AT-2 cells, AT-2 proliferating cells as well as transitional club-AT-2 cells.

The analysis showed that in case of the hAEPcs, on the day of the isolation (day 0) many transcripts which are related to airway epithelial cells (especially multiciliated nasal, multiciliated non-nasal and club non-nasal) are overrepresented indicating a presence of these cell types within the hAEPcs on day 0 from all donors. Interestingly, in one donor isolation the transcripts representative for rare ionocytes and tuft cells seem to be overrepresented (Figure 6A). It stands out however, that hAEPcs in general, but especially on day 7 as well as day 14 of culture, show a distinct overrepresentation of most transcripts representative

**Figure 4.** Similar expression of barrier relevant genes by “Arlo” in comparison to hAEPcs. A) Expression of 35 genes associated with regulating lung barrier integrity or barrier homeostasis by hAEPcs and the single cell clone “Arlo” cultured under ALI conditions was determined via bulk RNA-Sequencing. Genes were assigned the following classes: adherence junctions, desmosomes, gap junctions, receptors and tight junctions based on the function of their respective gene products. Data represent at least 2 biological replicates. B-C) Representative confocal maximum projections from “Arlo” cells on day 14 of culture under ALI conditions, demonstrating homogeneously connected networks of the barrier related proteins tight junction protein 1 (B, TJP1, cyan) and Occludin (C, yellow) stained by immunofluorescence. D) Orthogonal projection from confocal microscopy indicating an apically located Occludin signal. Nuclei stained with DAPI (gray) as well as F-Actin stained with phalloidin (magenta) were included as structural controls in all micrographs. Scale bar: 20  $\mu$ m.

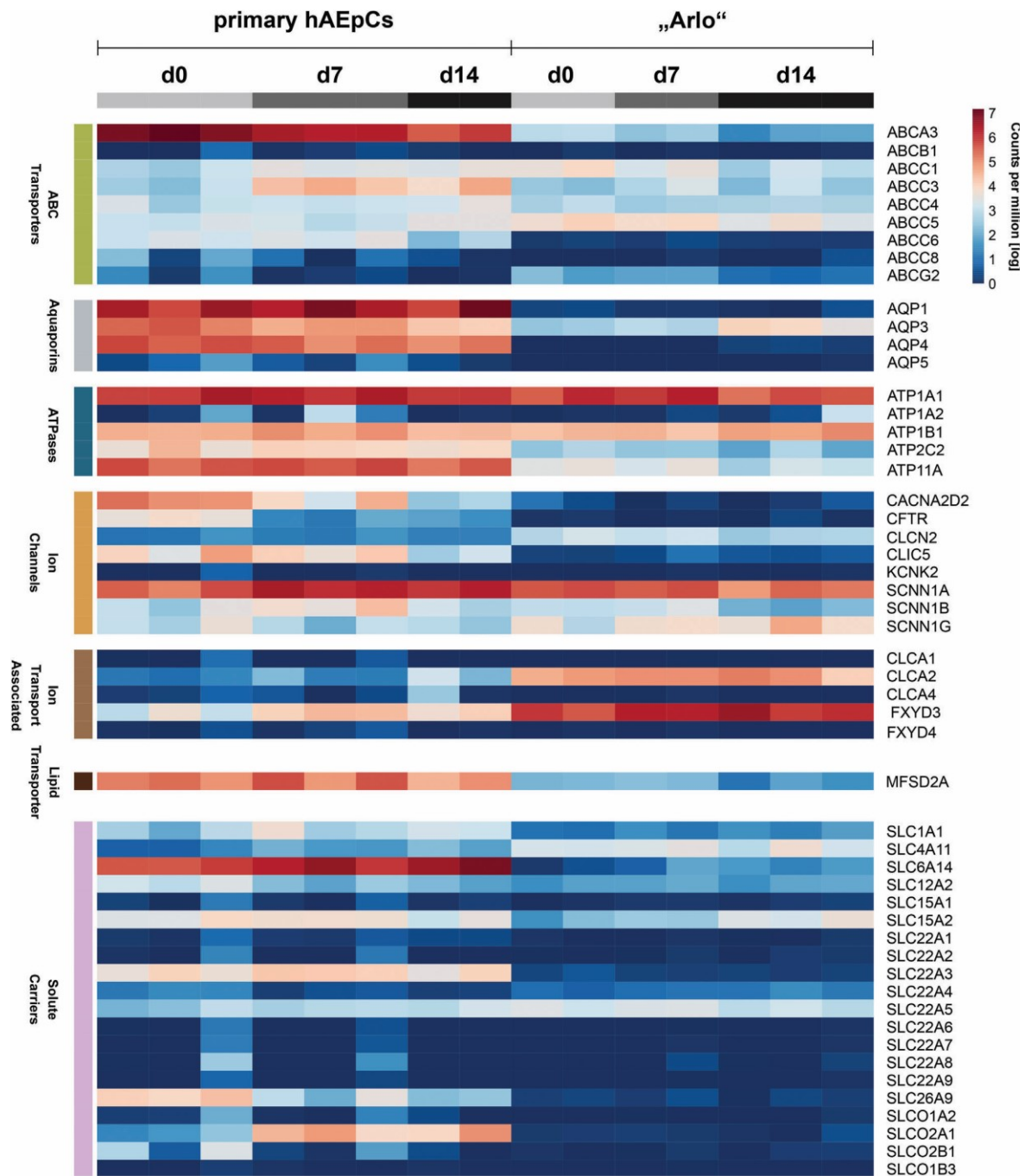
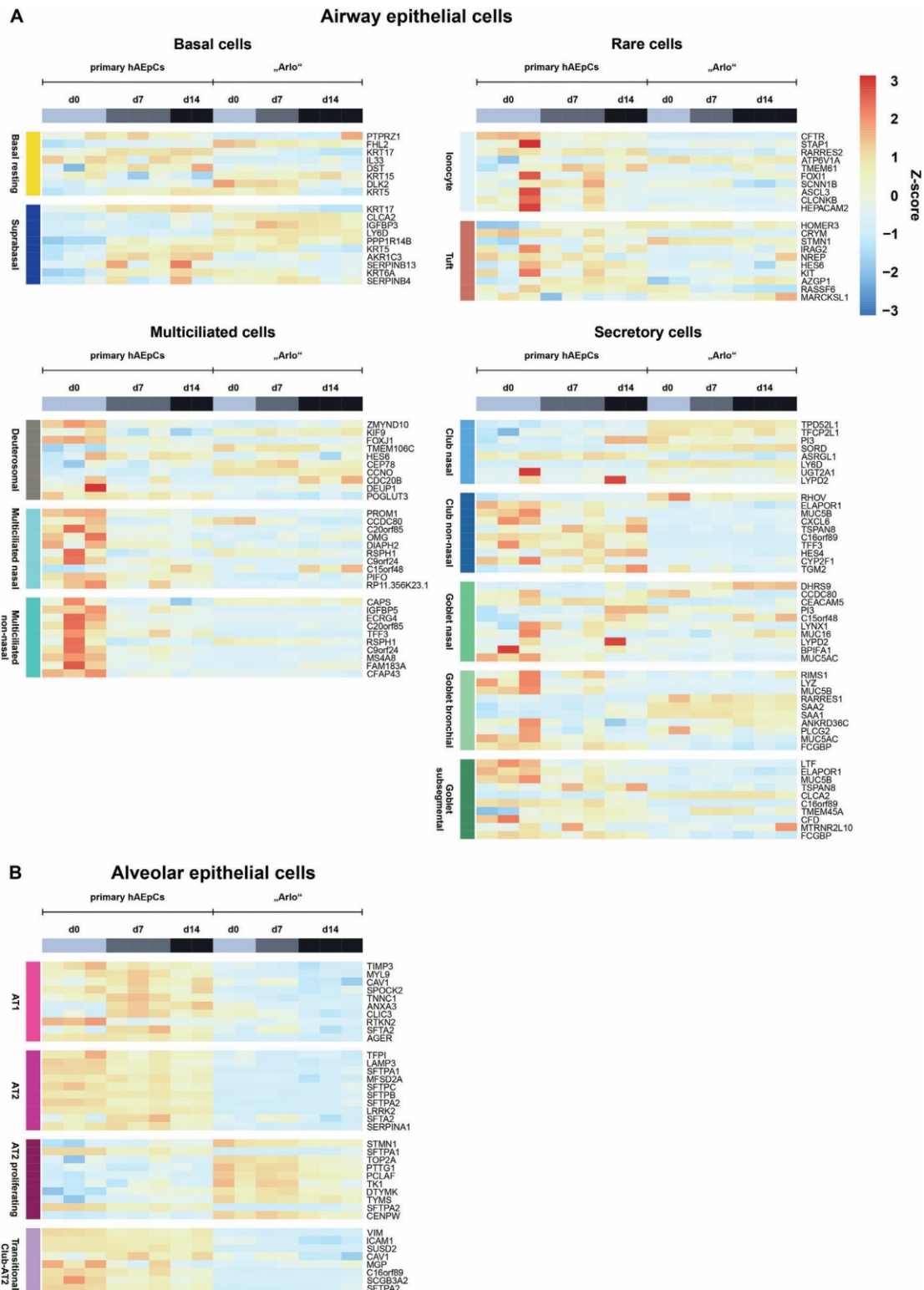


**Figure 5.** Expression of genes related to molecular and ion transport by "Arlo." Genes were assigned to the following classes: ABC transporters, aquaporins, ATPases, ion channels, ion transport associated, lipid transporter and solute carriers based on the function of their respective gene products. Genes showed expression in the human lung and were selected from literature.<sup>[56,59–62]</sup> Data represent at least 2 biological replicates of cells cultured under ALI conditions and were derived from bulk RNA-sequencing.





for alveolar epithelial cells (AT-1 cells, AT-2 cells, and transitional club-AT-2 cells) (Figure 6B).

Interestingly enough, in case of “Arlo” most of the overrepresented gene signatures could be referred to proliferating AT-2 cells. Although CAV1 as well as a few other AT-1 cell related genes (ANXA3, CLIC3 and SFTA2) seem to be overrepresented on day 0 and day 7 in the samples of “Arlo,” the majority of mature AT-1 as well as AT-2 related genes seemed to be underrepresented. The data further indicate that gene signatures of suprabasal as well as club cells from nasal origin are overrepresented within “Arlo” (Figure 6A).

In sum, the gene signatures present in “Arlo” seem to be representative of different cell types, but primarily match proliferating AT-2 cells. Gene signatures found in “Arlo” stand in contrast to the gene signatures observed in hAEPs, which mostly represent AT-1 cells, AT-2 cells, and transitional club-AT-2 cells.

In support of these findings, a gene ontology analysis demonstrated that hAEPs on day 0 (Figure 7A) of culture and “Arlo” on day 14 of culture (Figure 7B) share gene ontology terms that relate to the expression of surface antigens of the major histocompatibility complex (MHC) II. Expression of these surface antigens was shown for AT-2 cells.<sup>[67,68]</sup>

These findings were further supported when traditional, empirically derived markers for alveolar epithelial cells were analyzed (Figure S3, Supporting Information).<sup>[15]</sup> In the case of “Arlo,” some elevated transcripts of the AT-1-like marker CAV1 could be observed on day 0 and day 7, together with some elevation in the transcripts of the AT-2-like markers ABCA3, LAMP3 and MUC1 especially on day 0. These were however lower in abundance when compared to hAEPs. The basal cell marker KRT15, and the secretory club cell marker TUBB3 were the only transcripts from the empirical marker set which displayed higher abundance in “Arlo” than in hAEPs.

## 2.6. “Arlo” as a Use-Case to Study Viral Infections of the Deep Lung

The RNA expression data generated in this study were used to identify potential protein–protein association networks active in “Arlo.” To do so, the STRING resource, a comprehensive online database to discover protein–protein association networks from genome-wide gene expression datasets, was harnessed.<sup>[69,70]</sup> From the several clusters of potential protein–protein interactions obtained from the “Arlo” dataset at day 14 under ALI conditions, the cluster around the gene AGT, which indicated functional interactions also among EDN2, TAS1R3 as well as ACE2 was identified as basis for further studies in the context of infection research (Figure 8A). The pathogenic SARS-CoV-2 that first emerged in China in December 2019 and whose international pandemic spread led to a global health emergency, uses the angiotensin I converting enzyme 2, the protein encoded by ACE2, as an entry receptor for uptake by the host followed by the in-

tracellular priming of the SARS-CoV-2 S protein by the serine protease TMPRSS2.<sup>[74]</sup> In this context, SARS-CoV-2 infection experiments with “Arlo” were conducted as single biological experiments in a proof of principle study to determine the best time points for infection and to evaluate whether productive infection could be observed (Figure 8B,C). When “Arlo” was infected on day 7 of ALI culture, SARS-CoV-2 RNA-copies progressively increased until day 3 postinfection and remained elevated until day 5 postinfection (Figure 8B, upper panel). Productive infection was further supported by western blot, where SARS-CoV-2 nucleocapsid protein was detected in parallel to the rising RNA-copies (Figure 8B, lower panel). Infection of “Arlo” with SARS-CoV-2 on day 14 of ALI culture, also led to an increase in SARS-CoV-2 RNA-copies, accompanied by evidence of productive infection indicated by nucleocapsid protein synthesis from day 3 postinfection and onwards. The total number of RNA-copies, however, appeared to be reduced in comparison to the infection on day 7 (Figure 8C). Presence of the angiotensin I converting enzyme 2 as well as the serine protease TMPRSS2 was additionally confirmed in both experiments on the protein level (Figure 8B,C).

In patients that suffer from the coronavirus disease 2019 (COVID-19), the disease caused by a SARS-CoV-2 infection, a synergism of the cytokines TNF- $\alpha$  and INF- $\gamma$  triggers inflammatory cell death as well as tissue damage.<sup>[76]</sup> Based on the adaptation of an existing protocol where cells are cultured in absence of FCS and hydrocortisone as stimulation medium, TNF- $\alpha$  and INF- $\gamma$  stimulation was used to demonstrate cytokine induced reduction of barrier properties in case of “Arlo” (Figure 8D).<sup>[75]</sup> Synergistic stimulation with TNF- $\alpha$  and INF- $\gamma$  led to a relative decrease of  $\approx 50\%$  in TEER after 24 h compared to the TEER values before stimulation. After 48 h of stimulation with TNF- $\alpha$  and INF- $\gamma$  a significant reduction of TEER values was observed.

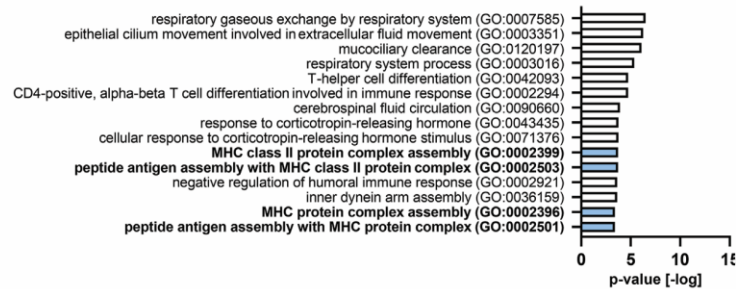
The findings from the single-variant infection studies described above were also used to infect “Arlo” with other variants of SARS-CoV-2 (FFM1, FFM 7, Alpha, Beta and Zeta) (Figure S4, Supporting Information). Although infection was not achieved for all of the variants, productive infection could be observed for some of them. Although investigation that is more thorough will be needed here, preliminary experiments suggest differences in barrier disruption responses to infection by the variants.

## 3. Discussion

We generated the single-cell clone “Arlo” in light of the growing demand for a reproducible cellular in vitro model of the alveolar epithelium for biopharmaceutical inhalation research. “Arlo” not only demonstrates robust barrier integrity with TEER values  $>3000 \Omega \text{ cm}^2$  under ALI conditions, but in addition also develops a polarized monolayer. These functional barrier properties are further supported on the molecular level by the expression of genes and proteins related to barrier integrity as well as homeostasis that largely correlates with hAEPs cultured in vitro.

**Figure 6.** Cell type specific gene signatures in the samples of hAEPs and “Arlo.” Cell type specific gene signatures of genes whose expression is representative for specific epithelial cell types within the human lung were defined by and derived from the integrated Human Lung Cell Atlas consortium.<sup>[59]</sup> A) Airway epithelial cell types are subdivided into basal cells, multiciliated cells, rare cells and secretory cells. Individual cell types are displayed on each heatmap (left, vertically). B) Alveolar epithelial cells are categorized into individual cell types without further sub-division. Data represent at least 2 biological replicates of cells cultured under ALI conditions and were derived from bulk RNA-Sequencing.

**A Primary hAEPs - highly expressed genes d0**



**B „Arlo“ - highly expressed genes d14**

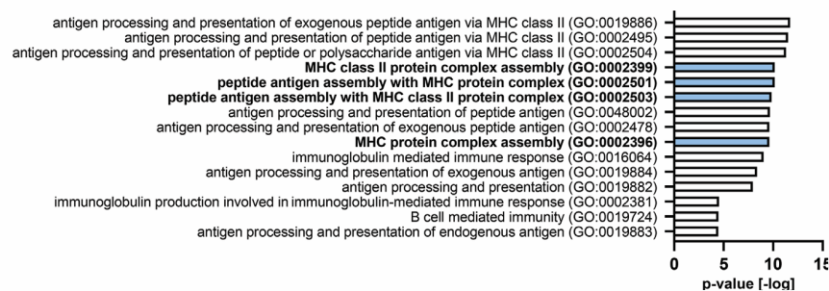


**Figure 7.** Gene ontology analysis reveals expression of MHC II surface antigens by hAEPs and “Arlo.” Gene ontology (GO) analysis of the top 15 highly expressed genes in hAEPs on A) day 0 after isolation and in “Arlo” on B) day 14 of culture under ALI conditions.<sup>[69–73]</sup> Shared gene ontology terms are marked in blue. Data represent at least 2 biological replicates of cells cultured under ALI conditions and were derived from bulk RNA-sequencing.

To be used in biopharmaceutical inhalation experiments, such tissue-specific barrier integrity provided by alveolar epithelial cells grown at the ALI could in the past almost exclusively be obtained *in vitro* by isolated primary hAEPs that were differentiated towards AT-1-like cells on Transwell inserts.<sup>[20,23,25,29]</sup> Primary cell isolations are costly and the trans-differentiation of these cells *in vitro* restricts their experimental use to only a few days. Sub-cultivation of hAEPs without the addition of feeder cells is possible for a very limited number of passages, but is mostly avoided due to rapid de-differentiation of the cells which might influence experimental readouts.<sup>[30]</sup>

The rapid advancement of culture models that are either generated from human adult stem cells or induced pluripotent stem cells (IPSCs) that are often further differentiated into organoids could offer an alternative to the use of freshly isolated hAEPs when modeling the alveolar epithelium *in vitro*.<sup>[33]</sup> Due to their intact stemness during *in vitro* culture, these cells can be continuously expanded. When cultured under ALI conditions on Transwell inserts or on basement membrane equivalents some models demonstrated AT-1 as well as AT-2 marker expression such as aquaporin 5 (AQP5), podoplanin (PDPN) or SFTPC after differentiation.<sup>[35–37,39]</sup> Another model which is based on alveospheres also showed enhanced expression of markers relevant for alveolar epithelial cells, but is not suitable for standardized drug transport studies over the alveolar epithelium yet because the closed spheres are fully embedded in 3D-culture matrices.<sup>[40]</sup> Other models were either not cultured under ALI conditions or demonstrated the formation of inhomogeneous cellular multilayers when seeded on Transwell inserts.<sup>[38,77]</sup> What all of the afore-

mentioned studies have in common, is that they either did not assess barrier integrity at all or reported TEER values <300 Ω cm<sup>2</sup> and/or have not been characterized in terms of drug transport. In a model reported by He et al., human IPSCs were differentiated to alveolar organoids and in parallel to endothelial cells before both cell types were seeded on artificial or reconstituted basement membranes under ALI-conditions. In this study, TEER values of ≈400 Ω cm<sup>2</sup> were reported, but drug transport was not assessed.<sup>[34]</sup> A further aggravating factor is that such models are experimentally challenging to establish, costly to implement and might hamper inter-laboratory comparison due to complex differentiation protocols.<sup>[77,78]</sup> One alveolar epithelial model which is based on differentiated human IPSCs grown on 96-well Transwell inserts under ALI conditions, reported tight barrier properties indicated by TEER values > 1000 Ω cm<sup>2</sup> and would thus be suitable for drug transport studies.<sup>[79]</sup> These TEER values, however, were measured using a custom-built device and were only compared to literature derived TEER values from hAEPs. Given the inter-laboratory variability of TEER measurements in general, side-by-side comparisons using the same experimental setup should be performed when assessing TEER values, as previously discussed and also conducted in the current study.<sup>[80]</sup> The provided confocal micrographs further indicated multilayered cellular clusters, which were not assessed quantitatively and could have influenced TEER development.

Although regarded as a promising *in vitro* model for the alveolar epithelium based on a continuous cell line, the polyclonal hAELVi cell line generated inconsistent results in the development of functional barrier properties as reported in the literature,



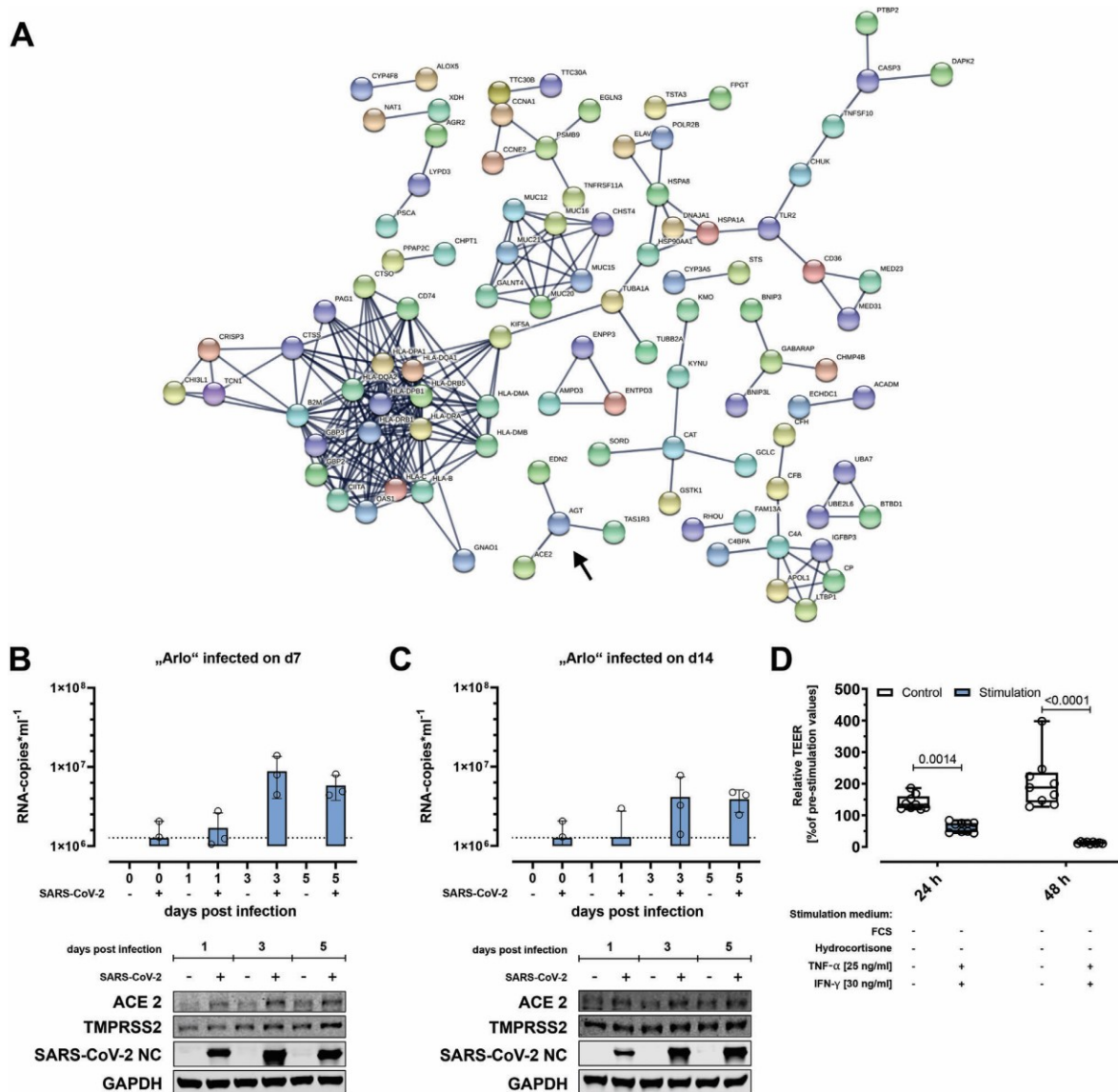


**Figure 8.** SARS-CoV-2/FFM7 infection as use-case for using “Arlo” for viral infection studies. A) Cluster analysis by the STRING resource to obtain potential protein-protein interactions present in samples of the single-cell clone “Arlo.” Arrow marks a cluster around the gene AGT that indicates an interaction with the gene ACE2. Analysis was derived from bulk RNA-Sequencing data of cells cultured until day 14 under ALI conditions. Data represent at least 2 biological replicates. B,C) Infection studies performed with “Arlo” either on A) day 7 or B) day 14 of culture under ALI conditions with SARS-CoV-2/FFM7 (MOI of 1) or mock (PBS). Upper panels show SARS-CoV-2/FFM7 RNA copy numbers (RNA-copies mL<sup>-1</sup>) derived from qRT-PCR of the RNA-dependent RNA polymerase (RdRp) gene copies present in single apical washes (30 min, PBS) on the given days post-infection. Lower panels show western blots indicating the cellular presence of angiotensin I converting enzyme 2 (ACE2), transmembrane serine protease 2 (TMPRSS2) and SARS-CoV-2/FFM7 nucleocapsid protein (SARS-CoV-2 NC) in samples infected with SARS-CoV-2/FFM7 (MOI of 1) or mock (PBS). Glyceraldehyde-3-phosphate dehydrogenase (GAPDH) was used as a control protein. Data represent single independent experiments. D) Reduction of barrier properties by stimulating “Arlo” monolayers synergistically with TNF- $\alpha$  [25 ng mL<sup>-1</sup>] and INF- $\gamma$  [30 ng mL<sup>-1</sup>] for 48 h. 24 h before the experiment, cells were incubated in stimulation medium without FCS and hydrocortisone as an adaptation of a previous protocol.<sup>[75]</sup> “Arlo” monolayers were grown under LCC for 10 d before the switch to stimulation medium. TEER values were normalized to the values before stimulation. Data represent mean  $\pm$  S.D.;  $n = 9$  for each group from 3 independent biological replicates.

most probably due to its polyclonality. The results reported in the current study for the polyclonal hAELVi cell line as well as experiments performed by other laboratories show that barrier properties developed differently over time than originally reported by Kuehn et al.<sup>[49–51]</sup> The reason for these conflicting reports most probably is that the polyclonal hAELVi cell line was generated by functional immortalization of multiple CD326/EpCAM-positive hAEPcS that have been cultured on a six-well cell culture plate for 5 days without clonal selection.<sup>[45,48]</sup> When isolating alveolar epithelial cells only via CD326/EpCAM as a positive molecular selection marker, not only AT-2-like cells are selected from a cell suspension but also AT-1-like as well as bronchiolar epithelial cells.<sup>[81]</sup> These findings are further supported by the transcriptomic analysis in this study, where gene signatures of these different epithelial cell types could also be detected in the hAEPcS on d0 after isolation, which have been isolated according to the same experimental protocol as the hAEPcS used for the generation of the polyclonal hAELVi cell line. Also in accordance with this hypothesis, other laboratories reported AT-2-like properties for a sub-population of the polyclonal hAELVi cell line, such as formation of microvilli or presence of surfactant as well as of proteins related to surfactant secretion.<sup>[82,83]</sup> It needs to be mentioned though, that propagation of sub-populations of the polyclonal hAELVi cell line could also be influenced by different growth media used to culture the polyclonal hAELVi cell line. We used equal culture conditions (cell culture medium and Transwell inserts) compared to the ones used by Kuehn et al. during the culture of all cellular models in the current study, whereas other reports used different growth media. Out of this reason, we highly recommend to follow the methods as well as to use the same culture media etc. described in this study, to ensure interlaboratory comparison of experimental results obtained from the single cell clone “Arlo” but also from the polyclonal cell line hAELVi.

The gene signatures representative for lung epithelial cells used in our study to assess the proportional cell types present in the primary hAEPcS isolations as well as in the “Arlo” samples were derived from the data published in the context of the human lung cell atlas.<sup>[6,59]</sup> To our knowledge, the data from the human lung cell atlas contain the most recent consensus-based as well as the largest set of annotations of the different cell types within the human lung and were thus selected for the gene signature analysis. Based on this data, the transcripts identified in “Arlo” seem to resemble proliferating AT-2 cells the most, followed by less abundant gene signatures representative for suprabasal as well as club cells of nasal origin. Apart from the abundance of gene signatures representative for proliferating AT-2 cells, we additionally identified the expression of transcripts related to the synthesis of MHC II in the samples of “Arlo,” as verified by the gene ontology as well as STRING network analysis. Surface antigens such as the MHC II molecules HLA-DR, HLA-DP, or HLA-DQ have been shown to be constitutively expressed by human AT-2 cells where they act as a major contributor to barrier immunity in vivo and are being discussed as exclusive selection markers to obtain pure AT-2 cell isolations.<sup>[67,68,84,85]</sup> Our gene ontology analysis data further indicate, that the expression of MHC II related molecules seems to be also highest in the hAEPcS samples immediately after isolation, before they decline over the course of in vitro culture. In the samples of “Arlo,” a contrary development was observed charac-

terized by a high presence of transcripts related to antigen presentation up to day 14 of culture.

In general, “Arlo” seems to show a marker expression profile that is distinct from the gene signatures obtained from hAEPcS. In the context of a potential AT-2-like phenotype of “Arlo,” this is most pronounced in the expression levels of surfactant related transcripts. Transcripts for SFTPA1, SFTPA2, SFTPB, SFTPC as well as SFTPD show no to very low expression in “Arlo.” Although SFTPC expression is considered the current gold standard to identify mature AT-2 cells, recent data suggest a heterogeneity among the adult AT-2 population in vivo.<sup>[6]</sup> In this context, AT-2 cells that show a low to absent SFTPC expression but a higher expression of ABCA3 seem to represent a proliferating progenitor cell type, while AT-2 cells that show high SFTPC levels together with a high expression of ABCA3 seem to rather represent mature AT-2 cells.<sup>[86]</sup> The authors speculated that these progenitor populations might be activated during early lung development, during disease or after lung damage. ABCA3 expression, however, declines in “Arlo” from day 0 to day 14 of culture, as seen in the empirically defined marker analysis.

Interestingly, the considerably high TEER values, functional barrier properties, and the polarized monolayer morphology demonstrated by “Arlo” seem to contradict a proliferating AT-2-like character. Primary human proliferating AT-2 cells, which were cocultured together with fibroblast feeder cells in addition to a treatment with the Rho kinase inhibitor Y-27632 in order to maintain active proliferation programs in vitro, only demonstrated TEER values of  $\approx 450 \Omega \text{ cm}^2$  when cultured under ALI conditions.<sup>[30]</sup>

In contrast, TEER values of  $\approx 3000 \Omega \text{ cm}^2$  as demonstrated by “Arlo” would be associated with an AT-1-like in vitro performance, as obtained by our lab for hAEPcS in the past and also demonstrated by one hAEPcS isolation in the current study.<sup>[29]</sup> But neither the cuboidal morphology of “Arlo” cells nor the gene signatures seem to support an AT-1-like phenotype. In this context, these new findings strongly challenge our previous assumption that the polyclonal hAELVi cell line is an AT-1-like cell line. Others also discussed the lack of strong evidence concerning an AT-1-like phenotype, besides CAV1 expression and elevated TEER values.<sup>[20]</sup>

The markers CLCA2, DAPL1, LY6D, and TUBB3 that were either defined in the empirical or consensus based marker sets, showed higher abundance in “Arlo” in comparison to hAEPcS. These markers were not only part of the transcriptomic gene signatures representative for basal cells, club cells of nasal origin as well as suprabasal cells but have also been shown to be upregulated in lung cancer patients.<sup>[87–90]</sup> As already mentioned in the results section, the gene product of CLCA2, the Chloride channel accessory 2 protein, is known to modulate calcium-activated chloride channel currents and could thus have an influence on the elevated PD values observed for “Arlo.”<sup>[64]</sup> However, the elevated expression of CLCA2 was also shown to be an important characteristic of epithelial differentiation and loss of CLCA2 was discussed to promote breast cancer metastasis.<sup>[91]</sup>

Within this context, the cell line NCI-H441 that was generated from a male patient with a papillary adenocarcinoma also demonstrated mixed characteristics of club cell-like and AT-2-like cells.<sup>[92]</sup> While the presence of SFTPA and SFTPB was detected in these early studies, also the AT-1 relevant marker RAGE has been



reported to be expressed by NCI-H441 in later studies.<sup>[93]</sup> Similar to the polyclonal hAELVi cell line, also for NCI-H441 no clonal selection was performed, which a study by Neuhaus et al. supported by identifying two distinct subpopulations of the NCI-H441 cell line. In one subpopulation the expression of the AT-1 related markers CAV1 as well as RAGE and in the other population the AT-2 related marker SFTPB could be detected.<sup>[93]</sup> A more recent comparison of the polyclonal cell line hAELVi and the cell line NCI-H441 identified SFTPC expression and presence of lamellar bodies in NCI-H441.<sup>[50]</sup> Although the cell lines NCI-H441 and the polyclonal hAELVi cell line have been suggested as promising models for the alveolar epithelium especially in the context of biopharmaceutical experiments, both share similar drawbacks in terms of reproducible barrier properties reported in literature. TEER value development of NCI-H441 seems to strongly depend on the seeded cell density and the addition of dexamethasone to the culture medium.<sup>[94]</sup> TEER values of  $\approx 1500 \Omega \text{ cm}^2$  have been recently described for NCI-H441 under ALI conditions, while earlier studies demonstrated TEER values of  $< 300 \Omega \text{ cm}^2$ .<sup>[46,47]</sup> In the study by Lochbaum et al., however, TEER values seem to rise until day 5 of culture to values  $\approx 1500 \Omega \text{ cm}^2$  and then seem to decline towards day 7, which strongly restricts the timespan at which experiments could be performed. Another study looked at culture times of 30 d, but only reported maximum TEER values of  $\approx 140 \Omega \text{ cm}^2$  at day 10 of culture for NCI-H441 cultured under ALI conditions, which also declined rapidly after this maximum.<sup>[50]</sup> In addition, multilayer formation was reported for NCI-H441 in several studies, further complicating the assessment of TEER development when no quantitative assessment of multilayer formation is performed in parallel.<sup>[50,95]</sup> Similarly, multilayer formation by the polyclonal cell line hAELVi was demonstrated in our study supporting the findings of others.<sup>[50,96,97]</sup>

The single-cell clone “Arlo,” however, demonstrated the formation of a polarized monolayer in a direct comparison with the polyclonal hAELVi cell line under equal culture conditions. The evaluation of the tissue morphology, which is based on quantitative image analysis, demonstrates that the monolayer morphology of “Arlo” is not limited to certain areas within selected sections—it represents the dominant tissue architecture. The tissue architecture of “Arlo” seems to be additionally supported by functional processes relevant to barrier integrity. This can not only be observed by the elevated TEER values together with increased transepithelial PD under LCC and ALI conditions, but also by the expression of genes and synthesis of proteins relevant to barrier formation as well as homeostasis. Among the largely similar gene expression patterns observed for “Arlo” in comparison to hAEPcs a large number of genes coding for the tight junction protein family of claudins can be found.

Especially, the claudins CLDN3, CLDN4, CLDN5, CLDN7, and CLDN18 have been reported to fulfill important functions in the lung epithelium.<sup>[55]</sup> While CLDN5 showed elevated expression in airway epithelial cells, others such as CLDN7 have been shown to be ubiquitously expressed by nearly all epithelial cells in the lung.<sup>[98,99]</sup> CLDN3, CLDN4, and CLDN18 seem to fulfill specific roles in the alveolar epithelium.<sup>[100]</sup> Remarkably, upregulation of CLDN4 and downregulation of CLDN3 through use of an adenoviral vector was reported to increase barrier properties of AT-1-like rat cells *in vitro*.<sup>[101]</sup> All of the patterns mentioned above could be observed in the samples of “Arlo” as well as in

the hAEPcs with the exception of CLDN18. The splice variant Claudin 18.1 by the CLDN18 gene is exclusively expressed in the lung and highly expressed in the alveolar epithelium.<sup>[102,103]</sup> While the highest abundance of CLDN18 transcripts could be observed on day 0 for hAEPcs, the abundance declined during the following days of culture. Within samples of “Arlo” transcripts of CLDN18 could not be detected. This finding is again supportive of the proliferating AT-2 character of “Arlo,” since proliferating AT-2 cells were highly abundant in CLDN18 double knockout mice.<sup>[104]</sup> Transcripts for CLDN10, which is specifically expressed by club cells, were also absent in “Arlo.”<sup>[105]</sup>

Homogenous distribution as well as localization of Occludin and Tight Junction Protein 1/ZO-1 in the samples of “Arlo” further indicate the presence of intact tight junctional complexes. These findings are also supported by the transcriptomic profiles of the genes coding for these proteins, OCLN and TJP1. Although these tight barrier properties also showed to enable vectorial ion transport in case of “Arlo,” identifying the reasons for the observed increase in transepithelial PD would have exceeded the methods that were available during this study. However, recent reports support our finding of an elevated expression of FXVD3 in alveolar and other respiratory epithelial cells, being highest in AT-1 cells.<sup>[106,107]</sup> Furthermore, FXVD3 mediated regulation of the sodium/potassium-transporting ATPase was linked to an increase in sodium absorption in proximal airway epithelia, which also positively stimulated the rate of liquid absorption.<sup>[108]</sup> Again, in the NCI-H441 cell line, FXVD3 overexpression did not lead to a significant increase in sodium absorption.<sup>[109]</sup> While the quantification of mRNA expression can be used to estimate transporter activity, future studies using “Arlo” would need to include functional assessments of the transport of specific transporter substrates in presence and absence of selective transport inhibitors, to draw conclusions about the elevated transepithelial PD values that are more robust.<sup>[110]</sup>

The paracellular transport studies with the low-permeability marker fluorescein sodium, under the additional influence of EDTA, moreover indicated that the tight junction complexes could be modulated. Modulation of barrier properties could also be seen under the synergistic influence of the inflammatory cytokines TNF- $\alpha$  and INF- $\gamma$ . The single-cell clone “Arlo” allowed for the rapid adaption of a protocol by Metz et al., that was established to assess barrier properties of the polyclonal cell line hAELVi under the influence of proinflammatory stimulants.<sup>[75]</sup> We omitted FCS as well as hydrocortisone in our adapted protocol only from the stimulation medium since longer cultivation of the polyclonal cell line hAELVi without FCS and hydrocortisone led to morphological changes.<sup>[75]</sup> Barrier properties of “Arlo” were not negatively affected by the stimulation medium, whereas the synergistic treatment with TNF- $\alpha$  and INF- $\gamma$  led to a collapse of barrier properties after 48 h treatment. We did, however, not assess, whether the reduction of barrier properties under the synergistic influence of TNF- $\alpha$  and INF- $\gamma$  was caused by panopsis, as also seen in COVID-19 patients, or stimulation of other cellular pathways such as NF- $\kappa$ B.<sup>[75,76]</sup> Further possible applications for “Arlo” beyond the use in classical biopharmaceutical experiments were revealed by the exploration of the RNA-Seq data for possible protein-protein interactions using the STRING resource. Interestingly, these data not only supported the findings of interactions among the MHC II surface antigens as also

seen in the gene ontology analysis, but also revealed an interaction network that included ACE2. Based on these results we not only verified angiotensin I converting enzyme 2 as well as the serine protease TMPRSS2 on the protein level, but in addition also demonstrated productive infection of “Arlo” with SARS-CoV-2. Although we saw productive infection in a total of three different biological replicates, these data need to be interpreted as a proof of principle, since the time points for infection differed with each replicate. Our findings are further supported by a recently published study, which provided evidence that the polyclonal hAELVi cell line could also be used to model productive viral infection, including variants of SARS-CoV-2.<sup>[111]</sup> In addition, the study by Mache et al., however, also demonstrated the multilayer formation by the polyclonal hAELVi cell line, which we quantified in the current study. Nonetheless, these findings offer new possibilities to use “Arlo” also as an epithelial model in the context of infection research. Given that ACE2 and other host factors are diversely expressed in the nasal, bronchial and alveolar epithelium by different cell types such as ciliated, club, secretory and alveolar cells, it will be interesting to see to which of these cell types “Arlo” corresponds the most.<sup>[112,113]</sup> Based on our results, the resemblance of an AT-2-like phenotype by “Arlo” is most likely and would also fit in vivo observations showing a higher preference of SARS-CoV-2 to infect AT-2 pneumocytes.<sup>[114]</sup>

#### 4. Limitations of the Study

As it is with most studies, also the results reported herein should be valued in light of some limitations. We have chosen to perform an untargeted bulk RNA-seq analysis over single-cell RNA-seq analysis of the hAEPs as well as “Arlo” samples, since bulk RNA-seq allowed us to obtain a deeper coverage of the total transcriptome and offered a simpler isolation of the RNA representative for all cells grown on the Transwell inserts. While this allowed us to identify many transcriptomic gene signatures that are representative for specific cell types or molecular complexes with confidence in the bulk samples due to a high level of mapped reads, we could not obtain defined clusters of specific cell types that share the same transcriptome. Assigning a specific cell type in the alveolar epithelium, especially given the intricacies of sample preparation and growing cells on Transwell inserts, requires identifying a multidimensional set of appropriate markers. Such future studies could build on advanced spatial proteomics techniques like, e.g., deep visual proteomics to fully unravel the cellular heterogeneity seen in the hAEPs as well as “Arlo” samples.<sup>[115]</sup>

#### 5. Conclusion

In vitro cultures of “Arlo” grown on Transwell inserts at the air interface reliably develop monolayers with functional tight junctions. Low paracellular permeability is the most essential feature of the alveolar epithelium for building a meaningful in vitro model in the context of biopharmaceutical inhalation research. The strong similarity between “Arlo” and primary hAEPs relating to gene expression involved in the formation of the junctional barriers in the human lung further opens opportunities to use “Arlo” in various other biomedical and biological disciplines. This especially holds true for infection research, where it will be

fascinating to study whether viral infection might trigger or even influence antigen presentation by these alveolar epithelial cells.

#### 6. Experimental Section

**Cell Culture:** The hAELVi polyclonal cell line (CI-hAELVi; InSCREENex GmbH, INS-CI-1015), passages 33 to 36, as well as the single cell clone “Arlo,” passages 1 to 20, were cultured in T25 cm<sup>2</sup> culture flasks containing 7 mL small airway growth medium (SAGM) Bullet kit (Lonza, CC-3118) supplemented with 100 U mL<sup>-1</sup> penicillin, 100 µg mL<sup>-1</sup> streptomycin (15140122) and 1% fetal calf serum (FCS) (all Gibco, Thermo Fisher Scientific Inc.), which was exchanged every two to three days. Cells were passaged after 7 d of culture. For that purpose, cells were washed twice with 7 mL PBS-buffer (Dulbecco’s PBS; Sigma-Aldrich, D8537) detached with 2 mL trypsin-EDTA 0.05% (Gibco, Thermo Fisher Scientific Inc., 25300-054) for 8 min., centrifuged at 300 rcf for 4 min. The cell suspension was reconstituted from the pellet in 5 mL SAGM Bullet kit including all supplements and cells were seeded into a new T25 cm<sup>2</sup> culture flask (0.7 × 10<sup>6</sup> cells per flask) and/or used for the experiments detailed in the following paragraphs. Before cell seeding, the cell culture flasks have been coated for 1 h at 37 °C by using a 2 mL solution of 1% volume/volume (v/v) fibronectin (human 1 mg mL<sup>-1</sup>; Corning, 356008) and 1% (v/v) collagen type 1 (bovine 3 mg mL<sup>-1</sup>, Sigma-Aldrich, C4243) in distilled and sterile-filtered H<sub>2</sub>O. The coating solution was completely aspirated shortly before cell seeding. All solutions were prewarmed to 37 °C before use and cells were maintained at 37 °C in a humidified atmosphere containing 5% CO<sub>2</sub>.

**Single-Cell Isolation and Clonal Expansion:** Polyclonal hAELVi cells have been cultured for 7 d in a T25 cm<sup>2</sup> cell culture flask containing 7 mL SAGM Bullet kit including all supplements until confluent and were handled in the same manner as they would have been for passaging. The only exception was that the cell suspension was reconstituted in HBSS and adjusted to a concentration of 0.7 × 10<sup>6</sup> cells per mL after the centrifugation step. Mean cell diameter as well as cell diameter distribution of the single cell suspension were measured using a cell counter and analyzer (CASY; OMNI Life Science). A volume of 500 µL of the single-cell suspension was transferred to a dispensing cartridge of the single-cell printer (c.sight; Cytena). To collect the printed single cells, a 96-well cell culture plate was precoated for 1 h with 50 µL per well of the coating solution from Section 1.1. The inner wells (60 wells) were then supplemented with 50 µL SAGM Bullet kit including all supplements and the outer wells (36 wells) were filled with 50 µL distilled and sterile-filtered H<sub>2</sub>O, to protect the single cell cultures from temperature changes as well as evaporation effects within the 96-well plate. In addition, the prepared 96-well plate was placed at 37 °C in a humidified atmosphere containing 5% CO<sub>2</sub> until the printing procedure started. Single-cell printing as well as culturing of the single cells was performed according to the manufacturer’s instructions with the parameters depicted in Figure 1B (Number of cells per well: 1; Cell diameter [µm]: 10–25; Cell roundness [a.u.]: 0.7–1), after performing a droplet quality control.<sup>[116]</sup> The inner 60 wells of the 96-well plate containing the printed single cells, whose mono-clonality was confirmed by the image-based algorithm, were fed with 8 µL SAGM Bullet kit including all supplements 48 h after the single cell printing without aspirating any medium from the culture wells every second day until bigger colonies of dividing cells (10–20 cells) could be observed. A volume of 8 µL of distilled and sterile-filtered H<sub>2</sub>O was added to the outer 36 wells. The cell culture medium of wells that contained colonies of dividing cells, was then aspirated every second day and replenished with fresh 200 µL SAGM Bullet kit including all supplements in case of the inner wells or 200 µL of distilled and sterile-filtered H<sub>2</sub>O in case of the outer wells until cells reached confluency. As exemplarily shown in Figure 1A for “Arlo,” monoclonal cultures were then serially transferred to bigger plate formats once they reached confluency. When cell numbers reached > 0.3 × 10<sup>6</sup> cells per well they were transferred to a T25 cm<sup>2</sup> culture flask. Cells from the single-cell clone “Arlo” were defined as passage 1, after they have been cultured for 7 d in a T25 cm<sup>2</sup> culture flask for the first time. Passage 1 as well as the consecutive passages were cryo-preserved for cell banking, where 1 × 10<sup>6</sup> cells per well were cryopreserved in cryo storage tubes in a cryopreservation medium

(35% SAGM Bullet kit including all supplements, 35% Dulbecco's modified Eagle medium/nutrient mixture F-12 (DMEM/F12; Gibco, Thermo Fisher Scientific Inc., 11320033), 20% FCS as well as 10% dimethyl sulfoxide (DMSO); all volume/volume).

**Isolation of Primary Alveolar Epithelial Cells:** Primary alveolar epithelial cells (hAEPcs) have been isolated from lung tissue which had been resected at the SHG clinics Völklingen, Germany according to the procedure described in Daum et al.<sup>[48]</sup> The local ethics committee of the state of Saarland, Germany, permitted the use of the patient material for the biomedical research performed in this study on 21 May 2019 under the sign 113/19. The committee has reviewed the patient consent forms in this process as well.

Briefly, the lung tissue was chopped into 5  $\mu\text{m}$  wide smaller pieces using a tissue chopper (Mcllwain Tissue Chopper, Plano GmbH). These pieces were collected in a 50 mL Falcon tube containing 30 mL balanced salt solution ( $137 \times 10^{-3}$  M NaCl,  $5 \times 10^{-3}$  M KCl  $0.7 \times 10^{-3}$  M,  $\text{Na}_2\text{HPO}_4$   $10 \times 10^{-3}$  M, HEPES,  $5.5 \times 10^{-3}$  M glucose, adjusted to pH 7.4) and washed three times by using a 100  $\mu\text{m}$  pore-sized cell strainer (Greiner, 542000) to recover the tissue remnants during each washing step. The tissue remnants were then enzymatically digested to generate a cell suspension, by using a combination of 1.5 mL trypsin ( $1 \times 10^6$  BAEE units  $\text{mL}^{-1}$ ; Sigma-Aldrich, T8003) and 300  $\mu\text{L}$  elastase ( $10 \text{ mg mL}^{-1}$ , Worthington, LS002279) for 40 min at 37  $^\circ\text{C}$ . After this incubation time, the cell suspension was serially washed again by using a 100  $\mu\text{m}$  pore-sized cell strainer first, followed by an washing step through a 50  $\mu\text{m}$  pore-sized cell strainer (Greiner, 542040). By incubating the cell suspension in cell culture petri dishes for 90 min at 37  $^\circ\text{C}$ , attaching immune cells as well as erythrocytes were excluded from the suspension. The cell suspension was then further purified using a Percoll gradient (Sigma-Aldrich, P1644) followed by a positive antibody selection for CD326 (EpCam) positive cells using a LS column (Micro beads; MACS column; Miltenyi Biotec, 130-061-101 (beads) or 130-042-401 (column)). The cell suspension of purified CD326-positive cells was recovered in 5 mL SAGM Bullet kit including all supplements and either seeded on Transwell inserts as described in the following paragraph, or used for isolation of RNA.

**Transwell Experiments:** Before cell seeding, Transwell inserts were coated for 1 h at 37  $^\circ\text{C}$  by adding a 100  $\mu\text{L}$  solution of 1% (v/v) fibronectin (human  $1 \text{ mg mL}^{-1}$ ; Corning, 356008) and 1% (v/v) collagen type 1 (bovine  $3 \text{ mg mL}^{-1}$ , Sigma-Aldrich, C4243) in distilled and sterile-filtered  $\text{H}_2\text{O}$  per Transwell. The coating solution was completely aspirated shortly before cell seeding.

$0.33 \times 10^5$  cells of the polyclonal cell line hAELVi as well as the single cell clone ‘Arlo’ or  $1 \times 10^5$  cells of the hAEPcs were seeded in 200  $\mu\text{L}$  SAGM Bullet kit including all supplements per apical compartment of a Transwell insert ( $0.33 \text{ cm}^2$ ; 400 nm pore size; Corning, 3470) ( $1 \times 10^5$  cells  $\text{cm}^{-2}$ , cell lines;  $3 \times 10^5$  cells  $\text{cm}^{-2}$ , hAEPcs). The basolateral compartment was supplemented with 800  $\mu\text{L}$  SAGM Bullet kit including all supplements. Every 2 to 3 d used medium was aspirated from the basolateral compartment first and then from the apical compartment. In the case of liquid-covered conditions (LCC) SAGM Bullet kit including all supplements was supplemented first in the apical compartment (200  $\mu\text{L}$ ) followed by the basolateral compartment (800  $\mu\text{L}$ ). Air-liquid interface (ALI) conditions were established on day 3 of culture by aspirating the medium from the apical compartment and supplementation of 400  $\mu\text{L}$  SAGM Bullet kit including all supplements in the basolateral compartment.

**Electrophysiological Measurements: Transepithelial Electrical Resistance (TEER) Measurements:** TEER measurements were conducted for all cells cultivated under LCC as well as ALI conditions on Transwell inserts, 2 h after LCC conditions have been restored by medium exchange. TEER was measured with a chopstick electrode connected to a Volt-Ohm-meter (STX2 and EVOM 2; World Precision instruments) according to the manufacturer's instructions. During the time of the measurement, the Transwell plate was placed on a heating plate (37  $^\circ\text{C}$ ). Ohmic resistance values ( $\Omega$ ) were corrected for the area of the Transwell insert ( $0.33 \text{ cm}^2$ ) as well as a blank (when no blank Transwell insert was available in the experiment, a value of  $100 \Omega$  was used by default) and reported as  $\Omega \text{ cm}^2$ . If not described differently, medium exchange was performed after each TEER measurement for cells cultured under LCC as well as ALI conditions.

**Epithelial Potential Difference (PD) Measurements:** The STX2 electrode was immersed in a solution of 0.15 (M) KCl in distilled and sterile-filtered  $\text{H}_2\text{O}$  for 2 h before every voltage measurement while connected to a switched off EVOM 2 according to the manufacturer's instructions. This procedure should assure voltage stability and a low inter-electrode potential difference. Voltage values (mV) for all cells cultivated under LCC as well as ALI conditions on Transwell inserts, were measured 2 h after LCC conditions have been restored by medium exchange and were corrected for the related blank. TEER measurements were always performed after PD measurements.

**Transport Experiments:** Before each transport experiment, TEER of the polyclonal hAELVi and the single cell clone ‘Arlo’ cell lines cultured until day 14 under LCC were measured to determine barrier integrity before the experiment (before). Cells were washed once with pre-warmed Hanks' balanced salt solution (HBSS) with  $\text{CaCl}_2$  as well as  $\text{MgCl}_2$  (HBSS (1x); Gibco, Thermo Fisher Scientific Inc., 14025050) and then equilibrated in HBSS (200  $\mu\text{L}$  apical; 800  $\mu\text{L}$  basolateral) for 1 h (1 h after switch) in case of the control group. To disrupt the integrity of tight junctions, the treatment group was equilibrated for 1 h (1 h after switch) in HBSS containing 2,2',2'',2'''-(ethane-1,2-diylidinitrilo)tetraacetic acid (EDTA) ( $16 \times 10^{-3}$  M). After measuring TEER, HBSS was aspirated from both, the apical and basolateral compartment. 200  $\mu\text{L}$  fluorescein sodium solution ( $2.5 \mu\text{g mL}^{-1}$  in HBSS) was added apically (donor) and 800  $\mu\text{L}$  HBSS was added to the basolateral compartment (acceptor). From the same solutions, 200  $\mu\text{L}$  each was transferred into a 96-well plate to determine the starting concentrations for each compartment. All steps were performed on a heating plate at 37  $^\circ\text{C}$ . Afterward, the Transwell plates were placed on a MTS orbital shaker (150 rpm; IKA, Germany) in the incubator and 200  $\mu\text{L}$  samples were taken every 1 h for a total of 5 h, from the basolateral compartment only. 200  $\mu\text{L}$  sampled at time points were immediately replenished with 200  $\mu\text{L}$  prewarmed HBSS. TEER was measured 30 min after the last sample was taken (after 6 h), 200  $\mu\text{L}$  from the apical as well as the basolateral compartment were sampled to determine the end concentrations and all samples were measured with a plate reader in a 96-well plate at 485 nm excitation and 530 nm emission wavelength. The concentration of fluorescein sodium in each sample was calculated using a calibration curve of defined concentrations of fluorescein sodium in HBSS.

**Calculation of the Apparent Permeability Coefficient ( $P_{\text{app}}$ ):** Sink conditions, where drug concentration in the receiver compartment should not exceed 10% of the drug concentration added to the donor compartment at the start of the experiment, were ensured during the assay. The flux of fluorescein sodium (J) [ $\text{ng cm}^{-2} \text{ s}^{-1}$ ] was calculated by dividing the slope from the linear section of the cumulative concentration–time curve (60–180 min) of the transported fluorescein sodium solution and divided by the area (A) [ $\text{cm}^2$ ] of the growth support. To obtain the apparent permeability ( $P_{\text{app}}$ ) [ $\text{cm s}^{-1}$ ] the following equation was applied, where the initial concentration in the donor compartment at the beginning of the experiment is defined as  $c_0$  [ $\text{ng cm}^{-3}$ ]:

$$P_{\text{app}} = \frac{J}{C_0} \quad (1)$$

**Growth Curve:** For the growth curve experiments, 3000 cells per well of the polyclonal hAELVi cell line and the single cell clone ‘Arlo’ were seeded on 24-well cell culture plates on day 0 which have been pre-coated with 400  $\mu\text{L}$  coating solution for 1 h at 37  $^\circ\text{C}$  as described above. Every day the cells from 3 wells per cell line were collected. This was done by washing each well first with 300  $\mu\text{L}$  PBS, followed by cell detachment with 200  $\mu\text{L}$  trypsin–EDTA 0.05% and the addition of 400  $\mu\text{L}$  PBS containing 1% FCS (v/v) to stop the trypsin reaction after the cells had been detached. The cell suspension was then transferred to a 2 mL reaction tube and centrifuged at 300 rcf for 4 min, before the cell suspension was reconstituted from the pellet in 400  $\mu\text{L}$  PBS containing 1% FCS (v/v). The cells were counted with a CASY cell counter (capillary size: 150  $\mu\text{m}$ , size scale 0–50  $\mu\text{m}$ , sample volume  $10 \times 400 \mu\text{L}$ ) by transferring 200  $\mu\text{L}$  of the cell suspension to 10 mL of CASY tone (dilution factor: 51). Total cell number was reported as total cells  $\text{cm}^{-2}$  after correcting for the dilution as well as the growth area of the culture well ( $0.95 \text{ cm}^2$ ).



**Inflammation Assay:** “Arlo” cells have been cultured for 10 days under LCC conditions on Transwell inserts in SAGM Bullet kit including all supplements as described in Section 1.1.3, as an adapted version of the protocol from Metz et al.<sup>[75]</sup> Last medium exchange with SAGM Bullet kit including all supplements was performed on day 9 of culture. On day 10 of culture TEER values (prestimulation values) were determined before SAGM Bullet kit including all supplements was exchanged either against stimulation medium or stimulation medium supplemented with tumor necrosis factor alpha (TNF  $\alpha$ ) (human 25 ng mL<sup>-1</sup>; Sigma-Aldrich, H8916-10UG) and interferon gamma (INF  $\gamma$ ) (human 30 ng mL<sup>-1</sup>; Sigma-Aldrich, I17001-100UG). The stimulation medium contains all the components of the SAGM Bullet kit, but hydrocortisone as well as FCS were omitted. “Arlo” cells were incubated in stimulation medium or stimulation medium supplemented with TNF  $\alpha$  and INF  $\gamma$  for 48 h without exchanging the cell culture medium. TEER measurements were performed after 24 and 48 h and normalized to the prestimulation values.

**Imaging: Confocal Laser Scanning Microscopy: Immunofluorescence Staining:** If not stated otherwise, cells prepared for immunofluorescence staining were cultured on Transwell inserts for 7 or 14 d under ALI conditions. First, the remaining medium was aspirated first from basolateral and then from the apical compartment of the Transwells, before the Transwells were washed starting with the apical compartment followed by the basolateral compartment with pre-warmed PBS (apical: 200  $\mu$ L, basolateral: 800  $\mu$ L). Fixation was performed with 200  $\mu$ L of 4% paraformaldehyde (in PBS) for 10 min at room temperature (RT) from apical only. Permeabilization as well as blocking of unspecific epitopes was conducted with blocking buffer (1% BSA (bovine serum albumin heat shock fraction; Sigma-Aldrich, A9647-50G), 0.05% Saponin (Saponin Quillaja sp.; Sigma-Aldrich, S4521-10G) in PBS (weight/weight/volume)) for 1 h at RT. Primary antibodies against tight junction proteins Occludin (monoclonal antibody, Thermo Fisher Scientific, Cat# 33-1500) or ZO-1 (monoclonal antibody, BD Biosciences, Cat# 610966) were both diluted (1:200 (v/v)) in blocking buffer and incubated for 12 h at 4 °C in cases where antibody stainings were performed. The related secondary antibody conjugated to Alexa 633 (polyclonal antibody, Thermo Fisher Scientific, Cat# A-21050) (1:2000 (v/v) in blocking buffer) was incubated for 1 h at RT. F-Actin staining via rhodamine phalloidin (1:200 (v/v) in blocking buffer) (Invitrogen, R415) was either conducted instead of the antibody staining, or conducted after the third washing step of the secondary antibody, for 45 min at RT. Nuclei were stained with DAPI (1  $\mu$ g mL<sup>-1</sup> in PBS (v/v)) for 30 min at RT. A volume of 200  $\mu$ L was used for all the steps mentioned above and Transwells were washed in between every step with PBS at RT three times for 10 min. After the staining procedure, the membrane of the Transwell was carefully detached from the plastic holder using a forceps, by slowly inserting a scalpel in the outer boundary of the membrane. Briefly, the membrane was cut from the plastic holder in a circular manner using a scalpel, mounted on a microscope slide (Superfrost; Menzel, AAAA000080##32E) and embedded with fluorescence mounting medium (DAKO, S3023). Samples were always kept moist by careful addition of PBS during the cutting and mounting procedure.

**Image Acquisition:** Representative micrographs of cells stained by indirect fluorescence were acquired as z-stacks with an inverted confocal laser scanning microscope (CLSM; Leica, TCS SP8). The microscope was equipped with a 25 $\times$  (Fluotar VISIR 25 $\times$ /0.95) as well as a 60 $\times$  water immersion objective (60 $\times$  HC PL APO CS2 63 $\times$ /1.20). The Resolution was set to 1024 $\times$ 1024 pixels, the scan speed to 200 Hz and the z-step size to 356 nm. Z-stacks were acquired as xy-scans moving in z-direction. Fluorescence of DAPI representing the cell nuclei was detected with the emission filter set to 463–494 nm excited by a diode laser at 405 nm. Fluorescence of rhodamine coupled to phalloidin representing the cellular F-Actin network was detected with the emission filter set to 580–609 nm excited by a laser line at 561 nm. ZO-1 or Occludin signals representative for the tight junctional networks were detected with the emission filter set to 650–681 nm excited by a laser line at 633 nm. Hybrid detectors (HyD) of the microscope were set to “photon-counting mode” with a line accumulation set to a value of 3, in order to improve the sequential quantification of the intensity signal, for the ZO-1 as well as Occludin signal. Orthogonal optical sections were either computationally reconstructed from

z-stack images using Fiji/Image or acquired directly on the microscope using the xzy-scan mode of the Leica SP8. Maximum intensity projections of z-stacks were created with the same settings for all images with Fiji/Image<sup>[117]</sup> and further equally processed using the BIOP Channel tools plugin ([https://c4science.ch/w/bioimaging\\_and\\_optics\\_platform\\_biop/image-processing/imagej\\_tools/ijab-biop\\_channel\\_tools/](https://c4science.ch/w/bioimaging_and_optics_platform_biop/image-processing/imagej_tools/ijab-biop_channel_tools/)).

**Computational Image Analysis:** Z-stacks which were used for the computational image analysis, were all acquired with the 25 $\times$  water immersion objective in a resolution of 1024  $\times$  1024 pixels, a thickness of 60  $\mu$ m, a z-step size of 1  $\mu$ m and a scan speed of 200 Hz from the center of each Transwell membrane. HyD detectors of the microscope were set to “photon-counting mode” with a line accumulation set to a value of 4, in order to improve the sequential quantification of the intensity signal. Fluorescence of DAPI representing the cell nuclei was detected with the emission filter set to 420–451 nm excited by a diode laser at 405 nm. Fluorescence of rhodamine coupled to phalloidin representing the cellular F-Actin network was detected with the emission filter set to 581–607 nm excited by a laser line at 561 nm. 3D surface creation with Imaris (Bitplane AG) generated individual 3D-objects based on the fluorescence intensity, in our case the DAPI signal of each nucleus, and allowed to extract individual statistics for each of these 3D-objects (in our case the 3D-position of the center of each nucleus in a z-stack). For the 3D-surface creation, a single image from each group (polyclonal cell line hAELVi ALI on day 14 vs single cell clone “Arlo” ALI on day 14) was used to define the parameters for the computational algorithm. All other samples were analyzed using these initially set parameters with the Imaris batch analysis, to reduce observer bias. Due to an error during the automated image-acquisition, the only parameter that differed between the two groups (polyclonal cell line hAELVi vs single cell clone “Arlo”) was the digital zoom (polyclonal cell line hAELVi: 1; single cell clone “Arlo”: 1.28). This difference had no influence on the relative nuclei position and was taken into account during the creation of the 3D surface by separating the two groups. Position statistics were exported and analyzed using GraphPad Prism 9.3.1. software.

**Histological Micrographs:** Samples of the polyclonal cell line hAELVi or the single cell clone “Arlo” were cultured under ALI conditions until day 7 or day 14 and then fixated as described in Section 1.2.1. They were covered afterward with HBSS (apical: 200  $\mu$ L, basolateral: 800  $\mu$ L). Samples were processed according to the following protocol of the supplier and stained with hematoxylin and eosin.<sup>[118]</sup>

**Bulk RNA-Sequencing and Analysis: RNA Library Preparation:** hAEPs and cells “Arlo” were prepared for RNA-isolation on day 0 (hAEPs: 300.000 cells, directly after the isolation; “Arlo” 300.000 cells, directly after passaging) or on day 7 as well as day 14 from cells grown under ALI conditions on Transwell inserts. Cells were washed twice with 200  $\mu$ L pre-warmed HBSS and RNA was subsequently isolated by using the Direct-zol RNA Microprep Kit (Zymo Research, R2062) following the manufacturer’s instructions. RNA from hAEPs on day 0 and day 7 in 100  $\mu$ L and on day 14 in 50  $\mu$ L TRI-reagent (Zymo Research, R2050-1-50) for 5 min at RT and directly put on ice. To isolate RNA from the cells of “Arlo” on day 0 100  $\mu$ L, on day 7 150  $\mu$ L and on day 14 200  $\mu$ L TRI-reagent was used to compensate for the higher cell numbers of “Arlo.” A modified SmartSeq 2 protocol was followed where total RNA between 2 and 100 ng was used as input for reverse transcription.

RNA was primed by adding 1  $\times$  10<sup>-6</sup> M Oligo-dT Primer (final conc.; 5’ AAGCAGTGGTATCAACGCAGAGTACTTTTTTTTTTTTTTTTTTTTTTTTTTTTTTTTTTTTTT; V = A/C/G, N = any base), 1  $\times$  10<sup>-3</sup> M dNTPs (final conc.) followed by a denaturation step at 72 °C for 3 min and immediately cooling on ice. Reverse transcription was performed in a 10  $\mu$ L volume reaction by using 0.5  $\mu$ L Superscript II RT (200 U  $\mu$ L<sup>-1</sup>, Thermo Fisher Scientific, 18064022), 0.4  $\mu$ L RNase inhibitor (40 U  $\mu$ L<sup>-1</sup>, Promega, N2515), 5  $\times$  10<sup>-3</sup> M DTT, 1 M Betaine, 6  $\times$  10<sup>-3</sup> M MgCl<sub>2</sub> and 1  $\times$  10<sup>-6</sup> M TSO (B-AAGCAGTGGTATCAACGCAGAGTACAT997, B = 5’ biotin, 7 = LNA g, 9 = RNA-G) under the following incubation conditions: 42 °C for 90 min, 10  $\times$  cycling of 50 °C for 2 min and 42 °C for 2 min, finalized by 70 °C for 15 min.

The preamplification of the cDNA was carried out by utilizing the KAPA HiFi HotStar Ready Mix (Roche, KK2601) and 0.1  $\times$  10<sup>-6</sup> M of the IS PCR primers (5’ AAGCAGTGGTATCAACGCAGAGT) in a 25  $\mu$ L volume reaction

under the following PCR conditions: 98 °C for 3 min, 10–12× cycling of 98 °C for 20 s, 67 °C for 15 s, 72 °C for 6 min and a final elongation at 72 °C for 5 min. The cDNA was purified by the use of 0.8× Agencourt AMPure XP Beads (Beckman Coulter, A63881), quantified by the help of Qubit dsDNA HS Assay Kit (Thermo Fisher Scientific, Q32851) and the cDNA integrity was examined via the analysis of the fragment size distribution by using the Agilent 2100 Bioanalyzer (High Sensitivity DNA Analysis Kit, Agilent, 5067-4626).

The libraries were prepared by applying a tagmentation-based approach using the Nextera DNA Library Preparation Kit (Illumina, FC-131-1024). 8 ng of each cDNA were tagmented for 10 min at 55 °C by the use of 1 µL of the Tagment DNA Enzyme 1 in a 20 µL reaction pursued immediately by the purification of the tagmented fragments by the use of the MinElute PCR Purification Kit (Qiagen, 28004) following the manufacturer's instructions. The amplification of the libraries was performed in a 30 µL reaction using the NEBNext High-Fidelity 2X PCR Master Mix (New England Biolabs, M0541S) and 0.33 × 10<sup>-6</sup> M indexed adapters (5' AATGATACGGC-GACCACCGAGATCTACAC[i5]TCGTCGGCAGCGTC and 5' CAAGCAGAA-GACGGCATACGAGAT[i7]GTCTCGTGGGCTCGG; Illumina). 8 PCR cycles were done of the following PCR program: 75 °C 5 min, 98 °C 10 s, cycling of 98 °C 30 s, 63 °C 30 s and 72 °C 1 min, finalized by a long elongation at 72 °C for 7 min. The libraries were purified by utilizing 0.9 × Agencourt AMPure XP Beads, the DNA concentrations were quantified by the help of the Qubit dsDNA HS Assay Kit and the size distribution of the amplified fragments was examined by the use of the Agilent 2100 Bioanalyzer (High Sensitivity DNA Analysis Kit). The libraries were sequenced on the Illumina HiSeq 2500 by using the 100 bp single read sequencing mode.

**m-RNA Sequencing Data Processing:** Adapter sequences of FastQ format RNA-seq reads were removed and trimmed of low-quality ends (phred score = 20) by the use of Trim Galore! (version 0.4.2).<sup>[119]</sup> The reads were aligned to the hg38 reference genome (Genbank: GCA\_000001405.15) by using grape-nf (version 433e7621f6),<sup>[120]</sup> which combines STAR (version 2.4.0j)<sup>[121]</sup> for the alignment and RSEM (version 1.2.21)<sup>[122]</sup> for the read assignment. Differential analysis was carried out by the utilization of the software R and the included R-package EdgeR (version 3.20.9).<sup>[123]</sup> Differentially expressed genes were defined by a maximal *p*-value of 0.01, a FDR ≤ 0.01 and a minimal log fold-change of | 1 |.

**Utilization of the STRING Database:** The differentially expressed genes resulting from the pairwise differential analyses by the use of EdgeR were loaded into the STRING database to detect possible protein–protein interactions.<sup>[69,70]</sup> In order to do so the minimum required interaction score was set to the highest confidence (0.9).

**Gene Ontology Annotations Using Gene Ontology:** Gene ontology annotations of the identified differentially expressed genes resulting from the pairwise comparisons were done by the use of GENEONTOLOGY.<sup>[72,73]</sup> The differentially expressed genes were restricted to those genes following a linear regression along the cultivation period (d0 to d14) derived by calculation using R. These genes (e.g., higher expressed in d0 and defined by a loss of transcription along the cultivation period) were loaded into GENEONTOLOGY and the resulting GO terms were filtered by a false discovery rate (FDR) of ≤ 0.01 as well as ranked by the enrichment score (provided by GENEONTOLOGY).

**SARS-CoV-2 Infection Experiments:** The isolates SARS-CoV-2/1/Human/2020/Frankfurt (SARS-CoV-2/FFM1), SARS-CoV-2/7/Human/2020/Frankfurt (SARS-CoV-2/FFM7), as well as the variants Alpha (B.1.1.7), Beta (B.1.351) and Zeta (P.) were isolated and produced in Caco-2-F03 cells as previously described.<sup>[124–126]</sup>

“Arlo” cells were cultured on Transwell inserts for 7 or 14 d under ALI conditions before infection with SARS-CoV-2/FFM7 was initiated. For the infection studies comprising the variants SARS-CoV-2/FFM1, SARS-CoV-2/FFM7, Alpha (B.1.1.7), Beta (B.1.351) and Zeta (P.2), “Arlo” cells were cultured on Transwell inserts for 12 d under ALI conditions. “Arlo” cells were infected at a multiplicity of infection (MOI) of 1 from the apical side. After 2 hours, the inoculum was removed by aspiration and cells were washed three times with PBS.

**Quantitative Reverse Transcription PCR (RT-qPCR) Analysis:** On d0 after the third wash with PBS, as well as on days 1, 3, and 5 postinfection, a 30 min wash with PBS was performed from apical to harvest SARS-CoV-

2 RNA for the RT-qPCR analysis, as previously described.<sup>[127,128]</sup> SARS-CoV-2 RNA was isolated from the apical wash samples via AVL lysis buffer (Qiagen, 19073) and the QIAamp Viral RNA Kit (Qiagen, 52904) following the instructions of the manufacturer. The RNA yield was quantified via absorbance measurement on a Genesys 10S UV-vis spectrophotometer (Thermo Fisher Scientific). After that a one-step RT-qPCR reaction was performed using the Luna Universal One-Step RT-qPCR Kit (New England Biolabs, E3006L) as well as a CFX96 Real-Time System, C1000 Touch Thermal Cycler (Bio-Rad). Primers, adapted from,<sup>[129]</sup> which target the open reading frame for RNA-dependent RNA polymerase (RdRp): RdRP\_SARSr-F2 (GTG ARA TGG TCA TGT GTG GCG G) and RdRP\_SARSr-R1 (CAR ATG TTA AAS ACA CTA TTA GCA TA) were used in a concentration of 0.4 × 10<sup>-6</sup> M per reaction.

**Western Blot Analysis:** On days 0, 1, 3, and 5 postinfection “Arlo” cells were lysed for Western blot analysis using Triton-X-100 sample buffer, as described previously.<sup>[130]</sup> Proteins were separated by SDS-PAGE. Specific antibodies against SARS-CoV-2 N (1:1000 dilution, SARS-CoV-2 Nucleocapsid Antibody, Rabbit monoclonal antibody (Mab), #40143-R019, Sino Biological), ACE2 (1:500 dilution, Anti-ACE2 antibody, #ab15348, Abcam), TMPRSS2 (1:1000 dilution, Recombinant Anti-TMPRSS2 antibody [EPR3861], #ab92323, Abcam), and GAPDH (1:1000 dilution, Anti-G3PDH Human Polyclonal Antibody, #2275-PC-100, Trevigen) allowed antigen detection. Protein bands were made visible by laser-induced fluorescence using an infrared scanner for protein quantification (Odyssey, Li-Cor Biosciences).

## Supporting Information

Supporting Information is available from the Wiley Online Library or from the author.

## Acknowledgements

P.C. received funding from the German-Israeli Foundation for Scientific Research and Development (GIF) (Grant: I-101-409.8-2015). In addition, the German Federal Ministry of Education and Research financially supported parts of the work from P.C., J.C., D.B., and M.B. in the context of the COVID-protect project (Grant: 01KI20143C & 01KI20143A). The authors would like to cordially thank Dr. med. Rainer G. Hanselmann (IB-Cancer Research Foundation, Germany) for providing access to the single-cell printer.

Open access funding enabled and organized by Projekt DEAL.

## Conflict of Interest

C.-M.L., N.S.-D., and P.C. are the creators of the cell line “Arlo”. A manufacture and distribution license for the cell line “Arlo” was granted to InSCREENeX GmbH, Germany by the Helmholtz Centre for Infection Research (Helmholtz-Zentrum für Infektionsforschung GmbH) (HZI), Germany. The authors declare that the research was conducted in the absence of any commercial or financial relationships that could be construed as a potential conflict of interest.

## Data Availability Statement

The data that support the findings of this study are available on request from the corresponding author. The RNA-Sequencing dataset is also available at the research data archive RADAR (number 893). These data are not publicly available due to privacy or ethical restrictions.

## Keywords

drug transport, lung, pulmonary drug delivery, tight junctions, Transwell inserts

Received: December 8, 2022  
Published online:

- [1] A. Artzy-Schnirman, C.-M. Lehr, J. Sznitman, *Expert Opin. Drug Delivery* **2020**, *17*, 621.
- [2] E. Fröhlich, *Pharmaceutics* **2019**, *11*, 316.
- [3] D. E. Ingber, *Adv. Sci.* **2020**, *7*, 2002030.
- [4] J. Seok, H. S. Warren, A. G. Cuenca, M. N. Mindrinos, H. V. Baker, W. Xu, D. R. Richards, G. P. McDonald-Smith, H. Gao, L. Hennessy, C. C. Finnerty, C. M. López, S. Honari, E. E. Moore, J. P. Minei, J. Cuschieri, P. E. Bankey, J. L. Johnson, J. Sperry, A. B. Nathens, T. R. Billiar, M. A. West, M. G. Jeschke, M. B. Klein, R. L. Gamelli, N. S. Gibran, B. H. Brownstein, C. Miller-Graziano, S. E. Calvano, P. H. Mason, et al., *Proc. Natl. Acad. Sci. USA* **2013**, *110*, 3507.
- [5] P. Carius, J. C. Horstmann, S. Carvalho-Wodarz, C. de, C.-M. Lehr, *Handb. Exp. Pharmacol.* **2021**, *265*, 157.
- [6] K. J. Travaglini, A. N. Nabhan, L. Penland, R. Sinha, A. Gillich, R. V. Sit, S. Chang, S. D. Conley, Y. Mori, J. Seita, G. J. Berry, J. B. Shrager, R. J. Metzger, C. S. Kuo, N. Neff, I. L. Weissman, S. R. Quake, M. A. Krasnow, *Nature* **2020**, *587*, 619.
- [7] J. R. Rock, S. H. Randell, B. L. M. Hogan, *Dis. Models Mech.* **2010**, *3*, 545.
- [8] P. Gehr, M. Bachofen, E. R. Weibel, *Respir. Physiol.* **1978**, *32*, 121.
- [9] C. Y. Dombu, D. Betbeder, *Biomaterials* **2013**, *34*, 516.
- [10] E. R. Weibel, *Am J. Respir. Crit. Care Med.* **2015**, *191*, 504.
- [11] J. D. Crapo, B. E. Barry, P. Gehr, M. Bachofen, E. R. Weibel, *Am. Rev. Respir. Dis.* **1982**, *125*, 740.
- [12] K. C. Stone, R. R. Mercer, P. Gehr, B. Stockstill, J. D. Crapo, *Am. J. Respir. Cell Mol. Biol.* **1992**, *6*, 235.
- [13] E. L. Herzog, A. R. Brody, T. V. Colby, R. Mason, M. C. Williams, *Proc. Am. Thorac. Soc.* **2008**, *5*, 778.
- [14] C. Garcia-Mouton, A. Hidalgo, A. Cruz, J. Pérez-Gil, *Eur. J. Pharm. Biopharm.* **2019**, *144*, 230.
- [15] K. V. Evans, J.-H. Lee, *Stem Cells Transl. Med.* **2020**, *9*, 867.
- [16] P. Bonniaud, A. Fabre, N. Frossard, C. Guignabert, M. Inman, W. M. Kuebler, T. Maes, W. Shi, M. Stampfli, S. Uhlig, E. White, M. Witzenthan, P.-S. Bellaye, B. Crestani, O. Eickelberg, H. Fehrenbach, A. Guenther, G. Jenkins, G. Joos, A. Magnan, B. Maitre, U. A. Maus, P. Reinhold, J. H. J. Vernooy, L. Richeldi, M. Kolb, *Eur. Respir. J.* **2018**, *51*, 1702133.
- [17] D. Movia, S. Bruni-Favier, A. Prina-Mello, *Front. Bioeng. Biotechnol.* **2020**, *8*, 549.
- [18] G. Lacroix, W. Koch, D. Ritter, A. C. Gutleb, S. T. Larsen, T. Loret, F. Zanetti, S. Constant, S. Chortarea, B. Rothen-Rutishauser, P. S. Hiemstra, E. Frejafon, P. Hubert, L. Gribaldo, P. Kearns, J.-M. Aublant, S. Diabaté, C. Weiss, A. d. Groot, I. Kooter, *Appl. In Vitro Toxicol.* **2018**, *4*, 91.
- [19] M. Hittinger, N. Schneider-Daum, C.-M. Lehr, *Eur. J. Pharm. Biopharm.* **2017**, *118*, 73.
- [20] M. A. Selo, J. A. Sake, K.-J. Kim, C. Ehrhardt, *Adv. Drug Delivery Rev.* **2021**, *177*, 113862.
- [21] S. Gordon, M. Daneshian, J. Bouwstra, F. Caloni, S. Constant, D. E. Davies, G. Dandekar, C. A. Guzman, E. Fabian, E. Haltner, T. Hartung, N. Hasiwa, P. Hayden, H. Kandarova, S. Khare, H. F. Krug, C. Kneuer, M. Leist, G. Lian, U. Marx, M. Metzger, K. Ott, P. Prieto, M. S. Roberts, E. L. Roggen, T. Tralau, C. van den Braak, H. Walles, C.-M. Lehr, *ALTEX* **2015**, *32*, 327.
- [22] M. Bur, H. Huwer, C.-M. Lehr, N. Hagen, M. Guldbrandt, K.-J. Kim, C. Ehrhardt, *Eur. J. Pharm. Biopharm.* **2006**, *28*, 196.
- [23] S. Fuchs, A. J. Hollins, M. Laue, U. F. Schaefer, K. Roemer, M. Gumbleton, C.-M. Lehr, *Cell Tissue Res.* **2003**, *311*, 31.
- [24] K. J. Kim, Z. Borok, E. D. Crandall, *Pharm. Res.* **2001**, *18*, 253.
- [25] K. J. Elbert, U. F. Schäfer, H. J. Schäfers, K. J. Kim, V. H. Lee, C. M. Lehr, *Pharm. Res.* **1999**, *16*, 601.
- [26] P. Zamprogno, S. Wüthrich, S. Achenbach, G. Thoma, J. D. Stucki, N. Hobi, N. Schneider-Daum, C.-M. Lehr, H. Huwer, T. Geiser, R. A. Schmid, O. T. Guenat, *Commun. Biol.* **2021**, *4*, 168.
- [27] J. D. Stucki, N. Hobi, A. Galimov, A. O. Stucki, N. Schneider-Daum, C.-M. Lehr, H. Huwer, M. Frick, M. Funke-Chambour, T. Geiser, O. T. Guenat, *Sci. Rep.* **2018**, *8*, 14359.
- [28] D. Huh, B. D. Matthews, A. Mammoto, M. Montoya-Zavala, H. Y. Hsin, D. E. Ingber, *Science* **2010**, *328*, 1662.
- [29] M. Hittinger, J. Janke, H. Huwer, R. Scherliess, N. Schneider-Daum, C.-M. Lehr, *ATLA, Altern. Lab. Anim.* **2016**, *44*, 337.
- [30] P. F. Bove, H. Dang, C. Cheluvvaraju, L. C. Jones, X. Liu, W. K. O'Neal, S. H. Randell, R. Schlegel, R. C. Boucher, *Am. J. Respir. Cell Mol. Biol.* **2014**, *50*, 767.
- [31] C. D. Foster, L. S. Varghese, R. B. Skalina, L. W. Gonzales, S. H. Guttentag, *Pediatr. Res.* **2007**, *61*, 404.
- [32] L. G. Dobbs, M. C. Williams, A. E. Brandt, *Biochim. Biophys. Acta* **1985**, *846*, 155.
- [33] J. van der Vaart, M. M. Lamers, B. L. Haagmans, H. Clevers, *Dis. Models Mech.* **2021**, *14*, dmm049060.
- [34] Y. He, E. Rofaani, X. Huang, B. Huang, F. Liang, L. Wang, J. Shi, J. Peng, Y. Chen, *Adv. Healthcare Mater.* **2022**, *11*, 2101972.
- [35] J.-W. Yang, Y.-R. Lin, Y.-L. Chu, J. H. Y. Chung, H.-E. Lu, G.-Y. Chen, *Commun. Biol.* **2022**, *5*, 70.
- [36] C. Tindle, M. Fuller, A. Fonseca, S. Taheri, S. Ibeawuchi, N. Beutler, G. D. Katkar, A. Claire, V. Castillo, M. Hernandez, H. Russo, J. Duran, L. E. C. Alexander, A. Tipps, G. Lin, P. A. Thistlethwaite, R. Chattopadhyay, T. F. Rogers, D. Sahoo, P. Ghosh, S. Das, *eLife* **2021**, *10*, e66417.
- [37] S. van Riet, D. K. Ninaber, H. M. M. Mikkers, T. D. Tetley, C. R. Jost, A. A. Mulder, T. Pasman, D. Baptista, A. A. Poot, R. Truckenmüller, C. L. Mummery, C. Freund, R. J. Rottier, P. S. Hiemstra, *Sci. Rep.* **2020**, *10*, 5499.
- [38] M. M. Lamers, J. van der Vaart, K. Knoops, S. Riesebosch, T. I. Breugem, A. Z. Mykytyn, J. Beumer, D. Schipper, K. Bezstarosti, C. D. Koopman, N. Groen, R. B. G. Ravelli, H. Q. Duimel, J. A. A. Demmers, G. M. G. M. Verjans, M. P. G. Koopmans, M. J. Muraro, P. J. Peters, H. Clevers, B. L. Haagmans, *EMBO J.* **2021**, *40*, 105912.
- [39] A. Jacob, M. Morley, F. Hawkins, K. B. McCauley, J. C. Jean, H. Heins, C.-L. Na, T. E. Weaver, M. Vedaie, K. Hurley, A. Hinds, S. J. Russo, S. Kook, W. Zacharias, M. Ochs, K. Traber, L. J. Quinton, A. Crane, B. R. Davis, F. V. White, J. Wambach, J. A. Whitsett, F. S. Cole, E. E. Morrissey, S. H. Guttentag, M. F. Beers, D. N. Kotton, *Cell Stem Cell* **2017**, *21*, 472.
- [40] H. Katsura, V. Sontake, A. Tata, Y. Kobayashi, C. E. Edwards, B. E. Heaton, A. Konkimalla, T. Asakura, Y. Mikami, E. J. Fritch, P. J. Lee, N. S. Heaton, R. C. Boucher, S. H. Randell, R. S. Baric, P. R. Tata, *Cell Stem Cell* **2020**, *27*, 890.
- [41] P. S. Hiemstra, T. D. Tetley, S. M. Janes, *Eur. Respir. J.* **2019**, *54*, 1900742.
- [42] H. L. Winton, H. Wan, M. B. Cannell, D. C. Gruenert, P. J. Thompson, D. R. Garrod, G. A. Stewart, C. Robinson, *Clin. Exp. Allergy* **1998**, *28*, 1273.
- [43] C. C. Tièche, Y. Gao, E. D. Bühner, N. Hobi, S. A. Berezowska, K. Wyler, L. Froment, S. Weis, R.-W. Peng, R. Bruggmann, P. Schär, M. A. Amrein, S. R. R. Hall, P. Dorn, G. Kocher, C. Riether, A. Ochsenbein, R. A. Schmid, T. M. Marti, *Neoplasia* **2019**, *21*, 185.
- [44] M. Sakagami, *Adv. Drug Delivery Rev.* **2020**, *161-162*, 63.
- [45] A. Kuehn, S. Kletting, S. Carvalho-Wodarz, C. de, U. Repnik, G. Grifiths, U. Fischer, E. Meese, H. Huwer, D. Wirth, T. May, N. Schneider-Daum, C.-M. Lehr, *ALTEX* **2016**, *33*, 251.
- [46] R. Lochbaum, C. Schilpp, L. Nonnenmacher, M. Frick, P. Dietl, O. H. Wittekindt, *Cell. Signalling* **2020**, *65*, 109421.



- [47] J. J. Salomon, V. E. Muchitsch, J. C. Gausterer, E. Schwagerus, H. Huwer, N. Daum, C.-M. Lehr, C. Ehrhardt, *Mol. Pharmaceutics* **2014**, *11*, 995.
- [48] N. Daum, A. Kuehn, S. Hein, U. F. Schaefer, H. Huwer, C.-M. Lehr, *Methods Mol. Biol.* **2012**, *806*, 31.
- [49] A. Artzy-Schnirman, H. Zidan, S. Elias-Kirma, L. Ben-Porat, J. Tenenbaum-Katan, P. Carius, R. Fishler, N. Schneider-Daum, C.-M. Lehr, J. Sznitman, *Adv. Biosyst.* **2019**, *3*, 1900026.
- [50] O. Brookes, S. Boland, R. Lai Kuen, D. Miremont, J. Movassat, A. Baeza-Squiban, *PLoS One* **2021**, *16*, e0248798.
- [51] L. Leibrock, S. Wagener, A. V. Singh, P. Laux, A. Luch, *Toxicol. Res.* **2019**, *8*, 1016.
- [52] C. Lipps, F. Klein, T. Wählich, V. Seiffert, M. Butueva, J. Zauers, T. Truschel, M. Luckner, M. Köster, R. MacLeod, J. Pezoldt, J. Hühn, Q. Yuan, P. P. Müller, H. Kempf, R. Zweigerdt, O. Dittrich-Breiholz, T. Pufe, R. Beckmann, W. Drescher, J. Riancho, C. Sañudo, T. Korff, B. Opalka, V. Rebmann, J. R. Göthert, P. M. Alves, M. Ott, R. Schucht, H. Hauser, et al., *Nat. Commun.* **2018**, *9*, 994.
- [53] M. Tomita, M. Hayashi, S. Awazu, *J. Pharm. Sci.* **1996**, *85*, 608.
- [54] T. Kulkarni, J. d. Andrade, Y. Zhou, T. Luckhardt, V. J. Thannickal, *Am. J. Physiol.: Lung Cell. Mol. Physiol.* **2016**, *311*, L185.
- [55] B. Schlingmann, S. A. Molina, M. Koval, *Sem. Cell Dev. Biol.* **2015**, *42*, 47.
- [56] K. Brune, J. Frank, A. Schwingshackl, J. Finigan, V. K. Sidhaye, *Am. J. Physiol.: Lung Cell. Mol. Physiol.* **2015**, *308*, L731.
- [57] J. M. Anderson, C. M. van Itallie, *Am. J. Physiol.* **1995**, *269*, G467.
- [58] C. Zihni, C. Mills, K. Matter, M. S. Balda, *Nat. Rev. Mol. Cell Biol.* **2016**, *17*, 564.
- [59] L. Sikkema, D. Strobl, L. Zappia, E. Madisson, N. S. Markov, L. Zaragosi, M. Ansari, M. Arguel, L. Apperloo, C. Bécavin, M. Berg, E. Chichelnitskiy, M. Chung, A. Collin, A. C. Gay, B. Hooshiar Kashani, M. Jain, T. Kapellos, T. M. Kole, C. Mayr, M. v. Papen, L. Peter, C. Ramírez-Suástegui, J. Schniering, C. Taylor, T. Walzthoeni, C. Xu, L. T. Bui, C. d. Donno, L. Dony, et al., *bioRxiv* **2022**, <https://doi.org/10.1101/2022.03.10.483747>.
- [60] M. A. Selo, J. A. Sake, C. Ehrhardt, J. J. Salomon, *Int. J. Mol. Sci.* **2020**, *21*, 9168.
- [61] O. H. Wittekindt, P. Dietl, *Pflugers Arch.: Eur. J. Physiol.* **2019**, *471*, 519.
- [62] A. Sakamoto, T. Matsumaru, N. Yamamura, Y. Uchida, M. Tachikawa, S. Ohtsuki, T. Terasaki, *J. Pharm. Sci.* **2013**, *102*, 3395.
- [63] S. Bibert, S. Roy, D. Schaer, E. Felley-Bosco, K. Geering, *J. Biol. Chem.* **2006**, *281*, 39142.
- [64] A. Sharma, G. Ramena, Y. Yin, L. Premkumar, R. C. Elble, *PLoS One* **2018**, *13*, e0196512.
- [65] M. F. Beers, Y. Moodley, *Am. J. Respir. Cell Mol. Biol.* **2017**, *57*, 18.
- [66] G. R. Newman, L. Campbell, C. Ruhland, B. von Jasani, M. Gumbleton, *Cell Tissue Res.* **1999**, *295*, 111.
- [67] K. Hasegawa, A. Sato, K. Tanimura, K. Uemasu, Y. Hamakawa, Y. Fuseya, S. Sato, S. Muro, T. Hirai, *Respir. Res.* **2017**, *18*, 150.
- [68] A. C. Cunningham, D. S. Milne, J. Wilkes, J. H. Dark, T. D. Tetley, J. A. Kirby, *J. Cell Sci.* **1994**, *107*, 443.
- [69] D. Szklarczyk, A. L. Gable, K. C. Nastou, D. Lyon, R. Kirsch, S. Pysalo, N. T. Doncheva, M. Legeay, T. Fang, P. Bork, L. J. Jensen, C. v. Mering, *Nucleic Acids Res.* **2021**, *49*, D605.
- [70] D. Szklarczyk, A. L. Gable, D. Lyon, A. Junge, S. Wyder, J. Huerta-Cepas, M. Simonovic, N. T. Doncheva, J. H. Morris, P. Bork, L. J. Jensen, C. v. Mering, *Nucleic Acids Res.* **2019**, *47*, D607.
- [71] H. Mi, A. Muruganujan, D. Ebert, X. Huang, P. D. Thomas, *Nucleic Acids Res.* **2019**, *47*, D419.
- [72] The Gene Ontology Consortium, *Nucleic Acids Res.* **2021**, *49*, D325.
- [73] M. Ashburner, C. A. Ball, J. A. Blake, D. Botstein, H. Butler, J. M. Cherry, A. P. Davis, K. Dolinski, S. S. Dwight, J. T. Eppig, M. A. Harris, D. P. Hill, L. Issel-Tarver, A. Kasarskis, S. Lewis, J. C. Matese, J. E. Richardson, M. Ringwald, G. M. Rubin, G. Sherlock, *Nat. Genet.* **2000**, *25*, 25.
- [74] M. Hoffmann, H. Kleine-Weber, S. Schroeder, N. Krüger, T. Herrler, S. Erichsen, T. S. Schiergens, G. Herrler, N.-H. Wu, A. Nitsche, M. A. Müller, C. Drosten, S. Pöhlmann, *Cell* **2020**, *181*, 271.
- [75] J. K. Metz, B. Wiegand, S. Schnur, K. Knoth, N. Schneider-Daum, H. Groß, G. Croston, T. M. Reinheimer, C.-M. Lehr, M. Hittinger, *ATLA, Altern. Lab. Anim.* **2020**, *48*, 252.
- [76] R. Karki, B. R. Sharma, S. Tuladhar, E. P. Williams, L. Zalduondo, P. Samir, M. Zheng, B. Sundaram, B. Banoth, R. K. S. Malireddi, P. Schreiner, G. Neale, P. Vogel, R. Webby, C. B. Jonsson, T.-D. Kaneganti, *Cell* **2021**, *184*, 149.
- [77] E. Tran, T. Shi, X. Li, A. Y. Chowdhury, D. Jiang, Y. Liu, H. Wang, C. Yan, W. D. Wallace, R. Lu, A. L. Ryan, C. N. Marconett, B. Zhou, Z. Borok, I. A. Offringa, *iScience* **2022**, *25*, 103780.
- [78] K. J. Wolf, J. D. Weiss, S. G. M. Uzel, M. A. Skylar-Scott, J. A. Lewis, *Cell Stem Cell* **2022**, *29*, 667.
- [79] T. Bluhmki, S. Traub, A.-K. Müller, S. Bitzer, E. Schruf, M.-T. Bammer, M. Leist, F. Gantner, J. P. Garnett, R. Heilker, *Sci. Rep.* **2021**, *11*, 17028.
- [80] P. Carius, A. Dubois, M. Ajarirad, A. Artzy-Schnirman, J. Sznitman, N. Schneider-Daum, C.-M. Lehr, *Front. Bioeng. Biotechnol.* **2021**, *9*, 743236.
- [81] N. Fujino, H. Kubo, C. Ota, T. Suzuki, S. Suzuki, M. Yamada, T. Takahashi, M. He, T. Suzuki, T. Kondo, M. Yamaya, *Am. J. Respir. Cell Mol. Biol.* **2012**, *46*, 422.
- [82] R. Brandt, S. Timm, J. L. Gorenflo López, J. Kwame Abledu, W. M. Kuebler, C. P. R. Hackenberger, M. Ochs, E. Lopez-Rodriguez, *Front. Bioeng. Biotechnol.* **2020**, *8*, 614357.
- [83] R. Mills-Goodlet, M. Schenck, A. Chary, M. Geppert, T. Serchi, S. Hofer, N. Hofstätter, A. Feinle, N. Hüsing, A. C. Gutleb, M. Himly, A. Duschl, *Environ. Sci.: Nano* **2020**, *7*, 2073.
- [84] A. T. Shenoy, C. Lyon De Ana, E. I. Arafa, I. Salwig, K. A. Barker, F. T. Korkmaz, A. Ramanujan, N. S. Etesami, A. M. Soucy, I. M. C. Martin, B. R. Tilton, A. Hinds, W. N. Goltry, H. Kathuria, T. Braun, M. R. Jones, L. J. Quinton, A. C. Belkina, J. P. Mizgerd, *Nat. Commun.* **2021**, *12*, 5834.
- [85] V. Corbière, V. Dirix, S. Norrenberg, M. Cappello, M. Rimmelink, F. Mascart, *Respir. Res.* **2011**, *12*, 15.
- [86] Y. L. Sun, K. Hurley, C. Villacorta-Martin, J. Huang, A. Hinds, K. Gopalan, I. S. Caballero, S. J. Russo, J. A. Kitzmiller, J. A. Whitsett, M. F. Beers, D. N. Kotton, *Am. J. Respir. Cell Mol. Biol.* **2021**, *65*, 442.
- [87] K. Xiao, Y. Wang, L. Zhou, J. Wang, Y. Wang, Z. de Tong, J. Jiang, *PLoS One* **2021**, *16*, e0259091.
- [88] K. Shinmura, H. Igarashi, H. Kato, Y. Kawanishi, Y. Inoue, S. Nakamura, H. Ogawa, T. Yamashita, A. Kawase, K. Funai, H. Sugimura, *Dis. Markers* **2014**, *2014*, 619273.
- [89] J. N. Jakobsen, E. Santoni-Rugiu, J. B. Sørensen, *Lung Cancer Manage.* **2015**, *4*, 97.
- [90] L. Fan, B. Li, Z. Li, L. Sun, *Front. Genet.* **2021**, *12*, 730003.
- [91] V. Wallia, Y. Yu, D. Cao, M. Sun, J. R. McLean, B. G. Hollier, J. Cheng, S. A. Mani, K. Rao, L. Premkumar, R. C. Elble, *Oncogene* **2012**, *31*, 2237.
- [92] A. F. Gazdar, R. I. Linnoila, Y. Kurita, H. K. Oie, J. L. Mulshine, J. C. Clark, J. A. Whitsett, *Cancer Res.* **1990**, *50*, 5481.
- [93] W. Neuhaus, F. Samwer, S. Kunzmann, R. M. Muellenbach, M. Wirth, C. P. Speer, N. Roewer, C. Y. Förster, *Differentiation* **2012**, *84*, 294.
- [94] H. Ren, N. P. Birch, V. Suresh, *PLoS One* **2016**, *11*, e0165225.
- [95] E. Dohle, S. Singh, A. Nishigushi, T. Fischer, M. Wessling, M. Möller, R. Sader, J. Kasper, S. Ghanaati, C. J. Kirkpatrick, *Tissue Eng., Part C* **2018**, *24*, 495.
- [96] A. Barilli, R. Visigalli, F. Ferrari, M. G. Bianchi, V. Dall'Asta, B. M. Rotoli, *Biomedicines* **2022**, *10*, 3085.

- [97] J. P. Joelsson, I. T. Myszor, S. Sigurdsson, F. Lehmann, C. P. Page, G. H. Gudmundsson, T. Gudjonsson, S. Karason, *ALTEX* **2020**, *37*, 545.
- [98] R. Kaarteenaho-Wiik, Y. Soini, *J. Histochem. Cytochem.* **2009**, *57*, 187.
- [99] C. B. Coyne, T. M. Gambling, R. C. Boucher, J. L. Carson, L. G. Johnson, *Am. J. Physiol.: Lung Cell. Mol. Physiol.* **2003**, *285*, L1166.
- [100] M. J. LaFemina, D. Rokkam, A. Chandrasena, J. Pan, A. Bajaj, M. Johnson, J. A. Frank, *Am. J. Physiol.: Lung Cell. Mol. Physiol.* **2010**, *299*, L724.
- [101] L. A. Mitchell, C. E. Overgaard, C. Ward, S. S. Margulies, M. Koval, *Am. J. Physiol.: Lung Cell. Mol. Physiol.* **2011**, *301*, L40.
- [102] H. Ohta, S. Chiba, M. Ebina, M. Furuse, T. Nukiwa, *Am. J. Physiol.: Lung Cell. Mol. Physiol.* **2012**, *302*, L193.
- [103] T. Niimi, K. Nagashima, J. M. Ward, P. Minoo, D. B. Zimonjic, N. C. Popescu, S. Kimura, *Mol. Cell. Biol.* **2001**, *21*, 7380.
- [104] B. Zhou, P. Flody, J. Luo, D. R. Castillo, Y. Liu, F.-X. Yu, A. McConnell, B. Varghese, G. Li, N.-O. Chimge, M. Sunohara, M. N. Koss, W. Elatre, P. Conti, J. M. Liebler, C. Yang, C. N. Marconett, I. A. Laird-Offringa, P. Minoo, K. Guan, B. R. Stripp, E. D. Crandall, Z. Borok, *J. Clin. Invest.* **2018**, *128*, 970.
- [105] A. C. Zemke, J. C. Snyder, B. L. Brockway, J. A. Drake, S. D. Reynolds, N. Kaminski, B. R. Stripp, *Am. J. Respir. Cell Mol. Biol.* **2009**, *40*, 340.
- [106] P. A. Reyfman, J. M. Walter, N. Joshi, K. R. Anekalla, A. C. McQuattipimentel, S. Chiu, R. Fernandez, M. Akbarpour, C.-I. Chen, Z. Ren, R. Verma, H. Abdala-Valencia, K. Nam, M. Chi, S. Han, F. J. Gonzalez-Gonzalez, S. Soberanes, S. Watanabe, K. J. N. Williams, A. S. Flozak, T. T. Nicholson, V. K. Morgan, D. R. Winter, M. Hinchcliff, C. L. Hrusch, R. D. Guzy, C. A. Bonham, A. I. Sperling, R. Bag, R. B. Hamanaka, et al., *Am. J. Respir. Crit. Care Med.* **2019**, *199*, 1517.
- [107] M. Karlsson, C. Zhang, L. Méar, W. Zhong, A. Digre, B. Katona, E. Sjöstedt, L. Butler, J. Odeberg, P. Dusart, F. Edfors, P. Oksvold, K. Feilitzen, M. von Zählen, M. Arif, O. Altay, X. Li, M. Ozcan, A. Mardinoglu, L. Fagerberg, J. Mulder, Y. Luo, F. Ponten, M. Uhlén, C. Lindskog, *Sci. Adv.* **2021**, *7*, eabh2169.
- [108] C. Cano Portillo, R. Villacreses, A. L. Thurman, A. A. Pezzulo, J. Zaber, I. M. Thornell, *Am. J. Physiol.: Cell Physiol.* **2022**, *323*, C1044.
- [109] Ł. A. Wujak, A. Blume, E. Baloghlu, M. Wygrecka, J. Wygowski, S. Herold, K. Mayer, I. Vadász, P. Besuch, H. Mairbäurl, W. Seeger, R. E. Morty, *Respir. Physiol. Neurobiol.* **2016**, *220*, 54.
- [110] F. Storelli, M. Yin, A. R. Kumar, M. K. Ladumor, R. Evers, P. P. Chothe, O. J. Enogieru, X. Liang, Y. Lai, J. D. Unadkat, *Pharmacol. Ther.* **2022**, *238*, 108271.
- [111] C. Mache, J. Schulze, G. Holland, D. Bourquain, J.-M. Gensch, D.-Y. Oh, A. Nitsche, R. Dürrwald, M. Laue, T. Wolff, *Commun. Biol.* **2022**, *5*, 1138.
- [112] J. P. Bridges, E. K. Vladar, H. Huang, R. J. Mason, *Thorax* **2022**, *77*, 203.
- [113] W. Sungnak, N. Huang, C. Bécavin, M. Berg, R. Queen, M. Litvinukova, C. Talavera-López, H. Maatz, D. Reichart, F. Sampaziotis, K. B. Worlock, M. Yoshida, J. L. Barnes, *Nat. Med.* **2020**, *26*, 681.
- [114] R. B. Martinez, J. M. Ritter, E. Matkovic, J. Gary, B. C. Bollweg, H. Bullock, C. S. Goldsmith, L. Silva-Flannery, J. N. Seixas, S. Reagan-Steiner, T. Uyeki, A. Denison, J. Bhatnagar, W.-J. Shieh, S. R. Zaki, *Emerging Infect. Dis.* **2020**, *26*, 2005.
- [115] A. Mund, F. Coscia, A. Kriston, R. Hollandi, F. Kovács, A.-D. Brunner, E. Migh, L. Schweizer, A. Santos, M. Bzorek, S. Naimy, L. M. Rahbek-Gjerdum, B. Dyring-Andersen, J. Bulkescher, C. Lukas, M. A. Eckert, E. Lengyel, C. Gnann, E. Lundberg, P. Horvath, M. Mann, *Nat. Biotechnol.* **2022**, *40*, 1231.
- [116] A. Gross, J. Schöndube, S. Niekrawitz, W. Streule, L. Riegger, R. Zengerle, P. Koltay, *J. Lab. Autom.* **2013**, *18*, 504.
- [117] J. Schindelin, I. Arganda-Carreras, E. Frise, et al., *Nat Methods* **2012**, *9*, 676.
- [118] Corning and Caradonna, P, <https://www.corning.com/catalog/cls/documents/protocols/CLS-AN-335.pdf> (accessed: July 2022).
- [119] F. Krueger, Trim Galore: a wrapper tool around Cutadapt and FastQC to consistently apply quality and adapter trimming to FastQ files, with some extra functionality for ..., [https://www.bioinformatics.babraham.ac.uk/projects/trim\\_galore/](https://www.bioinformatics.babraham.ac.uk/projects/trim_galore/) (accessed: July 2022).
- [120] E. Palumbo, P. di Tommaso, K. Nordström, An automated RNA-seq pipeline using Nextflow, <https://github.com/guigolab/grape-nf> (accessed: July 2022).
- [121] A. Dobin, C. A. Davis, F. Schlesinger, J. Drenkow, C. Zaleski, S. Jha, P. Batut, M. Chaisson, T. R. Gingeras, *Bioinformatics* **2013**, *29*, 15.
- [122] B. Li, C. N. Dewey, *BMC Bioinf.* **2011**, *12*, 323.
- [123] M. D. Robinson, D. J. McCarthy, G. K. Smyth, *Bioinformatics* **2010**, *26*, 139.
- [124] D. Bojkova, P. Reus, L. Panosch, M. Bechtel, T. Rothenburger, J. Kandler, A. Pfeiffer, J. U. Wagner, M. Shumliakivska, S. Dimmeler, R. Olmer, U. Martin, F. Vondran, T. Toptan, F. Rothweiler, R. Zehner, H. Rabenau, K. L. Osman, S. T. Pullan, M. Carroll, R. Stack, S. Ciesek, M. N. Wass, M. Michaelis, J. Cinatl, *iScience* **2023**, *26*, 105944.
- [125] S. Hoehl, H. Rabenau, A. Berger, M. Kortenbusch, J. Cinatl, D. Bojkova, P. Behrens, B. Böddinghaus, U. Götsch, F. Naujoks, P. Neumann, J. Schork, P. Tiarks-Jungk, A. Walczok, M. Eickmann, M. J. G. T. Vehreschild, G. Kann, T. Wolf, R. Gottschalk, S. Ciesek, *N. Engl. J. Med.* **2020**, *382*, 1278.
- [126] T. Toptan, S. Hoehl, S. Westhaus, D. Bojkova, A. Berger, B. Rotter, K. Hoffmeier, S. Ciesek, M. Wiedera, *Int. J. Mol. Sci.* **2020**, *21*, 4396.
- [127] D. Bojkova, K. Klann, B. Koch, M. Wiedera, D. Krause, S. Ciesek, J. Cinatl, C. Münch, *Nature* **2020**, *583*, 469.
- [128] B. Denisa, B. Marco, M. Katie-May, E. M. Jake, K. Kevin, B. Carla, R. Gernot, J. Danny, B. Peter, C. Sandra, M. Christian, N. W. Mark, M. Martin, C. Jindrich Jr, *Cells* **2020**, *9*, 2377.
- [129] V. Corman, T. Bleicker, S. Brünink, C. Drosten, M. Zambon, Diagnostic detection of 2019-nCoV by real-time RT-PCR, <https://www.who.int/docs/default-source/coronaviruse/protocol-v2-1.pdf> (accessed: July 2022).
- [130] D. Bojkova, R. Costa, M. Bechtel, S. Ciesek, M. Michaelis, J. Cinatl, *Metabolites* **2021**, *11*, 699.





## Supporting Information

for *Adv. Sci.*, DOI 10.1002/adv.202207301

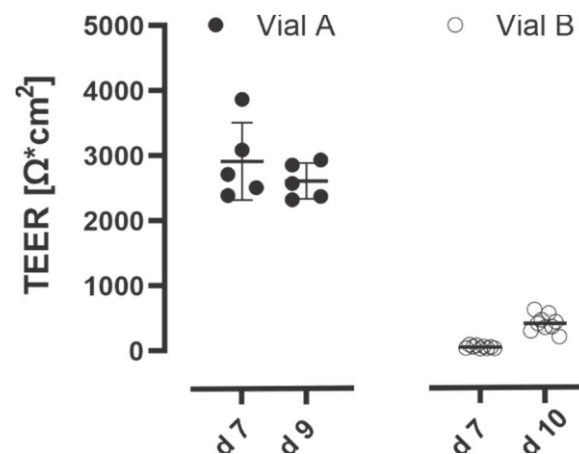
A Monoclonal Human Alveolar Epithelial Cell Line (“Arlo”) with Pronounced Barrier Function for Studying Drug Permeability and Viral Infections

*Patrick Carius, Annemarie Jungmann, Marco Bechtel, Alexander Grifßmer, Annette Boese, Gilles Gasparoni, Abdulrahman Salhab, Ralf Seipelt, Klaus Urbschat, Clémentine Richter, Carola Meier, Denisa Bojkova, Jindrich Cinatl, Jörn Walter, Nicole Schneider-Daum\* and Claus-Michael Lehr\**

## Supporting Information

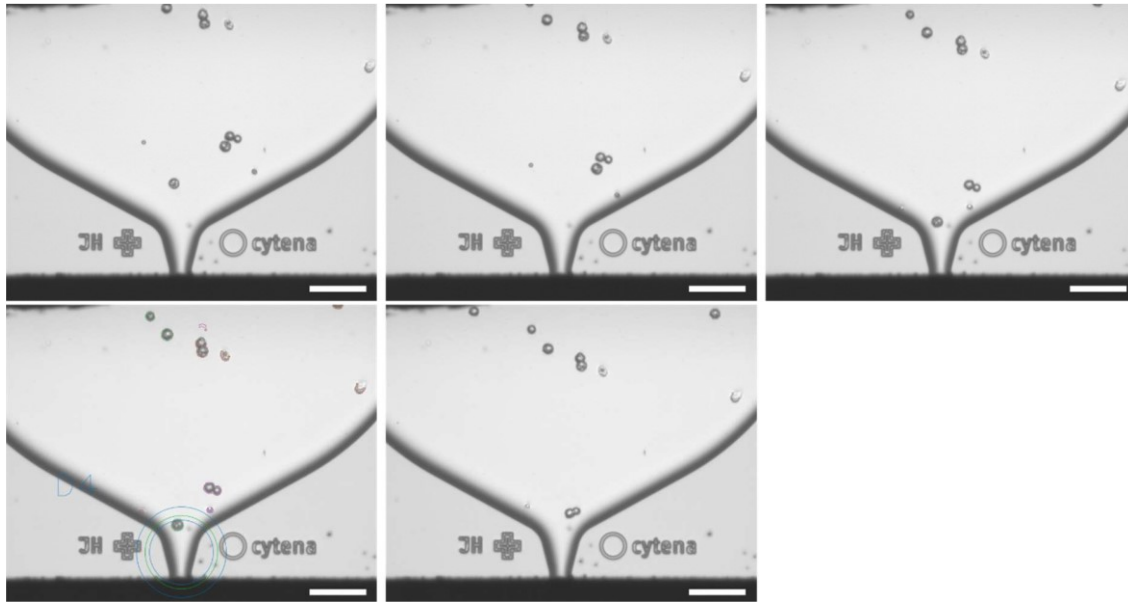
A monoclonal human alveolar epithelial cell line (“Arlo”) with pronounced barrier function for studying drug permeability and viral infections

Patrick Carius<sup>1,2</sup>, Annemarie Jungmann<sup>3</sup>, Marco Bechtel<sup>4</sup>, Alexander Grißmer<sup>5</sup>, Annette Boese<sup>1</sup>, Gilles Gasparoni<sup>3</sup>, Abdulrahman Salhab<sup>3</sup>, Ralf Seipelt<sup>6</sup>, Klaus Urbschat<sup>6</sup>, Clémentine Richter<sup>1,2</sup>, Carola Meier<sup>5</sup>, Denisa Bojkova<sup>4</sup>, Jindrich Cinatl<sup>4</sup>, Jörn Walter<sup>3</sup>, Nicole Schneider-Daum<sup>1\*</sup> and Claus-Michael Lehr<sup>1,2\*</sup>



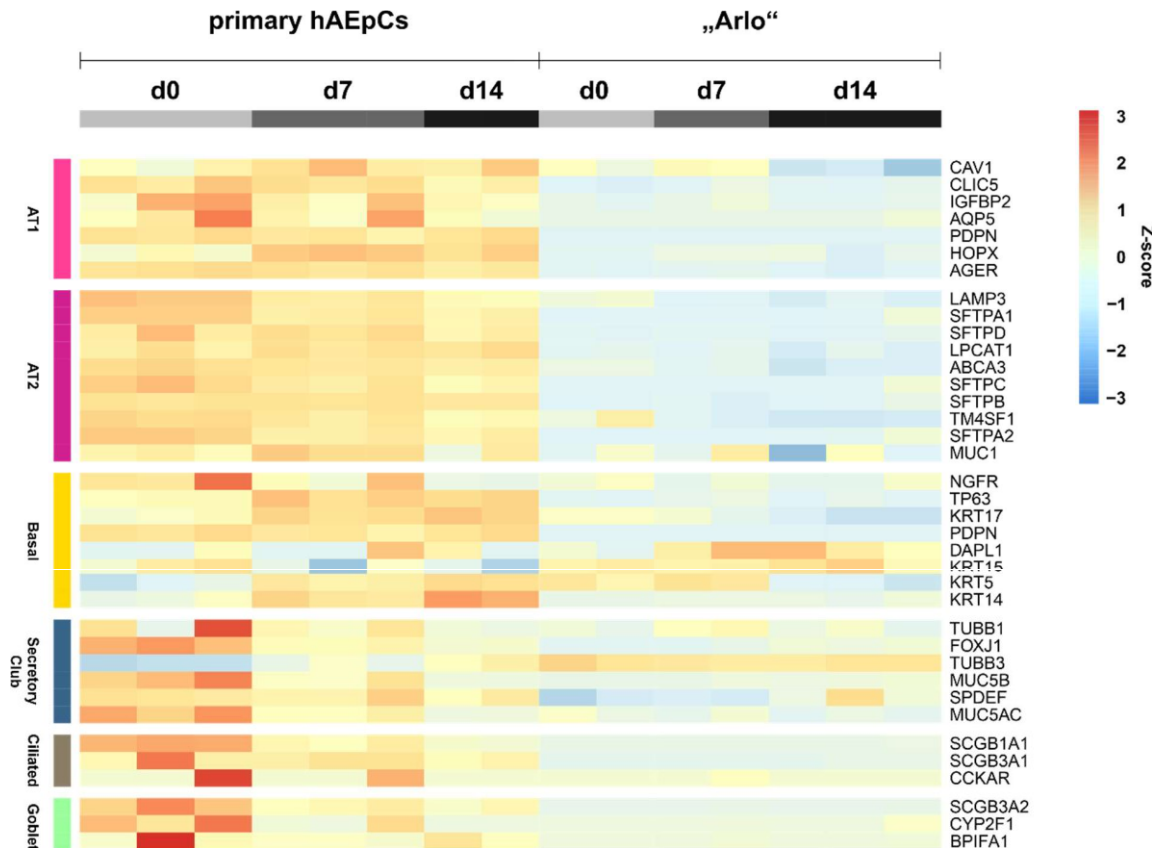
**Supplementary Figure 1 Impaired TEER development of the polyclonal hAELVi cell line.** Two vials, Vial A and Vial B, of the polyclonal hAELVi cell line were thawed and passaged once, before cells were seeded on Transwell® inserts as described in the Experimental section. Shown are mean values from TEER measurements from 3 individual experiments with technical replicates indicated in the plot.

## WILEY-VCH



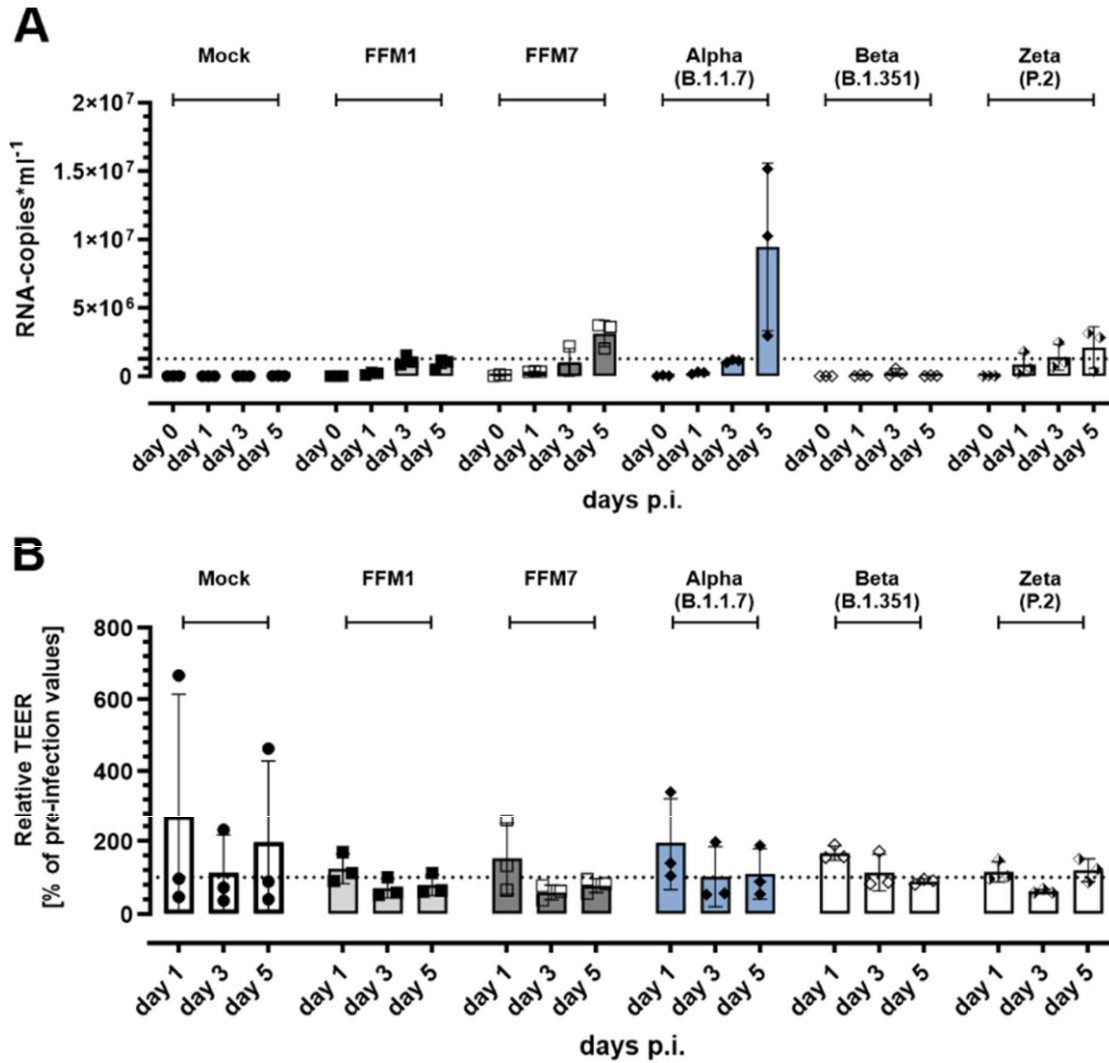
**Supplementary Figure 2 Single cell printing sequence.** The three pictures in the upper panel display the travel of cells to the printing nozzle before printing of the single cell that was used to generate hAELVI “Arlo“ in well D4 of a 96-well culture plate. The first picture of the bottom panel shows the event of single cell printing (detailed in Figure 1) and the last picture in the bottom panel shows the remaining cells after the printing of the single cell. Scale bar: 100  $\mu\text{m}$

WILEY-VCH



**Supplementary Figure 3 Empirical lung epithelial cell marker expressed by hAELVi “Arlo“.** Cell type specific gene signatures of genes whose expression is representative for specific epithelial cell types within the human lung were derived from [15]. Data represent at least 2 biological replicates of cells cultured under ALI conditions and were derived from bulk RNA-Sequencing.

WILEY-VCH



**Supplementary Figure 4 SARS-CoV-2 infection of hAELVi “Arlo” with different viral variants.**

A) Infection studies performed with the single cell clone hAELVi “Arlo” either on day 12 of culture under ALI conditions with SARS-CoV-2 (different variants are indicated) (MOI of 1) or mock (PBS). SARS-CoV-2 RNA copy numbers (RNA-copies\*ml<sup>-1</sup>) derived from qRT-PCR of the RNA-dependent RNA polymerase (RdRp) gene copies present in single apical washes (30 min, PBS) on the given days post-infection (days p.i.). B) Reduction of barrier properties of hAELVi “Arlo” after infection with the different variants. TEER values were normalized to the values before infection (dotted line). Data represent mean ± S.D.; n = 3 for each group from single biological specimen.

#### 4. Discussion and future perspectives

Ideally, results from preclinical or exploratory research models should well predict the various effects that a certain noxa could elicit in human subjects. Over recent years, rapid advances in novel *in vitro* technologies, such as organs-on-chip or the *in vitro* culture of human stem cells, led the scientific community to scrutinize the validity of the data stemming from animal models in terms of their predictivity for the effects observed in human subjects. Within this context, the FDA modernization act 2.0 marked a path-breaking political decision and a promising opportunity in the history of human-relevant *in vitro* models. However, it will still be a long way ahead before a wealth of validated human complex pulmonary *in vitro* models will generally be available for biopharmaceutical inhalation research, as exemplified by the work performed during this thesis.

In the coming years, biopharmaceutical research should focus on the development of technically accessible and reliable platforms with a higher throughput as well as a specific context of use in mind. Such ambitions should prioritize the inter-laboratory comparison of cell culture and other methodological protocols for better comparability as well as reproducibility. Examples of *in vitro* harmonization or standardization criteria have already been suggested in recent literature (Bonniaud et al. 2018; Movia et al. 2020; Rothen-Rutishauser et al. 2023). Using chemically defined cell culture media without the addition of animal-based supplements will be an essential standard to establish within this context. Such efforts will not only serve to improve complex pulmonary *in vitro* models of healthy origin, but they will also form the basis for better complex pulmonary *in vitro* models of respiratory disease. Precise 3D bioprinting of bacterial biofilms, on top of infected immunocompetent co-culture models of pulmonary epithelia, for example, could be combined with a perfused *in vitro* platform, such as PerfuPul, to enhance the reproducibility

as well as the longevity of such a future complex pulmonary *in vitro* model of infectious disease (Aliyazdi et al. 2023).

As suggested by Loewa et al. (2023), such complex *in vitro* models of human disease should among other things be benchmarked against human *in vivo* data and validated against robust as well as pre-defined performance criteria.

The perfusable platform (“PerfuPul”) and the cell line “Arlo” were inspired by the idea of providing better technical accessibility to such technologies. So far, these two examples of *in vitro* “software” and “hardware” represent early building blocks for the creation of complex pulmonary *in vitro* models; however, many researchers in standard bio-/pharmaceutical laboratories should be able to use, reproduce and further advance these tools in many areas of research. Through its reliable *in vitro* performance, especially the cell line “Arlo” could become an important *in vitro* tool to compare, for example, the performance of different lung-on-chip devices and thereby serve as a benchmark for barrier properties. Further, “Arlo” should be rigorously tested in bidirectional permeability experiments using specific substrates of drug-relevant transporters in the presence and absence of selective inhibitors. If successful, such experiments could be a valuable contribution not only to the biopharmaceutical field in general but also to initiatives like the inhalation-based biopharmaceutics classification system (iBCS), where standardized *in vitro* models to assess permeability in the lung are still missing (Hastedt et al. 2022).

## 5. Acknowledgements

Firstly, I would like to thank my “Doktorvater” Prof. Dr. Claus-Michael Lehr. He not only gave me the opportunity to work on such a fantastic project as a member of his research group, provided guidance and scientific advice, but more importantly, also was a great mentor who introduced me to the world of pharmaceutical sciences. I want to express my heartfelt thanks to my co-supervisor, Dr. Nicole Schneider-Daum, who provided invaluable support and always had attention to detail.

I also would further like to thank Prof. Dr.-Ing. Michael Vielhaber for his contributions and support as a scientific companion throughout this Ph.D. project.

The funding provided by the German-Israeli Foundation for Scientific Research and Development (GIF) did not only enable great science but also allowed me to visit and experience Israel during two research stays. Having had the opportunity to work closely with Prof. Dr. Sc. Josué Sznitman and Dr. Arbel Artzy-Schnirman as well as other Israeli scientists, during this exciting project, was a precious enrichment for which I am more than grateful. I also would like to express my sincere appreciation to Dr. Nina Hobi, including the whole Alveolix team, and Dr. Rainer Hanselmann from the IB-Cancer Research Foundation for providing access to innovative technologies as well as for giving me experienced scientific advice.

All co-authors and collaborators that have not been explicitly mentioned so far deserve my sincere appreciation for their help and dedication during this Ph.D. project.

Many colleagues are not listed as authors of scientific articles, yet they have played a significant role in the related success. Therefore, I would like to thank the office team around Karin Gross, Sarah Müller, and Annette Herkströter for their priceless assistance with the administrative work.



## Acknowledgements

---

I would also like to express my genuine appreciation to the hard-working team of technical assistants, namely Petra König, Jana Westhues, and Pascal Paul.

The students who contributed to this thesis as part of an internship or research stay also deserve an honorable mention. Lise Ripken, Aurélie Dubois, and Morvarid Ajdarirad, thank you for your creativity and interest in learning new things.

I was fortunate enough to meet many other great people during my time as a Ph.D. student, amongst them my long-term office companion Dr. Justus Horstmann and other great colleagues such as Dr. Brigitta Loretz or Dr. Annette Boese. The motivated students and scientists participating in the lung club, such as Dr. Cristiane de Souza Carvalho-Wodarz, Dr. Adriely Goes, Dr. Julia Metz, Dr. Robert Richter, Dr. Carla Sousa, Clémentine Richter, Samy Aliyadzdi and Aghiad Bali, helped to create a marvelous environment for scientific discussions, which I always will remember. The privilege of having met so many other wonderful people at HIPS in general, but especially within the teams of DDEL and BION, is something for which I am very grateful.

Profound experiences forge strong bonds, and the following people provided lots of kindness, friendship, and humor. They always had an open ear or an open beer for me.

Dr. Olga Hartwig, Dr. Alberto Hidalgo, Mariza Vaso, Dr. Sarah Nasr, and Dr. Carlos Montefusco Pereira, thank you very much for being such valuable friends.

My family has supported me throughout this journey in every way possible, and for that, I cannot thank them enough. To my dear friends who have stood by me for years, I express my deep appreciation for their incredible support.

Finally, HIPS was also where I first met Dr. Hanzey Carius, the woman who supports me the most, who understands and loves me unconditionally. The extent of my gratitude and love for her surpasses all boundaries. Our lovely daughter Enya, which always ensures that I do not dedicate too much time to science, delivered the needed energy and happiness to close this last chapter of my student life. I love both of you.

## 6. Publication bibliography

Aliyazdi, Samy; Frisch, Sarah; Hidalgo, Alberto; Frank, Nicolas; Krug, Daniel; Müller, Rolf et al. (2023): 3D bioprinting of *E. coli* MG1655 biofilms on human lung epithelial cells for building complex *in vitro* infection models. In *Biofabrication* 15 (3). DOI: 10.1088/1758-5090/acd95e.

AlveoliX (24.03.23): AXLung-on-Chip System - AlveoliX. Available online at <https://www.alveolix.com/axlung-on-chip-system/>, updated on 24.03.23, checked on 01.05.23.

Andes, D.; Craig, W. A. (2002): Animal model pharmacokinetics and pharmacodynamics: a critical review. In *International journal of antimicrobial agents* 19 (4), pp. 261–268. DOI: 10.1016/s0924-8579(02)00022-5.

Artzy-Schnirman, Arbel; Hobi, Nina; Schneider-Daum, Nicole; Guenat, Olivier T.; Lehr, Claus-Michael; Sznitman, Josué (2019a): Advanced *in vitro* lung-on-chip platforms for inhalation assays: From prospect to pipeline. In *European journal of pharmaceutics and biopharmaceutics : official journal of Arbeitsgemeinschaft fur Pharmazeutische Verfahrenstechnik e.V* 144, pp. 11–17. DOI: 10.1016/j.ejpb.2019.09.006.

Artzy-Schnirman, Arbel; Lehr, Claus-Michael; Sznitman, Josué (2020): Advancing human *in vitro* pulmonary disease models in preclinical research: opportunities for lung-on-chips. In *Expert opinion on drug delivery* 17 (5), pp. 621–625. DOI: 10.1080/17425247.2020.1738380.

Artzy-Schnirman, Arbel; Zidan, Hikaia; Elias-Kirma, Shani; Ben-Porat, Lee; Tenenbaum-Katan, Janna; Carius, Patrick et al. (2019b): Capturing the Onset of Bacterial Pulmonary Infection in Acini-On-Chips. In *Adv. Biosys.* 45, p. 1900026.

DOI: 10.1002/adbi.201900026.

Bai, Haiqing; Si, Longlong; Jiang, Amanda; Belgur, Chaitra; Zhai, Yunhao; Plebani, Roberto et al. (2022): Mechanical control of innate immune responses against viral infection revealed in a human lung alveolus chip. In *Nature communications* 13 (1), p. 1928.

DOI: 10.1038/s41467-022-29562-4.

Baptista, Danielle; Moreira Teixeira, Liliana; Barata, David; Tahmasebi Birgani, Zeinab; King, Jasia; van Riet, Sander et al. (2022): 3D Lung-on-Chip Model Based on Biomimetically Microcurved Culture Membranes. In *ACS biomaterials science & engineering* 8 (6), pp. 2684–2699. DOI: 10.1021/acsbmaterials.1c01463.

Boegh, Marie; Nielsen, Hanne Mørck (2015): Mucus as a barrier to drug delivery – understanding and mimicking the barrier properties. In *Basic & clinical pharmacology & toxicology* 116 (3), pp. 179–186. DOI: 10.1111/bcpt.12342.

Bonnaud, Philippe; Fabre, Aurélie; Frossard, Nelly; Guignabert, Christophe; Inman, Mark; Kuebler, Wolfgang M. et al. (2018): Optimising experimental research in respiratory diseases: an ERS statement. In *The European respiratory journal* 51 (5). DOI: 10.1183/13993003.02133-2017.

Bosquillon, Cynthia; Madlova, Michaela; Patel, Nilesh; Clear, Nicola; Forbes, Ben (2017): A Comparison of Drug Transport in Pulmonary Absorption Models. Isolated Perfused rat Lungs, Respiratory Epithelial Cell Lines and Primary Cell Culture. In *Pharmaceutical research* 34 (12), pp. 2532–2540. DOI: 10.1007/s11095-017-2251-y.

Bove, Peter F.; Dang, Hong; Cheluvvaraju, Chaitra; Jones, Lisa C.; Liu, Xuefeng; O’Neal, Wanda K. et al. (2014): Breaking the *in vitro* alveolar type II cell proliferation barrier while retaining ion transport properties. In *American journal of respiratory cell and molecular biology* 50 (4), pp. 767–776. DOI: 10.1165/rcmb.2013-00710C.

Brune, Kieran; Frank, James; Schwingshackl, Andreas; Finigan, James; Sidhaye, Venkataramana K. (2015): Pulmonary epithelial barrier function: some new players and mechanisms. In *American journal of physiology. Lung cellular and molecular physiology* 308 (8), L731-45. DOI: 10.1152/ajplung.00309.2014.

Bur, Michael; Huwer, Hanno; Lehr, Claus-Michael; Hagen, Nina; Guldbrandt, Mette; Kim, Kwang-Jin; Ehrhardt, Carsten (2006): Assessment of transport rates of proteins and peptides across primary human alveolar epithelial cell monolayers. In *European journal of pharmaceutical sciences : official journal of the European Federation for Pharmaceutical Sciences* 28 (3), pp. 196–203. DOI: 10.1016/j.ejps.2006.02.002.

Buzek, J.; Ask, B. (2009): Regulation (EC) No 1223/2009 of the European Parliament and of the Council of 30 November 2009 on cosmetic products. In *Off. J. Eur. Union L* 342, pp. 59–209.

Carius, Patrick; Dubois, Aurélie; Ajdarirad, Morvarid; Artzy-Schnirman, Arbel; Sznitman, Josué; Schneider-Daum, Nicole; Lehr, Claus-Michael (2021a): PerfuPul-A Versatile Perfusable Platform to Assess Permeability and Barrier Function of Air Exposed Pulmonary Epithelia. In *Frontiers in bioengineering and biotechnology* 9, p. 743236.

DOI: 10.3389/fbioe.2021.743236.

Carius, Patrick; Horstmann, Justus C.; Souza Carvalho-Wodarz, Cristiane de; Lehr, Claus-Michael (2021b): Disease Models: Lung Models for Testing Drugs Against Inflammation and Infection. In Monika Schäfer-Korting, Silvy Stuchi Maria-Engler, Robert Landsiedel (Eds.): *Organotypic models in drug development*, vol. 265. Cham, Switzerland: Springer (*Handbook of experimental pharmacology*, 0171-2004, 265), pp. 157–186. Available online at <https://link.springer.com/book/10.1007/978-3-030-70063-8>, checked on 14.05.23.

Carius, Patrick; Jungmann, Annemarie; Bechtel, Marco; Grißmer, Alexander; Boese, Annette; Gasparoni, Gilles et al. (2023): A Monoclonal Human Alveolar Epithelial Cell Line (“Arlo”) with Pronounced Barrier Function for Studying Drug Permeability and Viral Infections. In *Advanced science (Weinheim, Baden-Wurtemberg, Germany)*, e2207301. DOI: 10.1002/advs.202207301.

Cei, Daniele; Doryab, Ali; Lenz, Anke-Gabriele; Schröppel, Andreas; Mayer, Paula; Burgstaller, Gerald et al. (2021): Development of a dynamic *in vitro* stretch model of the alveolar interface with aerosol delivery. In *Biotechnology and bioengineering* 118 (2), pp. 690–702. DOI: 10.1002/bit.27600.

Ching, Terry; Toh, Yi-Chin; Hashimoto, Michinao; Zhang, Yu Shrike (2021): Bridging the academia-to-industry gap: organ-on-a-chip platforms for safety and toxicology assessment. In *Trends in pharmacological sciences* 42 (9), pp. 715–728.

DOI: 10.1016/j.tips.2021.05.007.

Chu, Xiaoyan; Bleasby, Kelly; Evers, Raymond (2013): Species differences in drug transporters and implications for translating preclinical findings to humans. In *Expert Opinion on Drug Metabolism & Toxicology* 9 (3), pp. 237–252.

DOI: 10.1517/17425255.2013.741589.

Committee for Medicinal Products for Human Use - EMA 2009: European Medicines Agency. ICH guideline M3(R2) on non-clinical safety studies for the conduct of human clinical trials and marketing authorisation for pharmaceuticals. EMA/CPMP/ICH/286/1995. Dec 2009. [http://www.ema.europa.eu/docs/en\\_GB/document\\_library/Scientific-guideline/2009/09/WC500002720.pdf](http://www.ema.europa.eu/docs/en_GB/document_library/Scientific-guideline/2009/09/WC500002720.pdf), checked on 05.06.23.

Cooper, James Ross; Abdullatif, Muhammad Bilal; Burnett, Edward C.; Kempself, Karen E.; Conforti, Franco; Tolley, Howard et al. (2016): Long Term Culture of the A549 Cancer Cell Line Promotes Multilamellar Body Formation and Differentiation towards an Alveolar Type II Pneumocyte Phenotype. In *PLOS ONE* 11 (10), e0164438.

DOI: 10.1371/journal.pone.0164438.

Crapo, J. D.; Barry, B. E.; Gehr, P.; Bachofen, M.; Weibel, E. R. (1982): Cell number and cell characteristics of the normal human lung. In *The American review of respiratory disease* 125 (6), pp. 740–745. DOI: 10.1164/arrd.1982.125.6.740.

Cunningham, A. C.; Milne, D. S.; Wilkes, J.; Dark, J. H.; Tetley, T. D.; Kirby, J. A. (1994): Constitutive expression of MHC and adhesion molecules by alveolar epithelial cells (type II pneumocytes) isolated from human lung and comparison with immunocytochemical findings. In *Journal of cell science* 107 (Pt 2), pp. 443–449. DOI: 10.1242/jcs.107.2.443.

Daum, Nicole; Kuehn, Anna; Hein, Stephanie; Schaefer, Ulrich F.; Huwer, Hanno; Lehr, Claus-Michael (2012): Isolation, cultivation, and application of human alveolar epithelial cells. In *Methods in molecular biology (Clifton, N.J.)* 806, pp. 31–42. DOI: 10.1007/978-1-61779-367-7\_3.

Di Huang; Liu, Tingting; Liao, Junlong; Maharjan, Sushila; Xie, Xin; Pérez, Montserrat et al. (2021): Reversed-engineered human alveolar lung-on-a-chip model. In *Proceedings of the National Academy of Sciences of the United States of America* 118 (19).

DOI: 10.1073/pnas.2016146118.

Dobbs, L. G.; Williams, M. C.; Brandt, A. E. (1985): Changes in biochemical characteristics and pattern of lectin binding of alveolar type II cells with time in culture. In *Biochimica et biophysica acta* 846 (1), pp. 155–166. DOI: 10.1016/0167-4889(85)90121-1.



Dombu, Christophe Y.; Betbeder, Didier (2013): Airway delivery of peptides and proteins using nanoparticles. In *Biomaterials* 34 (2), pp. 516–525.

DOI: 10.1016/j.biomaterials.2012.08.070.

Doryab, Ali; Heydarian, Motaharehsadat; Yildirim, Ali Önder; Hilgendorff, Anne; Behr, Jürgen; Schmid, Otmar (2023): Breathing-induced stretch enhances the efficacy of an inhaled and orally delivered anti-fibrosis drug *in vitro*. In *Journal of Drug Delivery Science and Technology* 82, p. 104316. DOI: 10.1016/j.jddst.2023.104316.

Doryab, Ali; Schmid, Otmar (2022): Bioactive Cell-Derived ECM Scaffold Forms a Unique Cellular Microenvironment for Lung Tissue Engineering. In *Biomedicines* 10 (8).

DOI: 10.3390/biomedicines10081791.

Doryab, Ali; Taskin, Mehmet Berat; Stahlhut, Philipp; Schröppel, Andreas; Orak, Sezer; Voss, Carola et al. (2021): A Bioinspired *in vitro* Lung Model to Study Particokinetics of Nano-/Microparticles Under Cyclic Stretch and Air-Liquid Interface Conditions. In *Front. Bioeng. Biotechnol.* 9, p. 616830. DOI: 10.3389/fbioe.2021.616830.

Dowden, Helen; Munro, Jamie (2019): Trends in clinical success rates and therapeutic focus. In *Nature reviews. Drug discovery* 18 (7), pp. 495–496. DOI: 10.1038/d41573-019-00074-z.

Dvorak, Anna; Tilley, Ann E.; Shaykhiev, Renat; Wang, Rui; Crystal, Ronald G. (2011): Do airway epithelium air-liquid cultures represent the *in vivo* airway epithelium transcriptome? In *American journal of respiratory cell and molecular biology* 44 (4), pp. 465–473.

DOI: 10.1165/rcmb.2009-04530C.

Elbert, K. J.; Schäfer, U. F.; Schäfers, H. J.; Kim, K. J.; Lee, V. H.; Lehr, C. M. (1999): Monolayers of human alveolar epithelial cells in primary culture for pulmonary absorption and transport studies. In *Pharmaceutical research* 16 (5), pp. 601–608.

DOI: 10.1023/a:1018887501927.

Emulate (05.04.23): Products & Services. Available online at <https://emulatebio.com/products-services/>, updated on 05.04.23, checked on 07.05.23.

European Commission, Joint Research Centre (2021): Establishing the scientific validity of complex *in vitro* models: results of a EURL ECVAM survey: Publications Office.

Evans, Kelly V.; Lee, Joo-Hyeon (2020): Alveolar wars: The rise of *in vitro* models to understand human lung alveolar maintenance, regeneration, and disease. In *Stem cells translational medicine* 9 (8), pp. 867–881. DOI: 10.1002/sctm.19-0433.

FDA (2018): The Drug Development Process. In *FDA*, 2018. Available online at <https://www.fda.gov/patients/learn-about-drug-and-device-approvals/drug-development-process>, checked on 14.05.23.

Forum of International Respiratory Societies (2021): The global impact of respiratory disease. European Respiratory Society. Available online at [firsnet.org/images/publications/FIRS\\_Master\\_09202021.pdf](https://firsnet.org/images/publications/FIRS_Master_09202021.pdf), checked on 22.09.21.

Foster, Cherie D.; Varghese, Linda S.; Skalina, Rachel B.; Gonzales, Linda W.; Guttentag, Susan H. (2007): *In vitro* transdifferentiation of human fetal type II cells toward a type I-like cell. In *Pediatric research* 61 (4), pp. 404–409. DOI: 10.1203/pdr.0b013e3180332c6d.

Fröhlich, Eleonore (2019): Biological Obstacles for Identifying *In vitro-In vivo* Correlations of Orally Inhaled Formulations. In *Pharmaceutics* 11 (7).

DOI: 10.3390/pharmaceutics11070316.

Fröhlich, Eleonore (2021): Replacement Strategies for Animal Studies in Inhalation Testing. In *Sci* 3 (4), p. 45. DOI: 10.3390/sci3040045.

Fuchs, Sabine; Hollins, Andrew John; Laue, Michael; Schaefer, Ulrich Friedrich; Roemer, Klaus; Gumbleton, Mark; Lehr, Claus-Michael (2003): Differentiation of human alveolar epithelial cells in primary culture: morphological characterization and synthesis of caveolin-1 and surfactant protein-C. In *Cell and tissue research* 311 (1), pp. 31–45.

DOI: 10.1007/s00441-002-0653-5.

Garcia-Mouton, Cristina; Hidalgo, Alberto; Cruz, Antonio; Pérez-Gil, Jesús (2019): The Lord of the Lungs: The essential role of pulmonary surfactant upon inhalation of nanoparticles. In *European journal of pharmaceutics and biopharmaceutics : official journal of Arbeitsgemeinschaft fur Pharmazeutische Verfahrenstechnik e.V* 144, pp. 230–243.

DOI: 10.1016/j.ejpb.2019.09.020.

Gautam, Shree Hari; Verhagen, Justus V. (2012): Direct behavioral evidence for retronasal olfaction in rats. In *PloS one* 7 (9), e44781. DOI: 10.1371/journal.pone.0044781.

Gehr, Peter; Bachofen, Marianne; Weibel, Ewald R. (1978): The normal human lung. Ultrastructure and morphometric estimation of diffusion capacity. In *Respiration Physiology* 32 (2), pp. 121–140. DOI: 10.1016/0034-5687(78)90104-4.

Giard, D. J.; Aaronson, S. A.; Todaro, G. J.; Arnstein, P.; Kersey, J. H.; Dosik, H.; Parks, W. P. (1973): *In vitro* cultivation of human tumors: establishment of cell lines derived from a series of solid tumors. In *J Natl Cancer Inst* 51 (5), pp. 1417–1423.

DOI: 10.1093/jnci/51.5.1417.

Gordon, Sarah; Daneshian, Mardas; Bouwstra, Joke; Caloni, Francesca; Constant, Samuel; Davies, Donna E. et al. (2015): Non-animal models of epithelial barriers (skin, intestine and lung) in research, industrial applications and regulatory toxicology. In *ALTEX* 32 (4), pp. 327–378. DOI: 10.14573/altex.1510051.

Haefeli-Bleuer, B.; Weibel, E. R. (1988): Morphometry of the human pulmonary acinus. In *The Anatomical record* 220 (4), pp. 401–414. DOI: 10.1002/ar.1092200410.

Hasegawa, Koichi; Sato, Atsuyasu; Tanimura, Kazuya; Uemasu, Kiyoshi; Hamakawa, Yoko; Fuseya, Yoshinori et al. (2017): Fraction of MHCII and EpCAM expression characterizes distal lung epithelial cells for alveolar type 2 cell isolation. In *Respiratory research* 18 (1), p. 150. DOI: 10.1186/s12931-017-0635-5.

Hastedt, Jayne E.; Bäckman, Per; Cabal, Antonio; Clark, Andy; Ehrhardt, Carsten; Forbes, Ben et al. (2022): iBCS: 1. Principles and Framework of an Inhalation-Based Biopharmaceutics Classification System. In *Molecular pharmaceutics* 19 (7), pp. 2032–2039. DOI: 10.1021/acs.molpharmaceut.2c00113.

Have-Opbroek, A. A. ten; Otto-Verberne, C. J.; Dubbeldam, J. A.; Dijkman, J. H. (1991): The proximal border of the human respiratory unit, as shown by scanning and transmission electron microscopy and light microscopical cytochemistry. In *The Anatomical record* 229 (3), pp. 339–354. DOI: 10.1002/ar.1092290308.

He, Yong; Rofaani, Elrade; Huang, Xiaochen; Huang, Boxin; Liang, Feng; Wang, Li et al. (2022): Generation of Alveolar Epithelium Using Reconstituted Basement Membrane and hiPSC-Derived Organoids. In *Advanced healthcare materials* 11 (6), e2101972.

DOI: 10.1002/adhm.202101972.

Herzog, Erica L.; Brody, Arnold R.; Colby, Thomas V.; Mason, Robert; Williams, Mary C. (2008): Knowns and unknowns of the alveolus. In *Proceedings of the American Thoracic Society* 5 (7), pp. 778–782. DOI: 10.1513/pats.200803-028HR.

Hiemstra, Pieter S.; Grootaers, Gwendolynn; van der Does, Anne M.; Krul, Cyrille A. M.; Kooter, Ingeborg M. (2018): Human lung epithelial cell cultures for analysis of inhaled toxicants: Lessons learned and future directions. In *Toxicology in vitro : an international journal published in association with BIBRA* 47, pp. 137–146.

DOI: 10.1016/j.tiv.2017.11.005.

Hiemstra, Pieter S.; Tetley, Teresa D.; Janes, Sam M. (2019): Airway and alveolar epithelial cells in culture. In *The European respiratory journal* 54 (5).

DOI: 10.1183/13993003.00742-2019.

Hittinger, Marius; Janke, Julia; Huwer, Hanno; Scherliess, Regina; Schneider-Daum, Nicole; Lehr, Claus-Michael (2016): Autologous co-culture of primary human alveolar macrophages and epithelial cells for investigating aerosol medicines. Part I. Model characterisation. In *Alternatives to laboratory animals : ATLA* 44 (4), pp. 337–347.

Hittinger, Marius; Schneider-Daum, Nicole; Lehr, Claus-Michael (2017): Cell and tissue-based *in vitro* models for improving the development of oral inhalation drug products. In *European journal of pharmaceutics and biopharmaceutics : official journal of Arbeitsgemeinschaft fur Pharmazeutische Verfahrenstechnik e.V.*

DOI: 10.1016/j.ejpb.2017.02.019.

Horstmann, Justus C.; Laric, Annabelle; Boese, Annette; Yildiz, Daniela; Röhrig, Teresa; Empting, Martin et al. (2022): Transferring Microclusters of *P. aeruginosa* Biofilms to the Air-Liquid Interface of Bronchial Epithelial Cells for Repeated Deposition of Aerosolized Tobramycin. In *ACS infectious diseases* 8 (1), pp. 137–149.

DOI: 10.1021/acsinfecdis.1c00444.

Horstmann, Justus C.; Thorn, Chelsea R.; Carius, Patrick; Graef, Florian; Murgia, Xabier; Souza Carvalho-Wodarz, Cristiane de; Lehr, Claus-Michael (2021): A Custom-Made Device for Reproducibly Depositing Pre-metered Doses of Nebulized Drugs on Pulmonary Cells *in vitro*. In *Front. Bioeng. Biotechnol.* 9, p. 643491. DOI: 10.3389/fbioe.2021.643491.

Huh, Dongeun; Matthews, Benjamin D.; Mammoto, Akiko; Montoya-Zavala, Martín; Hsin, Hong Yuan; Ingber, Donald E. (2010): Reconstituting organ-level lung functions on a chip. In *Science (New York, N.Y.)* 328 (5986), pp. 1662–1668.

DOI: 10.1126/science.1188302.

Hurst, Susan; Loi, Cho-Ming; Brodfuehrer, Joanne; El-Kattan, Ayman (2007): Impact of physiological, physicochemical and biopharmaceutical factors in absorption and metabolism mechanisms on the drug oral bioavailability of rats and humans. In *Expert Opinion on Drug Metabolism & Toxicology* 3 (4), pp. 469–489.

DOI: 10.1517/17425255.3.4.469.

Ingber, Donald E. (2020): Is it Time for Reviewer 3 to Request Human Organ Chip Experiments Instead of Animal Validation Studies? In *Adv. Sci.* 7 (22), p. 2002030.

DOI: 10.1002/advs.202002030.

InSCREENex (07.05.23): huArlo Alveolar Epithelial Cells. Available online at <https://www.inscreenex.de/products/human-immortalized-cell-lines/huarlo-alveolar-epithelial-cells-hu/>, updated on 07.05.23, checked on 07.05.23.



Jacob, Anjali; Morley, Michael; Hawkins, Finn; McCauley, Katherine B.; Jean, J. C.; Heins, Hillary et al. (2017): Differentiation of Human Pluripotent Stem Cells into Functional Lung Alveolar Epithelial Cells. In *Cell stem cell* 21 (4), 472-488.e10.

DOI: 10.1016/j.stem.2017.08.014.

Jong, P. M. de; van Sterkenburg, M. A.; Kempenaar, J. A.; Dijkman, J. H.; Ponec, M. (1993): Serial culturing of human bronchial epithelial cells derived from biopsies. In *In vitro cellular & developmental biology. Animal* 29A (5), pp. 379–387. DOI: 10.1007/BF02633985.

Juntke, Jenny; Murgia, Xabier; Günday Türeli, Nazende; Türeli, Akif Emre; Thorn, Chelsea R.; Schneider, Marc et al. (2021): Testing of aerosolized ciprofloxacin nanocarriers on cystic fibrosis airway cells infected with *P. aeruginosa* biofilms. In *Drug Deliv. and Transl. Res.* 11 (4), pp. 1752–1765. DOI: 10.1007/s13346-021-01002-8.

Kadzik, Rachel S.; Morrissey, Edward E. (2012): Directing lung endoderm differentiation in pluripotent stem cells. In *Cell stem cell* 10 (4), pp. 355–361.

DOI: 10.1016/j.stem.2012.03.013.

Karp, Philip H.; Moninger, Thomas O.; Pary Weber, S.; Nesselhauf, Tamara S.; Launspach, Janice L.; Zabner, Joseph; Welsh, Michael J. (2002): An *In vitro* Model of Differentiated Human Airway Epithelia. In : *Epithelial Cell Culture Protocols*: Humana Press, pp. 115–137.

Katsura, Hiroaki; Sontake, Vishwaraj; Tata, Aleksandra; Kobayashi, Yoshihiko; Edwards, Caitlin E.; Heaton, Brook E. et al. (2020): Human Lung Stem Cell-Based Alveolospheres Provide Insights into SARS-CoV-2-Mediated Interferon Responses and Pneumocyte Dysfunction. In *Cell stem cell* 27 (6), 890-904.e8. DOI: 10.1016/j.stem.2020.10.005.

Kim, K. J.; Borok, Z.; Crandall, E. D. (2001): A useful *in vitro* model for transport studies of alveolar epithelial barrier. In *Pharmaceutical research* 18 (3), pp. 253–255.

DOI: 10.1023/a:1011040824988.

Knight, Jean; Rovidia, Costanza; Kreiling, Reinhard; Zhu, Cathy; Knudsen, Mette; Hartung, Thomas (2021): Continuing animal tests on cosmetic ingredients for REACH in the EU. In *ALTEX* 38 (4), pp. 653–668. DOI: 10.14573/altex.2104221.

Knudsen, Lars; Ochs, Matthias (2018): The micromechanics of lung alveoli: structure and function of surfactant and tissue components. In *Histochemistry and cell biology* 150 (6), pp. 661–676. DOI: 10.1007/s00418-018-1747-9.

Koullapis, Pantelis; Ollson, Bo; Kassinos, Stavros C.; Sznitman, Josué (2019): Multiscale in silico lung modeling strategies for aerosol inhalation therapy and drug delivery. In *Current opinion in biomedical engineering* 11, pp. 130–136.

DOI: 10.1016/j.cobme.2019.11.003.

Kratochvil, Michael J.; Seymour, Alexis J.; Li, Thomas L.; Paşca, Sergiu P.; Kuo, Calvin J.; Heilshorn, Sarah C. (2019): Engineered materials for organoid systems. In *Nature reviews. Materials* 4 (9), pp. 606–622. DOI: 10.1038/s41578-019-0129-9.

Kuehn, Anna; Kletting, Stephanie; Souza Carvalho-Wodarz, Cristiane de; Repnik, Urska; Griffiths, Gareth; Fischer, Ulrike et al. (2016): Human alveolar epithelial cells expressing tight junctions to model the air-blood barrier. In *ALTEX* 33 (3), pp. 251–260.

DOI: 10.14573/altex.1511131.

Labode, Jonas; Dullin, Christian; Wagner, Willi L.; Myti, Despoina; Morty, Rory E.; Mühlfeld, Christian (2022): Evaluation of classifications of the monopodial bronchopulmonary vasculature using clustering methods. In *Histochemistry and cell biology* 158 (5), pp. 435–445. DOI: 10.1007/s00418-022-02116-x.

Lacroix, Ghislaine; Koch, Wolfgang; Ritter, Detlef; Gutleb, Arno C.; Larsen, Søren Thor; Loret, Thomas et al. (2018): Air-Liquid Interface *In vitro* Models for Respiratory Toxicology Research: Consensus Workshop and Recommendations. In *Applied in vitro toxicology* 4 (2), pp. 91–106. DOI: 10.1089/aivt.2017.0034.

LaFemina, Michael J.; Rokkam, Deepti; Chandrasena, Anita; Pan, Jue; Bajaj, Anisha; Johnson, Meshell; Frank, James A. (2010): Keratinocyte growth factor enhances barrier function without altering claudin expression in primary alveolar epithelial cells. In *American journal of physiology. Lung cellular and molecular physiology* 299 (6), L724-34.

DOI: 10.1152/ajplung.00233.2010.

Lamers, Mart M.; van der Vaart, Jelte; Knoop, Kevin; Riesebosch, Samra; Breugem, Tim I.; Mykytyn, Anna Z. et al. (2021): An organoid-derived bronchioalveolar model for SARS-CoV-2 infection of human alveolar type II-like cells. In *The EMBO Journal* 40 (5), e105912.

DOI: 10.15252/emj.2020105912.

Leenaars, Cathalijn H. C.; Kouwenaar, Carien; Stafleu, Frans R.; Bleich, André; Ritskes-Hoitinga, Merel; Vries, Rob B. M. de; Meijboom, Franck L. B. (2019): Animal to human translation: a systematic scoping review of reported concordance rates. In *Journal of translational medicine* 17 (1), p. 223. DOI: 10.1186/s12967-019-1976-2.

Lenz, Anke-Gabriele; Stoeger, Tobias; Cei, Daniele; Schmidmeir, Martina; Semren, Nora; Burgstaller, Gerald et al. (2014): Efficient bioactive delivery of aerosolized drugs to human pulmonary epithelial cells cultured in air-liquid interface conditions. In *American journal of respiratory cell and molecular biology* 51 (4), pp. 526–535. DOI: 10.1165/rcmb.2013-04790C.

Lin, J. H. (1995): Species similarities and differences in pharmacokinetics. In *Drug metabolism and disposition: the biological fate of chemicals* 23 (10), pp. 1008–1021, checked on 29.06.23.

Lipps, Christoph; Klein, Franziska; Wahlicht, Tom; Seiffert, Virginia; Butueva, Milada; Zauers, Jeannette et al. (2018): Expansion of functional personalized cells with specific transgene combinations. In *Nature communications* 9 (1), p. 994. DOI: 10.1038/s41467-018-03408-4.

Lochbaum, Robin; Schilpp, Carolin; Nonnenmacher, Lara; Frick, Manfred; Dietl, Paul; Wittekindt, Oliver H. (2020): Retinoic acid signalling adjusts tight junction permeability in response to air-liquid interface conditions. In *Cellular Signalling* 65, p. 109421.

DOI: 10.1016/j.cellsig.2019.109421.

Loewa, Anna; Feng, James J.; Hedtrich, Sarah (2023): Human disease models in drug development. In *Nature reviews bioengineering*, pp. 1–15. DOI: 10.1038/s44222-023-00063-3.

Low, Lucie A.; Mummery, Christine; Berridge, Brian R.; Austin, Christopher P.; Tagle, Danilo A. (2021): Organs-on-chips: into the next decade. In *Nat Rev Drug Discov* 20 (5), pp. 345–361. DOI: 10.1038/s41573-020-0079-3.

Mahto, Sanjeev Kumar; Tenenbaum-Katan, Janna; Greenblum, Ayala; Rothen-Rutishauser, Barbara; Sznitman, Josué (2014): Microfluidic shear stress-regulated surfactant secretion in alveolar epithelial type II cells *in vitro*. In *American journal of physiology. Lung cellular and molecular physiology* 306 (7), L672-83. DOI: 10.1152/ajplung.00106.2013.

Metz, Julia; Knoth, Katharina; Groß, Henrik; Lehr, Claus-Michael; Stäbler, Carolin; Bock, Udo; Hittinger, Marius (2018): Combining MucilAir™ and Vitrocell® Powder Chamber for the *In vitro* Evaluation of Nasal Ointments in the Context of Aerosolized Pollen. In *Pharmaceutics* 10 (2), p. 56. DOI: 10.3390/pharmaceutics10020056.

Mieke A. Dentener; Anita C. E. Vreugdenhil; Peter H. M. Hoet; Juanita H. J. Vernooy; Fred H. M. Nieman; Didier Heumann et al. (2000): Production of the Acute-Phase Protein Lipopolysaccharide-Binding Protein by Respiratory Type II Epithelial Cells 23(2), pp. 146–153, checked on 04.07.23.

Montefusco-Pereira, Carlos Victor; Horstmann, Justus C.; Ebensen, Thomas; Beisswenger, Christoph; Bals, Robert; Guzmán, Carlos A. et al. (2020): *P. aeruginosa* Infected 3D Co-Culture of Bronchial Epithelial Cells and Macrophages at Air-Liquid Interface for Preclinical Evaluation of Anti-Infectives. In *Journal of visualized experiments : JoVE* (160).

DOI: 10.3791/61069.

Movia, Dania; Bruni-Favier, Solene; Prina-Mello, Adriele (2020): *In vitro* Alternatives to Acute Inhalation Toxicity Studies in Animal Models-A Perspective. In *Frontiers in bioengineering and biotechnology* 8, p. 549. DOI: 10.3389/fbioe.2020.00549.

Murgia, Xabier; Loretz, Brigitta; Hartwig, Olga; Hittinger, Marius; Lehr, Claus-Michael (2018): The role of mucus on drug transport and its potential to affect therapeutic outcomes. In *Advanced drug delivery reviews* 124, pp. 82–97.

DOI: 10.1016/j.addr.2017.10.009.

Niimi, T.; Nagashima, K.; Ward, J. M.; Minoo, P.; Zimonjic, D. B.; Popescu, N. C.; Kimura, S. (2001): claudin-18, a novel downstream target gene for the T/EBP/NKX2.1 homeodomain transcription factor, encodes lung- and stomach-specific isoforms through alternative splicing. In *Molecular and cellular biology* 21 (21), pp. 7380–7390.

DOI: 10.1128/MCB.21.21.7380-7390.2001.

Nof, Eliram; Zidan, Hikaia; Artzy-Schnirman, Arbel; Mouhadeb, Odelia; Beckerman, Margarita; Bhardwaj, Saurabh et al. (2022): Human Multi-Compartment Airways-on-Chip Platform for Emulating Respiratory Airborne Transmission: From Nose to Pulmonary Acini. In *Frontiers in physiology* 13, p. 853317. DOI: 10.3389/fphys.2022.853317.

Ochs, Matthias; Nyengaard, Jens R.; Jung, Anja; Knudsen, Lars; Voigt, Marion; Wahlers, Thorsten et al. (2004): The number of alveoli in the human lung. In *American journal of respiratory and critical care medicine* 169 (1), pp. 120–124.

DOI: 10.1164/rccm.200308-1107OC.

Perlman, Carrie E.; Bhattacharya, Jahar (2007): Alveolar expansion imaged by optical sectioning microscopy. In *Journal of applied physiology (Bethesda, Md. : 1985)* 103 (3), pp. 1037–1044. DOI: 10.1152/jappphysiol.00160.2007.

Pound, Pandora; Ritskes-Hoitinga, Merel (2018): Is it possible to overcome issues of external validity in preclinical animal research? Why most animal models are bound to fail. In *Journal of translational medicine* 16 (1), pp. 1–8.

Prior, Helen; Haworth, Richard; Labram, Briony; Roberts, Ruth; Wolfreys, Alison; Sewell, Fiona (2020): Justification for species selection for pharmaceutical toxicity studies. In *Toxicol Res* 9 (6), pp. 758–770. DOI: 10.1093/toxres/tfaa081.

Punde, Tushar H.; Wu, Wen-Hao; Lien, Pei-Chun; Chang, Ya-Ling; Kuo, Ping-Hsueh; Chang, Margaret Dah-Tsyr et al. (2015): A biologically inspired lung-on-a-chip device for the study

of protein-induced lung inflammation. In *Integrative biology : quantitative biosciences from nano to macro* 7 (2), pp. 162–169. DOI: 10.1039/c4ib00239c.

Rock, Jason R.; Randell, Scott H.; Hogan, Brigid L. M. (2010): Airway basal stem cells: a perspective on their roles in epithelial homeostasis and remodeling. In *Disease models & mechanisms* 3 (9-10), pp. 545–556.

DOI: 10.1242/dmm.006031.

Rothen-Rutishauser, Barbara; Gibb, Matthew; He, Ruiwen; Petri-Fink, Alke; Sayes, Christie M. (2023): Human lung cell models to study aerosol delivery - considerations for model design and development. In *European journal of pharmaceutical sciences : official journal of the European Federation for Pharmaceutical Sciences* 180, p. 106337.

DOI: 10.1016/j.ejps.2022.106337.

Ruge, Christian A.; Kirch, Julian; Lehr, Claus-Michael (2013): Pulmonary drug delivery. From generating aerosols to overcoming biological barriers—therapeutic possibilities and technological challenges. In *The Lancet Respiratory Medicine* 1 (5), pp. 402–413.

DOI: 10.1016/S2213-2600(13)70072-9.

Russel, W. M.S.; Burch, R. L. (1959): *The principles of humane experimental technique*: London: Methuen. Available online at <https://caat.jhsph.edu/principles/the-principles-of-humane-experimental-technique>, checked on 26.02.23

S. R. Bates; C. Dodia; and A. B. Fisher (1994): Surfactant protein A regulates uptake of pulmonary surfactant by lung type II cells on microporous membranes. In *The American Journal of Physiology* (267), L753-60. DOI: 10.1152/ajplung.1994.267.6.l753.

Schittny, Johannes C. (2017): Development of the lung. In *Cell and tissue research* 367 (3), pp. 427–444. DOI: 10.1007/s00441-016-2545-0.



Schlingmann, Barbara; Molina, Samuel A.; Koval, Michael (2015): Claudins. Gatekeepers of lung epithelial function. In *Seminars in cell & developmental biology* 42, pp. 47–57.

DOI: 10.1016/j.semcdb.2015.04.009.

Selo, Mohammed Ali; Sake, Johannes A.; Kim, Kwang-Jin; Ehrhardt, Carsten (2021): *In vitro* and ex vivo models in inhalation biopharmaceutical research - advances, challenges and future perspectives. In *Advanced drug delivery reviews* 177, p. 113862.

DOI: 10.1016/j.addr.2021.113862.

Sengupta, Arunima; Dorn, Aurélien; Jamshidi, Mohammad; Schwob, Magali; Hassan, Widad; Maddalena, Lea Lara de et al. (2023): A multiplex inhalation platform to model in situ like aerosol delivery in a breathing lung-on-chip. In *Frontiers in pharmacology* 14, p. 1114739. DOI: 10.3389/fphar.2023.1114739.

Sengupta, Arunima; Roldan, Nuria; Kiener, Mirjam; Froment, Laurène; Raggi, Giulia; Imler, Theo et al. (2022): A New Immortalized Human Alveolar Epithelial Cell Model to Study Lung Injury and Toxicity on a Breathing Lung-On-Chip System. In *Front. Toxicol.* 4, p. 840606.

DOI: 10.3389/ftox.2022.840606.

Seyhan, Attila A. (2019): Lost in translation: the valley of death across preclinical and clinical divide – identification of problems and overcoming obstacles. In *transl med commun* 4 (1). DOI: 10.1186/s41231-019-0050-7.

Shanks, Niall; Greek, Ray; Greek, Jean (2009): Are animal models predictive for humans? In *Philos Ethics Humanit Med* 4 (1), p. 2. DOI: 10.1186/1747-5341-4-2.

Stucki, Andreas O.; Stucki, Janick D.; Hall, Sean R. R.; Felder, Marcel; Mermoud, Yves; Schmid, Ralph A. et al. (2015): A lung-on-a-chip array with an integrated bio-inspired respiration mechanism. In *Lab on a Chip* 15 (5), pp. 1302–1310.

DOI: 10.1039/C4LC01252F.

Stucki, Janick D.; Hobi, Nina; Galimov, Artur; Stucki, Andreas O.; Schneider-Daum, Nicole; Lehr, Claus-Michael et al. (2018): Medium throughput breathing human primary cell alveolus-on-chip model. In *Sci Rep* 8 (1), p. 14359. DOI: 10.1038/s41598-018-32523-x.

Tièche, Colin Charles; Gao, Yanyun; Bühner, Elias Daniel; Hobi, Nina; Berezowska, Sabina Anna; Wyler, Kurt et al. (2019): Tumor Initiation Capacity and Therapy Resistance Are Differential Features of EMT-Related Subpopulations in the NSCLC Cell Line A549. In *Neoplasia* 21 (2), pp. 185–196. DOI: 10.1016/j.neo.2018.09.008.

Tindle, Courtney; Fuller, Mackenzie; Fonseca, Ayden; Taheri, Sahar; Ibeawuchi, Stella-Rita; Beutler, Nathan et al. (2021): Adult stem cell-derived complete lung organoid models emulate lung disease in COVID-19. In *eLife Sciences Publications, Ltd* 10.

DOI: 10.7554/eLife.66417.

Tyler, Walter S.; Julian, M. Dolores (1992): Gross and subgross anatomy of lungs, pleura, connective tissue septa, distal airways, and structural units. In *Comparative biology of the normal lung* 1, pp. 37–48.

van Michael J. Evans, Laura S. Wink (2001): CELLULAR AND MOLECULAR CHARACTERISTICS OF BASAL CELLS IN AIRWAY EPITHELIUM. In *Experimental Lung Research* 27 (5), pp. 401–415. DOI: 10.1080/01902140120740.

van Riet, Sander; Ninaber, Dennis K.; Mikkers, Harald M. M.; Tetley, Teresa D.; Jost, Carolina R.; Mulder, Aat A. et al. (2020): *In vitro* modelling of alveolar repair at the air-liquid interface using alveolar epithelial cells derived from human induced pluripotent stem cells. In *Scientific reports* 10 (1), p. 5499. DOI: 10.1038/s41598-020-62226-1.

van Riet, Sander; van Schadewijk, Annemarie; Khedoe, P. Padmini S. J.; Limpens, Ronald W. A. L.; Bárcena, Montserrat; Stolk, Jan et al. (2022): Organoid-based expansion of patient-derived primary alveolar type 2 cells for establishment of alveolus epithelial Lung-Chip cultures. In *American journal of physiology. Lung cellular and molecular physiology* 322 (4), L526-L538. DOI: 10.1152/ajplung.00153.2021.

Vos, Theo; Lim, Stephen S.; Abbafati, Cristiana; Abbas, Kaja M.; Abbasi, Mohammad; Abbasifard, Mitra et al. (2020): Global burden of 369 diseases and injuries in 204 countries and territories, 1990-2019: a systematic analysis for the Global Burden of Disease Study 2019. In *Lancet (London, England)* 396 (10258), pp. 1204–1222.

DOI: 10.1016/S0140-6736(20)30925-9.

Weibel, E. R. (1973): Morphological basis of alveolar-capillary gas exchange. In *Physiological Reviews* 53 (2), pp. 419–495. DOI: 10.1152/physrev.1973.53.2.419.

Weibel, E. R.; Courmand, A. F.; Richards, D. W. (1963): Morphometry of the human lung: Springer (1).

Whitcutt, M. J.; Adler, K. B.; Wu, R. (1988): A biphasic chamber system for maintaining polarity of differentiation of cultured respiratory tract epithelial cells. In *In vitro cellular & developmental biology : journal of the Tissue Culture Association* 24 (5), pp. 420–428. DOI: 10.1007/BF02628493.

Winton, H. L.; Wan, H.; Cannell, M. B.; Gruenert, D. C.; Thompson, P. J.; Garrod, D. R. et al. (1998): Cell lines of pulmonary and non-pulmonary origin as tools to study the effects of house dust mite proteinases on the regulation of epithelial permeability. In *Clinical and experimental allergy : journal of the British Society for Allergy and Clinical Immunology* 28 (10), pp. 1273–1285. DOI: 10.1046/j.1365-2222.1998.00354.x.

Wittekindt, Oliver H.; Dietl, Paul (2019): Aquaporins in the lung. In *Pflugers Archiv : European journal of physiology* 471 (4), pp. 519–532. DOI: 10.1007/s00424-018-2232-y.

World Health Organization (2020): The top 10 causes of death. Available online at <https://www.who.int/news-room/fact-sheets/detail/the-top-10-causes-of-death>, updated on 08.02.23, checked on 26.02.23.

Wu, Reen; Sato, Gordon H.; Whitcutt, M. J. (1986): Developing Differentiated Epithelial Cell Cultures: Airway Epithelial Cells. In *Toxicol Sci* 6 (4), pp. 580–590.

DOI: 10.1093/toxsci/6.4.580.

Yang, Jia-Wei; Lin, Yu-Rou; Chu, Ying-Ling; Chung, Johnson H. Y.; Lu, Huai-En; Chen, Guan-Yu (2022): Tissue-level alveolar epithelium model for recapitulating SARS-CoV-2 infection and cellular plasticity. In *Communications biology* 5 (1), p. 70.

DOI: 10.1038/s42003-022-03026-3.

Yaqub, Naheem; Wayne, Gareth; Birchall, Martin; Song, Wenhui (2022): Recent advances in human respiratory epithelium models for drug discovery. In *Biotechnology advances* 54, p. 107832. DOI: 10.1016/j.biotechadv.2021.107832.

Zamprogno, Pauline; Wüthrich, Simon; Achenbach, Sven; Thoma, Giuditta; Stucki, Janick D.; Hobi, Nina et al. (2021): Second-generation lung-on-a-chip with an array of stretchable alveoli made with a biological membrane. In *Commun Biol* 4 (1), p. 168.

DOI: 10.1038/s42003-021-01695-0.